The bone and cartilage interplay in osteoarthritis: key to effective treatment strategy

Tuerlings, M.

The bone and cartilage interplay in osteoarthritis:

key to effective treatment strategy

Margo Tuerlings

The bone and cartilage interplay in osteoarthritis: key to effective treatment strategy
M. Tuerlings, MSc
ISBN: 978-94-6483-191-7

The bone and cartilage interplay in osteoarthritis:

key to effective treatment strategy
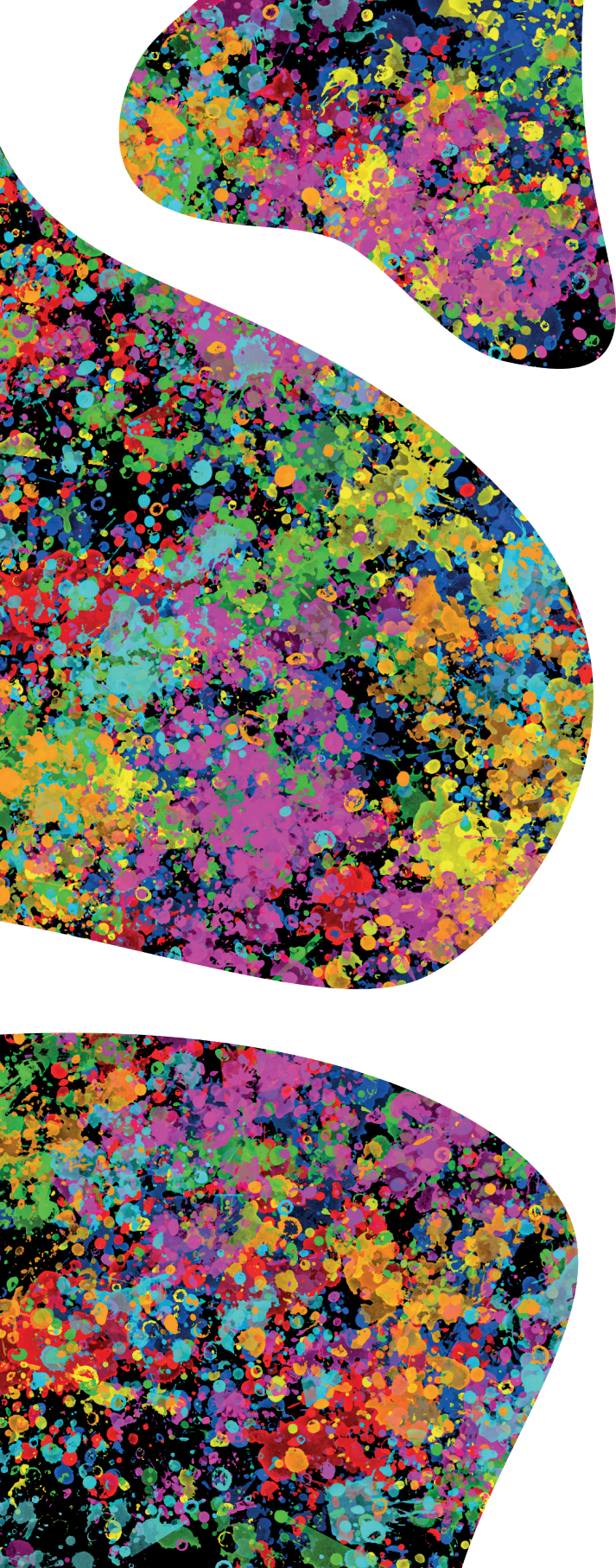
Proefschrift

ter verkrijging van

de graad van doctor aan de Universiteit Leiden,

op gezag van rector magnificus prof.dr.ir. H. Bijl,

volgens besluit van het college voor promoties

te verdedigen op woensdag 27 september 2023

klokke 15.00 uur

door

Margo Tuerlings

geboren te Eindhoven

in 1992

Contents

CHAPTER 1

General introduction

Burden of Osteoarthritis

Osteoarthritis (OA) is a prevalent degenerative, yet irreversible, disease of the articular joints. Globally, 7% percent of the population is affected by OA and in 2019 OA was the 15th highest cause of years lived with disability (YLDs) [1]. Prevalence of OA increases significantly with increasing age and incidence rate is higher in women than in men, especially between 55 and 59 years of age [2]. OA pathophysiology is characterized by progressive and heterogeneous deterioration and loss of articular cartilage, remodeling of subchondral bone, osteophyte formation, and inflammation (**Figure 1**) [3]. Clinical symptoms of OA are pain, (morning) stiffness, crepitus, and reduced range of motion [4, 5]. Therefore, OA has a negative impact on patient quality of life and with progression of the disease it could even result in complete disability. So far, no disease modifying treatments are available, except for costly total joint replacement surgery at end-stage disease. This results in high social and economic burden to society [2, 6, 7]. OA pathophysiology is a complex process in which initiation and progression of the disease is mostly multifactorial [8]. Risk factors for OA include age, sex, metabolic health, aberrant loading, trauma, and genetics [9, 10].
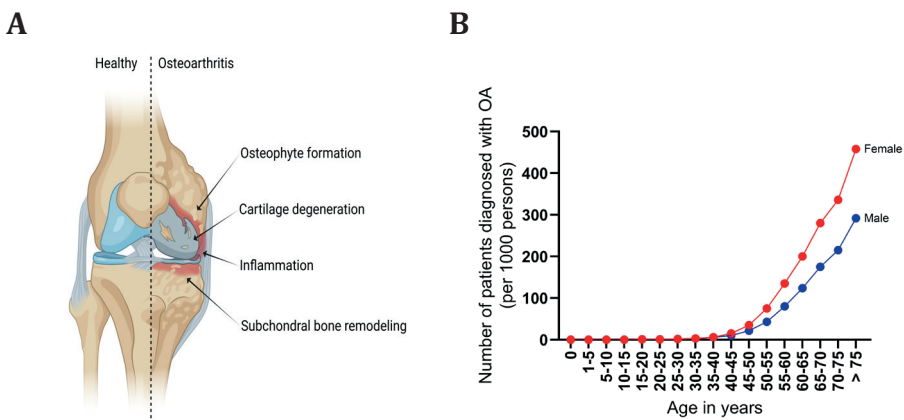
Figure 1 – Overview of osteoarthritis pathophysiology as age-related disease.
(A) Schematic overview of OA pathophysiology including cartilage degeneration, subchondral bone remodeling, osteophyte formation, and inflammation (created with Biorender.com). (B) Overview of number of patients diagnosed with OA in the Netherlands in 2020 according to CBS, stratified by age.

(Patho-)physiology of the osteochondral unit

Development and growth of longitudinal bones relies on a process called endochondral ossification (**Figure 2**). During prenatal development a cartilage template is formed, which is pre- and postnatally replaced by bone tissue. During endochondral ossification, chondrocytes present in the cartilage template become hypertrophic and start to secrete factors such as runt-related transcription factor 2 (*RUNX2*), vascular endothelial growth factor (*VEGF*), and collagen type 10 (*COL10*) [11]. Subsequently, the cartilage template is invaded by osteoblast progenitors, blood vessels, endothelial cells, and hematopoietic

cells that give rise to formation of osteoclasts, together resulting in resorption of hypertrophic cartilage and deposition of trabecular bone and bone marrow tissue in the so-called primary ossification center [12]. This primary ossification center expands and a secondary ossification center appears in the epiphysis of the developing bone, leaving the epiphyseal growth plate in between. The epiphyseal growth plate is responsible for the longitudinal growth of bones. With age this growth plate gets thinner, until both ossification centers fuse.

The cartilage at the end of bones escapes the endochondral ossification process, forming an avascular load-bearing structure called articular cartilage (**Figure 2**) [13, 14]. Chondrocytes are thought to be the only cell type present in articular cartilage and they reside in a maturational arrest state and do not proliferate. Chondrocytes are responsible for structural integrity of cartilage extracellular matrix (ECM), which consists of four zones: superficial, middle, deep, and calcified zone, with each zone having its specific fiber and cell organization **(Figure 3)** [13]. Main cartilage ECM components are collagens, such as collagen type 2 (*COL2*), and proteoglycans, such as aggrecan (*ACAN*). With OA, chondrocytes lose their maturational arrested state and become hypertrophic-like, resembling growth plate morphology. Thereby, they start to actively produce catabolic enzymes, such as matrix metalloproteinases (*MMPs*) and disintegrin and metalloproteinase with thrombospondin motifs 4 and 5 (ADAMTS-4 and -5) [15-17]. These enzymes result in fragmentation and degradation of collagens and proteoglycans, respectively. Moreover, the reactivated chondrocytes secrete
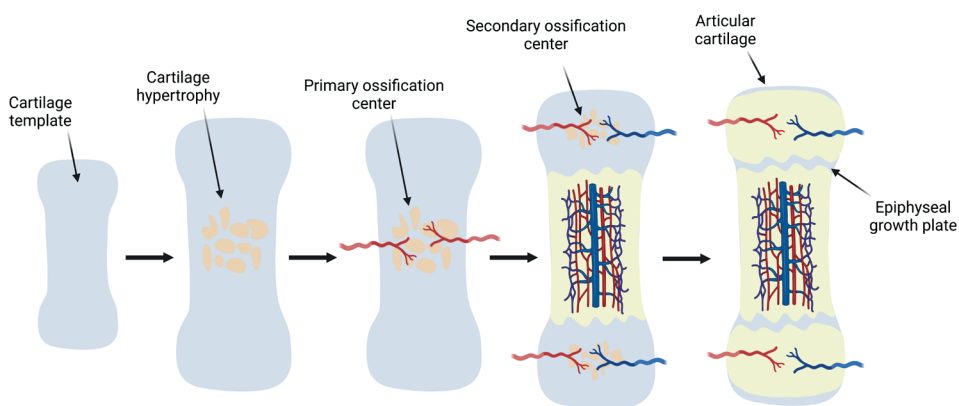
Figure 2 – Schematic overview of endochondral ossification process.
A cartilage template is pre- and postnatally replaced by bone tissue. First, chondrocytes become hypertrophic and a primary ossification center is formed. This primary ossification center expands and a secondary ossification center develops in the epiphysis of the cartilage template, leaving the epiphyseal growth plate in between. With age this growth plate gets thinner, until both ossification centers fuse (created with Biorender. com).
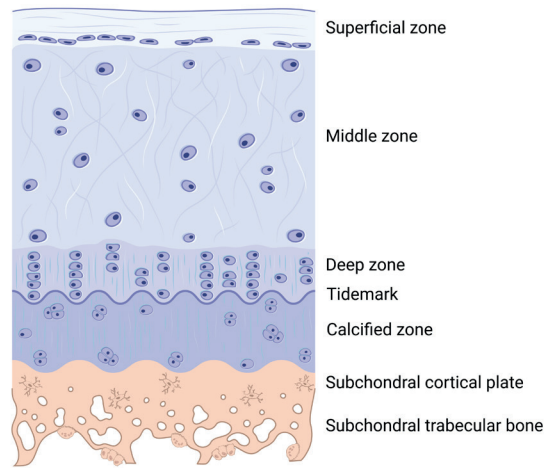
Figure 3 – Schematic overview of osteochondral structure.
Cartilage consist of multiple zones, including the superficial, middle, deep, and calcified zone. The subchondral bone can be divided in the subchondral cortical plate and subchondral trabecular bone (created with Biorender.com).

factors promoting calcification and vascularization of the ECM, such as runt-related transcription factor 2 (RUNX2), vascular endothelial growth factor (VEGF), and collagen type X (COL10A1) [18, 19]. The degeneration and mineralization of cartilage in OA is accompanied with alterations in the subchondral bone.

The subchondral bone consists of subchondral cortical plate and subchondral trabecular bone. The subchondral cortical plate is defined as a thin cortical bone structure beneath the calcified cartilage, which is invaded with blood vessels and nerves. The subchondral trabecular bone is more porous, contains even more blood vessels and nerves compared to the cortical plate and is important in shock-absorbing [20]. Cell types residing in the subchondral bone are osteoblasts, osteocytes, and osteoclasts. Osteoblasts and osteocytes are responsible for production and maintenance of bone matrix, while osteoclasts are responsible for bone resorption in response to environmental factors, such as mechanical loading [21]. Main constituent of subchondral bone is collagen type 1 (COL1), which forms a network that serves as a scaffold for hydroxyapatite crystal deposition [22, 23]. In healthy bone, there is a balance between bone ECM production and resorption. However, with OA, this balance gets disturbed, resulting in increased subchondral bone plate thickness and decreased bone mineral density (BMD) in end-stage OA [22, 24, 25]. Together, increased subchondral bone plate thickness and mineralization of articular cartilage result in joint space narrowing, a typical characteristic of OA [5]. Another feature commonly seen in OA is the formation of bony

structures along the joint margins, called osteophytes. Osteophytes are formed through endochondral ossification in presence of growth factors transforming growth factor beta (TGF-β) and bone morphogenic protein 2 (BMP2) and they are hypothesized to increase joint stability in response to the enlarged mechanical load applied [26, 27].

Genetics

Although development of OA is multifactorial, genetic predisposition is one of the strongest determinants of the disease [10]. To identify genetic variants and/or genes conferring risk to OA, comprehensive genome-wide association studies (GWASs) have been performed [28-33]. In GWASs genetic variants, called single nucleotide polymorphisms (SNPs), are being statistically associated to a specific disease or trait [34]. Since OA is a polygenic disease, with multiple causal genes showing small effects, effect sizes of OA susceptibility SNPs are generally low and large sample sizes are required to identify these SNPs [35]. The largest GWAS meta-analysis so far identifying OA risk SNPs is performed recently by Boer and colleagues [28]. This study included 826,690 individuals, of which 177,517 were diagnosed with OA and resulted in identification of 100 independent SNPs being associated with OA. These variants were located near genes including WW domain containing E3 ubiquitin protein ligase 2 (*WWP2*), interleukin 11 (*IL11*), transforming growth factor alpha (*TGF-α*), and aldehyde dehydrogenase 1 family member A2 (*ALDH1A2*) (**Table 1**). These genes are involved in maintenance processes in both bone and cartilage, confirming that both tissues have a substantial role in initiation and development of OA and stressing the importance of including both tissues and their interaction in OA research.

Functional genomics

Next to identification of OA susceptibility genes, better understanding of molecular OA pathogenesis is required towards development of disease modifying treatments. A valuable tool for this is transcriptomic data, such as RNA-sequencing data, as it can be used to identify genes that mark OA pathophysiology, identify OA subtypes, and it can be used to determine the direction of effect of compelling OA risk genes.

Differential expression analysis

To identify underlying genes and pathways that mark OA pathophysiology, multiple studies have been performed comparing healthy or macroscopically preserved and lesioned OA areas of the joint on transcriptomic level [61-63]. In this respect, RNA-sequencing (RNA-seq) was performed on articular cartilage from patients who underwent total joint replacement surgery due to OA as part of the Research in Articular osteoArthritis Cartilage (RAAK) study. Upon comparing gene expression levels of macroscopically preserved and lesioned OA articular cartilage, 2387 genes

Table 1 – Notable examples of OA susceptibility SNPs, identified in genome wide association studies, with their mapped genes and hypothesized direction of effect.
These genes are all involved in maintenance processes of both articular cartilage and subchondral bone.

Mapped gene	Function of protein	SNP	Risk allele	Trait	Annotation	Gene expression risk	References
IL11	Regulates bone formation, remodeling, and resorption	rs4252548	T	Hip OA	Missense	Decreased expression	[28, 31, 32, 36]
SMAD3	Prevents chondrocyte hypertrophy	rs12908498	C	Hip OA	Intron	Decreased expression	[28, 37-39]
DIO2	Induces chondrocyte hypertrophy	rs225014	T	Symptomatic OA	Exon	Increased expression	[40, 41]
TNC	Promotes cartilage repair	rs1330349	C	Hip OA	Intron	Decreased expression	[28, 32, 42, 43]
COL27A1	Involved in transition from cartilage to bone	rs72760655	A	Knee and hip OA	Upstream gene	Decreased expression	[28, 38, 44, 45]
GDF5	Involved in joint development and cartilage repair	rs143384	A	Knee OA	5' UTR	Decreased expression	[28, 31, 32, 44, 46-48]
WWP2	Plays a role in chondrogenesis	rs34195470	A	Knee OA	Intron	Increased expression	[28, 31, 38, 42, 49]
MGP	Regulates cartilage calcification	rs1800801	C	Hand OA	Exon	Decreased expression	[50-52]
TGF-α	Involved in transition from cartilage to bone	rs3771501	T	Hip OA	Intron	Increased expression	[28, 32, 53, 54]
ALDH1A2	Involved in maintenance of cartilage and bone	rs11071366	A	Hand OA	Intron	Decreased expression	[28, 55]
CHADL	Negative modulator of chondrocyte differentiation	rs117018441	T	Hip OA	Intron	Increased expression	[29, 31]
COL11A1	Involved in endochondral ossification and microarchitecture of developing bone	rs3753841	T	Hip OA	Missense	Decreased expression	[31, 56]
FRZB	Involved in endochondral ossification	rs288326	G	Hip OA	Exon	Decreased expression	[57-60]

were identified as being false discovery rate (FDR) significantly differentially expressed [63]. These differentially expressed genes were enriched for processes involved in extracellular matrix organization, characterized by upregulation of periostin (*POSTN),* TNF receptor superfamily member 11b (*TNFRSF11B*) and secreted phosphoprotein 1 (*SPP1*) and processes involved in skeletal system development, characterized by upregulation of bone morphogenic protein 3 (*BMP3*) and 6 (*BMP6*) and downregulation of frizzled related protein (*FRZB*) and growth differentiation factor 10 (*GDF10*). In another large transcriptomic analysis study, RNA-seq was performed on paired preserved and lesioned cartilage of 124 OA patients [64]. Differentially expressed genes found in this study were enriched for, amongst others, cytokine activity, characterized by upregulation of cytokine receptor like factor 1 (*CRLF1*), *IL11*, and *IL1-β*, suggesting OA-related inflammation is driven by the interleukin 6 (IL6) super family (**Table 2**).

While valuable extensive effort has been made to characterize the pathophysiological process in articular cartilage, the pathophysiology of underlying subchondral bone is less explored. This despite the fact that there is accumulating evidence that subchondral bone, in interaction with articular cartilage, contributes to both OA onset and progression [24, 27, 65, 66]. Chou and colleagues used microarray analysis to identify differentially expressed genes between OA and non-OA subchondral bone [62]. Among the differentially expressed genes were *TNF,* collagen type 12 alpha 1 (*COL12A1),* sclerostin (*SOST*), bone morphogenic protein 7 (*BMP7*), and chordin-like 2 (*CHRDL2*) (**Table 2**). Another study used microarray analysis to identify differential expression of genes between OA bone marrow lesion and control bone samples [67]. They found genes involved in osteochondral turnover, neurogenesis, and inflammation. However, both of these studies only included knee samples and in both studies microarray analysis was performed. The disadvantage of microarray analysis is that it only profiles predefined genes, while RNA-seq, for example, results in transcriptome-wide gene expression profiling. Therefore, valuable information might be missed by microarray analysis

Characterization of OA subtypes
Recently, OA is more recognized to be a heterogeneous disease with variable characteristics across OA patients. For that matter, transcriptomic analysis of articular cartilage can also be used to identify OA subtypes to better understand heterogeneity of the underlying molecular disease process. Yuan and colleagues identified four subtypes of knee OA by performing unsupervised clustering based on top 4000 genes that showed highest variation across patients [70]. These four subtypes represented GAG metabolic disorder, collagen metabolic disorder, activated sensory neurons, and inflammation. In another study, two OA subtypes were identified also in knee OA samples [71]. These two subtypes were associated to chondrocyte hypertrophy and immune response,

Table 2 – Differential expression between macroscopically preserved and lesioned OA articular cartilage and subchondral bone.

Articular Cartilage

Pathway	Gene	Fold change	FDR	Reference FC and FDR	Similar direction of effect shown by:
Extracellular matrix	POSTN	2.04	3.4E-02	[63]	[64, 68]
	TNFRSF11B	3.01	7.1E-12	[63]	[61, 64, 68]
	SPP1	3.14	9.0E-07	[63]	[61, 64]
Skeletal system development	BMP3	0.28	2.9E-03	[63]	[69]
	BMP6	2.43	1.6E-09	[63]	[61]
	FRZB	0.27	1.9E-09	[63]	[61, 64, 68]
	GDF10	0.35	1.0E-08	[63]	[61, 64, 68]
Cytokine activity	IL11	22.79	1.6E-20	[63]	[64, 68]
	CRLF1	3.04	3.0E-10	[63]	[61, 64, 68]

Subchondral bone

Pathway	Gene	Fold change	FDR	Reference FC and FDR	Similar direction of effect shown by:
Bone mineral density	SOST	2.51	2.59E-04	[62]	-
Abnormal bone morphology	COL12A1	2.26	6.55E-08	[62]	-
	TNF	0.32	1.17E-08	[62]	-
Mineralization of cells	BMP7	0.40	1.65E-09	[62]	-
	CHRDL2	0.25	1.40E-04	[62]	-

respectively. Recently, Coutinho de Almeida and colleagues also identified two OA subtypes using RNA-seq data of both hip and knee OA samples, representing similar processes [72]. More importantly, they showed that these subtypes were associated with phenotypic differences. Identification of these OA subtypes enables better predictions of clinical outcomes of OA treatments [70]. However, to distinguish OA subtypes in clinical practice, non-invasive biomarkers are necessary to stratify patients on OA subtype before treatments start.

Allelic imbalanced expression
While some OA risk variants are missense mutations located in the protein-coding region of a gene and thereby directly affecting protein structure, most SNPs conferring risk to OA are located in non-coding regions. Functional follow-up studies have shown that SNPs in non-coding regions frequently act via altered expression of positional genes in *cis*, also known as allelic imbalanced expression (AIE) [73, 74]. Transcriptomic data can also be used to screen for allelic imbalance. In this respect, den Hollander and colleagues used RNA-seq data of preserved and lesioned OA articular cartilage to screen for transcriptome-wide AIE [42]. As a result, 2,070 SNPs were identified marking AIE of 1,031 genes, including 18 genes that were also identified as OA susceptibility genes in GWASs. Among these 18 genes were *WWP2, FRZB*, and matrix gla protein (*MGP*) identified as highly significant. More recently, Coutinho de Almeida and colleagues also screened for AIE in both articular cartilage and subchondral bone OA samples [75]. In this study, 26 SNPs were identified being subjected to AIE in cartilage, and 7 SNPs were identified in subchondral bone. These studies on AIE are extremely valuable as they can be used to make firm hypothesis on the direction of effect of identified compelling OA risk genes. However, for translation of these OA risk genes towards development of disease modifying OA treatments, functional follow-up studies are required to elucidate molecular mechanisms and targets of these genes [76-78].

Epigenetics in osteoarthritis
Epigenetics refers to changes in heritable phenotype without alterations in the genetic code. Epigenetic regulation provides cells with a mechanism to respond to environmental cues such as mechanical stress and microtraumas by changing gene and protein expression levels temporarily [79]. Epigenetic mechanisms include DNA methylation, histone modification, and non-coding RNA expression, all being extensively associated to OA pathophysiology [80].

DNA methylation and histone modifications
DNA consist of a sequence of adenine, thymine, cytosine, and guanine and cytosine followed by guanine, is called a CpG site. In a CpG site, the cytosine can be converted

to 5-methylcytosine (5mC) by methylation catalyzed by methyltransferases. This processes is called DNA methylation and this process alters the binding of proteins, such as transcription factors, to the DNA and therefore it changes gene expression levels (**Figure 4A**) [81]. DNA is condensed around histone proteins (H3, H4, H2A, and H2B). To modulate gene expression, histone proteins undergo modifications such as methylation and acetylation (**Figure 4B**) [82, 83]. Histone methylation mainly inhibits gene transcription by blocking binding of transcription factors, while histone acetylation is associated with increased gene transcription. Histone modifications are executed by histone methyl transferases, histone acetyl transferases, histone deacetylases, and histone demethylases [80].
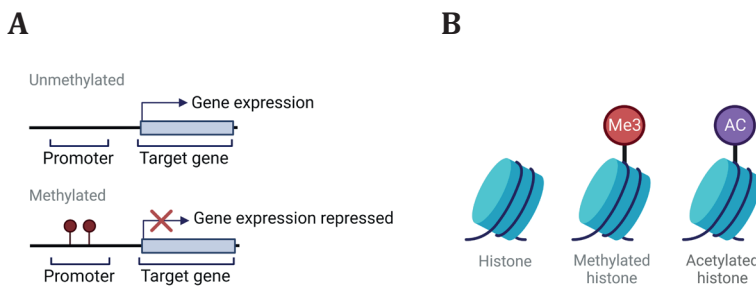
Figure 4 – Overview of epigenetic processes.
(A) overview of DNA methylation. Methylation of the DNA alters the binding of proteins, such as transcription factors, to the DNA (created with Biorender.com) (B) Schematic overview of histone modifications. Methylation of histones is associated with decreased gene transcription, while acetylation of histones is associated with increased gene transcription (created with Biorender.com)

MicroRNA expression
While DNA methylation and histone modifications are mainly regulating transcription of genes, non-coding RNAs are a class of transcriptional and (post-)translational regulators. Non-coding RNAs are classified based on their size in micro-RNAs (miRNAs) and long non-coding RNAs (lncRNAs). MiRNAs are typically between 18 and 25 nucleotides in length and they negatively regulate translation of mRNA to protein. Most miRNAs bind to the 3' untranslated region (UTR) of their target mRNA, thereby inhibiting translation and/or reducing mRNA stability [84, 85]. The number of base pairs that overlap between miRNAs and their target mRNA determine whether the mRNA is degraded via Argonaute RISC Catalytic Component 2 (Ago2) or repressed via Argonaute RISC Catalytic Component 1 (Ago1). The target mRNA will be degraded when there is (almost) a perfect overlap between miRNA and target mRNA, while translation of the target mRNA will be repressed when there is only partial overlap (**Figure 5A**) [86].

As dysregulated miRNAs mark complex diseases, such as OA, multiple studies focused on characterization of miRNA expression and identification of their mRNA targets in OA pathophysiology. To date, the role of miRNAs in OA has mainly been studied in articular cartilage. For example, Iliopoulos and colleagues compared expression levels of 365 miRNAs in cartilage of 33 OA joints and cartilage of 10 non-OA joints [87]. This resulted in the identification of 16 differentially expressed miRNAs, including upregulation of miR-22 and downregulation of miR-140 in OA cartilage. In another study, miRNAs were identified being differentially expressed between OA and non-OA cartilage and bone, including miR-9 and miR-98[88]. Upon gene targeting prediction and pathway analysis, these miRNAs seem to play a role in inflammation. More recently, integration of transcriptome-wide miRNA-seq and mRNA-seq of OA articular cartilage resulted in identification of 143 miRNAs differentially expressed between macroscopically preserved and lesioned OA cartilage [63]. possible mRNA target was identified for 62 of these differentially expressed miRNAs, including *RGS4*. *RGS4* expression was found to be regulated by mir-140, which is abundantly expressed in articular cartilage and known to be involved in chondrogenesis and osteoarthritis [89, 90]. Mir-140 is co-transcribed with its host gene *WWP2* and regulated by *SOX9*. Moreover, miR-140 is shown to be involved in endochondral ossification, as loss of miR-140 expression in mice results in bone defects and malformations [91].

Long non-coding RNA expression
In contrast to miRNAs, lncRNAs are less frequently investigated mainly because of the poor evolutionary conservation between species and because of their generally low expression levels [92, 93]. LncRNAs are typically over 200 nucleotides in length and while lncRNAs lack protein-coding ability, they share similarities with mRNAs, as most lncRNAs have a 5' 7-methylguanosine cap and a 3' poly A tail and are transcribed by RNA polymerase II [94]. LncRNAs are involved in various transcriptional and (post-)translational processes, including chromatin remodeling, mRNA translation, transcription factor activity, and mRNA and protein stability (**Figure 5B**) [95, 96]**.** Moreover, lncRNA expression can be highly tissue- and disease specific [97]. Multiple lncRNAs have been reported to be involved in chondrogenesis and osteogenesis [93, 98]. Similar to miRNAs, in OA pathophysiology currently lncRNAs have been exclusively studied in articular cartilage. Upon comparing macroscopically preserved and lesioned OA cartilage, 191 lncRNAs were identified to be differentially expressed [99]. Among these differentially expressed lncRNAs was prolyl 3-hydroxylase 2 antisense RNA 1 (*P3H2-AS1*), which was shown to regulate expression levels of its sense gene prolyl 3-hydroxylase 2 (*P3H2*). In another study comparing OA and non-OA articular cartilage, maternally expressed 3 (*MEG3*) was found to be downregulated in both OA hips and knees [100]. As lncRNAs tend to be tissue- and disease specific, identification of

A

B
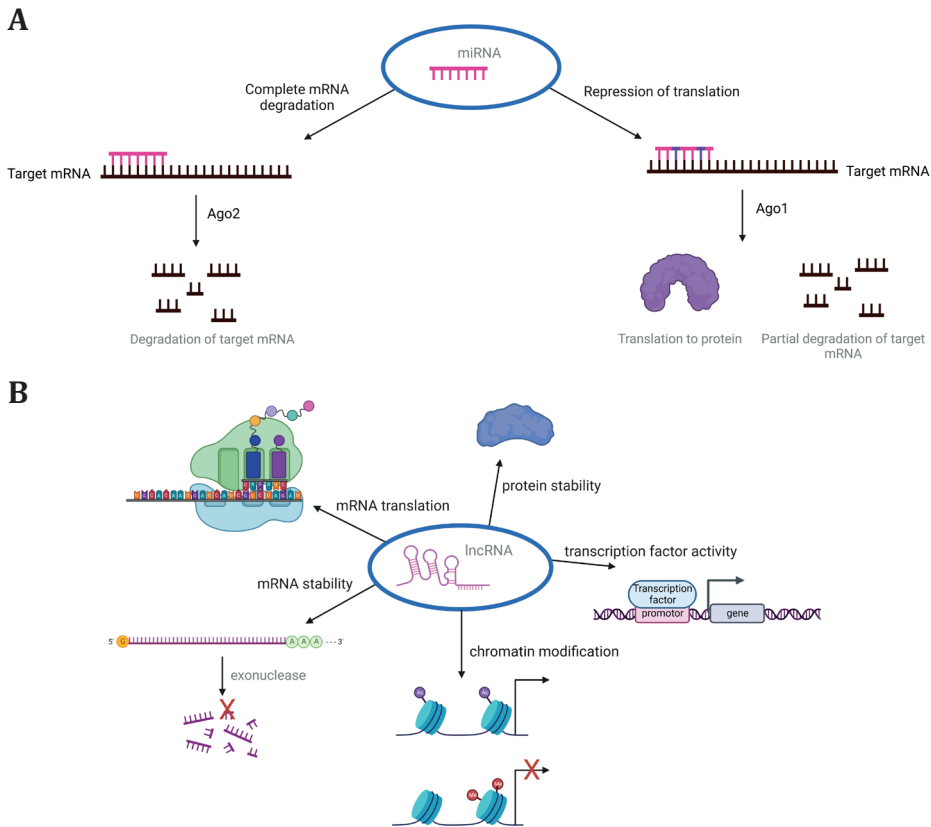
Figure 5 – Overview of non-coding mode-of-actions.
(A) Most miRNAs bind to the 3'UTR of their target mRNA, thereby (partly) inhibiting translation to protein (created with Biorender.com). (B) LncRNAs have various mode-of-actions both on a transcriptional, translational, and post-translational level (Created with Biorender.com).

lncRNAs that mark OA pathophysiological processes might bring new opportunities in development of joint tissue- and disease specific therapeutic strategies. Although multiple lncRNAs are identified marking OA in articular cartilage, studies on lncRNAs marking OA pathophysiology in subchondral bone are still lacking.

Biomarkers in osteoarthritis
To date, there are no reliable biomarkers that reflect ongoing processes in joint tissues. Classification and/or diagnosis of OA is therefore only based on imaging (radiography, MRI) and clinical symptoms, such as pain and stiffness of the affected joint [101]. Consequently, early diagnosis of OA, information on OA prognosis, and ability to predict treatment outcomes are still lacking [102]. To overcome this knowledge gap, research started focusing on identification of potential OA biomarkers using relatively easily accessible sites, such as synovial fluid, urine, and blood. For example, Soul and

colleagues identified a set of proteins, including POSTN, TNC, and MGP, that were predicted to be secreted in the synovial fluid. This set of proteins in synovial fluid could reflect whether a patient is subjected to inflammation-driven or chondrocyte hypertrophy-driven OA [71]. Another study identified six proteins in measured in synovial fluid that were in association with synovial inflammation, severity of cartilage loss, and joint pain [103]. These synovial fluid proteins included MMP3 and soluble vascular cell adhesion molecule 1 (sVCAM1). Nonetheless, urine and blood are more easily accessible and therefore less invasive compared to synovial fluid. OA biomarkers that can be measured in urine are mostly based on breakdown products of main cartilage components collagen type 2 (COL2) and aggrecan (ACAN) [104]. For instance, urinary levels of C-terminal crosslinking telopeptide of type II collagen (CTX-II) are shown to be associated with radiographic signs of OA in multiple studies [105, 106]. Moreover, CTX-II were higher in OA patients compared to healthy controls [107]. Nevertheless, these levels are solely reflecting collagen type II breakdown and do not provide insight in other ongoing OA-related processes. Recently, circulating miRNAs gained interest and Ramos and colleagues showed for the first time that miRNA expression levels in plasma could reflect changes in mRNA expression patterns in articular cartilage [108]. They identified 7 miRNAs, including miR-140-3p, miR-181a-3p, and miR-4443, that were able to predict OA progression. In another study, circulating miR-140-3p, miR-33b-3p, and miR-671-3p were identified in serum as OA biomarker and reflecting metabolic processes in articular cartilage [109]. Finally, Murata and colleagues identified miR-132 being predictive for rheumatoid arthritis and OA [110].

In vitro osteoarthritis disease models

To study compelling OA risk genes appropriate *in vitro* human OA disease models are required that incorporate disease relevant tissues, e.g. bone and cartilage [111]. To date, available *in vitro* model systems for osteochondral tissues include 2D cell cultures, 3D pellet cultures, 3D multi tissue co-cultures (**Figure 6**).

2D cell cultures

The simplest *in vitro* models are 2D cell cultures of OA relevant cells, such as chondrocytes, bone-marrow derived mesenchymal stromal cells (hBMSCs), osteoblasts, osteocytes, and osteoclasts. These 2D cell cultures can be exposed to OA-related cytokines or to conditioned media to study their cellular response [112]. For example in the study of Van Geffen and colleagues [113], human chondrocytes were cultured in 2D and exposed to IL1-β, TNF-α, or human OA synovium-conditioned medium to study the effect of inflammation on interleukin 37 (*IL37*) expression levels. To incorporate intercellular communication in 2D cell cultures co-cultures can be performed in Transwells, for example to study intercellular communication between chondrocytes and bone
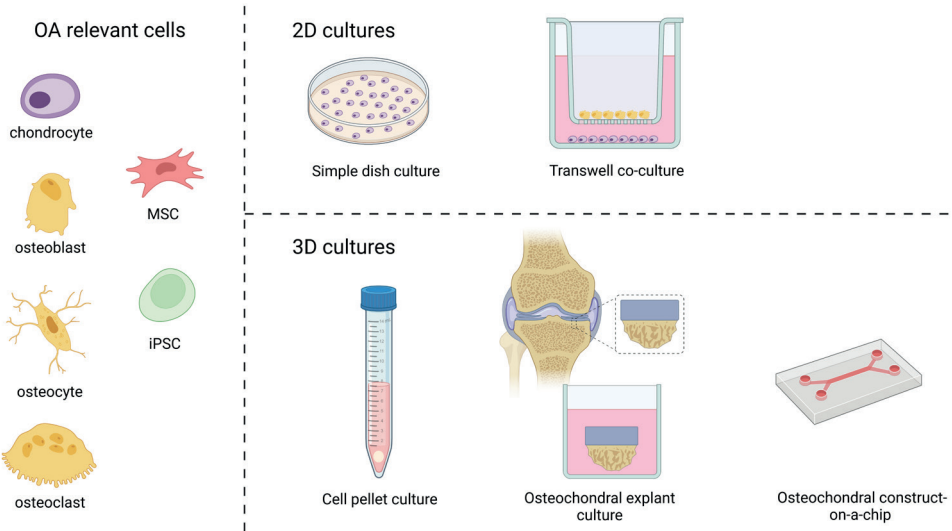
Figure 6 – Overview of OA relevant cells and some available OA models.

cells [114]. While being a useful tool, Transwell co-cultures still lack complexity and interaction of the ECM, and it is known that cells are prone to lose their specific phenotype on 2D surfaces [115].

3D pellet cultures

To include the effect of extracellular matrix and minimize dedifferentiation of cells, 3D cell pellet cultures or micro mass cultures are extensively used to model cartilaginous and osseous tissue [116, 117]. Caron and colleagues showed that chondrocytes in 3D pellet cultures are less prone to become hypertrophic compared to 2D cell cultures [115]. On another level, Bömer and colleagues showed that DNA methylation profile was 99% similar between 3D human chondrocyte pellet cultures and autologous articular cartilage [118]. Subsequently, these 3D human chondrocyte pellet cultures were used to study the effect of silencing OA risk gene fibronectin (*FN1*) [119]. In this study, it was shown that downregulation of *FN1* had detrimental effects on cartilage matrix deposition. These changes in cartilage matrix deposition can only be shown in 3D structures as no ECM is produced by 2D cell cultures, further stressing the advantage of using 3D model systems. In another study, lentiviral particle-mediated overexpression of *TNFRSF11B* in 3D human chondrocyte pellet cultures resulted in enhanced chondrocyte to osteoblast transition, thereby underscoring the role of *TNFRSF11B* in OA development [120]. Altogether, these studies show that 3D chondrocyte cell pellet are a suitable and valuable model for OA articular cartilage.

Multi-tissue culture systems

Given the tissue cross-talk, however, translation of strong OA risk genes towards their underlying mechanism is ideally performed in *in vitro* models that incorporate at least functional bone and cartilage tissue units. Therefore, human osteochondral explants might be an alternative. Osteochondral explants are directly derived from patient material and the main advantage is that cells maintain their natural aged 3D environment [121]. Houtman and colleagues explored the response of osteochondral explants upon exposure to IL1-β, triiodothyronine (T3), and 65% mechanical strain, and confirmed suitability of osteochondral explants as OA models for inflammation, hypertrophy, and posttraumatic OA, respectively [122]. Subsequently, the posttraumatic OA model was used to study potential pharmacological OA treatment with deiodinase inhibitor iopanoic acid (IOP), an FDA approved medication [123]. OA susceptibility gene *DIO2* encodes Iodothyronine deiodinase type 2 enzyme (D2), which is known to convert thyroxine (T4) to T3, thereby inducing hypertrophy [40]. IOP is known to inhibit D2 activity and therefore IOP was hypothesized to be a potential OA treatment. Upon exposing osteochondral explants to 65% mechanical strain to induce posttraumatic OA, with and without IOP treatment, Houtman and colleagues showed that IOP treatment was able to prevent posttraumatic OA-related changes in articular cartilage [123]. Together, these studies show that osteochondral explants provide major advantages in studying potential disease modifying OA treatments using a reliable human biomimetic model and complying to the principle of reduction, refinement, and replacement of animal models. Yet, use of osteochondral explants limits scalability as collection of explants is dependent on patients undergoing joint replacement surgery. Moreover, long-term cultures of osteochondral explants might be challenging, as their properties change over time [112]. Finally, genetic manipulation such as upregulation or silencing of genes cannot be performed in osteochondral explants, limiting these models to study OA related perturbations and treatment options. Henceforth, more state-of-the-art model systems are needed that are based on microfluidic tissue-on-chip principles.

Lin and colleagues developed a microfluidic osteochondral system that consists of a chondrogenic and osteogenic microenvironment [124]. Human bone marrow derived stem cells (hBMSCs) were seeded in hydrogels in these two compartments and chondrogenesis and osteogenesis was induced. More recently, to overcome the limited availability of hBMSCs, the same system was used to create osteochondral tissues using induced pluripotent stem cells (iPSCs) [125]. These iPSCs were first differentiated towards induced mesenchymal stem cells (iMSC) and these iMSCs were seeded in hydrogels. Upon culturing these hydrogels for 28 days within the microfluidic chip, the two compartments showed a chondrogenic and osteogenic phenotype, respectively. Subsequently, joint inflammation was mimicked by exposing the chondrogenic compartment to IL1-β and this inflammation was then treated by addition of anti-

inflammatory drug Celecoxib. Even though this system represents an elegant manner to study disease mechanisms and response to disease modifying OA drugs, the use of hydrogels has some disadvantages. Hydrogels require crosslinking methods, such as temperature changes, UV exposure, or enzymatic crosslinking, to form a stable network [126]. These crosslinking methods often are known to negatively affect cells, adding an uncertainty to the model. Moreover, hydrogels still fail to accurately mimic the 3D joint environment and reoccurring problems using hydrogels are formation of matrix islands and limited cell proliferation within hydrogels, which occur because of the elastic nature of the material [127]. Furthermore, tissue damage cannot be studied using hydrogels. Consequently, there are still shortcomings to bridge towards development of osteochondral constructs-on-a-chip consisting of biological ECM instead of hydrogels.

Outline of this thesis

In this thesis, we tried to make a step forward in transition from bench-to-bedside in OA by combining transcriptomic data from OA articular cartilage, subchondral bone, and plasma, with previously reported genetic studies, and OA disease modelling. In **chapter 2** and **chapter 3** we used RNA-sequencing data of subchondral bone to identify genes and lncRNAs that mark OA pathophysiology, by comparing macroscopically preserved and lesioned OA subchondral bone. Subsequently, we integrated these findings with previously reported findings on articular cartilage (partially of same patients) and genetics to identify potential druggable targets with possibly effects in both tissues.

In **chapter 4** and **chapter 5** we gained more insight in previously identified OA molecular endotypes in articular cartilage. To make OA molecular endotypes applicable to clinical practice, we first identified non-invasive biomarkers in plasma that allow stratification of patients based on their endotype before treatment (**chapter 4**). These OA molecular endotypes were identified based on articular cartilage, leaving the underlying subchondral bone unexplored. Therefore, we used RNA-sequencing data of the underlying subchondral bone to characterize these OA molecular endotypes in bone by performing differential expression analysis between these endotypes (**chapter 5**).

To translate genetic findings towards OA drug development, functional investigation is necessary to unravel underlying biological mechanisms of how these OA risk genes affect articular cartilage and/or subchondral bone matrix deposition. As proof-of-concept, in **chapter 6** and **chapter 7** we functionally investigated *WWP2* and *IL11* in two different models of joint tissue. The effect of *WWP2* upregulation on cartilage matrix deposition was explored using 3D human chondrocyte pellet cultures (**chapter 6**), while the effects of hrIL11 on both articular cartilage and subchondral bone were explored using osteochondral explant cultures (**chapter 7**).

Finally, we developed a new *in vitro* biomimetic model system representing functional articular cartilage and subchondral bone to study OA-related perturbations and/or OA susceptibility genes (**chapter 8**). This osteochondral-unit-on-a-chip allows in depth investigations of underlying mechanisms of OA risk genes in both tissues.

References
1. Hunter, D.J., L. March, and M. Chew, *Osteoarthritis in 2020 and beyond: a Lancet Commission.* Lancet, 2020. **396**(10264): p. 1711-1712.
2. Safiri, S., et al., *Global, regional and national burden of osteoarthritis 1990-2017: a systematic analysis of the Global Burden of Disease Study 2017.* Annals of the Rheumatic Diseases, 2020. **79**(6): p. 819.
3. Loeser, R.F., et al., *Osteoarthritis: a disease of the joint as an organ.* Arthritis Rheum, 2012. **64**(6): p. 1697-707.
4. Marshall, M., et al., *Hand osteoarthritis: clinical phenotypes, molecular mechanisms and disease management.* Nature Reviews Rheumatology, 2018. **14**(11): p. 641-656.
5. Katz, J.N., K.R. Arant, and R.F. Loeser, *Diagnosis and Treatment of Hip and Knee Osteoarthritis: A Review.* JAMA, 2021. **325**(6): p. 568-578.
6. Litwic, A., et al., *Epidemiology and burden of osteoarthritis.* Br Med Bull, 2013. **105**: p. 185-99.
7. Woolf, A.D., J. Erwin, and L. March, *The need to address the burden of musculoskeletal conditions.* Best Pract Res Clin Rheumatol, 2012. **26**(2): p. 183-224.
8. Johnson, V.L. and D.J. Hunter, *The epidemiology of osteoarthritis.* Best Practice & Research Clinical Rheumatology, 2014. **28**(1): p. 5-15.
9. Palazzo, C., et al., *Risk factors and burden of osteoarthritis.* Annals of Physical and Rehabilitation Medicine, 2016. **59**(3): p. 134-138.
10. Spector, T.D. and A.J. MacGregor, *Risk factors for osteoarthritis: genetics11Supported by Procter & Gamble Pharmaceuticals, Mason, OH.* Osteoarthritis and Cartilage, 2004. **12**: p. 39-44.
11. Mackie, E.J., et al., *Endochondral ossification: How cartilage is converted into bone in the developing skeleton.* The International Journal of Biochemistry & Cell Biology, 2008. **40**(1): p. 46-62.
12. Berendsen, A.D. and B.R. Olsen, *Bone development.* Bone, 2015. **80**: p. 14-18.
13. Sophia Fox, A.J., A. Bedi, and S.A. Rodeo, *The basic science of articular cartilage: structure, composition, and function.* Sports health, 2009. **1**(6): p. 461-468.
14. Bhosale, A.M. and J.B. Richardson, *Articular cartilage: structure, injuries and review of management.* British Medical Bulletin, 2008. **87**(1): p. 77-95.
15. van der Kraan, P.M. and W.B. van den Berg, *Chondrocyte hypertrophy and osteoarthritis: role in initiation and progression of cartilage degeneration?* Osteoarthritis and Cartilage, 2012. **20**(3): p. 223-232.
16. Dreier, R., *Hypertrophic differentiation of chondrocytes in osteoarthritis: the developmental aspect of degenerative joint disorders.* Arthritis Res Ther, 2010. **12**(5): p. 216.
17. Goldring, M.B. and K.B. Marcu, *Cartilage homeostasis in health and rheumatic diseases.* Arthritis Research & Therapy, 2009. **11**(3): p. 224.
18. Goldring, M.B. and S.R. Goldring, *Osteoarthritis.* J Cell Physiol, 2007. **213**(3): p. 626-34.
19. Xiao, Z.F., et al., *Cartilage degradation in osteoarthritis: A process of osteochondral remodeling resembles the endochondral ossification in growth plate?* Med Hypotheses, 2018. **121**: p. 183-187.
20. Li, G., et al., *Subchondral bone in osteoarthritis: insight into risk factors and microstructural changes.* Arthritis Research & Therapy, 2013. **15**(6): p. 223.
21. Karsdal, M.A., et al., *The coupling of bone and cartilage turnover in osteoarthritis: opportunities for bone antiresorptives and anabolics as potential treatments?* Ann Rheum Dis, 2014. **73**(2): p. 336-48.
22. Zhu, X., et al., *Subchondral Bone Remodeling: A Therapeutic Target for Osteoarthritis.* Frontiers in cell and developmental biology, 2021. **8**: p. 607764-607764.
23. Madry, H., C.N. van Dijk, and M. Mueller-Gerbl, *The basic science of the subchondral bone.* Knee Surgery, Sports Traumatology, Arthroscopy, 2010. **18**(4): p. 419-433.
24. Funck-Brentano, T. and M. Cohen-Solal, *Crosstalk between cartilage and bone: when bone cytokines matter.* Cytokine Growth Factor Rev, 2011. **22**(2): p. 91-7.
25. Funck-Brentano, T. and M. Cohen-Solal, *Subchondral bone and osteoarthritis.* Curr Opin Rheumatol, 2015. **27**(4): p. 420-6.
26. Goldring, M.B. and S.R. Goldring, *Articular cartilage and subchondral bone in the pathogenesis of osteoarthritis.* Ann N Y Acad Sci, 2010. **1192**: p. 230-7.
27. Goldring, S.R. and M.B. Goldring, *Changes in the osteochondral unit during osteoarthritis: structure, function and cartilage-bone crosstalk.* Nat Rev Rheumatol, 2016. **12**(11): p. 632-644.
28. Boer, C.G., et al., *Deciphering osteoarthritis genetics across 826,690 individuals from 9 populations.* Cell, 2021.
29. Styrkarsdottir, U., et al., *Whole-genome sequencing identifies rare genotypes in COMP and CHADL associated with high risk of hip osteoarthritis.* Nat Genet, 2017. **49**(5): p. 801-805.
30. Zengini, E., et al., *Genome-wide analyses using UK Biobank data provide insights into the genetic architecture of osteoarthritis.* Nat Genet, 2018. **50**(4): p. 549-558.
31. Styrkarsdottir, U., et al., *Meta-analysis of Icelandic and UK data sets identifies missense variants in SMO, IL11, COL11A1 and 13 more new loci associated with osteoarthritis.* Nat Genet, 2018. **50**(12): p. 1681-1687.
32. Tachmazidou, I., et al., *Identification of new therapeutic targets for osteoarthritis through genome-wide analyses of UK Biobank data.* Nat Genet, 2019. **51**(2): p. 230-236.
33. Zeggini, E., et al., *Identification of new susceptibility loci for osteoarthritis (arcOGEN): a genome-wide association study.* Lancet, 2012. **380**(9844): p. 815-23.
34. Uffelmann, E., et al., *Genome-wide association studies.* Nature Reviews Methods Primers, 2021. **1**(1): p. 59.
35. Aubourg, G., et al., *Genetics of osteoarthritis.* Osteoarthritis and Cartilage, 2021.
36. Kespohl, B., et al., *The cytokine interleukin-11 crucially links bone formation, remodeling and resorption.* Cytokine & Growth Factor Reviews, 2021. **60**: p. 18-27.

37. Valdes, A.M., et al., *Genetic variation in the SMAD3 gene is associated with hip and knee osteoarthritis.* Arthritis Rheum, 2010. **62**(8): p. 2347-52.
38. *The Genotype-Tissue Expression (GTEx) project.* Nat Genet, 2013. **45**(6): p. 580-5.
39. Yang, X., et al., *TGF-beta/Smad3 signals repress chondrocyte hypertrophic differentiation and are required for maintaining articular cartilage.* J Cell Biol, 2001. **153**(1): p. 35-46.
40. Meulenbelt, I., et al., *Identification of DIO2 as a new susceptibility locus for symptomatic osteoarthritis.* Human Molecular Genetics, 2008. **17**(12): p. 1867-1875.
41. Bomer, N., et al., *Underlying molecular mechanisms of DIO2 susceptibility in symptomatic osteoarthritis.* Ann Rheum Dis, 2015. **74**(8): p. 1571-9.
42. den Hollander, W., et al., *Annotating Transcriptional Effects of Genetic Variants in Disease-Relevant Tissue: Transcriptome-Wide Allelic Imbalance in Osteoarthritic Cartilage.* Arthritis Rheumatol, 2019. **71**(4): p. 561-570.
43. Hasegawa, M., T. Yoshida, and A. Sudo, *Tenascin-C in Osteoarthritis and Rheumatoid Arthritis.* Frontiers in Immunology, 2020. **11**.
44. Meng, W., et al., *Genome-wide association study of knee pain identifies associations with GDF5 and COL27A1 in UK Biobank.* Commun Biol, 2019. **2**: p. 321.
45. Hjorten, R., et al., *Type XXVII collagen at the transition of cartilage to bone during skeletogenesis.* Bone, 2007. **41**(4): p. 535-42.
46. Evangelou, E., et al., *Large-scale analysis of association between GDF5 and FRZB variants and osteoarthritis of the hip, knee, and hand.* Arthritis Rheum, 2009. **60**(6): p. 1710-21.
47. Chapman, K., et al., *A meta-analysis of European and Asian cohorts reveals a global role of a functional SNP in the 5' UTR of GDF5 with osteoarthritis susceptibility.* Hum Mol Genet, 2008. **17**(10): p. 1497-504.
48. Kania, K., et al., *Regulation of Gdf5 expression in joint remodelling, repair and osteoarthritis.* Sci Rep, 2020. **10**(1): p. 157.
49. Nakamura, Y., et al., *Wwp2 is essential for palatogenesis mediated by the interaction between Sox9 and mediator subunit 25.* Nat Commun, 2011. **2**: p. 251.
50. Houtman, E., et al., *Characterization of dynamic changes in Matrix Gla Protein (MGP) gene expression as function of genetic risk alleles, osteoarthritis relevant stimuli, and the vitamin K inhibitor warfarin.* Osteoarthritis and Cartilage, 2021. **29**(8): p. 1193-1202.
51. den Hollander, W., et al., *Genome-wide association and functional studies identify a role for matrix Gla protein in osteoarthritis of the hand.* 2017. **76**(12): p. 2046-2053.
52. Misra, D., et al., *Matrix Gla protein polymorphism, but not concentrations, is associated with radiographic hand osteoarthritis.* The Journal of rheumatology, 2011. **38**(9): p. 1960-1965.
53. Usmani, S.E., et al., Context-specific protection of TGFα null mice from osteoarthritis. Sci Rep, 2016. 6: p. 30434.
54. Usmani, S.E., et al., Transforming growth factor alpha controls the transition from hypertrophic cartilage to bone during endochondral bone growth. Bone, 2012. 51(1): p. 131-41.
55. Styrkarsdottir, U., et al., Severe osteoarthritis of the hand associates with common variants within the ALDH1A2 gene and with rare variants at 1p31. Nat Genet, 2014. 46(5): p. 498-502.
56. Hafez, A., et al., Col11a1 Regulates Bone Microarchitecture during Embryonic Development. J Dev Biol, 2015. 3(4): p. 158-176.
57. Loughlin, J., et al., Functional variants within the secreted frizzled-related protein 3 gene are associated with hip osteoarthritis in females. Proc Natl Acad Sci U S A, 2004. 101(26): p. 9757-62.
58. Leijten, J.C., et al., GREM1, FRZB and DKK1 mRNA levels correlate with osteoarthritis and are regulated by osteoarthritis-associated factors. Arthritis Res Ther, 2013. 15(5): p. R126.
59. Lories, R.J., et al., Articular cartilage and biomechanical properties of the long bones in Frzb-knockout mice. Arthritis Rheum, 2007. 56(12): p. 4095-103.
60. Enomoto-Iwamoto, M., et al., The Wnt antagonist Frzb-1 regulates chondrocyte maturation and long bone development during limb skeletogenesis. Dev Biol, 2002. 251(1): p. 142-56.
61. Ramos, Y.F., et al., Genes involved in the osteoarthritis process identified through genome wide expression analysis in articular cartilage; the RAAK study. PLoS One, 2014. 9(7): p. e103056.
62. Chou, C.H., et al., Genome-wide expression profiles of subchondral bone in osteoarthritis. Arthritis Res Ther, 2013. 15(6): p. R190.
63. Coutinho de Almeida, R., et al., RNA sequencing data integration reveals an miRNA interactome of osteoarthritis cartilage. Ann Rheum Dis, 2019. 78(2): p. 270-277.
64. Katsoula, G., et al., A molecular map of long non-coding RNA expression, isoform switching and alternative splicing in osteoarthritis. Human Molecular Genetics, 2022: p. ddac017.
65. Fellows, C.R., C. Matta, and A. Mobasheri, Applying Proteomics to Study Crosstalk at the Cartilage-Subchondral Bone Interface in Osteoarthritis: Current Status and Future Directions. EBioMedicine, 2016. 11: p. 2-4.
66. Pan, J., et al., Elevated cross-talk between subchondral bone and cartilage in osteoarthritic joints. Bone, 2012. 51(2): p. 212-7.
67. Kuttapitiya, A., et al., Microarray analysis of bone marrow lesions in osteoarthritis demonstrates upregulation of genes implicated in osteochondral turnover, neurogenesis and inflammation. Ann Rheum Dis, 2017. 76(10): p. 1764-1773.
68. Dunn, S.L., et al., Gene expression changes in damaged osteoarthritic cartilage identify a signature of non-chondrogenic and mechanical responses. Osteoarthritis Cartilage, 2016. 24(8): p. 1431-40.
69. Li, H., et al., Whole-transcriptome sequencing of knee joint cartilage from osteoarthritis patients. Bone Joint Res, 2019. 8(7): p. 290-303.
70. Yuan, C., et al., Classification of four distinct osteoarthritis subtypes with a knee joint tissue transcriptome atlas. Bone Research, 2020. 8(1): p. 38.
71. Soul, J., et al., Stratification of knee osteoarthritis: two major patient subgroups identified by genome-wide expression analysis of articular cartilage. Ann Rheum Dis, 2018. 77(3): p. 423.
72. Coutinho de Almeida, R., et al., Identification and characterization of two consistent osteoarthritis subtypes by transcriptome and clinical data integration. Rheumatology (Oxford), 2020.
73. Raine, E.V., et al., Allelic expression analysis of the osteoarthritis susceptibility gene COL11A1 in human joint tissues. BMC Musculoskelet Disord, 2013. 14: p. 85.
74. Gee, F., et al., Allelic expression analysis of the osteoarthritis susceptibility locus that maps to chromosome 3p21 reveals cis-acting eQTLs at GNL3 and SPCS1. BMC Med Genet, 2014. 15: p. 53.
75. Coutinho de Almeida, R., et al., Allelic expression imbalance in articular cartilage and subchondral bone refined genome-wide association signals in osteoarthritis. medRxiv, 2022: p. 2022.04.07.22273552.
76. Loughlin, J., Translating osteoarthritis genetics research: challenging times ahead. Trends in Molecular Medicine, 2022. 28(3): p. 176-182.
77. Ramos, Y.F.M. and I. Meulenbelt, Implementation of Functional Genomics for Bench-to-Bedside Transition in

1

Osteoarthritis. Current Rheumatology Reports, 2015. 17(8): p. 53.

78. Bomer, N., et al., Translating genomics into mechanisms of disease: Osteoarthritis. Best Pract Res Clin Rheumatol, 2015. 29(6): p. 683-91.

79. Coutinho de Almeida, R., Y.F.M. Ramos, and I. Meulenbelt, Involvement of epigenetics in osteoarthritis. Best Pract Res Clin Rheumatol, 2017. 31(5): p. 634-648.

80. Ramos, Y.F. and I. Meulenbelt, The role of epigenetics in osteoarthritis: current perspective. Curr Opin Rheumatol, 2017. 29(1): p. 119-129.

81. den Hollander, W. and I. Meulenbelt, DNA Methylation in Osteoarthritis. Curr Genomics, 2015. 16(6): p. 419-26.

82. Letarouilly, J.-G., O. Broux, and A. Clabaut, New insights into the epigenetics of osteoporosis. Genomics, 2019. 111(4): p. 793-798.

83. Park, J., et al., The role of histone modifications: from neurodevelopment to neurodiseases. Signal Transduction and Targeted Therapy, 2022. 7(1): p. 217.

84. Bartel, D.P., MicroRNAs: genomics, biogenesis, mechanism, and function. Cell, 2004. 116(2): p. 281-97.

85. Swingler, T.E., et al., The function of microRNAs in cartilage and osteoarthritis. Clin Exp Rheumatol, 2019. 37 Suppl 120(5): p. 40-47.

86. Le, L.T.T., T.E. Swingler, and I.M. Clark, Review: The Role of MicroRNAs in Osteoarthritis and Chondrogenesis. Arthritis & Rheumatism, 2013. 65(8): p. 1963-1974.

87. Iliopoulos, D., et al., Integrative microRNA and proteomic approaches identify novel osteoarthritis genes and their collaborative metabolic and inflammatory networks. PLoS One, 2008. 3(11): p. e3740.

88. Jones, S.W., et al., The identification of differentially expressed microRNA in osteoarthritic tissue that modulate the production of TNF-α and MMP13. Osteoarthritis and Cartilage, 2009. 17(4): p. 464-472.

89. Yang, J., et al., MiR-140 is co-expressed with Wwp2-C transcript and activated by Sox9 to target Sp1 in maintaining the chondrocyte proliferation. FEBS Lett, 2011. 585(19): p. 2992-7.

90. Endisha, H., et al., The complex landscape of microRNAs in articular cartilage: biology, pathology, and therapeutic targets. JCI Insight, 2018. 3(17).

91. Nakamura, Y., et al., Chondrocyte-specific microRNA-140 regulates endochondral bone development and targets Dnpep to modulate bone morphogenetic protein signaling. Mol Cell Biol, 2011. 31(14): p. 3019-28.

92. Rice, S.J., et al., Interplay between genetics and epigenetics in osteoarthritis. Nature Reviews Rheumatology, 2020. 16(5): p. 268-281.

93. Ghafouri-Fard, S., et al., The Emerging Role of Non-Coding RNAs in Osteoarthritis. Frontiers in Immunology, 2021. 12.

94. Marchese, F.P., I. Raimondi, and M. Huarte, The multidimensional mechanisms of long noncoding RNA function. Genome Biology, 2017. 18(1): p. 206.

95. Statello, L., et al., Gene regulation by long non-coding RNAs and its biological functions. Nature Reviews Molecular Cell Biology, 2021. 22(2): p. 96-118.

96. Morlando, M., M. Ballarino, and A. Fatica, Long Non-Coding RNAs: New Players in Hematopoiesis and Leukemia. Frontiers in medicine, 2015. 2: p. 23-23.

97. Quinn, J.J. and H.Y. Chang, Unique features of long non-coding RNA biogenesis and function. Nature Reviews Genetics, 2016. 17(1): p. 47-62.

98. Sun, H., et al., Emerging roles of long noncoding RNA in chondrogenesis, osteogenesis, and osteoarthritis. Am J Transl Res, 2019. 11(1): p. 16-30.

99. van Hoolwerff, M., et al., Elucidating Epigenetic Regulation by Identifying Functional cis-Acting Long Noncoding RNAs and Their Targets in Osteoarthritic Articular Cartilage. Arthritis Rheumatol, 2020. 72(11): p. 1845-1854.

100. Ajekigbe, B., et al., Identification of long non-coding RNAs expressed in knee and hip osteoarthritic cartilage. Osteoarthritis Cartilage, 2019. 27(4): p. 694-702.

101. Bernotiene, E., et al., Emerging Technologies and Platforms for the Immunodetection of Multiple Biochemical Markers in Osteoarthritis Research and Therapy. Frontiers in Medicine, 2020. 7.

102. Hunter, D.J., et al., Biomarkers for osteoarthritis: current position and steps towards further validation. Best practice & research. Clinical rheumatology, 2014. 28(1): p. 61-71.

103. Haraden, C.A., et al., Synovial fluid biomarkers associated with osteoarthritis severity reflect macrophage and neutrophil related inflammation. Arthritis Research & Therapy, 2019. 21(1): p. 146.

104. Bay-Jensen, A.C., et al., Blood and urine biomarkers in osteoarthritis – an update on cartilage associated type II collagen and aggrecan markers. Current Opinion in Rheumatology, 2022. 34(1).

105. Cheng, H., et al., C-Terminal Cross-Linked Telopeptides of Type II Collagen as Biomarker for Radiological Knee Osteoarthritis: A Meta-Analysis. Cartilage, 2020. 11(4): p. 512-520.

106. Meulenbelt, I., et al., Urinary CTX-II levels are associated with radiographic subtypes of osteoarthritis in hip, knee, hand, and facet joints in subject with familial osteoarthritis at multiple sites: the GARP study. Annals of the rheumatic diseases, 2006. 65(3): p. 360-365.

107. Arunrukthavon, P., et al., Can urinary CTX-II be a biomarker for knee osteoarthritis? Arthroplasty, 2020. 2(1): p. 6.

108. Ramos, Y.F.M., et al., Circulating MicroRNAs Highly Correlate to Expression of Cartilage Genes Potentially Reflecting OA Susceptibility-Towards Identification of Applicable Early OA Biomarkers. Biomolecules, 2021. 11(9): p. 1356.

109. Ntoumou, E., et al., Serum microRNA array analysis identifies miR-140-3p, miR-33b-3p and miR-671-3p as potential osteoarthritis biomarkers involved in metabolic processes. Clin Epigenetics, 2017. 9: p. 127.

110. Murata, K., et al., Plasma and synovial fluid microRNAs as potential biomarkers of rheumatoid arthritis and osteoarthritis. Arthritis Res Ther, 2010. 12(3): p. R86.

111. Alexander, P.G., et al., Three-dimensional osteogenic and chondrogenic systems to model osteochondral physiology and degenerative joint diseases. Exp Biol Med (Maywood), 2014. 239(9): p. 1080-95.

112. Piluso, S., et al., Mimicking the Articular Joint with In Vitro Models. Trends Biotechnol, 2019. 37(10): p. 1063-1077.

113. van Geffen, E.W., et al., IL37 dampens the IL1β-induced catabolic status of human OA chondrocytes. Rheumatology, 2017. 56(3): p. 351-361.

114. Carpintero-Fernandez, P., et al., Intercellular communication via gap junction channels between chondrocytes and bone cells. Biochimica et Biophysica Acta (BBA) - Biomembranes, 2018. 1860(12): p. 2499-2505.

115. Caron, M.M., et al., Redifferentiation of dedifferentiated human articular chondrocytes: comparison of 2D and 3D cultures. Osteoarthritis Cartilage, 2012. 20(10): p. 1170-8.

116. Otero, M., et al., Human chondrocyte cultures as models of cartilage-specific gene regulation. Methods Mol Biol, 2012. 806: p. 301-36.

117. Gerber, I., et al., Stimulatory effects of creatine on metabolic activity, differentiation and mineralization of primary osteoblast-like cells in monolayer and micromass cell cultures. Eur Cell Mater, 2005. 10: p. 8-22.

118. Bomer, N., et al., Neo-cartilage engineered from primary chondrocytes is epigenetically similar to autologous cartilage, in contrast to using mesenchymal stem cells. Osteoarthritis Cartilage, 2016. 24(8): p. 1423-30.

119. van Hoolwerff, M., et al., Identification and functional characterization of imbalanced osteoarthritis associated fibronectin splice variants. Rheumatology (Oxford), 2022.

120. Rodríguez Ruiz, A., et al., The role of TNFRSF11B in development of osteoarthritic cartilage. Rheumatology (Oxford), 2022. 61(2): p. 856-864.

121. Geurts, J., et al., Novel Ex Vivo Human Osteochondral Explant Model of Knee and Spine Osteoarthritis Enables Assessment of Inflammatory and Drug Treatment Responses. Int J Mol Sci, 2018. 19(5).

122. Houtman, E., et al., Human Osteochondral Explants: Reliable Biomimetic Models to Investigate Disease Mechanisms and Develop Personalized Treatments for Osteoarthritis. Rheumatology and Therapy, 2021. 8(1): p. 499-515.

123. Houtman, E., et al., Inhibiting thyroid activation in aged human explants prevents mechanical induced detrimental signalling by mitigating metabolic processes. Rheumatology, 2022.

124. Lin, H., et al., Stem cell-based microphysiological osteochondral system to model tissue response to interleukin-1β. Mol Pharm, 2014. 11(7): p. 2203-12.

125. Lin, Z., et al., Osteochondral Tissue Chip Derived From iPSCs: Modeling OA Pathologies and Testing Drugs. Front Bioeng Biotechnol, 2019. 7: p. 411.

126. Hu, W., et al., Advances in crosslinking strategies of biomedical hydrogels. Biomater Sci, 2019. 7(3): p. 843-855.

127. Lee, H.-p., et al., Mechanical confinement regulates cartilage matrix formation by chondrocytes. Nature Materials, 2017. 16(12): p. 1243-1251.

1
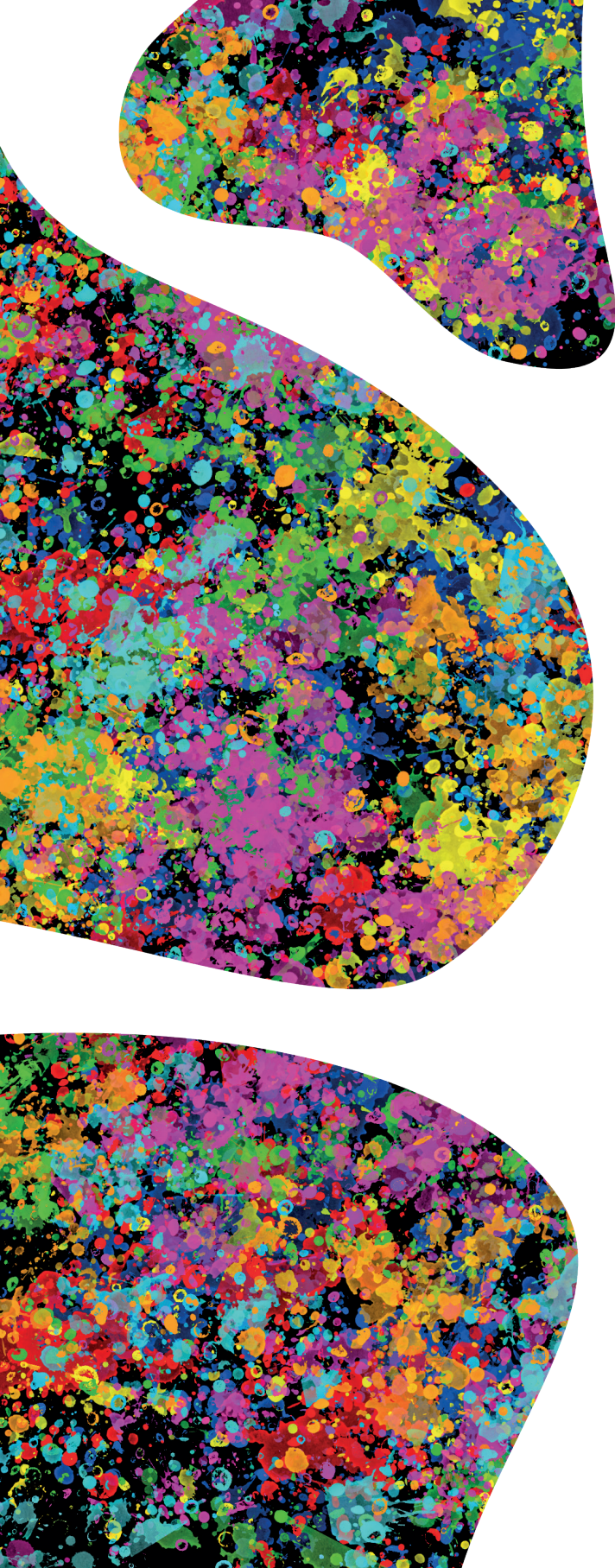
CHAPTER 2

RNA sequencing reveals interacting key determinants of osteoarthritis acting in subchondral bone and articular cartilage

Margo Tuerlings[1], Marcella van Hoolwerff[1], Evelyn Houtman[1], H. Eka D. Suchiman[1], Nico Lakenberg[1], Hailiang Mei[1], Enrike H.M.J. van der Linden[2], Rob G.H.H. Nelissen[2], Yolande F.M. Ramos[1], Rodrigo Coutinho de Almeida[1], Ingrid Meulenbelt[1]

[1] Dept. of Biomedical Data Sciences, Leiden University Medical Center, Leiden, The Netherlands.
[2] Dept. Orthopaedics Leiden University Medical Center, Leiden, The Netherlands.

Abstract

Objective: To identify key determinants of the interactive pathophysiologic processes in subchondral bone and cartilage in osteoarthritis (OA).

Methods: We performed RNA sequencing on macroscopically preserved and lesioned OA subchondral bone from patients in the Research Arthritis and Articular Cartilage study who underwent joint replacement surgery due to OA (n = 24 sample pairs: 6 hips and 18 knees). Unsupervised hierarchical clustering and differential expression analyses were conducted. Results were combined with data on previously identified differentially expressed genes in cartilage (partly overlapping samples) as well as data on recently identified OA risk genes.

Results: We identified 1569 genes significantly differentially expressed between lesioned and preserved subchondral bone, including *CNTNAP2* (fold change (FC)=2.4, false discovery rate (FDR)=3.36×10^{-5}) and *STMN2* (FC=9.6, FDR=3.36×10^{-3}). Among these 1569 genes, 305 were also differentially expressed, and with same direction of effects, in cartilage, including the recently recognized OA susceptibility genes *IL11* and *CHADL*. Upon differential expression analysis with stratification for joint site, we identified 509 genes exclusively differentially expressed in subchondral bone of the knee, including *KLF11* and *WNT4*. These genes that were differentially expressed exclusively in the knee were enriched for involvement in epigenetic processes, characterized by, e.g., *HIST1H3J* and *HIST1H3H*.

Conclusion: Among the most consistently differentially expressed genes with OA pathophysiology in both bone and cartilage were *IL11* and *CHADL*. As these genes were recently also identified as robust OA risk genes they classify as attractive druggable targets acting on two OA disease relevant tissues.

2

Introduction

Osteoarthritis (OA) represents multiple subtypes of degenerative joint diseases, characterized by progressive and irreversible degeneration of the articular cartilage and structural changes in the subchondral bone. Globally, OA is a highly prevalent and disabling disease that results in high social and economic burdens to society [1]. Yet, there is no proven therapy to prevent OA or slow down its progression. Development of OA is dependent on multiple factors, with both environmental and genetic components [2, 3]. To discover genes and underlying disease pathways, genetic investigations, such as large genome wide association studies, have been performed, identifying compelling OA risk single-nucleotide polymorphisms (SNPs) [4-6]. Functional follow-up studies involve exploring the expression patterns in disease-relevant tissues, behavior with pathophysiology, and/or expression quantitative trait locus (eQTL) or cis-eQTL analysis. To date, major efforts have been made to characterize pathophysiological processes of OA in articular cartilage. However, only few studies have focused on OA pathophysiologic processes in the underlying bone [7, 8].

In recent decades, there has been accumulating evidence that subchondral bone contributes to both onset and progression of OA [9-12]. In healthy bone, there is a balanced process between bone resorption and bone deposition, as a consequence of dynamic adaptation to mechanical load. In OA this balance is disturbed, which results in changes in the architecture of the subchondral trabecular bone, increased thickness of the subchondral bone plate, formation of new bony structures, called osteophytes, at the joint margins, and development of subchondral bone cysts [2, 13, 14]. In addition, studies have shown an association between the bone mineral density and development of OA, which suggest that subchondral bone is involved in the early stages of OA [13, 15]. This was also suggested by studies regarding subchondral bone marrow lesions, showing these to be very early markers of OA [8, 16].

In contrast to cartilage and despite its relevance, only a limited number of studies have focused on the characterization of OA disease processes at the gene expression level in subchondral bone. Chou et al. [7] performed whole-genome expression profiling of non-OA and OA subchondral bone using microarray analysis, which led to identification of genes involved in pathways such as lipid metabolism and mineral metabolism. Kuttapitiya et al. [8] used microarray analysis to identify genes involved in bone remodeling, pain sensitization, and matrix turnover being differentially expressed between OA bone marrow lesioned tissue and controls. However, both of these studies included samples from the knee only.

In the present study, we explored RNA sequencing data on preserved and lesioned OA

subchondral bone to identify genes that change with progression of OA. The samples used were obtained from the joints of patients in the Research Arthritis and Articular Cartilage (RAAK) study who underwent total joint replacement surgery due to OA. In total, we compared paired subchondral bone samples (preserved and lesioned) from 24 OA patients from whom preserved and lesioned cartilage was also collected. The results presented here contribute to further understanding of the ongoing OA process in the subchondral bone and provide give insight into the pathophysiology of the disease in bone relative to cartilage.

Methods

Sample description

The current investigation includes 26 participants from the RAAK study who underwent joint replacement surgery due to OA. Macroscopically preserved and lesioned OA subchondral bone was collected from the joints of these patients. Of note, classification of OA subchondral bone as preserved or lesioned was based on classification of its overlying cartilage as preserved or lesioned, as described previously [17]. The results reported here were compared to the results of our earlier study of macroscopically preserved and lesioned OA articular cartilage from 35 patients from the RAAK study [18]. Fourteen of these 35 patients were included in the present study, as samples of both preserved and lesioned subchondral bone and preserved and lesioned articular cartilage was available. The sample size for the current study was determined using the R package ssize.fdr v1.2 [19], with parameters based on our previous similar analysis of articular cartilage [18] and a desired power of 0.8 (Supplementary Figure 1). Since the parameters were based on cartilage, whereas bone is known to be more heterogeneous, we decided to include an excess of samples. The samples were either randomly selected or selected based on their overlap with the cartilage data. Informed consent was obtained from all participants in the RAAK study, and ethical approval for the RAAK study was granted by the medical ethics committee of Leiden University Medical Center (P08.239/P19.013).

RNA sequencing

RNA was isolated from subchondral bone using an RNeasy Mini Kit (Qiagen). Paired-end 2×100 bp RNA-sequencing (Illumina TruSeq RNA Library Prep Kit, Illumina HiSeq2000 and Illumina HiSeq4000) was performed. Strand-specific RNA-seq libraries were generated, which yielded a mean of 20 million reads per sample. Data from both Illumina platforms were integrated and analyzed with the same in-house pipeline. RNA-seq reads were aligned using GSNAP [20] against GRCh38, with default parameters. Read abundances per sample was estimated using HTSeq count v0.11.1 [21]. Only uniquely mapping reads were used for estimating expression. The quality of the raw

reads for RNA-seq was checked using MultiQC v1.7. [22] The adaptors were clipped using Cutadapt v1.1 [23], applying default settings (min overlap 3, min length). To identify outliers, principal component analysis (PCA) and hierarchical clustering on the samples were applied, and one extreme outlier was identified. A sensitivity analysis was performed, which showed that the outlier had a large effect on the results in the overall data set. Based on this, the outlier was removed from the data set. There was one sample without paired data, which was also removed from the data set. After removal of these samples, only 24 participants were included for further analysis. The RNA-seq data are deposited at the European Genome-Phenome Archive (accession number: EGAS00001004476).

Cluster analysis

Prior to the cluster analysis, variance stabilizing transformation was performed on the data and 1000 genes were selected based on the highest coefficient of variation [24, 25]. To identify the optimal number of clusters in the unsupervised hierarchical clustering the silhouette width score approach was used, with a higher average silhouette width score indicating a more optimal number of clusters [26]. Details on the cluster analyses and the stability of cluster solutions have been reported previously [25].

Differential expression analysis and pathway enrichment

Differential expression analysis was performed on paired lesioned and preserved subchondral bone samples, using the DESeq2 R package, version 1.24.0 [27]. A general linear model assuming a negative binomial distribution was applied, followed by a paired Wald-test between lesioned and preserved OA samples, with the preserved samples set as a reference. The Benjamini-Hochberg method was used to correct for multiple testing, as indicated by the false discovery rate (FDR), with a significance cutoff value of 0.05. Gene enrichment was performed using the online functional annotation tool DAVID, selecting for the gene ontology terms Biological Processes (GOTERM_BP_DIRECT), Cellular Component (GOTERM_CC_DIRECT) and Molecular Function (GOTERM_MF_DIRECT) and for the Reactome Homo Sapiens (R-HAS) and the KEGG pathways [28]. Moreover, the protein-protein interactions were analyzed using the online tool STRING, version 11.0 [29]. An analysis summary scheme is shown in **Figure 1**.

RT-qPCR validation

Complementary DNA (cDNA) synthesis was performed using Transcriptor First Strand cDNA Synthesis Kit (Roche), using 400 ng of RNA. We used RT-qPCR to quantitatively determine gene expression of *FRZB, CNTNAP2, STMN2, CHRDL2, POSTN*, and *ASPN*. Relative gene expression was evaluated using -ΔCT values, using *GAPDH* and *SDHA* as internal controls. Generalized estimating equation (GEE) analysis was performed to

calculate the significance of differences between the lesioned and preserved samples.

Comparison subchondral bone and articular cartilage
The 1569 genes that were significantly differentially expressed (by FDR) between preserved and lesioned OA subchondral bone (24 paired samples) reported here were compared to the 2387 genes that were significantly differentially expressed between preserved and lesioned OA articular cartilage (35 paired samples) as determined in our earlier study [18]. Genes that were significantly differentially expressed in both tissues were selected, and the directions of effect were explored.
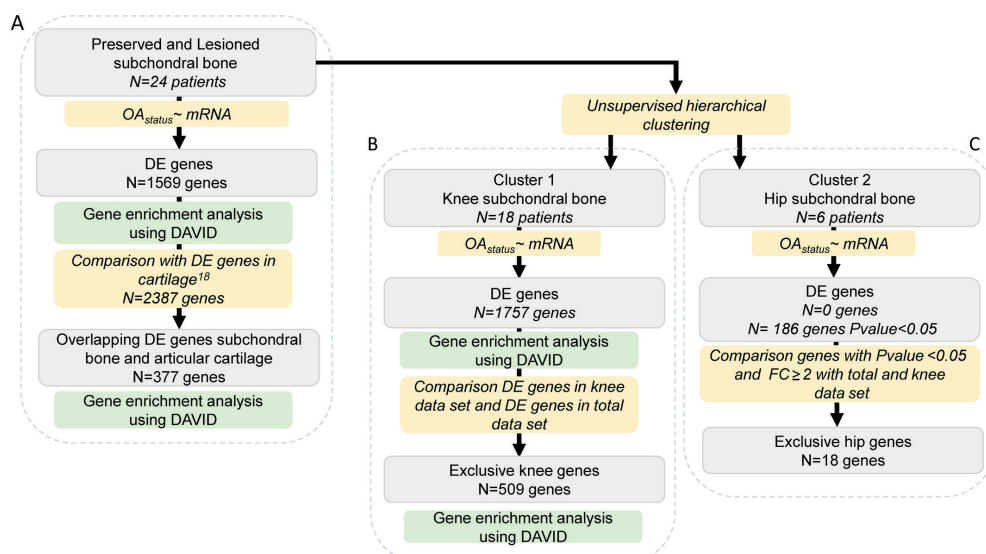
Figure 1 – Overview of applied strategy.
Number of genes represents the FDR-significant differentially expressed (DE) genes, except for the hip genes.

Results

Sample characteristics

To characterize the pathophysiologic process in subchondral bone with ongoing OA, we performed RNA-seq on macroscopically preserved and lesioned OA subchondral bone samples from patients in the RAAK study who underwent joint replacement surgery due to OA. The RNA-seq was performed on 24 paired samples (6 from hips and 18 from knees, **Supplementary Table 1**).

Prior to the differential expression analysis, we tested possible contamination of cartilage tissue in the subchondral bone samples. We used RNA-seq data on both tissue types from the same joint and evaluated the relative difference in expression levels of three cartilage-specific genes (*COL2A1, COMP, CRTAC1*) and three bone-specific genes (*COL1A1, SPP1, BGLAP*), as described previously [30]. As shown in **Supplementary Table 2**, we observed relatively low levels of cartilage-specific genes and high levels

of bone-specific genes in the subchondral bone data set under study, suggesting no-to-minimal cross-contamination. Next, we explored whether the expression pattern in subchondral bone was associated with any baseline characteristics of the patients (**Supplementary Table 1**), by performing unsupervised hierarchical clustering. To include the most informative genes in the cluster analysis, 1000 genes were selected based on the highest coefficient of variation in the total data set (preserved and lesioned, N=24 pairs). As shown in **Figure 2** and **Supplementary Figure 2**), we identified two clusters. These appeared to be based on joint site, indicating an inherent difference between hip and knee subchondral bone.
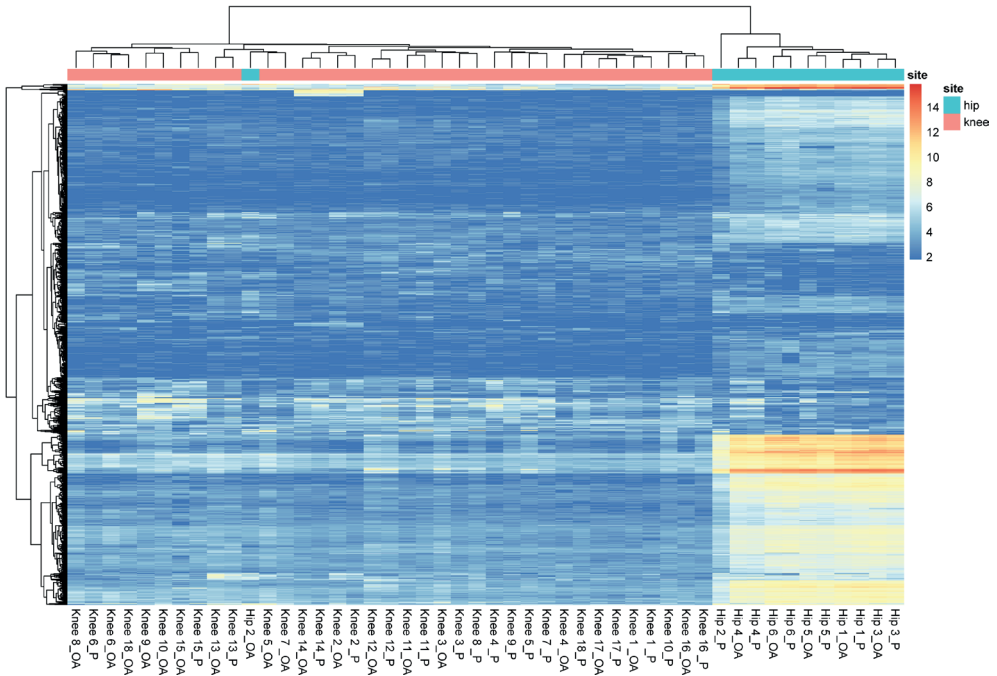
Figure 2 – Cluster analysis based on the 1000 genes selected for their highest COV.
Two clusters were identified based on knee samples (left) and hip samples (right).

Differential expression analysis and pathway enrichment

We first determined the genes that were consistently differentially expressed between preserved and lesioned OA subchondral bone in the overall data set, to explore the most consistent OA pathways (**Figure 1A**). Upon differential expression analysis in the 24 samples, we identified 1569 genes that were genome-wide significantly differentially expressed between lesioned and preserved OA subchondral bone tissue. Of these differentially expressed genes, 750 were up-regulated and 819 were down-regulated (**Figure 3** and **Supplementary Table 3**). The most significantly down-regulated gene was *FRZB* (FC=0.53, FDR=3.99x10^{-7}), encoding the frizzled-related protein, which is

a well-known OA gene showing consistently lower expression in lesioned relative to preserved OA articular cartilage [17, 18]. The most significantly up-regulated gene was *CNTNAP2* (FC=2.42, FDR=3.36×10^{-5}), encoding the contactin-associated protein-like 2 protein (CASPR2). Among the 1569 differentially expressed genes, 53 genes had an absolute FC of ≥2 (35 up-regulated and 18 down-regulated). The most highly up-regulated gene was *STMN2* (FC=9.56, FDR=2.36×10^{-3}), encoding stathmin 2, while the most down-regulated gene was *CHRDL2* (FC=0.14, FDR=1.20×10^{-4}), encoding chordin-like protein 2.

Next, we explored whether the 1569 significant differentially expressed genes were enriched in relation to particular pathways or processes, using DAVID. The results demonstrated significantly enriched Gene Ontology (GO) terms regarding processes involved in translational and posttranslational processes, such as signal recognition particle-dependent co-translational protein targeting to membrane (GO:0006614, 33 genes, FDR=4.27×10^{-7}) and translational initiation (GO:0006413, 36 genes, FDR=1.95×10^{-4}). These processes were both mainly characterized by ribosomal proteins such as *RPS24*, *RPS4X* and *RPS18* (**Supplementary Table 4)**. Gene enrichment analysis of the genes selected for the highest FC (FC≥2, N=53 genes), showed significant enrichment of processes regarding the extracellular matrix (GO:0005615, 16 genes, FDR=1.19×10^{-5}), characterized by the up-regulation of *WNT16* (FC=4.35, FDR= 6.88×10^{-4}) , *CRLF1* (FC=2.32, FDR=2.86×10^{-2}) and *OGN* (FC=3.43, FDR= 4.62×10^{-3}),
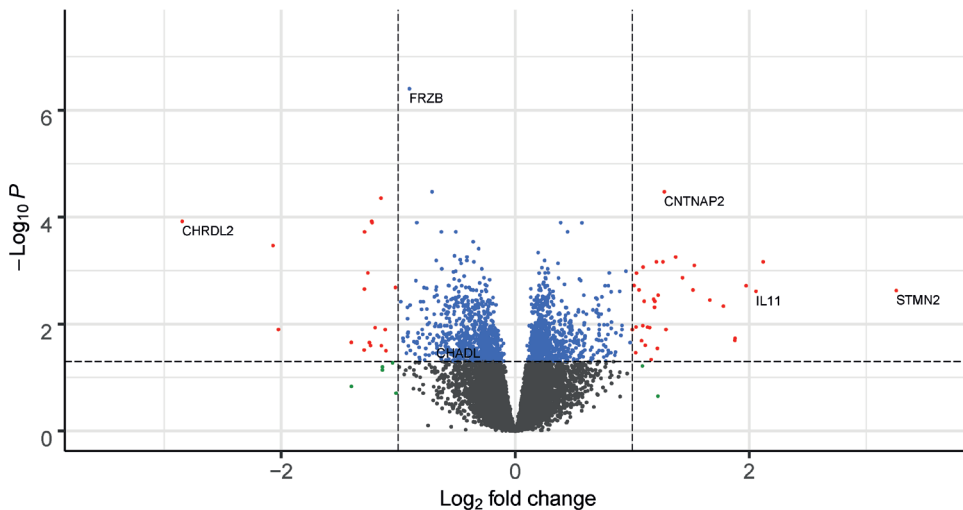
Figure 3 – Volcano plot of differential expressed genes in the subchondral bone.
The dots in the figure represent genes expressed in bone. Blue dots represent genes that are significantly differentially expressed, red dots represent genes that are significantly differentially expressed and have an absolute fold change of 2 or higher, and green dots represent the genes with an absolute fold change of two or higher that are not significantly differentially expressed.

and the proteinaceous extracellular matrix (GO:0005578, 7 genes, FDR=4.50x10^{-2}), characterized by up-regulation of *POSTN* (FC=2.04, FDR=3.44x10^{-2}), *ASPN* (FC=3.17, FDR=3.56x10^{-3}) and *CTHRC1* (FC=2.15, FDR=3.75x10^{-3}) (**Supplementary Table 5**). To explore interactions between proteins encoded by the 53 differentially expressed genes with an FC of ≥2, we used the online tool STRING. We identified significant enrichment for protein-protein interactions (PPI) among 22 of 44 proteins (P=3.20x10^{-9}, **Figure 4**).

Comparison subchondral bone and articular cartilage

To investigate interacting OA pathophysiologic processes in subchondral bone and articular cartilage, we compared differentially expressed genes identified in bone with our previously reported results on differentially expressed genes in articular cartilage [18] (**Figure 1A**, 24 sample pairs from bone and 35 from cartilage; 14 patients with available sample pairs from both bone and cartilage). This analysis revealed 337 genes that were differentially expressed in both subchondral bone and articular cartilage (**Supplementary Figure 3**). Of these 337 overlapping genes, the majority (305 genes) showed similar directions of effect in cartilage and bone (**Supplementary Table 6**), while 32 genes showed opposite directions of effect between the two tissue types
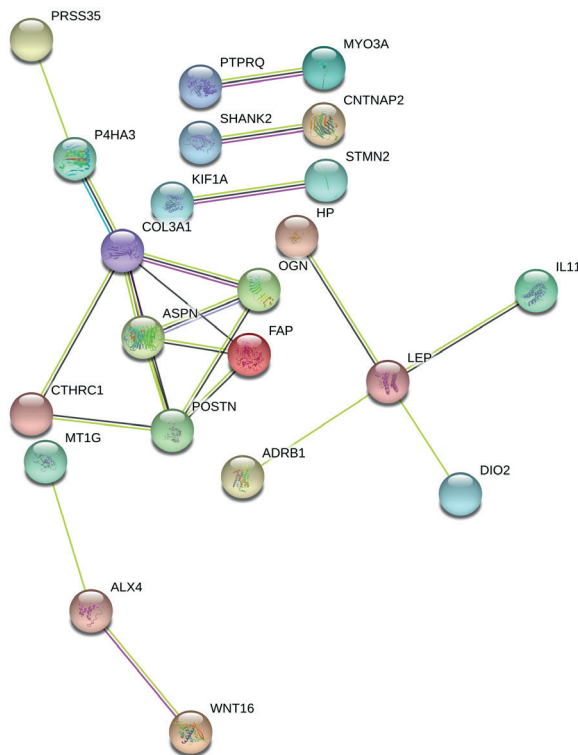
Figure 4 – Protein-protein interaction network of proteins encoded by genes that show an absolute fold change of 2 or higher (N=53 genes) created by STRING.

(**Supplementary Table 7**). *ALX4,* encoding aristaless-like homeobox 4, was notable gene among the genes showing opposite directions of effects. *ALX4* is known to be involved in osteogenesis and was one of the most highly up-regulated genes in bone (**Table 1**). Among the 305 genes showing similar direction of effects, 14 were among the top 25 genes with the highest FC in both tissues, such as *WNT16*, *IL11*, *CRLF1* and *FRZB* (**Table 1**).

To explore common underlying pathways in subchondral bone and articular cartilage, we performed gene enrichment analysis with the 305 genes that showed similar directions of effect in cartilage and bone. We found significant enrichment for the GO terms extracellular region (GO:0005576, 36 genes, FDR= 4.56×10^{-3}), characterized by the expression of, for example, *COL6A3*, *FGF14* and *GDF6*, proteinaceous extracellular matrix (GO:0005578, 17 genes, FDR= 7.98×10^{-3}), characterized by the expression of, for example, *CHADL*, *ADAMTS17* and *SPOCK3,* and extracellular space (GO:0005615, 37 genes, FDR= 4.42×10^{-3}), characterized by the expression of, for example, *CD63*, *SPP1* and *RELN* (**Supplementary Table 8**).

Differential expression analysis stratified for joint site
Since hip and knee samples showed different gene expression profiles in the cluster analysis (**Figure 2**), we repeated the differential expression analysis with stratification by joint site to explore whether we could identify exclusive OA pathways that occur in subchondral bone of knees only or hips only. Differential expression analysis of the 18 knee sample pairs revealed 1757 genes that were significantly differentially expressed (**Figure 1B**), of which 902 genes were up-regulated and 855 genes were down-regulated in lesioned compared to preserved OA subchondral bone (**Supplementary Table 9**). Moreover, we identified 509 genes that were differentially expressed exclusively in the knee (**Supplementary Table 10**); i.e. these genes were not differentially expressed in analysis of the total data set (**Supplementary Table 3**) or the hip data set (**Supplementary Table 12**). Enrichment analysis of these genes that were differentially expressed exclusively in the knee showed significant enrichment for processes involved in epigenetic regulation, such as nucleosome (GO:0000786, 20 genes, 1.81×10^{-9}), DNA methylation (R-HSA-5334118, 15 genes, 2.48×10^{-6}) and regulation of gene silencing (GO:0060968, 6 genes, 1.90×10^{-2}), all characterized by members of H3 histone family, such as *HIST1H3J* and *HIST1H3H* (**Supplementary Table 11).**

Differential expression analysis using only the hip samples (6 pairs) did not reveal any genes that were significantly differentially expressed by the FDR method when comparing preserved and lesioned subchondral bone (**Figure 1C**). However, among the genes with a P-value <0.05 and an absolute FC ≥2 (**Supplementary Table 12),** 18

Table 1 – Genes that belonged to the top 25 genes based on the highest absolute foldchange in either bone or cartilage.
Of these genes, 14 appear to be in the top 25 highest FC genes in both tissues.

Ensemble ID	Gene name	Subchondral bone		Articular Cartilage		Top 25 absolute foldchange	
		FC	FDR	FC	FDR	SB	AC
ENSG00000002745	WNT16	4,35	$6,88 \times 10^{-4}$	8,48	$1,10 \times 10^{-13}$	x	x
ENSG00000095752	IL11	4,16	$2,44 \times 10^{-3}$	22,8	$1,53 \times 10^{-20}$	x	x
ENSG00000156466	GDF6	3,67	$2,02 \times 10^{-2}$	1,58	$3,19 \times 10^{-2}$	x	
ENSG00000106809	OGN	3,43	$4,62 \times 10^{-3}$	2,00	$1,02 \times 10^{-3}$	x	
ENSG00000106819	ASPN	3,17	$3,56 \times 10^{-3}$	1,65	$3,04 \times 10^{-2}$	x	
ENSG00000095777	MYO3A	2,44	$1,27 \times 10^{-2}$	2,25	$1,16 \times 10^{-4}$	x	
ENSG00000006016	CRLF1	2,32	$2,86 \times 10^{-2}$	3,04	$2,96 \times 10^{-10}$	x	x
ENSG00000151025	GPR158	2,31	$6,88 \times 10^{-4}$	2,73	$3,63 \times 10^{-3}$	x	x
ENSG00000198729	PPP1R14C	2,19	$1,14 \times 10^{-2}$	2,52	$1,33 \times 10^{-11}$	x	
ENSG00000125144	MT1G	2,16	$2,50 \times 10^{-2}$	1,97	$1,72 \times 10^{-4}$	x	
ENSG00000052850	ALX4	2,08	$2,30 \times 10^{-3}$	0,55	$2,75 \times 10^{-2}$	x	
ENSG00000149380	P4HA3	2,05	$1,12 \times 10^{-3}$	1,84	$1,49 \times 10^{-5}$	x	
ENSG00000078098	FAP	2,05	$1,14 \times 10^{-2}$	1,69	$1,09 \times 10^{-3}$	x	
ENSG00000133110	POSTN	2,04	$3,44 \times 10^{-2}$	2,06	$3,20 \times 10^{-2}$	x	
ENSG00000230148	HOXB-AS1	2,00	$1,27 \times 10^{-2}$	1,64	$4,86 \times 10^{-2}$	x	
ENSG00000112984	KIF20A	1,97	$2,22 \times 10^{-2}$	1,59	$4,44 \times 10^{-2}$	x	
ENSG00000123610	TNFAIP6	1,93	$1,03 \times 10^{-3}$	3,58	$2,48 \times 10^{-8}$	x	x
ENSG00000178752	ERFE	1,87	$1,63 \times 10^{-2}$	3,44	$8,82 \times 10^{-12}$	x	x
ENSG00000148344	PTGES	1,64	$1,63 \times 10^{-2}$	3,06	$3,61 \times 10^{-12}$		x
ENSG00000006327	TNFRSF12A	1,50	$2,31 \times 10^{-2}$	2,68	$1,14 \times 10^{-8}$		x
ENSG00000169884	WNT10B	1,49	$3,25 \times 10^{-2}$	3,47	$1,52 \times 10^{-6}$		x
ENSG00000100473	COCH	1,46	$4,21 \times 10^{-2}$	3,30	$1,01 \times 10^{-8}$		x
ENSG00000196352	CD55	1,46	$2,48 \times 10^{-2}$	2,96	$1,05 \times 10^{-14}$		x
ENSG00000090530	P3H2	1,37	$1,14 \times 10^{-2}$	3,23	$4,71 \times 10^{-18}$		x
ENSG00000134259	NGF	1,36	$3,26 \times 10^{-2}$	4,91	$2,53 \times 10^{-14}$		x
ENSG00000118785	SPP1	1,36	$4,81 \times 10^{-2}$	3,14	$8,98 \times 10^{-7}$		x
ENSG00000140538	NTRK3	0,70	$3,56 \times 10^{-3}$	0,31	$2,64 \times 10^{-5}$		x
ENSG00000048540	LMO3	0,58	$3,82 \times 10^{-3}$	0,28	$1,67 \times 10^{-5}$		x
ENSG00000162998	FRZB	0,53	$3,99 \times 10^{-7}$	0,27	$1,87 \times 10^{-9}$	x	x
ENSG00000189056	RELN	0,53	$2,56 \times 10^{-2}$	0,22	$7,37 \times 10^{-12}$	x	x
ENSG00000141469	SLC14A1	0,53	$1,71 \times 10^{-2}$	0,51	$7,05 \times 10^{-6}$	x	
ENSG00000121005	CRISPLD1	0,51	$1,84 \times 10^{-2}$	0,36	$9,29 \times 10^{-6}$	x	x
ENSG00000187595	ZNF385C	0,51	$3,82 \times 10^{-3}$	0,43	$2,30 \times 10^{-6}$	x	
ENSG00000124440	HIF3A	0,49	$2,07 \times 10^{-3}$	0,58	$2,72 \times 10^{-2}$	x	
ENSG00000259916	AL845331.2	0,46	$3,16 \times 10^{-2}$	0,34	$3,50 \times 10^{-2}$	x	x
ENSG00000179399	GPC5	0,43	$1,27 \times 10^{-4}$	0,36	$1,47 \times 10^{-8}$	x	x
ENSG00000223561	AC005165.1	0,43	$1,20 \times 10^{-4}$	0,45	$5,31 \times 10^{-4}$	x	
ENSG00000102466	FGF14	0,41	$1,89 \times 10^{-4}$	0,58	$2,01 \times 10^{-4}$	x	
ENSG00000256995	AC084816.1	0,38	$2,20 \times 10^{-2}$	0,45	$2,20 \times 10^{-5}$	x	

Ensemble ID	Gene name	Subchondral bone		Articular Cartilage		Top 25 absolute foldchange	
		FC	FDR	FC	FDR	SB	AC
ENSG00000130294	KIF1A	0,25	$1,27 \times 10^{-2}$	0,37	$8,64 \times 10^{-8}$	x	x
ENSG00000196104	SPOCK3	0,24	$3,41 \times 10^{-4}$	0,22	$1,56 \times 10^{-9}$	x	x
ENSG00000054938	CHRDL2	0,14	$1,20 \times 10^{-4}$	0,13	$7,07 \times 10^{-9}$	x	x

genes appeared to be differentially expressed exclusively in the hip; i.e. not differentially expressed in an analysis of the total data set (**Supplementary Table 3**) or the knee dataset (**Supplementary Table 9**). Included among these genes with differential expression exclusively in the hip were *CALCR*, *LGR5* and *COL2A1* (**Supplementary Table 13**).

Validation of differentially expressed genes
To validate and replicate the findings of the differential expression analysis performed using RNA-seq, we used a set of 20 samples to conduct both technical replication (10 samples) and biological replication (10 samples) by RT-qPCR. Validation analysis of six genes, *FRZB*, *CNTNAP2*, *STMN2*, *CHRDL2*, *POSTN*, and *ASPN,* showed significant differences between preserved and lesioned subchondral bone, with directions of effects similar to those found by RNA-seq. Replication analysis also showed significant differences, with the same direction of effects as shown by RNA-seq (**Supplementary Table 14**).

Differential expression of previously identified risk genes
In recent genome-wide association studies of hip and knee OA [5, 6], 27 loci conferring risk to OA were identified (**Table 2**). To assess whether those OA susceptibility genes are also involved in OA pathophysiology in articular cartilage, subchondral bone, or both, we explored their expression levels and differential expression between lesioned and preserved tissue in our data sets. As shown in **Table 2**, we identified two risk genes, *IL11* and *CHADL,* that were differentially expressed in both subchondral bone and articular cartilage. In addition, *IL11* showed both significant differential expression in knee subchondral bone (FC=4.07, FDR=7.00×10^{-3}) and a high FC (FC=4.77, Pval= $4,43 \times 10^{-02}$) in hip subchondral bone. This indicates that, based on our data sets, *IL11* has an effect in both tissues and at both joint sites, albeit not significant according to FDR in hip subchondral bone.

Discussion
Differential expression analysis of gene expression levels in preserved and lesioned OA subchondral bone (N=24 paired samples) revealed 1569 genes that were significantly

Table 2 – Expression levels and differential expression of new risk genes reported in two recent GWAS.

	Bone - total dataset			Cartilage - total dataset		
	Expression*	FC P vs. OA	FDR	Expression*	FC P vs. OA	FDR
COL11a1	1	1,19	$6,21 \times 10^{-1}$	1	1,07	$7,59 \times 10^{-1}$
HDAC9	2	0,97	$6,75 \times 10^{-1}$	1	0,59	$9,10 \times 10^{-6}$
SMO	2	1,00	$9,91 \times 10^{-1}$	1	0,69	$7,85 \times 10^{-5}$
TNC	1	1,18	$2,58 \times 10^{-1}$	1	1,41	$1,09 \times 10^{-2}$
LMX1B	Not expressed	NA	NA	3	0,99	$9,80 \times 10^{-1}$
LTBP3	1	0,87	$3,08 \times 10^{-1}$	1	1,08	$6,95 \times 10^{-1}$
FAM101A (RFLNA)	4	0,99	$9,77 \times 10^{-1}$	2	0,49	$6,48 \times 10^{-5}$
IL11	3	4,16	$2,44 \times 10^{-3}$	1	22,80	$1,53 \times 10^{-20}$
ITIH1	Not expressed	NA	NA	Not expressed	NA	NA
FILIP1	2	0,84	$7,07 \times 10^{-2}$	3	1,23	$2,38 \times 10^{-1}$
RUNX2	1	1,07	$4,75 \times 10^{-1}$	2	0,93	$7,79 \times 10^{-1}$
ASTN2	4	0,87	$2,42 \times 10^{-1}$	4	0,82	$2,43 \times 10^{-1}$
SMAD3	1	0,93	$3,74 \times 10^{-1}$	1	0,84	$2,83 \times 10^{-2}$
HFE	3	1,01	$9,07 \times 10^{-1}$	2	0,88	$1,32 \times 10^{-1}$
CHADL	4	0,63	$2,33 \times 10^{-2}$	1	0,63	$1,29 \times 10^{-2}$
LTBP1	1	0,97	$6,91 \times 10^{-1}$	1	1,15	$1,70 \times 10^{-1}$
SBNO1	1	0,98	$6,79 \times 10^{-1}$	1	1,10	$3,94 \times 10^{-1}$
WWP2	1	0,82	$2,47 \times 10^{-1}$	1	0,79	$3,43 \times 10^{-2}$
GDF5	4	0,92	$8,08 \times 10^{-1}$	1	1,23	$3,09 \times 10^{-1}$
TGFB1	Not expressed	NA	NA	Not expressed	NA	NA
TNFSF15	4	1,23	$2,42 \times 10^{-1}$	3	1,00	$9,91 \times 10^{-1}$
FGF18	Not expressed	NA	NA	2	1,58	$9,51 \times 10^{-4}$
CTSK	1	1,41	$3,23 \times 10^{-1}$	1	1,03	$8,91 \times 10^{-1}$
DPEP1 (MBD1)	1	0,95	$2,83 \times 10^{-1}$	1	0,96	$6,20 \times 10^{-1}$
DIABLO	4	0,95	$7,37 \times 10^{-1}$	3	1,08	$6,46 \times 10^{-1}$
CRHR1	Not expressed	NA	NA	4	0,62	$5,10 \times 10^{-1}$
MAPT	3	0,61	$3,47 \times 10^{-2}$	4	0,70	$1,56 \times 10^{-1}$

* Expression in quartiles, with 1 being the highest expressed quartile and 4 being the lowest expressed quartile

differentially expressed, including *CNTNAP2* and *STMN2*. Upon comparing these 1569 differentially expressed genes with the 2387 genes previously shown to be differentially expressed with OA pathophysiology in cartilage, we found an overlap of 305 genes that had the same direction of effect. These 305 overlapping genes were enriched for processes related to the extracellular matrix, characterized by the expression of, amongst others, *COL6A3, GDF6* and *SPP1*. Moreover, among the 305 overlapping genes were *IL11* and *CHADL* (**Supplementary Table 6**), which were previously identified as

being OA risk genes (**Table 2**). By applying hierarchical clustering on the overall RNA-seq data set from subchondral bone, we observed two clusters based on joint site (knee and hip). When stratifying the analysis for joint site, we identified 1759 genes that were differentially expressed between preserved and lesioned knee OA bone, 509 of which were differentially expressed in the knee exclusively, including genes such as *WNT4* and *KLF11*. These OA genes that were differentially expressed exclusively in the knee were enriched for regulation of gene silencing by epigenetic processes, such as DNA methylation and histone modification, characterized by genes such as *HIST1H3J* and *HIST1H3H*, as well as being enriched for other processes.

Among the 1569 genes that were significantly differentially expressed between lesioned and preserved OA subchondral bone using the FDR method in the complete data set, we identified *CNTNAP2* (FC=2.42, FDR=3.36×10^{-5}) and *STMN2* (FC=9.56, FDR=2.36×10^{-3}) as the most significantly up-regulated gene and the gene with the highest FC, respectively. *CNTNAP2*, encoding CASPR2, is known for its effect on cell-cell interactions in the nervous system, synapse development, neural migration, and neural connectivity [31, 32]. Neither *CNTNAP2* nor its encoded protein were previously identified as being related to OA. *STMN2* also plays a role in the control of neuronal differentiation. Moreover, *STMN2* is expressed during osteogenesis and it was previously shown to be highly up-regulated in OA bone marrow lesions as compared to control bone samples [8, 33]. In addition, we found other neural markers to be up-regulated in lesioned compared to preserved OA subchondral bone, such as *NGF* and *THBS3* (**Supplementary Table 3**). Based on these findings, we hypothesize that the formation of new neuronal structures in bone is increased with ongoing OA, which might suggest that OA-related pain originates from bone [8]. However, functional follow up research is needed to confirm this hypothesis.

The hierarchical clustering was done on the top 1000 genes that showed the highest coefficient of variation between samples; hence, the clusters reflect particularly large differences. Based on the results observed here, it could thus be concluded that these highly variable genes reflect consistent differences between subchondral bone in the knees and subchondral bone in the hip, which was not previously seen in similar analyses of the cartilage [25]. Consequently, the fact that neither preserved and lesioned samples from the same individual nor preserved samples or lesioned samples as a group cluster together, indicated that the 1000 genes with the highest coefficient of variation are marking differences between knees and hips only. This does not rule out the relevance of the highly consistently differentially expressed genes reflecting OA subchondral bone pathology described here.

Upon differential expression analysis with stratification by joint site, we discovered 509

genes that were unique to the knee compared to the complete data set, which were significantly enriched for epigenetic processes such as DNA methylation, reflected by the expression of, among others, *HIST1H3J* and *HIST1H3H*. The significant enrichment of these epigenetic processes among the knee-exclusive genes indicates a change in epigenetics with ongoing knee OA, which is not seen with ongoing hip OA. This was also previously demonstrated in articular cartilage, where hip and knee methylation profiles clustered apart irrespective of the OA status. However, this was characterized by the expression of different genes, such as the homeobox genes [34, 35]. We did not find FDR-significant genes when selecting the hip samples, which is likely due to the small sample size (6 sample pairs). Nonetheless, we identified 18 genes that were exclusively differentially expressed in the hip based on the nominal P-value and an absolute FC ≥2, including genes such as *CALCR*, *LGR5* and *COL2A1*. However, replication is needed to confirm our findings regarding these genes differentially expressed exclusively in the hip.

Given the accumulating awareness of cross-talk between articular cartilage and subchondral bone during OA [10, 36], we compared RNA-seq data from subchondral bone and from articular cartilage (24 sample pairs, and 35 sample pairs, respectively, with an overlap of 14 patients). Compared to the number of genes identified as being significantly differentially expressed between preserved and lesioned OA articular cartilage based on FDR (2387 genes), we found fewer genes that were significantly differentially expressed by FDR between preserved and lesioned OA subchondral bone (1569 genes). This difference might be due to the difference in sample size. However, it could also reflect the fact that bone as multicellular tissue is more heterogeneous. The relatively small overlap in genes that were differentially expressed in the same direction in both subchondral bone and cartilage (9.31%, 305 genes), suggest that there is a difference in OA pathophysiology between the two tissues.

To find genes that are most likely causal in OA, we explored 27 previously published genes with SNPs that were identified as being genome-wide significantly associated with OA (**Table 2**), suggesting that those genes have a more causal relationship to OA and making them attractive potential drug targets [5, 6]. To examine whether the previously identified OA risk genes are involved in the OA pathophysiological process in both tissues, we compared the expression levels and the differential expression between preserved and lesioned samples (**Table 2**). We found the OA risk genes *IL11* and *CHADL* were differentially expressed in both articular cartilage and subchondral bone and with the same direction of effect, thus making them attractive potential drug targets with effects in both tissues. *CHADL*, encoding chondroadherin-like protein, is involved in collagen binding and is a negative modulator of chondrocyte differentiation.

The OA susceptibility allele rs117018441-T, located in an intron of *CHADL*, marks higher expression of *CHADL* compared to rs117018441-G in skeletal muscle and adipose tissue according to the Genotype-Tissue Expression Project [5, 37]. This may indicate that increased expression of *CHADL* has a negative regulatory role both in bone and cartilage and that inhibition of this gene could be a therapeutic strategy. However, when stratifying for joint site, we found *CHADL* to be differentially expressed specifically in the knee subchondral bone, suggesting that it is a treatment target for knee OA exclusively.

IL11, encoding Interleukin 11 (IL-11), is known for its role in bone remodelling and lack of IL-11 function is associated with impaired bone formation [38]. Notably, IL-11 is recently proposed as potential therapeutic target for OA in cartilage [6], since OA risk allele rs4252548-T, a missense variant p.Arg112His, acts via reduced function of the IL-11 protein. As such, increasing IL-11 protein levels was proposed as a strategy for treatment of OA. In this study we have again shown that *IL11* is highly up-regulated in lesioned versus preserved OA tissue in both subchondral bone and articular cartilage (FC=4.16 and FC=22.8, respectively). Taken together, these data indicate that reduced function of IL-11 predisposes to OA onset and that the up-regulation of *IL11* with OA pathophysiology could be considered an attempt of the chondrocytes to enhance extracellular matrix integrity. Nonetheless, the consistent and considerable up-regulation of *IL11* in both subchondral bone and articular cartilage may not necessarily reflect a lack of potency to produce IL-11, unless translation of the protein is hampered. This requires further functional investigation preferably in an *in vitro* model of OA. *CHADL* and *IL11* could both be highly suitable treatment targets with effects in both bone and cartilage. However, further functional research is needed to confirm the effects of these genes on bone and cartilage metabolism.

The classification of OA subchondral bone as preserved or lesioned is derived from its overlying cartilage. We acknowledge that this ascertainment strategy is bound to introduce heterogeneity between samples. Nonetheless, we find FDR-significant, and hence very consistent, differentially expressed genes. In other words, despite the fact that there may be heterogeneity in the preserved cartilage, we found consistent markers of the OA pathophysiological process in subchondral bone.

To our knowledge, we are the first reported study of large-scale differential gene expression patterns in OA subchondral, performed using RNA-seq in both hip and knee samples. We identified distinct differences in expression patterns between hips and knees. Moreover, we identified multiple genes that were previously demonstrated in OA articular cartilage, in addition to genes that were subchondral bone specific. These results will contribute to a better understanding of the pathophysiological processes

underlying the development of OA.

Declarations

Disclosures

The authors have declared no conflicts of interest.

References

1. Woolf, A.D., J. Erwin, and L. March, *The need to address the burden of musculoskeletal conditions.* Best Pract Res Clin Rheumatol, 2012. **26**(2): p. 183-224.
2. Goldring, M.B. and S.R. Goldring, *Articular cartilage and subchondral bone in the pathogenesis of osteoarthritis.* Ann N Y Acad Sci, 2010. **1192**: p. 230-7.
3. Vina, E.R. and C.K. Kwoh, *Epidemiology of osteoarthritis: literature update.* Curr Opin Rheumatol, 2018. **30**(2): p. 160-167.
4. Zeggini, E., et al., *Identification of new susceptibility loci for osteoarthritis (arcOGEN): a genome-wide association study.* Lancet, 2012. **380**(9844): p. 815-23.
5. Styrkarsdottir, U., et al., *Meta-analysis of Icelandic and UK data sets identifies missense variants in SMO, IL11, COL11A1 and 13 more new loci associated with osteoarthritis.* Nat Genet, 2018. **50**(12): p. 1681-1687.
6. Tachmazidou, I., et al., *Identification of new therapeutic targets for osteoarthritis through genome-wide analyses of UK Biobank data.* Nat Genet, 2019. **51**(2): p. 230-236.
7. Chou, C.H., et al., *Genome-wide expression profiles of subchondral bone in osteoarthritis.* Arthritis Res Ther, 2013. **15**(6): p. R190.
8. Kuttapitiya, A., et al., *Microarray analysis of bone marrow lesions in osteoarthritis demonstrates upregulation of genes implicated in osteochondral turnover, neurogenesis and inflammation.* Ann Rheum Dis, 2017. **76**(10): p. 1764-1773.
9. Fellows, C.R., C. Matta, and A. Mobasheri, *Applying Proteomics to Study Crosstalk at the Cartilage-Subchondral Bone Interface in Osteoarthritis: Current Status and Future Directions.* EBioMedicine, 2016. **11**: p. 2-4.
10. Goldring, S.R. and M.B. Goldring, *Changes in the osteochondral unit during osteoarthritis: structure, function and cartilage-bone crosstalk.* Nat Rev Rheumatol, 2016. **12**(11): p. 632-644.
11. Funck-Brentano, T. and M. Cohen-Solal, *Crosstalk between cartilage and bone: when bone cytokines matter.* Cytokine Growth Factor Rev, 2011. **22**(2): p. 91-7.
12. Pan, J., et al., *Elevated cross-talk between subchondral bone and cartilage in osteoarthritic joints.* Bone, 2012. **51**(2): p. 212-7.
13. Funck-Brentano, T. and M. Cohen-Solal, *Subchondral bone and osteoarthritis.* Curr Opin Rheumatol, 2015. **27**(4): p. 420-6.
14. Loeser, R.F., et al., *Osteoarthritis: a disease of the joint as an organ.* Arthritis Rheum, 2012. **64**(6): p. 1697-707.
15. Barbour, K.E., et al., *Bone Mineral Density and the Risk of Hip and Knee Osteoarthritis: The Johnston County Osteoarthritis Project.* Arthritis Care Res (Hoboken), 2017. **69**(12): p. 1863-1870.
16. Roemer, F.W., et al., *Change in MRI-detected subchondral bone marrow lesions is associated with cartilage loss: the MOST Study. A longitudinal multicentre study of knee osteoarthritis.* Ann Rheum Dis, 2009. **68**(9): p. 1461-5.
17. Ramos, Y.F., et al., *Genes involved in the osteoarthritis process identified through genome wide expression analysis in articular cartilage; the RAAK study.* PLoS One, 2014. **9**(7): p. e103056.
18. Coutinho de Almeida, R., et al., *RNA sequencing data integration reveals an miRNA interactome of osteoarthritis cartilage.* Ann Rheum Dis, 2019. **78**(2): p. 270-277.

19. Liu, P. and J.T.G. Hwang, *Quick calculation for sample size while controlling false discovery rate with application to microarray analysis.* Bioinformatics, 2007. **23**(6): p. 739-746.
20. Wu, T.D. and C.K. Watanabe, *GMAP: a genomic mapping and alignment program for mRNA and EST sequences.* Bioinformatics, 2005. **21**(9): p. 1859-75.
21. Anders, S., P.T. Pyl, and W. Huber, *HTSeq--a Python framework to work with high-throughput sequencing data.* Bioinformatics, 2015. **31**(2): p. 166-9.
22. Ewels, P., et al., *MultiQC: summarize analysis results for multiple tools and samples in a single report.* Bioinformatics, 2016. **32**(19): p. 3047-8.
23. Martin, M., *Cutadapt removes adapter sequences from high-throughput sequencing reads.* 2011, 2011. **17**(1): p. 3 %J EMBnet.journal.
24. Li, W., M. Fan, and M. Xiong, *SamCluster: an integrated scheme for automatic discovery of sample classes using gene expression profile.* Bioinformatics, 2003. **19**(7): p. 811-817.
25. Coutinho de Almeida, R., et al., *Identification and characterization of two consistent osteoarthritis subtypes by transcriptome and clinical data integration.* Rheumatology (Oxford), 2020.
26. Charrad, M., et al., *NbClust: An R Package for Determining the Relevant Number of Clusters in a Data Set.* 2014, 2014. **61**(6): p. 36 %J Journal of Statistical Software.
27. Love, M.I., W. Huber, and S. Anders, *Moderated estimation of fold change and dispersion for RNA-seq data with DESeq2.* Genome Biology, 2014. **15**(12): p. 550.
28. Huang da, W., B.T. Sherman, and R.A. Lempicki, *Systematic and integrative analysis of large gene lists using DAVID bioinformatics resources.* Nat Protoc, 2009. **4**(1): p. 44-57.
29. Szklarczyk, D., et al., *STRING v11: protein-protein association networks with increased coverage, supporting functional discovery in genome-wide experimental datasets.* Nucleic Acids Res, 2019. **47**(D1): p. D607-d613.
30. Chou, C.H., et al., *Direct assessment of articular cartilage and underlying subchondral bone reveals a progressive gene expression change in human osteoarthritic knees.* Osteoarthritis Cartilage, 2013. **21**(3): p. 450-61.
31. Lu, Z., et al., *Molecular Architecture of Contactin-associated Protein-like 2 (CNTNAP2) and Its Interaction with Contactin 2 (CNTN2).* J Biol Chem, 2016. **291**(46): p. 24133-24147.
32. Rodenas-Cuadrado, P., J. Ho, and S.C. Vernes, *Shining a light on CNTNAP2: complex functions to complex disorders.* Eur J Hum Genet, 2014. **22**(2): p. 171-8.
33. Chiellini, C., et al., *Stathmin-like 2, a developmentally-associated neuronal marker, is expressed and modulated during osteogenesis of human mesenchymal stem cells.* Biochem Biophys Res Commun, 2008. **374**(1): p. 64-8.
34. Reynard, L.N., *Analysis of genetics and DNA methylation in osteoarthritis: What have we learnt about the disease?* Semin Cell Dev Biol, 2017. **62**: p. 57-66.
35. den Hollander, W., et al., *Knee and hip articular cartilage have distinct epigenomic landscapes: implications for future cartilage regeneration approaches.* Ann Rheum Dis, 2014. **73**(12): p. 2208-12.
36. Kwan Tat, S., et al., *Targeting subchondral bone for treating osteoarthritis: what is the evidence?* Best Pract Res Clin Rheumatol, 2010. **24**(1): p. 51-70.
37. Styrkarsdottir, U., et al., *Whole-genome sequencing identifies rare genotypes in COMP and CHADL associated with high risk of hip osteoarthritis.* Nat Genet, 2017. **49**(5): p. 801-805.
38. Lokau, J., et al., *The SNP rs4252548 (R112H) which is associated with reduced human height compromises the stability of IL-11.* Biochim Biophys Acta Mol Cell Res, 2018. **1865**(3): p. 496-506.

2

Supplementary data

Supplementary figures
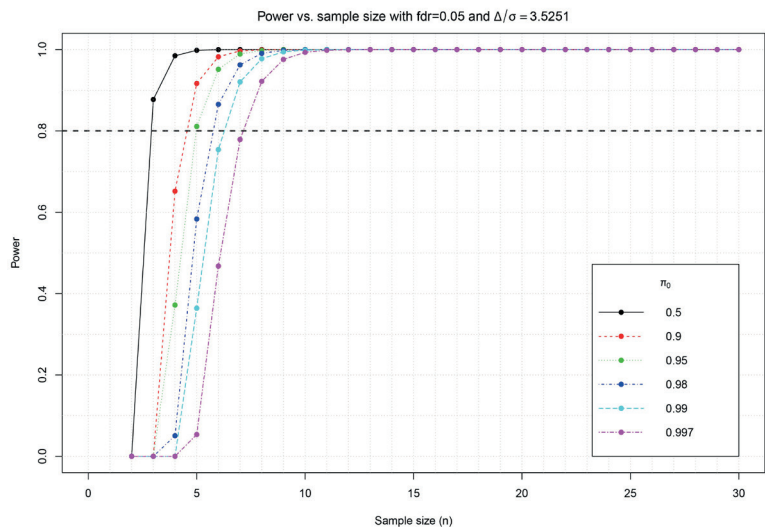
Supplementary Figure 1 – Power calculations to determine the sample size of the current study. The parameters used to generate the graph are based on similar analysis on articular cartilage
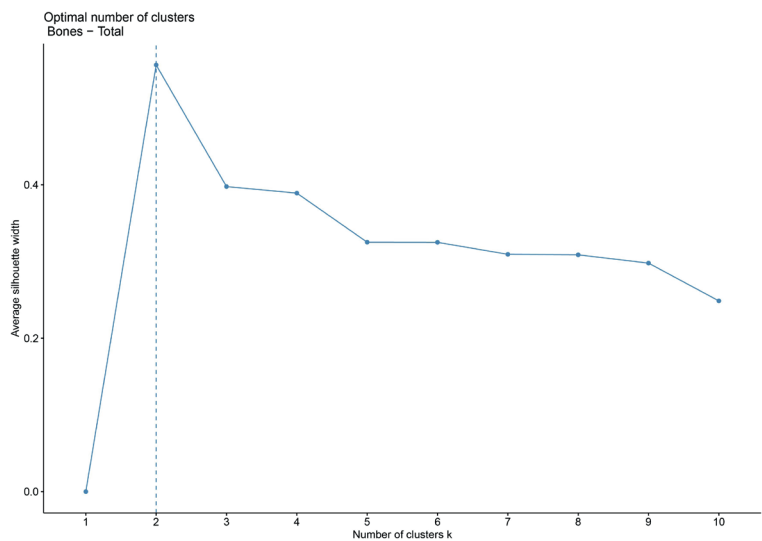
Supplementary Figure 2 – Silhouette width score showing an optimal number of two clusters.
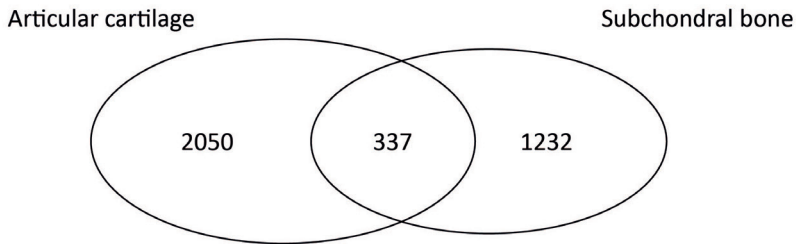
Supplementary Figure 3 – Venn diagram of differentially expressed genes in the articular cartilage (N=2387) and in the subchondral bone (N=1569).
337 genes were overlapping between cartilage and bone, of which 305 genes show similar direction of effects between cartilage and bone.

Supplementary tables

Supplementary table 1 – Baseline characteristics of subchondral bone samples included in the study

	Total (N=34)	RNAseq - hips (N=6)	RNAseq - knees (N=18)	RT-qPCR - biological (N=10)	RT-qPCR - technical (N=10)
Age (SD)	68,1 (9,5)	67,8 (8,8)	65,7 (8,5)	72,4 (10)	67,6 (7,8)
Females (total)	27 (34)	6 (6)	16 (18)	5 (10)	8 (10)

Supplementary table 2 – Gene expression levels of cartilage and bone markers measured in preserved and lesioned bone and cartilage tissue.
In the statistical analysis cartilage is set as the reference.

Marker	Genes	Preserved Cartilage vs. Bone		Lesioned Cartilage vs. Bone	
		Fold change	FDR	Fold change	FDR
Cartilage	COL2A1	0.02	7.46E-48	0.01	7.93E-24
Cartilage	COMP	0.01	1.03E-60	0.01	2.76E-47
Cartilage	CRTAC1	0.01	1.64E-112	0.01	1.88E-75
Bone	COL1A1	1.85	1.78E-01	4.31	2.25E-03
Bone	SPP1	8.85	3.54E-19	2.56	3.56E-04
Bone	BGLAP	9.17	5.92E-08	11.19	1.59E-11

Supplementary table 3 (partially) – Significantly differentially expressed genes between lesioned and preserved OA subchondral bone.
Top 50 most significantly differentially expressed genes are shown here, the rest of the table can be found in the online supplement: https://doi.org/10.1002/art.41600

Ensembl gene ID	Gene	P-value	FDR	Log 2 fold change	Fold change
ENSG00000162998	FRZB	2.52E-11	3.99E-07	-0.90	0.53
ENSG00000174469	CNTNAP2	6.16E-09	3.36E-05	1.27	2.42
ENSG00000157103	SLC6A1	6.36E-09	3.36E-05	-0.71	0.61
ENSG00000162105	SHANK2	1.12E-08	4.43E-05	-1.15	0.45
ENSG00000054938	CHRDL2	4.10E-08	1.20E-04	-2.85	0.14
ENSG00000223561	AC005165.1	4.54E-08	1.20E-04	-1.23	0.43
ENSG00000179399	GPC5	7.22E-08	1.27E-04	-1.22	0.43
ENSG00000159307	SCUBE1	6.66E-08	1.27E-04	-0.84	0.56
ENSG00000198918	RPL39	7.12E-08	1.27E-04	0.39	1.31
ENSG00000116285	ERRFI1	8.10E-08	1.28E-04	0.57	1.48
ENSG00000102466	FGF14	1.67E-07	1.89E-04	-1.29	0.41
ENSG00000007314	SCN4A	1.42E-07	1.89E-04	-0.63	0.65
ENSG00000251322	SHANK3	1.61E-07	1.89E-04	-0.51	0.70
ENSG00000144867	SRPRB	1.67E-07	1.89E-04	0.45	1.36
ENSG00000037042	TUBG2	2.74E-07	2.89E-04	-0.36	0.78
ENSG00000196104	SPOCK3	3.44E-07	3.41E-04	-2.07	0.24
ENSG00000169871	TRIM56	4.18E-07	3.90E-04	-0.31	0.81
ENSG00000134014	ELP3	5.24E-07	4.61E-04	0.20	1.15
ENSG00000106511	MEOX2	6.35E-07	5.30E-04	-0.52	0.70
ENSG00000257017	HP	7.30E-07	5.57E-04	1.37	2.59
ENSG00000130158	DOCK6	7.38E-07	5.57E-04	-0.41	0.75
ENSG00000136237	RAPGEF5	8.72E-07	6.28E-04	-0.47	0.72
ENSG00000163884	KLF15	9.79E-07	6.46E-04	-0.67	0.63
ENSG00000204301	NOTCH4	9.58E-07	6.46E-04	-0.41	0.75
ENSG00000234797	RPS3AP6	1.02E-06	6.46E-04	0.25	1.19
ENSG00000002745	WNT16	1.26E-06	6.88E-04	2.12	4.35
ENSG00000064886	CHI3L2	1.22E-06	6.88E-04	1.26	2.40
ENSG00000151025	GPR158	1.17E-06	6.88E-04	1.21	2.31
ENSG00000154783	FGD5	1.21E-06	6.88E-04	-0.35	0.78
ENSG00000130300	PLVAP	1.42E-06	7.33E-04	-0.46	0.73
ENSG00000252835	SCARNA21	1.43E-06	7.33E-04	0.37	1.29
ENSG00000115616	SLC9A2	1.62E-06	8.01E-04	1.53	2.89
ENSG00000232044	SILC1	1.79E-06	8.60E-04	1.09	2.13

Ensembl gene ID	Gene	P-value	FDR	Log 2 fold change	Fold change
ENSG00000112306	RPS12	1.89E-06	8.81E-04	0.23	1.17
ENSG00000128917	DLL4	2.13E-06	9.31E-04	-0.63	0.65
ENSG00000146830	GIGYF1	2.07E-06	9.31E-04	-0.29	0.82
ENSG00000225178	RPSAP58	2.17E-06	9.31E-04	0.28	1.21
ENSG00000123610	TNFAIP6	2.53E-06	1.03E-03	0.95	1.93
ENSG00000173801	JUP	2.48E-06	1.03E-03	-0.51	0.70
ENSG00000148400	NOTCH1	2.67E-06	1.06E-03	-0.53	0.69
ENSG00000089157	RPLP0	2.84E-06	1.10E-03	0.28	1.22
ENSG00000229847	EMX2OS	3.07E-06	1.11E-03	-1.26	0.42
ENSG00000148848	ADAM12	3.02E-06	1.11E-03	0.80	1.75
ENSG00000115128	SF3B6	2.98E-06	1.11E-03	0.25	1.19
ENSG00000149380	P4HA3	3.24E-06	1.12E-03	1.04	2.05
ENSG00000163902	RPN1	3.18E-06	1.12E-03	0.20	1.15
ENSG00000078018	MAP2	3.77E-06	1.27E-03	-0.44	0.74
ENSG00000166426	CRABP1	4.26E-06	1.36E-03	1.43	2.69

2

Supplementary table 4 (partially) – Gene enrichment analysis on differentially expressed genes (N=1569 genes) in OA subchondral bone.
The five most significant processes are shown here, the rest of the table can be found in the online supplement: https://doi.org/10.1002/art.41600

Category	Term	Count	%	Genes	P-value	FDR
Biological processes	GO:0006614~SRP-dependent cotranslational protein targeting to membrane	33	2.2	RPL26L1, SEC61A1, RPL6, RPLP0, RPL34, RPS13, RPS12, RPL5, RPL23, RPL27, RPS6, RPS24, RPL11, RPS8, SRPRB, RPS3A, RPL7, RPL7A, RPL27A, RPSA, RPS7, RPL4, RPS17, RPL35A, RPS23, RPL37A, RPL12, RPS4X, RPL23A, RPL10A, RPL39, RPL41, RPS18	2.29E-10	4.27E-07
Biological processes	GO:0000184~nuclear-transcribed mRNA catabolic process, nonsense-mediated decay	36	2.4	RPL26L1, SMG6, RPL6, RPLP0, EIF3E, RPL34, RPS13, RPS12, RPL5, RPL23, RPL27, CTIF, NCBP1, RPS6, RPS24, EIF4A3, RPL11, RPS8, RPS3A, RPL7, RPL7A, RPL27A, RPSA, RPS7, RPL4, RPS17, RPL35A, RPS23, RPL37A, RPL12, RPS4X, RPL23A, RPL10A, RPL39, RPL41, RPS18	2.83E-09	5.28E-06
Biological processes	GO:0019083~viral transcription	33	2.2	RPL26L1, RPL6, RPLP0, RPL34, RPS13, RPS12, RPL5, RPL23, NUP214, RPL27, RPS6, RPS24, RPL11, RPS8, RPS3A, RPL7, RPL7A, RPL27A, RPSA, RPS7, RPL4, RPS17, RPL35A, RPS23, POM121, RPL37A, RPL12, RPS4X, RPL23A, RPL10A, RPL39, RPL41, RPS18	4.32E-08	8.06E-05
Biological processes	GO:0006413~translational initiation	36	2.4	RPL26L1, RPL6, RPLP0, EIF3E, RPL34, RPS13, RPS12, RPL5, RPL23, EIF2S2, RPL27, EIF2S1, RPS6, RPS24, RPL11, RPS8, EIF2A, RPS3A, RPL7, RPL7A, EIF3M, RPL27A, RPSA, RPS7, RPL4, RPS17, RPL35A, RPS23, RPL37A, RPL12, RPS4X, RPL23A, RPL10A, RPL39, RPL41, RPS18	1.04E-07	1.95E-04
Biological processes	GO:0018279~protein N-linked glycosylation via asparagine	16	1.1	FUT8, LMAN1, MAGT1, TUSC3, RPN2, ALG5, DAD1, UGGT1, ST6GAL2, ST6GALNAC6, STT3B, RPN1, MGAT2, UBE2J1, OSTC, DDOST	2.95E-06	5.51E-03
Cellular component	GO:0022625~cytosolic large ribosomal subunit	22	1.5	RPL26L1, RPL6, RPLP0, RPL34, RPL5, RPL23, RPL27, RPL11, RPL7L1, RPL7, SURF6, RPL7A, RPL22L1, RPL27A, RPL4, RPL35A, RPL37A, RPL12, RPL23A, RPL10A, RPL39, RPL41	7.73E-07	1.17E-03
Cellular component	GO:0008250~oligosaccharyltransferase complex	8	0.5	MAGT1, TUSC3, RPN2, DAD1, STT3B, RPN1, OSTC, DDOST	5.07E-06	7.66E-03

Supplementary table 5 – Gene enrichment analysis on differentially expressed genes in OA subchondral bone showing an absolute fold change of 2 or higher (N=53 genes)

Category	Term	Count	%	Genes	FDR
Cellular component	GO:0005615~extracellular space	16	32.7	WNT16, CRLF1, CHRDL2, CHI3L2, FAP, IL11, OGN, POSTN, GDF6, CTHRC1, LEP, GPC5, SPOCK3, MSMP, HP, CCL18	1.19E-05
Cellular component	GO:0005578~proteinaceous extracellular matrix	7	14.3	WNT16, OGN, ASPN, POSTN, CTHRC1, GPC5, SPOCK3	4.50E-02

Chapter 2

Supplementary table 6 (partially) - Overlapping differentially expressed genes between the subchondral bone and the articular cartilage with similar direction of effect.
Top 50 genes differentially expressed genes in subchondral bone and articular cartilage are shown here, the rest of the table can be found online: https://doi.org/10.1002/art.41600

Ensembl ID	Gene name	Subchondral bone		Articular Cartilage	
		Fold change	FDR	Fold change	FDR
ENSG00000054938	CHRDL2	0.14	1.20E-04	0.13	7.07E-09
ENSG00000002745	WNT16	4.35	6.88E-04	8.48	1.10E-13
ENSG00000095752	IL11	4.16	2.44E-03	22.80	1.53E-20
ENSG00000196104	SPOCK3	0.24	3.41E-04	0.22	1.56E-09
ENSG00000130294	KIF1A	0.25	1.27E-02	0.37	8.64E-08
ENSG00000006016	CRLF1	2.32	2.86E-02	3.04	2.96E-10
ENSG00000179399	GPC5	0.43	1.27E-04	0.36	1.47E-08
ENSG00000189056	RELN	0.53	2.56E-02	0.22	7.37E-12
ENSG00000123610	TNFAIP6	1.93	1.03E-03	3.58	2.48E-08
ENSG00000151025	GPR158	2.31	6.88E-04	2.73	3.63E-03
ENSG00000259916	AL845331.2	0.46	3.16E-02	0.34	3.50E-02
ENSG00000162998	FRZB	0.53	3.99E-07	0.27	1.87E-09
ENSG00000178752	ERFE	1.87	1.63E-02	3.44	8.82E-12
ENSG00000198729	PPP1R14C	2.19	1.14E-02	2.52	1.33E-11
ENSG00000121005	CRISPLD1	0.51	1.84E-02	0.36	9.29E-06
ENSG00000048540	LMO3	0.58	3.82E-03	0.28	1.67E-05
ENSG00000095777	MYO3A	2.44	1.27E-02	2.25	1.16E-04
ENSG00000256995	AC084816.1	0.38	2.20E-02	0.45	2.20E-05
ENSG00000223561	AC005165.1	0.43	1.20E-04	0.45	5.31E-04
ENSG00000187595	ZNF385C	0.51	3.82E-03	0.43	2.30E-06
ENSG00000106809	OGN	3.43	4.62E-03	2.00	1.02E-03
ENSG00000148344	PTGES	1.64	1.63E-02	3.06	3.61E-12
ENSG00000159307	SCUBE1	0.56	1.27E-04	0.42	2.15E-06
ENSG00000166033	HTRA1	1.73	1.57E-02	2.39	1.65E-11
ENSG00000133110	POSTN	2.04	3.44E-02	2.06	3.20E-02
ENSG00000120149	MSX2	1.64	3.13E-02	2.44	2.45E-05
ENSG00000125144	MT1G	2.16	2.50E-02	1.97	1.72E-04
ENSG00000134198	TSPAN2	1.64	1.51E-02	2.42	1.51E-08
ENSG00000094963	FMO2	0.63	2.56E-02	0.38	2.20E-03
ENSG00000169884	WNT10B	1.49	3.25E-02	3.47	1.52E-06
ENSG00000007314	SCN4A	0.65	1.89E-04	0.38	4.36E-03
ENSG00000141469	SLC14A1	0.53	1.71E-02	0.51	7.05E-06
ENSG00000149380	P4HA3	2.05	1.12E-03	1.84	1.49E-05

54

Ensembl ID	Gene name	Subchondral bone		Articular Cartilage	
		Fold change	FDR	Fold change	FDR
ENSG00000148848	ADAM12	1.75	1.11E-03	1.98	1.85E-04
ENSG00000263155	MYZAP	0.60	1.55E-02	0.47	3.56E-04
ENSG00000089685	BIRC5	1.59	3.77E-02	2.30	2.12E-03
ENSG00000006327	TNFRSF12A	1.50	2.31E-02	2.68	1.14E-08
ENSG00000100473	COCH	1.46	4.21E-02	3.30	1.01E-08
ENSG00000102466	FGF14	0.41	1.89E-04	0.58	2.01E-04
ENSG00000171017	LRRC8E	1.72	3.89E-02	1.99	1.11E-04
ENSG00000280339	AP001528.3	0.66	2.65E-02	0.38	1.28E-06
ENSG00000167037	SGSM1	0.63	2.89E-03	0.47	1.30E-06
ENSG00000196352	CD55	1.46	2.48E-02	2.96	1.05E-14
ENSG00000116147	TNR	0.65	1.98E-02	0.44	1.08E-03
ENSG00000142149	HUNK	1.71	4.91E-02	1.94	1.04E-03
ENSG00000140538	NTRK3	0.70	3.56E-03	0.31	2.64E-05
ENSG00000106819	ASPN	3.17	3.56E-03	1.65	3.04E-02
ENSG00000124440	HIF3A	0.49	2.07E-03	0.58	2.72E-02

2

Supplementary table 7 – Overlapping differentially expressed genes between the subchondral bone and the articular cartilage with opposite direction of effect.

Ensembl ID	Gene name	Subchondral bone		Articular Cartilage	
		Fold change	FDR	Fold change	FDR
ENSG00000074181	NOTCH3	0.70	1.44E-03	2.03	1.13E-03
ENSG00000081277	PKP1	0.57	5.32E-03	1.62	4.84E-03
ENSG00000082175	PGR	0.73	2.79E-02	1.49	2.02E-02
ENSG00000088387	DOCK9	0.88	2.90E-02	1.32	2.17E-02
ENSG00000100234	TIMP3	0.70	4.39E-03	1.54	9.97E-06
ENSG00000103528	SYT17	0.80	4.66E-02	1.21	2.56E-02
ENSG00000109846	CRYAB	0.67	2.83E-02	1.32	6.16E-03
ENSG00000110092	CCND1	0.84	3.29E-02	1.63	1.14E-04
ENSG00000119185	ITGB1BP1	0.81	2.45E-02	1.22	5.71E-04
ENSG00000120278	PLEKHG1	0.85	4.29E-02	1.77	7.93E-04
ENSG00000120318	ARAP3	0.85	3.56E-03	1.34	4.38E-03
ENSG00000144476	ACKR3	0.76	3.99E-02	1.34	7.96E-03
ENSG00000145911	N4BP3	0.68	1.92E-03	2.18	3.27E-03
ENSG00000146674	IGFBP3	0.78	2.63E-02	2.65	1.12E-07
ENSG00000156453	PCDH1	0.82	2.19E-02	1.91	4.02E-05
ENSG00000157510	AFAP1L1	0.80	1.93E-02	2.08	9.44E-04
ENSG00000157617	C2CD2	0.74	2.45E-02	1.28	1.98E-03
ENSG00000158258	CLSTN2	0.66	6.38E-03	1.83	1.40E-02
ENSG00000173210	ABLIM3	0.76	3.70E-03	1.98	9.31E-06
ENSG00000173599	PC	0.83	3.60E-02	1.25	3.51E-03
ENSG00000197183	NOL4L	0.84	2.56E-02	1.25	1.02E-03
ENSG00000198517	MAFK	0.86	2.43E-02	1.35	4.36E-03
ENSG00000198742	SMURF1	0.90	4.93E-02	1.55	3.32E-07
ENSG00000205336	ADGRG1	0.78	3.59E-02	1.73	1.39E-03
ENSG00000052850	ALX4	2.08	2.30E-03	0.55	2.75E-02
ENSG00000099284	H2AFY2	1.23	2.32E-02	0.85	2.07E-02
ENSG00000106066	CPVL	1.26	8.94E-03	0.53	9.16E-03
ENSG00000144649	GASK1A	1.48	1.49E-02	0.54	1.86E-03
ENSG00000165973	NELL1	1.74	3.11E-02	0.47	2.05E-02
ENSG00000182326	C1S	1.29	1.37E-02	0.77	7.74E-03
ENSG00000182853	VMO1	1.58	4.38E-02	0.53	1.63E-03
ENSG00000264672	SEPT4-AS1	1.44	2.30E-02	0.60	1.94E-02

Supplementary table 8 – Gene enrichment analysis on overlapping genes with similar direction of effect between the subchondral bone and the articular cartilage (N= 305 genes).

Category	Term	Count	%	Genes	FDR
Cellular Component	GO:0005615~extracellular space	37	12	WNT16, CRLF1, VCAN, DKK3, CHRDL2, FAP, DLG3, WNT11, IL11, CCN4, OGN, TPI1, FRMD4B, SPP1, TNFSF11, TNFAIP6, OMD, POSTN, CD63, GGH, LUM, MANF, LGI4, SEMA3D, GDF6, SCUBE1, FRZB, COL6A3, FSTL1, HTRA1, GPRC5B, ERFE, GPC5, RELN, SPOCK3, S100A4, GPX3	4.42E-03
Cellular Component	GO:0005576~extracellular region	36	12	WNT16, CRLF1, VCAN, DKK3, WNT11, IL11, FGF14, OGN, TNR, SPP1, TNFSF11, CRISPLD1, OMD, CALU, FGF13, SPATA6, PDZD2, NGF, FST, LUM, ADAM12, PAMR1, CRIM1, LGI4, GDF6, FRZB, COL6A3, FSTL1, HTRA1, THBS3, HTRA3, ERFE, GPC5, PLAC9, CD55, GPX3	4.56E-03
Cellular Component	GO:0005578~proteinaceous extracellular matrix	17	6	WNT16, VCAN, WNT11, CHADL, COCH, CCN4, OGN, ASPN, TNR, OMD, POSTN, LUM, ADAMTS17, COL6A3, GPC5, RELN, SPOCK3	7.98E-03

2

Supplementary table 9 (partially) – Significantly differentially expressed genes in OA knee subchondral bone.
Top 50 most significantly differentially expressed genes in knee subchondral bone are shown here, the rest of the table can be found online: https://doi.org/10.1002/art.41600

Ensembl gene ID	Gene	P-value	FDR	Log 2 fold change	Fold change
ENSG00000162998	FRZB	3.07E-12	5.13E-08	-1.05	0.48
ENSG00000174469	CNTNAP2	4.05E-10	3.38E-06	1.54	2.90
ENSG00000054938	CHRDL2	7.41E-10	4.13E-06	-3.47	0.09
ENSG00000116285	ERRFI1	1.61E-09	6.70E-06	0.68	1.60
ENSG00000157103	SLC6A1	3.77E-09	1.16E-05	-0.76	0.59
ENSG00000178445	GLDC	4.16E-09	1.16E-05	1.78	3.44
ENSG00000113594	LIFR	1.96E-08	4.68E-05	0.43	1.34
ENSG00000179399	GPC5	3.64E-08	7.59E-05	-1.36	0.39
ENSG00000198918	RPL39	4.15E-08	7.71E-05	0.42	1.34
ENSG00000115616	SLC9A2	4.72E-08	7.88E-05	1.75	3.35
ENSG00000102466	FGF14	5.51E-08	7.97E-05	-1.41	0.38
ENSG00000151025	GPR158	5.73E-08	7.97E-05	1.34	2.54
ENSG00000223561	AC005165.1	7.31E-08	9.39E-05	-1.31	0.40
ENSG00000257017	HP	9.28E-08	1.11E-04	1.79	3.46
ENSG00000154783	FGD5	1.17E-07	1.23E-04	-0.40	0.76
ENSG00000145934	TENM2	1.22E-07	1.23E-04	0.72	1.64
ENSG00000130158	DOCK6	1.26E-07	1.23E-04	-0.45	0.73
ENSG00000229847	EMX2OS	1.45E-07	1.34E-04	-1.52	0.35
ENSG00000106511	MEOX2	1.56E-07	1.34E-04	-0.51	0.70
ENSG00000168685	IL7R	1.64E-07	1.34E-04	1.07	2.10
ENSG00000171517	LPAR3	1.75E-07	1.34E-04	1.11	2.15
ENSG00000175161	CADM2	1.81E-07	1.34E-04	-1.46	0.36
ENSG00000002745	WNT16	1.85E-07	1.34E-04	2.39	5.23
ENSG00000144057	ST6GAL2	2.31E-07	1.61E-04	2.29	4.88
ENSG00000249306	LINC01411	2.54E-07	1.70E-04	2.65	6.27
ENSG00000104435	STMN2	2.74E-07	1.76E-04	4.52	23.00
ENSG00000159307	SCUBE1	3.10E-07	1.92E-04	-0.92	0.53
ENSG00000144867	SRPRB	3.95E-07	2.36E-04	0.51	1.43
ENSG00000187244	BCAM	4.10E-07	2.36E-04	-0.61	0.66
ENSG00000169871	TRIM56	4.26E-07	2.37E-04	-0.36	0.78
ENSG00000110237	ARHGEF17	6.59E-07	3.55E-04	-0.39	0.76
ENSG00000123610	TNFAIP6	6.95E-07	3.63E-04	1.17	2.26
ENSG00000148400	NOTCH1	8.50E-07	4.30E-04	-0.65	0.64

Ensembl gene ID	Gene	P-value	FDR	Log 2 fold change	Fold change
ENSG00000232044	SILC1	9.27E-07	4.55E-04	1.19	2.28
ENSG00000138829	FBN2	1.13E-06	5.37E-04	1.01	2.02
ENSG00000146830	GIGYF1	1.18E-06	5.49E-04	-0.33	0.80
ENSG00000074181	NOTCH3	1.27E-06	5.74E-04	-0.61	0.66
ENSG00000150938	CRIM1	1.42E-06	6.22E-04	-0.55	0.68
ENSG00000196104	SPOCK3	1.81E-06	7.25E-04	-2.43	0.19
ENSG00000159200	RCAN1	1.81E-06	7.25E-04	0.57	1.49
ENSG00000171714	ANO5	1.82E-06	7.25E-04	0.92	1.89
ENSG00000134014	ELP3	1.82E-06	7.25E-04	0.22	1.17
ENSG00000107719	PALD1	2.21E-06	8.59E-04	-0.34	0.79
ENSG00000125869	LAMP5	2.31E-06	8.63E-04	0.92	1.90
ENSG00000066056	TIE1	2.33E-06	8.63E-04	-0.40	0.76
ENSG00000162105	SHANK2	2.60E-06	9.45E-04	-1.10	0.47
ENSG00000166426	CRABP1	2.82E-06	9.84E-04	1.54	2.91
ENSG00000140464	PML	2.83E-06	9.84E-04	-0.37	0.78
ENSG00000172986	GXYLT2	3.32E-06	1.10E-03	0.69	1.61

2

Ensembl gene ID	Gene	P-value	FDR	Log 2 fold change	Fold change
ENSG00000249306	LINC01411	2.54E-07	1.70E-04	2.65	6.27
ENSG00000072041	SLC6A15	4.09E-06	1.22E-03	-1.73	0.30
ENSG00000113263	ITK	9.38E-06	1.76E-03	0.58	1.49
ENSG00000196787	HIST1H2AG	9.75E-06	1.76E-03	0.58	1.50
ENSG00000275221	HIST1H2AK	1.18E-05	1.90E-03	0.58	1.49
ENSG00000101057	MYBL2	1.20E-05	1.91E-03	1.07	2.10
ENSG00000122966	CIT	1.24E-05	1.93E-03	0.51	1.43
ENSG00000274997	HIST1H2AH	1.37E-05	1.98E-03	0.55	1.47
ENSG00000278272	HIST1H3C	1.64E-05	2.19E-03	0.84	1.79
ENSG00000138160	KIF11	1.89E-05	2.39E-03	0.68	1.60
ENSG00000100593	ISM2	1.91E-05	2.39E-03	1.77	3.40
ENSG00000162739	SLAMF6	2.05E-05	2.47E-03	0.79	1.73
ENSG00000169679	BUB1	2.50E-05	2.81E-03	0.79	1.73
ENSG00000090382	LYZ	2.56E-05	2.82E-03	0.64	1.56
ENSG00000277224	HIST1H2BF	2.59E-05	2.83E-03	0.58	1.49
ENSG00000253141	AC008632.1	2.76E-05	2.91E-03	-1.68	0.31
ENSG00000019505	SYT13	2.81E-05	2.92E-03	2.33	5.04
ENSG00000185730	ZNF696	2.81E-05	2.92E-03	-0.39	0.77
ENSG00000136167	LCP1	3.09E-05	2.98E-03	0.45	1.37
ENSG00000158481	CD1C	3.08E-05	2.98E-03	0.69	1.61
ENSG00000274267	HIST1H3B	3.20E-05	3.05E-03	0.75	1.69
ENSG00000205268	PDE7A	4.93E-05	4.07E-03	0.39	1.31
ENSG00000184357	HIST1H1B	5.70E-05	4.40E-03	0.61	1.53
ENSG00000171388	APLN	5.81E-05	4.43E-03	-0.51	0.70
ENSG00000126787	DLGAP5	5.91E-05	4.44E-03	1.23	2.35
ENSG00000276410	HIST1H2BB	7.06E-05	4.89E-03	0.57	1.49
ENSG00000117724	CENPF	7.62E-05	5.07E-03	0.71	1.64
ENSG00000125354	SEPT6	7.86E-05	5.10E-03	0.30	1.23
ENSG00000197635	DPP4	8.10E-05	5.20E-03	0.76	1.69
ENSG00000131747	TOP2A	8.28E-05	5.28E-03	0.77	1.71
ENSG00000130812	ANGPTL6	9.02E-05	5.54E-03	1.34	2.53
ENSG00000131475	VPS25	9.78E-05	5.90E-03	0.26	1.19
ENSG00000197153	HIST1H3J	1.15E-04	6.24E-03	0.94	1.91

Ensembl gene ID	Gene	P-value	FDR	Log 2 fold change	Fold change
ENSG00000169385	RNASE2	1.18E-04	6.35E-03	1.22	2.33
ENSG00000273703	HIST1H2BM	1.21E-04	6.48E-03	0.91	1.88
ENSG00000105639	JAK3	1.24E-04	6.57E-03	0.54	1.45
ENSG00000049540	ELN	1.40E-04	7.03E-03	-0.55	0.68
ENSG00000140157	NIPA2	1.59E-04	7.49E-03	0.33	1.26
ENSG00000273983	HIST1H3G	1.60E-04	7.49E-03	0.88	1.84
ENSG00000172575	RASGRP1	1.64E-04	7.54E-03	0.60	1.51
ENSG00000197057	DTHD1	1.68E-04	7.55E-03	0.97	1.95
ENSG00000103145	HCFC1R1	1.78E-04	7.74E-03	0.30	1.23
ENSG00000085265	FCN1	1.85E-04	7.75E-03	0.55	1.47
ENSG00000128641	MYO1B	1.84E-04	7.75E-03	0.39	1.31
ENSG00000139734	DIAPH3	1.82E-04	7.75E-03	1.05	2.07
ENSG00000118193	KIF14	2.03E-04	8.28E-03	0.73	1.66
ENSG00000266524	GDF10	2.11E-04	8.40E-03	-0.79	0.58
ENSG00000076685	NT5C2	2.23E-04	8.62E-03	0.19	1.14
ENSG00000182566	CLEC4G	2.22E-04	8.62E-03	0.99	1.99

2

Chapter 2

Supplementary table 11 (partially) – Gene enrichment analysis on genes exclusively differentially expressed in knee OA subchondral bone samples (N=509 genes).
The five most significant processes are shown here, the rest of the table can be found in the online supplement: https://doi.org/10.1002/art.41600

Category	Term	Count	%	Genes	FDR
Biological process	GO:0006334~nucleosome assembly	15	3.0	HIST1H1B, H1FX, HIST1H2BL, HIST1H3J, HIST1H4K, HIST1H2BM, HIST1H3G, HIST1H3B, HIST1H2BH, HIST1H2BB, HIST1H2BF, HIST1H3F, HIST1H3C, HIST1H2BI, HIST1H3H	2.91E-03
Biological process	GO:0060968~regulation of gene silencing	6	1.2	HIST1H3J, HIST1H3G, HIST1H3B, HIST1H3F, HIST1H3C, HIST1H3H	1.90E-02
Cellular component	GO:0000786~nucleosome	20	4.1	HIST1H1B, H1FX, HIST1H2BL, HIST1H2AG, HIST1H3J, HIST1H4K, HIST1H2BM, HIST1H3G, HIST1H3B, HIST1H2AH, HIST1H2AK, HIST1H2BH, HIST1H2AJ, HIST1H2BB, HIST1H2BF, HIST1H3F, HIST1H3C, HIST1H2AB, HIST1H2BI, HIST1H3H	1.81E-09
Cellular component	GO:0000788~nuclear nucleosome	12	2.4	HIST1H2BL, HIST1H3J, HIST1H2BM, HIST1H3G, HIST1H3B, HIST1H2BH, HIST1H2BB, HIST1H2BF, HIST1H3F, HIST1H3C, HIST1H2BI, HIST1H3H	4.37E-06
Reactome pathway	R-HSA-2299718:Condensation of Prophase Chromosomes	17	3.5	PLK1, CDK1, HIST1H2BL, HIST1H3J, HIST1H4K, HIST1H2BM, HIST1H3G, HIST1H3B, HIST1H2AJ, HIST1H2BB, HIST1H2BF, HIST1H3F, HIST1H3C, HIST1H2AB, HIST1H2BI, HIST1H3H	2.52E-07

Supplementary table 12 - Differentially expressed genes in hip samples selected on their nominal p-value.

Ensembl gene ID	Gene Name	P-value	Log 2 fold change	Fold change
ENSG00000064886	CHI3L2	5.08E-05	1.047	2.07
ENSG00000120738	EGR1	1.17E-04	-1.367	0.39
ENSG00000106809	OGN	5.06E-04	2.646	6.26
ENSG00000279407	AC007191.1	4.39E-03	-1.292	0.41
ENSG00000143512	HHIPL2	7.41E-03	1.515	2.86
ENSG00000131459	GFPT2	7.63E-03	1.199	2.30
ENSG00000169884	WNT10B	8.43E-03	1.236	2.35
ENSG00000139219	COL2A1	8.72E-03	2.514	5.71
ENSG00000162105	SHANK2	1.14E-02	-1.350	0.39
ENSG00000100302	RASD2	1.18E-02	-1.602	0.33
ENSG00000280800	FP671120.4	1.34E-02	-1.827	0.28
ENSG00000167094	TTC16	1.35E-02	-1.306	0.40
ENSG00000180389	ATP5F1EP2	1.60E-02	1.131	2.19
ENSG00000260105	AOC4P	2.09E-02	-1.706	0.31
ENSG00000006016	CRLF1	2.27E-02	1.232	2.35
ENSG00000279662	AC131649.2	2.72E-02	-1.192	0.44
ENSG00000149380	P4HA3	2.95E-02	0.997	2.00
ENSG00000261026	AC105046.1	3.09E-02	-1.338	0.40
ENSG00000004948	CALCR	3.12E-02	-1.223	0.43
ENSG00000125740	FOSB	3.32E-02	-1.696	0.31
ENSG00000275765	AC091982.3	3.42E-02	1.048	2.07
ENSG00000283199	C13orf46	3.51E-02	-1.227	0.43
ENSG00000267653	AC002546.1	3.63E-02	-1.214	0.43
ENSG00000106819	ASPN	3.65E-02	1.770	3.41
ENSG00000233013	FAM157B	3.73E-02	-1.144	0.45
ENSG00000116147	TNR	3.75E-02	-1.052	0.48
ENSG00000139292	LGR5	4.27E-02	-1.454	0.36
ENSG00000095752	IL11	4.43E-02	2.253	4.77
ENSG00000253132	IGHV3-62	4.79E-02	1.064	2.09

Supplementary table 13 - Significant differentially expressed genes exclusive for hip OA subchondral bone

Ensembl gene ID	Gene Name	P-value	Log 2 Fold Change	Fold Change
ENSG00000004948	CALCR	3.12E-02	-1.22	0.43
ENSG00000120738	EGR1	1.17E-04	-1.37	0.39
ENSG00000125740	FOSB	3.32E-02	-1.70	0.31
ENSG00000139292	LGR5	4.27E-02	-1.45	0.36
ENSG00000167094	TTC16	1.35E-02	-1.31	0.40
ENSG00000233013	FAM157B	3.73E-02	-1.14	0.45
ENSG00000260105	AOC4P	2.09E-02	-1.71	0.31
ENSG00000261026	AC105046.1	3.09E-02	-1.34	0.40
ENSG00000279407	AC007191.1	4.39E-03	-1.29	0.41
ENSG00000279662	AC131649.2	2.72E-02	-1.19	0.44
ENSG00000280800	FP671120.4	1.34E-02	-1.83	0.28
ENSG00000283199	C13orf46	3.51E-02	-1.23	0.43
ENSG00000131459	GFPT2	7.63E-03	1.20	2.30
ENSG00000139219	COL2A1	8.72E-03	2.51	5.71
ENSG00000143512	HHIPL2	7.41E-03	1.52	2.86
ENSG00000180389	ATP5F1EP2	1.60E-02	1.13	2.19
ENSG00000253132	IGHV3-62	4.79E-02	1.06	2.09
ENSG00000275765	AC091982.3	3.42E-02	1.05	2.07

Supplementary table 14 - Validation and replication of the RNAseq findings. The preserved samples are set as the reference.

Genes	RNAseq (N=18 samples)			Validation (N=10 technial replicates)			Replication (N=10 biological replicates)		
	β	FC	FDR	β	FC	Pval	β	FC	Pval
FRZB	-6.97	0.48	5.13E-08	-1.82	0.28	2.00E-06	-2.27	0.27	4.10E-05
CHRDL2	-6.16	0.09	4.13E-06	-3.46	0.08	1.00E-03	-3.93	0.10	2.00E-03
POSTN	3.89	2.55	5.99E-03	2.32	5.01	2.93E-04	2.52	3.37	5.00E-04
ASPN	3.52	3.10	1.24E-02	2.33	5.04	1.40E-02	2.21	2.34	1.00E-03
CNTNAP2	6.25	2.90	3.38E-06	1.38	2.60	1.60E-02	1.17	2.14	3.10E-02
STMN2	5.14	23.0	1.76E-04	3.04	7.86	1.20E-02	4.52	9.33	5.77E-07
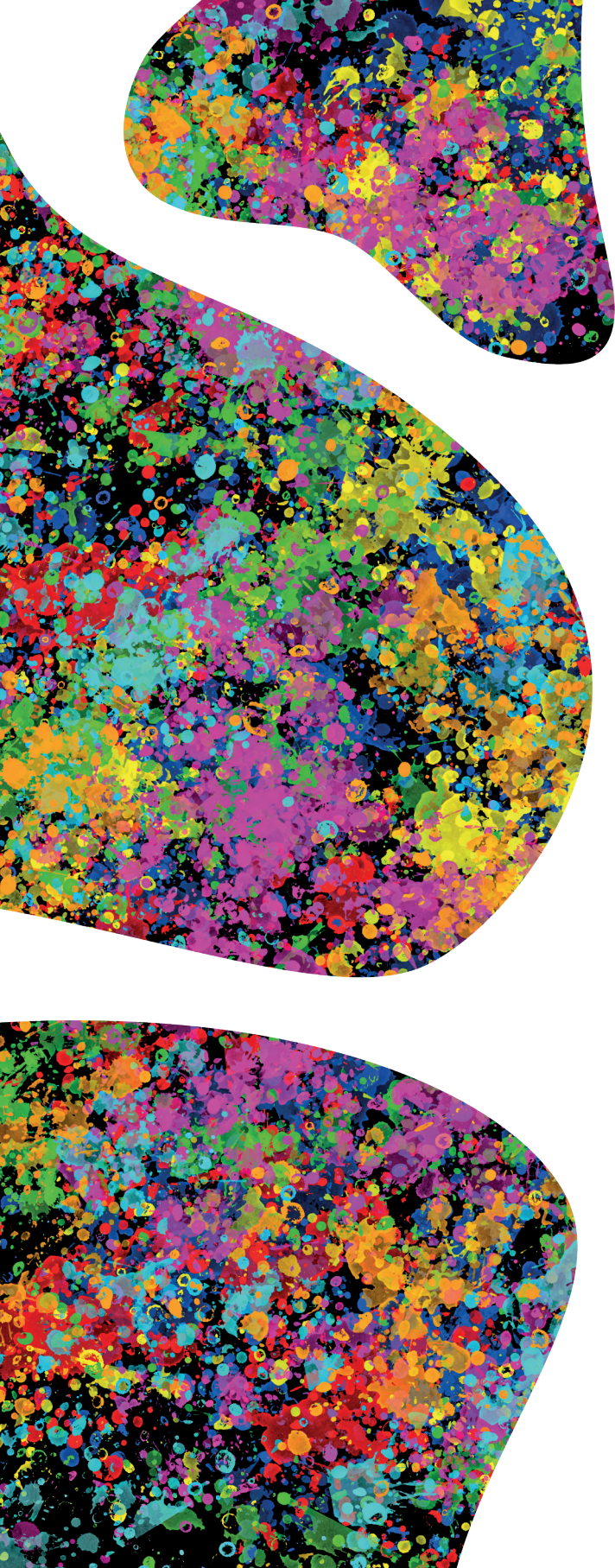
CHAPTER 3

Long non-coding RNA expression profiling of subchondral bone reveals AC005165.1 modifying FRZB expression during osteoarthritis

Margo Tuerlings[1], Marcella van Hoolwerff[1], Evelyn Houtman[1], H. Eka D. Suchiman[1], Nico Lakenberg[1], Hailiang Mei[1], Enrike H.M.J. van der Linden[2], Rob G.H.H. Nelissen[2], Yolande F.M. Ramos[1], Rodrigo Coutinho de Almeida[1], Ingrid Meulenbelt[1]

[1] Dept. of Biomedical Data Sciences, Leiden University Medical Center, Leiden, The Netherlands.
[2] Dept. Orthopaedics Leiden University Medical Center, Leiden, The Netherlands.

Abstract

Objective: To gain insight in the expression profile of long non-coding RNAs (lncRNAs) in OA subchondral bone.

Methods: RNA sequencing data of macroscopically preserved and lesioned OA subchondral bone of patients that underwent joint replacement surgery due to OA (N=22 pairs; 5 hips, 17 knees, RAAK-study) was run through an in-house pipeline to detect expression of lncRNAs. Differential expression analysis between preserved and lesioned bone was performed. Spearman correlations were calculated between differentially expressed lncRNAs and differentially expressed mRNAs identified previously in the same samples. Primary osteogenic cells were transfected with Locked nucleic acid (LNA) GapmeRs targeting *AC005165.1* lncRNA, to functionally investigate its potential mRNA targets.

Results: In total, 2816 lncRNAs were well-expressed in subchondral bone and we identified 233 lncRNAs exclusively expressed in knee and 307 lncRNAs exclusively in hip. Differential expression analysis, using all samples (N=22 pairs; 5 hips, 17 knees), resulted in 21 differentially expressed lncRNAs (false discovery rate (FDR)<0.05, Fold change (FC) range:1.19-7.39), including long intergenic non-protein coding RNA (LINC) 1411 (*LINC01411,* FC=7.39, FDR=2.20×10^{-8}), *AC005165.1* (FC=0.44, FDR=2.37×10^{-6}), and embtyp spiracles homeobox 2 opposite strand RNA (*EMX2OS,* FC=0.41, FDR=7.64×10^{-3}). Among the differentially expressed lncRNAs, five were also differentially expressed in articular cartilage, including *AC005165.1,* showing similar direction of effect. Downregulation of *AC005165.1* in primary osteogenic cells resulted in consistent downregulation of highly correlated frizzled related protein (*FRZB*).

Conclusion: The current study identified a novel lncRNA, *AC005165.1,* being dysregulated in OA articular cartilage and subchondral bone. Downregulation of *AC005165.1* caused a decreased expression of OA risk gene *FRZB*, an important member of the wnt pathway, suggesting that *AC005165.1* could be an attractive potential therapeutic target with effects in articular cartilage and subchondral bone.

Introduction

OA is a highly prevalent degenerative joint disease, characterised by articular cartilage degradation and subchondral bone remodelling [1-3]. Since OA is now considered a disease of the whole joint, recently focus has shifted towards characterization of gene expression profiles in OA synovium and subchondral bone [4, 5]. In this respect, we reported on mRNA expression profiling of OA subchondral bone of knee and hip joints [6]. We observed clustering of the samples based on joint site, suggesting distinct subchondral bone OA pathophysiological processes. This indicates that future therapeutic strategies particularly targeting bone should consider such differences between joint sites.

Different epigenetic mechanisms are described in OA, each of them modifying gene expression upon environmental cues such as mechanical stress or disease, without changing the genetic code. Among these, DNA methylation, histone modifications and miRNA expression are most frequently studied in OA articular cartilage [1, 7-11]. In contrast, the role of long non-coding RNAs (lncRNAs) with OA pathophysiology is less explored as they show poor conservation between species [9]. LncRNAs are typically defined as RNAs >200 nucleotides in length, with little or no coding potential, and they are known to be involved in various transcriptional and (post-)translational processes, such as chromatin remodelling, mRNA/protein stabilization, production of short interfering RNAs (siRNAs) and recruitment of scaffolding proteins, or they might act as pseudogenes [12, 13]. Moreover, the expression of lncRNAs can be highly tissue- and disease specific [14, 15]. Due to the fact that OA is a disease of the whole joint, it is of added value to identify disease specific lncRNAs that are expressed in various tissues involved in the OA pathophysiology, since these lncRNAs might serve as a potential druggable target with effects in several disease-relevant tissues.

Upon applying an in-house developed pipeline to reliably detect lncRNAs from RNA sequencing, we recently reported on the characterization of lncRNAs in OA cartilage. Notably, we identified prolyl 3-hydroxylase 2 antisense (*P3H2-AS1*) as being differentially expressed between macroscopically preserved and lesioned OA cartilage and this was shown to regulate prolyl 3-hydroxylase 2 (*P3H2*) in *cis* [16]. Ajekigbe et al. [17] also reported on the expression levels of lncRNAs in OA cartilage, identifying among others *LINC01411* and *AC003090.1* as being differentially expressed between intact and damage OA cartilage from knees. Furthermore, Sun et al. [14] summarized the findings on the identification of lncRNAs involved in osteogenesis, such as maternally expressed 3 (*MEG3*), metastasis associated lung adenocarcinoma transcript 1 (*MALAT1*), and differentiation antagonizing non-protein coding RNA (D*ANCR*)*.* To our knowledge, however, there are no studies yet focussing on the characterization of

lncRNA expression profiles with ongoing OA in subchondral bone.

In the current study, we set out to characterize the lncRNA expression profile in subchondral bone using RNA sequencing data of patients that underwent joint replacement surgery due to OA (RAAK study). First, joint-specific lncRNAs expressed in OA subchondral bone were identified. Differential expression analysis comparing macroscopically preserved and lesioned OA bone (N=22 paired samples) was then performed to identify robust differentially expressed lncRNAs. To investigate the role of the differentially expressed lncRNAs identified herein with OA pathophysiology, we correlated the expression levels of these lncRNAs with the expression levels of our previously identified differentially expressed mRNAs in subchondral bone of the same patients [6]. Finally, we functionally investigated the effect of a specific lncRNA on mRNA expression levels in primary osteogenic cells.

Methods

Sample description

The current study includes N=41 participants of the RAAK study [2], who underwent a joint replacement surgery due to OA (**Supplementary Table 1**). Macroscopically preserved and lesioned subchondral bone were collected from the joints of 37 of the 41 participants, for either RNA-sequencing (N=22) or replication by means of reverse transcriptase-quantitative PCR (RT-qPCR) (N=15) (**Supplementary Table 1A-1B)**. Osteogenic cells were collected from 4 of the 41 participants (**Supplementary Table 1C**). The classification of macroscopically preserved and lesioned OA subchondral bone was based on its preserved and lesioned classified overlying cartilage as described previously [2]. The results reported here were compared to our recently reported results on the expression of lncRNAs in OA articular cartilage [16], in which 98 samples were used (65 knees, 33 hips). Of these OA articular cartilage samples, 10 paired samples did overlap with the OA subchondral bone samples, i.e. of these 10 patients we had preserved and lesioned OA articular cartilage and OA subchondral bone. Written informed consent was obtained from all participants of the RAAK study and ethical approval for the RAAK study was given by the medical ethics committee of the Leiden University Medical Center (P08.239/P19.013).

RNA sequencing

Sequencing was performed on preserved and lesioned OA subchondral on the Illumina HiSeq4000 (San Francisco, California, USA). Detailed information on the RNA isolation, alignment, mapping, and filtering on lncRNAs is available in the **Supplementary methods**. To identify outliers, principal component analysis and hierarchical clustering

on the samples was applied. Three extreme outliers were identified (**Supplementary Figure 1**) and upon performing sensitivity analysis, these outliers were removed from the dataset. Finally, non-paired samples were removed from the dataset resulting in 22 paired samples (N=17 paired knee samples, N=5 paired hip samples) for further analysis, of which 10 paired samples were overlapping with the cartilage samples of our previous study [16].

LncRNA expression
To identify the lncRNAs that are expressed in subchondral bone, we filtered the lncRNAs identified by our in-house pipeline on a minimal average read count of four and a minimal count of two in at least 80% of the samples, indicated as robustly expressed. Cluster analysis was based on Euclidean distance and a heatmap was created using the lncRNAs that were expressed in the total dataset, the knee dataset, and the hip dataset.

Differential expression analysis
Prior to the differential expression analysis, the lncRNAs were filtered on a minimum average read counts of 4 to allow variation. Differential expression analysis was performed between preserved and lesioned OA subchondral bone. The results were validated and replicated by means of RT-qPCR. Additional information is available in the **Supplementary Methods**.

Correlation analysis
Correlation between the expression levels of previously identified differentially expressed mRNAs in subchondral bone [6] and the expression levels of the here identified differentially expressed lncRNAs in subchondral bone was calculated using a Spearman correlation. Additional information is available in the **Supplementary Methods**.

Functional validation of AC005165.1
Primary osteogenic cells were isolated from the OA joints (**Supplementary Table 1C**), resulting in isolation of a mixture of bone cells, which was characterized by measuring osteogenic and chondrogenic markers (**Supplementary Figure 2**). Subsequently, osteogenic cells were transfected with antisense locked nucleic acid (LNA) GapmeRs (Qiagen, Hilden, Germany) targeting *AC005165.1* or GapmeR negative control. RT-qPCR was performed to measure gene expression levels. Additional information is available in **Supplementary methods**.

Data availability
The RNA-sequencing data is deposited at the European Genome-Phenome Archive

(accession number: EGAS00001004476).

A complete overview of the approach applied to identify lncRNAs being expressed in subchondral bone is shown in **Figure 1A**. An overview of the approach applied on identification of differential expressed lncRNAs with OA pathophysiology is shown in **Figure 1B**.
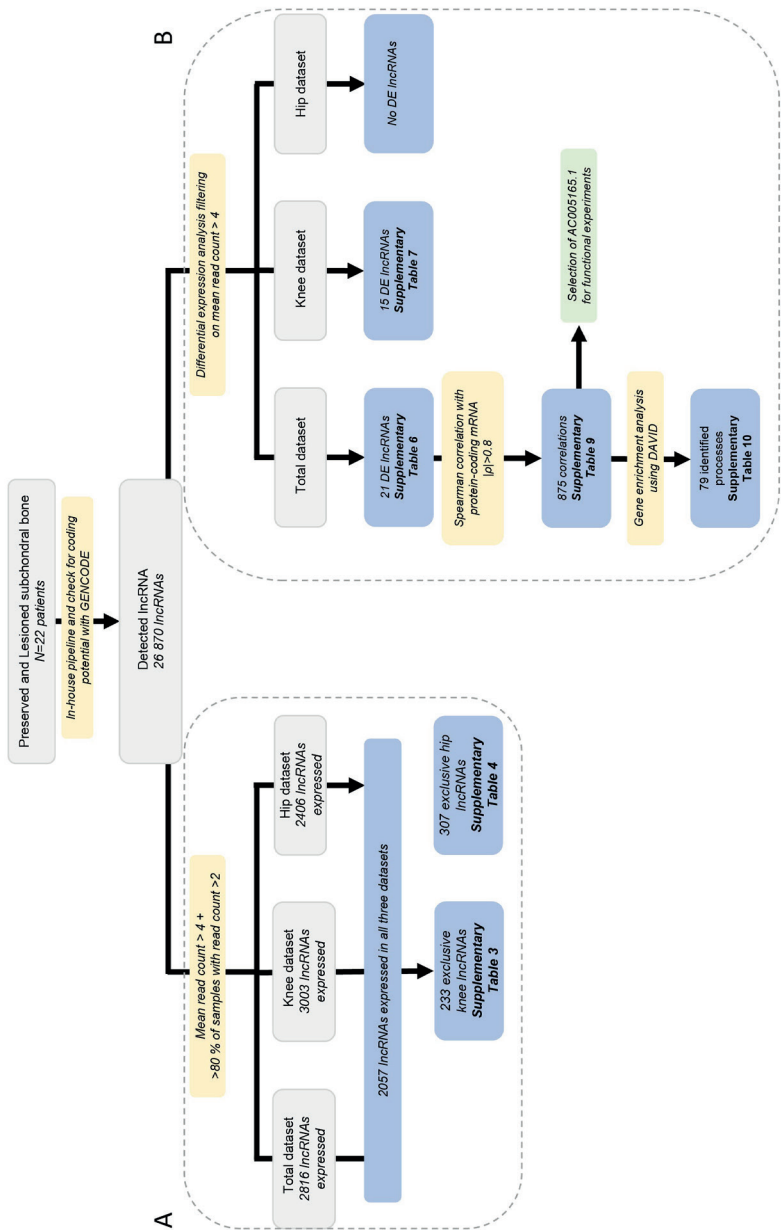
Results

Expression of lncRNAs in OA subchondral bone

Initially, we explored the expression profile of lncRNAs in OA subchondral bone (**Figure 1A**). We applied our in house pipeline [16] on an RNA sequencing dataset of 22 paired samples (5 hips, 17 knees, **Supplementary Table 1A**) of macroscopically lesioned and preserved OA subchondral bone. Henceforth, we filtered on a minimal average read count of four and a minimal count of two in at least 80% of the samples, and we identified 2816 lncRNAs robustly expressed in OA subchondral bone.

Since we observed major differences in mRNA expression levels between knee and hip OA subchondral bone in our previous study [6], we also explored lncRNA expression patterns in knee and hip subchondral bone separately, while including both preserved and lesioned samples. As shown in **Figure 2**, we identified 2057 overlapping lncRNAs commonly expressed in the hip, knee, and total datasets (mean counts between 4.02 and 3.40×10^5; **Supplementary Table 2**). Moreover, we identified 233 exclusive knee lncRNAs (mean counts between 4.0 and 23; **Supplementary Table 3**) and 307 exclusive hip lncRNAs (mean counts between 4.0- 892; **Supplementary Table 4**).

To investigate differences in expression levels of commonly expressed lncRNAs in knee and hip subchondral bone samples (N=2057 lncRNAs, **Figure 2**), we performed cluster analysis based on these commonly expressed lncRNAs using the Euclidian distance (**Figure 3**). We observed, similar to the mRNA profile of subchondral bone, clustering of lncRNA expression profiles based on joint site. To investigate which lncRNAs are most contributing to this clustering, we performed differential expression analysis between the two clusters, with the hip cluster set as a reference. More specifically, we found 1069 lncRNAs being significantly differentially expressed between the two clusters (**Supplementary Table 5**). The lncRNAs showing the highest fold difference (FD), i.e. lncRNAs highly expressed in knee samples, were *AC068724.4* (FD=158.87), *AL034397.3* (FD=157.82), and *LINC02009* (FD=89.21), while the lncRNAs with the lowest FD, i.e. highly expressed in hip samples, were *AC105046.1* (FD=0.15), *TGFB2-OT1* (FD=0.21), and *LINC02328* (FD=0.21).

Figure 1 - Schematic overview of applied strategy
(A) Identification of expressed lncRNAs. (B) identification of lncRNAs differentially expressed between macroscopically preserved and lesioned OA subchondral bone. DE: differentially expressed; lncRNA: long non-coding RNA.
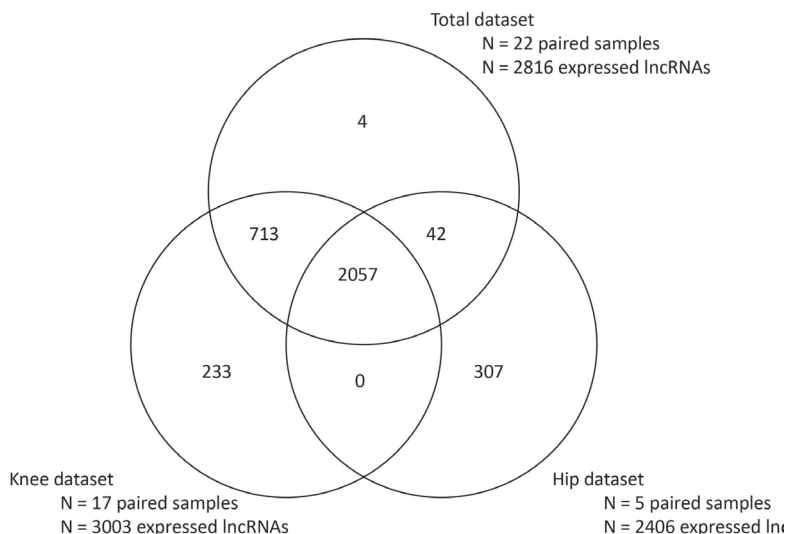

3

Total dataset
N = 22 paired samples
N = 2816 expressed lncRNAs

4

713

42

2057

233

0

307

Knee dataset
N = 17 paired samples
N = 3003 expressed lncRNAs

Hip dataset
N = 5 paired samples
N = 2406 expressed lnc

Figure 2 - Venn diagram of lncRNAs being expressed in the total, knee, and hip dataset of preserved and lesioned OA subchondral bone.

Differential expression analysis of lncRNAs in OA subchondral bone

Next, we explored lncRNAs that change expression levels with OA pathophysiology, using a slightly different selection criteria to allow more variation (**Figure 1B**). To identify robust lncRNAs that are associated with the OA pathophysiological process in subchondral bone, we filtered lncRNAs on a minimal average read count of four and we performed differential expression analysis between preserved and lesioned OA subchondral bone samples (knees and hips together). We identified 21 lncRNAs being false discovery rate (FDR) significantly differentially expressed between preserved and lesioned OA subchondral bone (**Figure 4, Supplementary Table 6**). Among these, *LINC01411* (FC=7.39, FDR=2.20×10^{-8}) showed the highest and most significant upregulation, while *AC005165.1* (FC=0.44, FDR=2.37×10^{-6}) showed the most significant downregulation and *EMX2OS* (FC=0.41, FDR=7.64×10^{-3}) the largest downregulation in lesioned compared to preserved OA subchondral bone. Differential expression analysis stratifying for joint site resulted in the identification of 15 lncRNAs being FDR significantly differentially expressed between preserved and lesioned knee samples (N=17 paired samples, **Supplementary Figure 3A**), of which cancer susceptibility 15 (*CASC15*, FC=1.48, FDR=2.67×10^{-2}) and *AL135926.1* (FC=1.70, FDR=9.92×10^{-5}) appeared to be exclusive knee lncRNAs, i.e. not significantly differentially expressed in the total nor the hip dataset (**Supplementary Table 7**). We did not find any significantly differentially expressed lncRNAs between preserved and lesioned hip samples (N=6 paired samples, **Supplementary Figure 3B**). To validate and replicate the results of the differential

Figure 3 - Heatmap of sample distance
Heatmap is based on lncRNA expression levels of lncRNAs (N = 2057) expressed in all three datasets (i.e. total, hip and knee dataset of preserved and lesioned OA subchondral bone).

expression analysis by means of RT-qPCR, we included 9 paired samples for technical validation, i.e. samples overlapping with the RNA-sequencing dataset, and 15 paired samples for biological validation, i.e. additional preserved and lesioned OA subchondral bone samples (**Supplementary Table 1B**). A selection of seven lncRNAs was measured in these samples: *LINC01411*, growth arrest specific 5 (*GAS5*), *EMX2OS*, *PVT*, *LINC01060*, sciatic injury induced lincRNA upregulator of SOX11 (*SILC1*), and *AC005165.1*. These lncRNAs showed similar directions of effect in the technical validation and the biological replication samples as compared to the direction of effect measured in the RNA-seq data, except for *EMX2OS* (**Supplementary Table 8**).

Correlation of mRNA and lncRNA in OA subchondral bone
To identify possible mRNA targets of the differentially expressed lncRNAs i.e. lncRNAs regulating mRNAs with OA pathophysiology in subchondral bones, we filtered our recently reported differentially expressed mRNAs in subchondral bone [6] for protein-coding mRNAs (N=1417 protein-coding differentially expressed mRNAs) and correlated them with expression levels of the differentially expressed lncRNAs (N=21 lncRNAs) of the same patients (N=22 paired samples). Upon prioritizing on high correlations ($-0.8 > \rho > 0.8$) and significance (FDR<0.05), we found 875 significant correlations between 16
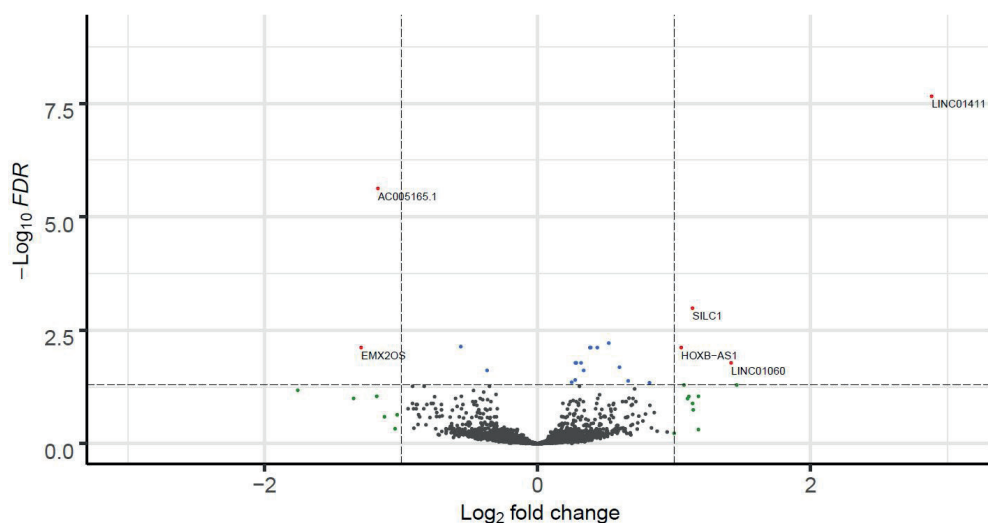
Figure 4 - Volcano plot of differentially expressed lncRNAs in OA subchondral bone.
The dots in the figure represent lncRNAs expressed in bone. Blue dots represent lncRNAs that are significantly differentially expressed, red dots represent lncRNAs that are significantly differentially expressed and have an absolute fold change of ≥2 and green dots represent the lncRNAs with an absolute fold change of ≥2 that are not significantly differentially expressed.

lncRNAs and 378 mRNAs (**Supplementary Table 9**). LncRNA small nucleolar RNA host gene 3 (*SNHG3*) showed the most interactions to mRNAs, with 174 significant correlations. In addition, the highest negative correlation was seen between *SNHG3* and *PTPRM* (ρ= -0.92), encoding Protein Tyrosine Phosphatase Receptor Type M, whereas the highest positive correlation was seen between *AC144548.1* and *ILF2* (ρ=0.92), encoding Interleukin Enhancer-binding Factor 2. Other notable interactions were those between *AC005165.1* and *FRZB* (ρ=0.85), encoding Frizzled Related Protein, and between *SILC1* and *POSTN* (ρ=0.81), encoding Periostin, which are both well-known OA genes.

To explore whether the differentially expressed lncRNAs are involved in certain processes or pathways, we performed gene enrichment analysis on their correlating mRNAs (**Supplementary Table 10**). Genes correlated to 9 out of 16 lncRNAs showed significant enrichment. The genes correlated to *AC006511.5* were enriched for Extracellular exosome (GO:0070062, FDR=3.67×10^{-4}) and Myelin sheath (GO:0043209, FDR=3.67×10^{-4}). Genes correlated to *SILC1* were significantly enriched for the GO-terms proteinaceous extracellular matrix (GO:0005578, FDR= 1.07×10^{-4}) and endoplasmic reticulum lumen (GO:0005788, FDR=4.62×10^{-2}), while for example genes correlated to *AC116533.1*, *AC245033.4* and *GAS5* were all significantly enriched for transcriptional and translational processes such as translational initiation (GO:0006413), poly(A) RNA binding (GO:0044822) and viral transcription (GO:0019083).

Functional investigation of AC005165.1

AC005165.1 was identified as the most significantly downregulated lncRNA (**Supplementary Table 6**) and, among others, it showed high correlation with well-known OA gene *FRZB* (ρ=0.85, **Supplementary Table 9**). Therefore, we selected *AC005165.1* to functionally investigate its possible mRNA targets *in vitro.* As shown in **Figure 5**, upon downregulation of *AC005165.1* (FC=0.55, *P*=0.51) by transfecting primary osteogenic cells (collected from N=4 knees) with an LNA GapmeR targeting *AC005165.1*, we observed consistent downregulation of *FRZB* (FC=0.54), which was in line with the observed positive correlation (ρ=0.85). However, the downregulation of *FRZB* did not reach statistical significance (*P*=0.08). Other mRNAs highly correlating with *AC0051651.1*, such as cysteine rich transmembrane BMP regulator 1 (*CRIM1, ρ*=0.82) and laeverin *LVRN* (ρ=-0.84), showed more donor-dependent variation upon downregulation of *AC005165.1*.

Comparison of lncRNAs between subchondral bone and articular cartilage

Since subchondral bone and the articular cartilage are interacting tissues, we used our previously published results on lncRNAs in OA articular cartilage [16] to compare the identified differentially expressed lncRNAs between preserved and lesioned OA articular cartilage and preserved and lesioned subchondral bone. First, we selected the overlapping samples of which we had RNA-seq data of subchondral bone and articular cartilage (N=10 paired samples, **Supplementary Table 1C**). As shown in **Supplementary Figure 4A**, we found 1763 exclusive subchondral bone lncRNAs, 590 exclusive cartilage lncRNAs, and 1090 lncRNAs that were expressed in both tissues (**Supplementary Table 11**). Upon comparing the here identified differentially expressed lncRNAs in subchondral bone with our previously identified differentially expressed in
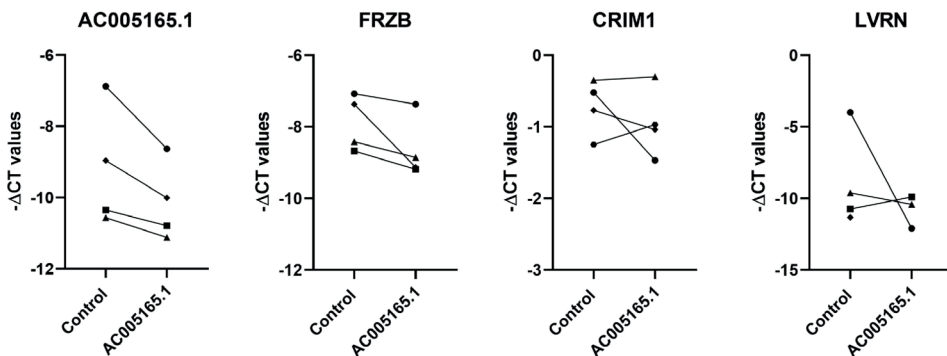

Figure 5 - Expression levels of AC005165.1, FRZB, CRIM1 and LVRN upon either transfecting primary osteogenic cells with LNA GapmeRs targeting AC005165.1 (indicated with AC005165.1) or transfecting primary osteogenic cells with a negative control (cells were collected from N = 4 knee joints).

articular cartilage [16], we found five lncRNAs being differentially expressed in both tissues: *AC005165.1*, *SILC1*, *LINC01411*, *AL590560.2* and *AC079781.5* (**Supplementary Figure 4B, Supplementary Table 12**). These five overlapping lncRNAs showed all similar directions of effect between preserved and lesioned samples in articular cartilage and subchondral bone. .

Discussion

We set out to study lncRNAs in subchondral bone as function of joint site and OA pathophysiology. In doing so, we identified 2057 lncRNAs commonly expressed in subchondral bone of hip and knee joints, 233 exclusive knee lncRNAs and 307 exclusive hip lncRNAs. Moreover, we observed additionally clustering on joint site based on level of lncRNA expression (**Figure 3**) among the commonly expressed lncRNA, signifying the difference between hip and knee OA subchondral bone pathophysiology. Differential expression analysis further identified 21 lncRNAs being differentially expressed between preserved and lesioned OA subchondral bone. Among the 21 differentially expressed lncRNAs we found *AC005165.1,* which was highly correlated to well-known OA gene *FRZB* (ρ=0.86). Upon functional investigation of *AC005165.1 in vitro* by downregulating *AC005165.1* using LNA GapmeRs, we observed a concurrent downregulation of *FRZB*. As lncRNAs tend to be highly tissue specific, lncRNAs, such as *AC005165.1*, could be attractive therapeutic OA targets with tissue specific effects.

Among the 21 differentially expressed lncRNAs, we identified *LINC01411* (FC=6.19, FDR=2.20x10^{-8}) as the most significantly and highest upregulated lncRNA, *AC005165.1* (FC=0.44, FDR=2.37x10^{-6}) as the most significantly downregulated lncRNA, and *EMX2OS* as the most downregulated lncRNA (FC=0.41, FDR=7.64x10^{-3}). The function of *LINC0411* remains unknown, however in a recent study it was found to be differentially expressed between healthy and OA articular cartilage and between healthy and OA synovium, indicating its role in OA across multiple tissues [18]. According to biotype classification of Ensembl v97 [19], *AC005165.1* was classified as a novel transcript and its function is still unknown. *AC005165.1* is genomically located at chromosome 7, with no coding genes lying within a 200-kb window. *EMX2OS* is an antisense RNA to *EMX2*, encoding Empty Spiracles Homeobox 2, which is a transcription factor crucial for the central nervous system. Multiple differentially methylated sites between preserved and lesioned OA articular cartilage have been reported in both *EMX2OS* and its antisense gene *EMX2* [20]. However, we did not find *EMX2* among the differentially expressed genes in our cartilage dataset [1] nor among the differentially expressed genes in bone [6]. Notably, we were not able to either validate or replicate the differential expression of *EMX2OS* by means of RT-qPCR, which might be due to its low expression levels and its consistency across individuals. Other notable differentially expressed lncRNAs were

GAS5 (FC=1.21, FDR=1.66x10^{-2}) and *PVT1* (FC=1.52, FDR=2.07x10^{-2}), as they both have been previously associated with OA pathophysiology [14, 17, 21].

To explore the potential targets and interactions of the 21 differentially expressed lncRNAs identified here, we calculated Spearman correlations between these lncRNAs and the previously identified differentially expressed mRNAs in the same OA subchondral bone samples and gene enrichment analysis was performed (**Supplementary Table 9, Supplementary Table 10**). *AC005165.1* was highly correlated with nine mRNAs, including *FRZB*, *CRIM1*, and *LVRN*. *FRZB* is a known OA gene and absence of FRZB in mice was previously shown to result in increased bone stiffness and increased cartilage degeneration [22]. CRIM1 is involved the TGF-β pathways by its binding to BMP-4 and BMP-7 [23], and LVRN is a metalloprotease which was previously linked to rheumatoid arthritis [24]. Despite the fact that *LINC0411* showed a higher FC than *AC005165.1*, we selected *AC005165.1* for functional investigation to see the functional relation between *AC005165.1* and the correlated mRNAs. Upon downregulation of *AC005165.1* in primary osteogenic cells, we observed consistent downregulation of *FRZB*, while *CRIM1* and *LVRN* expression levels did not change consistently. This suggests that *AC005165.1* directly or indirectly targets *FRZB* gene expression, while *CRIM1* and *LVRN* are functioning upstream of *AC005165.1*.

Similar to our mRNA expression profiling in OA subchondral bone [6], we here identified 233 exclusive knee, and 307 exclusive hip lncRNAs (**Supplementary Table 3, Supplementary Table 4**) indicating that lncRNA are not only tissue specific [14, 15], but also joint site specific. Additionally we showed (**Figure 3**) that such differences are also captured by quantitative differences in expression levels. Consecutively, we showed knee joint specific differentially expressed lncRNAs between preserved and lesioned OA subchondral bone, such as *CASC15* and *AL135926.1* (**Supplementary Table 7**). *CASC15,* which has not previously been associated to OA, is associated to cancer and involved in cell proliferation and migration [25]. *AL135926.1* was classified as novel transcript by Ensembl v97 [19] and its exact function is still unknown. However, *AL135926.1* is genomically located sense to protein-coding gene *DPT*, encoding dermatopontin, which was previously shown to inhibit BMP2 activity in mice [26]. We did not find any FDR significantly differentially expressed lncRNAs when stratifying for hip samples, which is likely due to the low sample size. Together, the here detected tissue and joint site specificity of lncRNA's qualifies them as eligible personalized therapeutic targets.

Although lncRNAs are known for their tissue specificity, we found a relatively large overlap of lncRNAs expressed in both articular cartilage and subchondral bone (N=1090 lncRNAs), which might be due to their common origin. Among the overlapping

differentially expressed between preserved and lesioned OA articular cartilage and subchondral bone, we found *AC005165.1*, making this lncRNA an attractive potential druggable target with effects in both tissues. The relative low number of differentially expressed lncRNAs identified in bone (N=21) compared to those found in cartilage (N=191) might be explained by the fact that cartilage is a single cell type tissue and subchondral bone multicellular and therefore more heterogeneous [27]. Moreover, the analysis on the subchondral bone included a lower sample size (N= 23 paired samples bone, N=32 paired samples cartilage) and stricter threshold for in- or excluding lncRNAs from the analysis.

The RNA-seq dataset that we used in this study was primarily obtained for mRNA expression profiling. Nonetheless, by applying our in-house pipeline we were able to characterize robust lncRNA expression in the same samples. It should be noted, however, that the lncRNA that entered the analyses had relatively high expression levels, while lncRNAs generally tend to be expressed at low levels [28]. To this end, we used two different selection criteria. In our initial, descriptive analyses on the lncRNA being expressed in our (knee and hip) subchondral bone samples we used more stringent selection criteria than in our pairwise differential expression analysis. This because per definition differential pairwise expression analysis is less sensitive for confounding factors. However, in future research the identification of lncRNAs associated with OA pathophysiology might be improved by increasing the sequencing depth.

In conclusion, the current study identified differences between hip and knee OA subchondral bone based on robust lncRNA expression levels. Moreover, *AC005165.1* was identified as an attractive potential therapeutic target, as it was here shown to be differentially expressed between preserved and lesioned OA subchondral bone and previously it was shown to be differentially expressed between preserved and lesioned OA articular cartilage. Furthermore, *AC005165.1* was here shown to regulate well-known OA gene *FRZB in vitro*. Finally, *AC005165.1* was not significantly differentially expressed between the hip and knee clusters, which could make *AC005165.1* a suitable druggable target in OA articular cartilage and OA subchondral bone of both hips and knees. More research is still needed to further elucidate the role and mode of action of *AC005165.1* in the OA pathophysiology. Together, this study shows that lncRNAs could bring new opportunities regarding joint tissue specific therapeutic strategies.

Declarations

Hasan, Maartje Meijer, Daisy Latijnhouwers and Geert Spierenburg for collecting the RAAK material. Moreover, data was generated within the scope of the Medical Delta programs Regenerative Medicine 4D: Generating complex tissues with stem cells and printing technology and Improving Mobility with Technology. The study was funded by the Dutch Scientific Research council NWO /ZonMW VICI scheme (nr 91816631/528), Dutch Arthritis Society (DAA-10-1-402, DAF-16-1-405).

Disclosures

The authors have declared no conflicts of interest.

References
1. Coutinho de Almeida, R., et al., RNA sequencing data integration reveals an miRNA interactome of osteoarthritis cartilage. Ann Rheum Dis, 2019. 78(2): p. 270-277.
2. Ramos, Y.F., et al., Genes involved in the osteoarthritis process identified through genome wide expression analysis in articular cartilage; the RAAK study. PLoS One, 2014. 9(7): p. e103056.
3. Dunn, S.L., et al., Gene expression changes in damaged osteoarthritic cartilage identify a signature of non-chondrogenic and mechanical responses. Osteoarthritis Cartilage, 2016. 24(8): p. 1431-40.
4. Chou, C.H., et al., Direct assessment of articular cartilage and underlying subchondral bone reveals a progressive gene expression change in human osteoarthritic knees. Osteoarthritis Cartilage, 2013. 21(3): p. 450-61.
5. Kuttapitiya, A., et al., Microarray analysis of bone marrow lesions in osteoarthritis demonstrates upregulation of genes implicated in osteochondral turnover, neurogenesis and inflammation. Ann Rheum Dis, 2017. 76(10): p. 1764-1773.
6. Tuerlings, M., et al., RNA sequencing reveals interacting key determinants of osteoarthritis acting in subchondral bone and articular cartilage. Arthritis Rheumatol, 2020.
7. Coutinho de Almeida, R., Y.F.M. Ramos, and I. Meulenbelt, Involvement of epigenetics in osteoarthritis. Best Pract Res Clin Rheumatol, 2017. 31(5): p. 634-648.
8. Reynard, L.N. and M.J. Barter, Osteoarthritis year in review 2019: genetics, genomics and epigenetics. Osteoarthritis Cartilage, 2020. 28(3): p. 275-284.
9. Rice, S.J., et al., Interplay between genetics and epigenetics in osteoarthritis. Nature Reviews Rheumatology, 2020. 16(5): p. 268-281.
10. Yang, J., et al., MiR-140 is co-expressed with Wwp2-C transcript and activated by Sox9 to target Sp1 in maintaining the chondrocyte proliferation. FEBS Lett, 2011. 585(19): p. 2992-7.
11. Endisha, H., et al., The complex landscape of microRNAs in articular cartilage: biology, pathology, and therapeutic targets. JCI Insight, 2018. 3(17).
12. Frankish, A., et al., GENCODE reference annotation for the human and mouse genomes. Nucleic Acids Res, 2019. 47(D1): p. D766-d773.
13. Marchese, F.P., I. Raimondi, and M. Huarte, The multidimensional mechanisms of long noncoding RNA function. Genome Biology, 2017. 18(1): p. 206.
14. Sun, H., et al., Emerging roles of long noncoding RNA in chondrogenesis, osteogenesis, and osteoarthritis. Am J Transl Res, 2019. 11(1): p. 16-30.
15. Quinn, J.J. and H.Y. Chang, Unique features of long non-coding RNA biogenesis and function. Nature Reviews Genetics, 2016. 17(1): p. 47-62.
16. van Hoolwerff, M., et al., Elucidating Epigenetic Regulation by Identifying Functional cis-Acting Long Noncoding RNAs and Their Targets in Osteoarthritic Articular Cartilage. Arthritis Rheumatol, 2020. 72(11): p. 1845-1854.
17. Ajekigbe, B., et al., Identification of long non-coding RNAs expressed in knee and hip osteoarthritic cartilage. Osteoarthritis Cartilage, 2019. 27(4): p. 694-702.
18. Li, C. and Z. Zheng, Identification of Novel Targets of Knee Osteoarthritis Shared by Cartilage and Synovial Tissue. Int J Mol Sci, 2020. 21(17).
19. Cunningham, F., et al., Ensembl 2019. Nucleic Acids Research, 2018. 47(D1): p. D745-D751.
20. Zhang, Y., et al., Genome-wide DNA methylation profile implicates potential cartilage regeneration at the late stage of knee osteoarthritis. Osteoarthritis and Cartilage, 2016. 24(5): p. 835-843.
21. Xing, D., et al., Identification of long noncoding RNA associated with osteoarthritis in humans. Orthop Surg, 2014. 6(4): p. 288-93.
22. Lories, R.J., et al., Articular cartilage and biomechanical properties of the long bones in Frzb-knockout mice. Arthritis Rheum, 2007. 56(12): p. 4095-103.
23. Wilkinson, L., et al., CRIM1 regulates the rate of processing and delivery of bone morphogenetic proteins to the cell surface. J Biol Chem, 2003. 278(36): p. 34181-8.
24. Haas, C.S., et al., Identification of genes modulated in rheumatoid arthritis using complementary DNA microarray analysis of lymphoblastoid B cell lines from disease-discordant monozygotic twins. Arthritis Rheum, 2006. 54(7): p. 2047-60.
25. Sheng, L. and R. Wei, Long Non-Coding RNA-CASC15 Promotes Cell Proliferation, Migration, and Invasion by Activating

Wnt/β-Catenin Signaling Pathway in Melanoma. Pathobiology, 2020. 87(1): p. 20-29.

26. Behnam, K., S.S. Murray, and E.J. Brochmann, BMP stimulation of alkaline phosphatase activity in pluripotent mouse C2C12 cells is inhibited by dermatopontin, one of the most abundant low molecular weight proteins in demineralized bone matrix. Connect Tissue Res, 2006. 47(5): p. 271-7.

27. Goldring, M.B. and S.R. Goldring, Articular cartilage and subchondral bone in the pathogenesis of osteoarthritis. Ann N Y Acad Sci, 2010. 1192: p. 230-7.

28. Jarroux, J., A. Morillon, and M. Pinskaya, History, Discovery, and Classification of lncRNAs, in Long Non Coding RNA Biology, M.R.S. Rao, Editor. 2017, Springer Singapore: Singapore. p. 1-46.

3

Supplementary data
Supplementary methods

RNA sequencing
Preserved and lesioned subchondral bone were collected from the joint and stored in liquid nitrogen. Subsequently, the subchondral bone was pulverized and homogenized in TRIzol reagent (Invitrogen, USA) using a Mixer mill 200 (Retch, Germany). Total RNA was isolated from the subchondral bone using Qiagen RNeasy Mini Kit (Qiagen, Germany). Paired-end 2×100 bp RNA-sequencing (Illumina TruSeq RNA Library Prep Kit, Illumina HiSeq4000) was performed. Strand specific RNA-seq libraries were generated which yielded a mean of 20 million reads per sample. Data from both Illumina platforms were integrated and analysed with the same in-house pipeline. The quality of the raw reads for RNA-sequencing was checked using MultiQC v1.7. [1]. The adaptors were clipped using Cutadapt v1.1 [2] applying default settings (min overlap 3, min length). RNA-seq reads were aligned using Hisat2 v.2.1.0 against GRCh38 using default parameters. The aligned reads were processed into individual transcripts by StringTie v1.3.4 [3] and potential lncRNAs were identified by mapping the transcripts to GENCODE v29 [4] and Ensembl v97 [5]. The annotation of GENCODE v34 was used to filter the transcript on coding potential.

Differential expression analysis
Differential expression analysis was then performed in two ways: between hip and knee subchondral bone samples (preserved and lesioned tissue together); and between paired lesioned and preserved subchondral bone samples. The DESeq2 R package version 1.26.0 [6] was used to apply a general linear model assuming a negative binomial distribution, followed by a paired Wald-test. The Benjamini-Hochberg method was used to correct for multiple testing, as indicated by the false discovery rate (FDR), with a significance cut-off value of 0.05. Hip samples were set as a reference in the differential expression analysis between hip and knee subchondral bone and preserved samples were set as a reference in the analysis between preserved and lesioned OA subchondral bone.

RT-qPCR validation and replication
cDNA synthesis was done using Transcriptor First Strand cDNA Synthesis Kit (Roche, Switzerland), using 400 ng of RNA (Supplementary Table 1B). RT-qPCR was performed to quantitatively determine the lncRNA expression levels. The relative gene expression was evaluated by the -ΔCT values, using GAPDH and SDHA as internal controls. Paired T-test was performed to calculate the statistical difference in -ΔCT values between the lesioned and preserved OA subchondral bone samples.

Spearman correlation and gene ontology enrichment analysis

Prior to correlation, the differentially expressed mRNAs were filtered on protein-coding mRNAs using Ensembl v97 21. The Benjamini-Hochberg method was used to correct for multiple testing, as indicated by the FDR. Correlations with an FDR below 0.05 and an absolute correlation coefficient of 0.8 or higher were considered significantly correlated. Gene ontology enrichment was performed using the online functional annotation tool DAVID, selecting for the gene ontology terms Biological Processes (GOTERM_BP_DIRECT), Cellular Component (GOTERM_CC_DIRECT) and Molecular Function (GOTERM_MF_DIRECT). Genes expressed in OA subchondral bone were used as a background in the gene ontology enrichment analysis. Gene ontology terms with an FDR<0.05 were considered significant.

Functional validation of AC005165.1

Primary osteogenic cells were isolated from the preserved subchondral bone part of OA joints as described previously [7] and expanded in 2D (Supplementary Table 1C). This osteogenic cell isolation results in a mixture of bone cells, i.e. MSCs, osteoblasts, and osteocytes. To characterize this mixture of cells, we measured osteogenic and chondrogenic markers (SPP1, COL1A1, BGLAP, COL2A1, and COMP) using RT-qPCR and we compared these expression levels to the expression levels in preserved subchondral bone (Supplementary Figure-2), showing similar expression profiles. Then, the osteogenic cells were transfected with antisense locked nucleic acid (LNA) GapmeRs (Qiagen, Hilden, Germany) targeting AC005165.1 (GATAAAACCTGTAACT) or GapmeR negative control (AACACGTCTATACGC) at 10 nM final concentration using Lipofectamine RNAiMax Transfection reagent (Invitrogen, USA) according to manufacturer's protocol. After 30 hours, the cells were lysed using TRIzol (Invitrogen, USA) for RNA isolation. cDNA synthesis and RT-qPCR were performed to measure gene expression levels.

Comparison subchondral bone and articular cartilage

LncRNA expression between subchondral bone and articular cartilage was compared in the overlapping samples (N=10 paired samples: preserved and lesioned OA cartilage and bone, Supplementary Table 1D). Mapping of the RNA sequencing data was done using different versions of Ensembl between subchondral bone (v97) and articular cartilage (v94). To be able to compare the expressed and differentially expressed lncRNAs between the two tissues, we selected the lncRNAs that were mapped with both versions.

References methods
1.   Ewels, P., et al., MultiQC: summarize analysis results for multiple tools and samples in a single report. Bioinformatics, 2016. 32(19): p. 3047-8.
2.   Martin, M., Cutadapt removes adapter sequences from high-throughput sequencing reads. 2011, 2011. 17(1): p. 3 %J EMBnet.journal.
3.   Pertea, M., et al., StringTie enables improved reconstruction of a transcriptome from RNA-seq reads. Nature

Biotechnology, 2015. 33(3): p. 290-295.
4.   Frankish, A., et al., GENCODE reference annotation for the human and mouse genomes. Nucleic Acids Res, 2019. 47(D1): p. D766-d773.
5.   Cunningham, F., et al., Ensembl 2019. Nucleic Acids Research, 2018. 47(D1): p. D745-D751.
6.   Love, M.I., W. Huber, and S. Anders, Moderated estimation of fold change and dispersion for RNA-seq data with DESeq2. Genome Biology, 2014. 15(12): p. 550.
7.   Stern, A.R., et al., Isolation and culture of primary osteocytes from the long bones of skeletally mature and aged mice. Biotechniques, 2012. 52(6): p. 361-73.

Supplementary figures
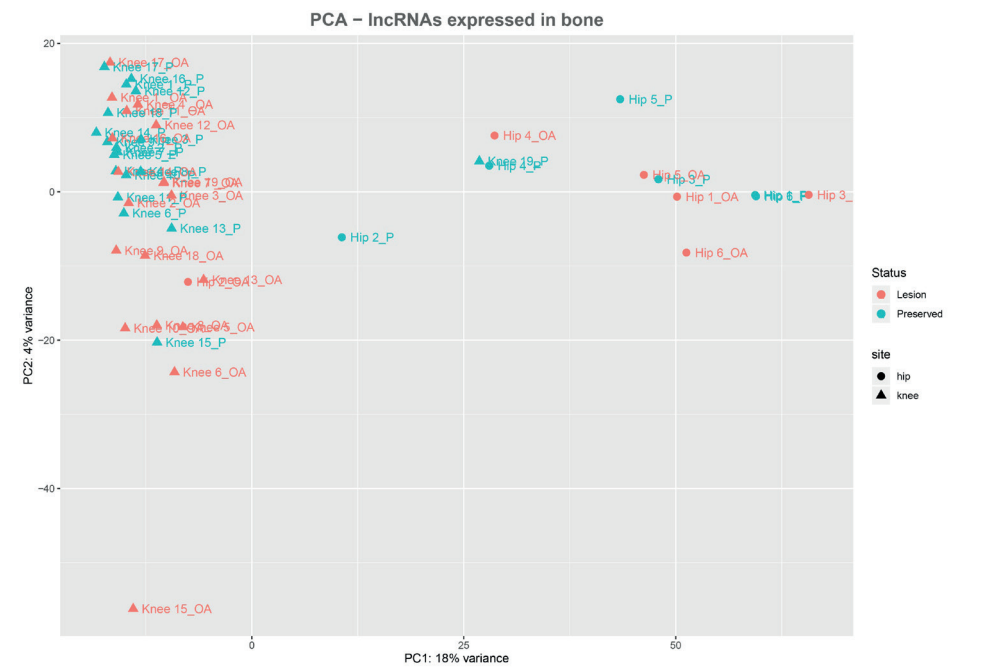
Supplementary Figure 1 – PCA in quality control identifying Knee_15, Knee_19, and Hip_2 as outliers.
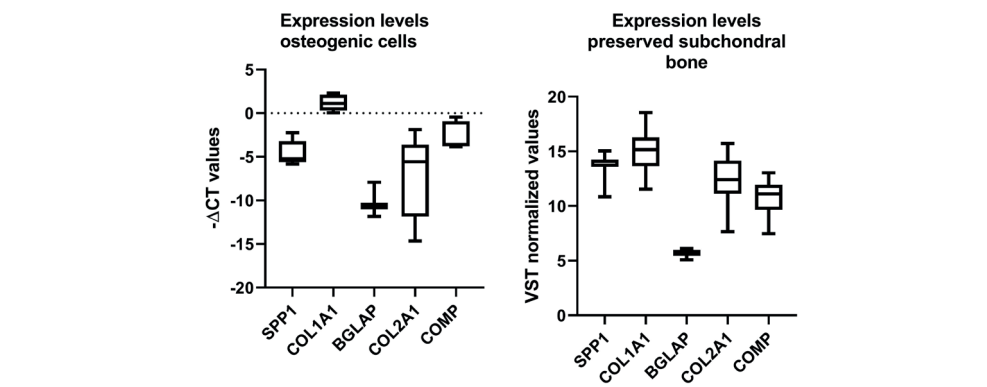
Supplementary Figure 2 – Expression levels of osteogenic and chondrogenic markers.
(A) Expression levels in -ΔCT values of the primary osteogenic cells. (B) Expression levels in VST normalized values of preserved subchondral bone.
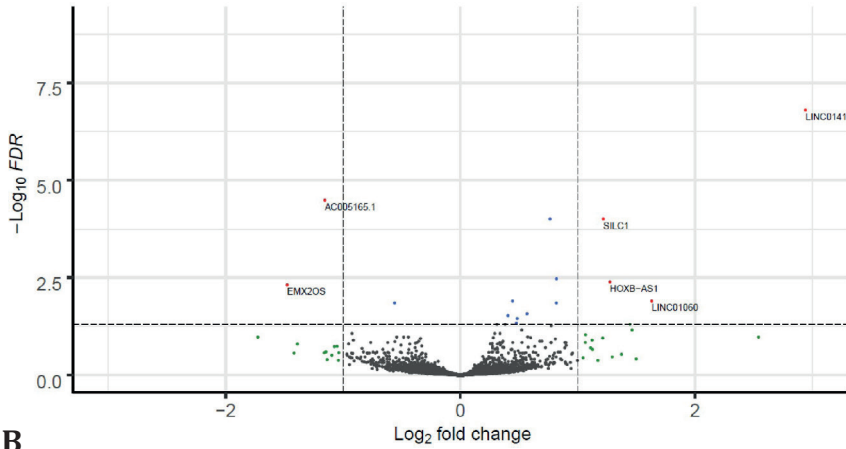
A

B
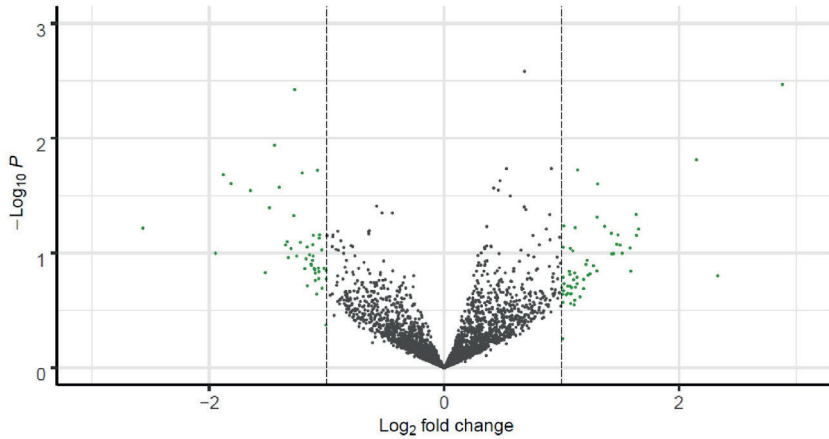
3

Supplementary Figure 3 – Volcano plot of differentially expressed lncRNAs in OA subchondral bone of knees (A) and hips (B).
The dots in the figure represent lncRNAs expressed. Blue dots represent lncRNAs that are significantly differentially expressed, red dots represent lncRNAs that are significantly differentially expressed and have an absolute fold change of 2 or higher, and green dots represent the lncRNAs with an absolute fold change of two or higher that are not significantly differentially expressed.
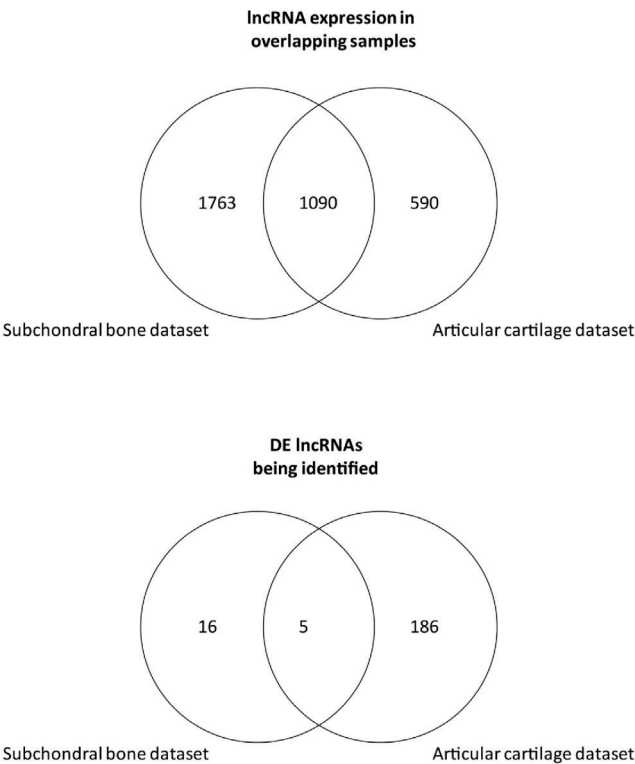
Supplementary Figure 4 – (A) Venn diagram of expressed lncRNAs in articular cartilage and subchondral bone, with 1090 lncRNAs expressed in both tissues. **(B)** Venn diagram of significantly differentially expressed lncRNAs between preserved and lesioned articular cartilage and subchondral bone, with 5 lncRNAs differentially expressed in both tissues.

Supplementary tables

Supplementary Table 1 – Baseline characteristics of material included in the current study

Supplementary Table 1A – Sample characteristics of lncRNA- and mRNA-seq data subchondral bone (N=44 samples, 22 pairs of preserved and lesioned subchondral bone)

	Hip	Knee	Total
Participants	5	17	22
Mean age	68.40	66.12	66.64
SD age	9.65	8.44	8.67
Female (%)	100.00	88.24	91.00

Supplementary Table 1B – Characteristics of samples used for technical validation (N= 18 samples, 9 pairs of preserved and lesioned subchondral bone) and biological replication (N=30 samples, 15 pairs of preserved and lesioned subchondral bone).

	Technical validation			Biological replication		
	Hip	Knee	Total	Hip	Knee	Total
Participants	-	9	9	5	10	15
Mean age	-	68.67	68.67	67.80	72.40	70.87
SD age	-	7.42	7.42	6.06	10.07	8.98
Female (%)	-	77.78	77.78	20.00	50.00	60.00

Supplementary Table 1C – Characteristics of samples used to transfect primary cells with LNA GapmeRs (N=4 participants)

	Hip	Knee
Participants	-	4
Mean age	-	67.50
SD age	-	8.10
Female (%)	-	25.00

Supplementary Table 1D – Characteristics of samples used in overlapping RNA-seq data of articular cartilage and subchondral bone (N=20 samples, 10 pairs of preserved and lesioned articular cartilage and subchondral bone)

	Hip	Knee	Total
participants	1	9	10
Mean age	56.00	67.44	66.30
SD age	-	8.81	9.05
Female (%)	100.00	88.89	90.00

Supplementary Table 2 **(partially) – LncRNAs expressed in the knee, the hip, and the total datasets of subchondral bone.**
The top 50 lncRNAs with highest expression levels in subchondral bone are shown here, the rest of the table can be found in the online supplement: https://doi.org/10.1093/rheumatology/keab826

Ensembl ID	lncRNA	Mean Expression
ENSG00000282885	AL627171.2	340390.89
ENSG00000259001	AL355075.4	48251.77
ENSG00000269900	RMRP	42482.57
ENSG00000251562	MALAT1	38905.93
ENSG00000229807	XIST	7801.50
ENSG00000281181	FP236383.3	6396.73
ENSG00000245532	NEAT1	5659.95
ENSG00000260032	NORAD	4049.39
ENSG00000264772	AC016876.2	3596.00
ENSG00000270066	AL356488.2	3231.50
ENSG00000284803	AC245033.4	2501.48
ENSG00000259976	AC093010.3	1924.68
ENSG00000276232	AC006064.5	1758.39
ENSG00000242125	SNHG3	1665.55
ENSG00000240801	AC132217.1	1634.43
ENSG00000175061	SNHG29	1504.66
ENSG00000253352	TUG1	1412.27
ENSG00000247092	SNHG10	1393.16
ENSG00000247556	OIP5-AS1	1320.75
ENSG00000224078	SNHG14	1233.25
ENSG00000261771	DNAAF4-CCPG1	1201.68
ENSG00000280614	FP236383.2	1188.66
ENSG00000225733	FGD5-AS1	1095.93
ENSG00000257379	AC023509.1	1091.86
ENSG00000274536	AL034397.3	1073.93
ENSG00000279738	AL022311.1	958.75
ENSG00000203930	LINC00632	934.77
ENSG00000263244	AC087190.3	930.82
ENSG00000230590	FTX	861.39
ENSG00000273189	AC010619.2	773.16
ENSG00000249669	CARMN	766.27
ENSG00000230551	AC021078.1	748.86

Ensembl ID	lncRNA	Mean Expression
ENSG00000234456	MAGI2-AS3	660.55
ENSG00000285565	AL671762.1	642.93
ENSG00000267009	AC007780.1	595.41
ENSG00000262202	AC007952.4	576.36
ENSG00000256028	AC026362.1	575.20
ENSG00000163597	SNHG16	570.59
ENSG00000234741	GAS5	554.84
ENSG00000269821	KCNQ1OT1	501.52
ENSG00000237298	TTN-AS1	501.23
ENSG00000263798	AC018521.1	467.14
ENSG00000203875	SNHG5	460.61
ENSG00000272888	LINC01578	431.84
ENSG00000196295	GARS-DT	424.18
ENSG00000267519	AC020916.1	411.95
ENSG00000215386	MIR99AHG	400.34
ENSG00000263753	LINC00667	398.73
ENSG00000285622	AL135926.1	397.48

3

Supplementary Table 3 (partially) – LncRNAs exclusively expressed in knee OA subchondral bone.
The top 50 lncRNAs with highest expression levels exclusively in knee OA subchondral bone are shown here, the rest of the table can be found in the online supplement: https://doi.org/10.1093/rheumatology/keab826

Ensembl ID	lncRNA	Mean Expression
ENSG00000258820	AF111167.1	22.76
ENSG00000260653	AC237221.1	12.21
ENSG00000261713	SSTR5-AS1	11.82
ENSG00000285051	SLC7A14-AS1	11.12
ENSG00000287415	AC099541.2	10.91
ENSG00000271239	AC007423.1	10.65
ENSG00000287620	AC092053.4	10.65
ENSG00000286113	AC022868.2	10.50
ENSG00000272256	AC044849.1	9.94
ENSG00000213025	COX20P1	9.00
ENSG00000260192	LINC02240	8.76
ENSG00000238042	LINC02257	8.59
ENSG00000258910	LINC01956	8.47
ENSG00000286598	AC100756.4	8.38
ENSG00000267737	AC087645.2	8.29
ENSG00000226581	AC092634.3	8.26
ENSG00000258334	AC125611.4	8.21
ENSG00000261083	LINC02516	8.03
ENSG00000260278	AC098818.2	7.91
ENSG00000253434	LINC02237	7.71
ENSG00000275830	AL390755.1	7.56
ENSG00000265485	LINC01915	7.53
ENSG00000235619	RPL36AP33	7.24
ENSG00000234626	AL021937.3	7.21
ENSG00000256984	AC008013.2	7.12
ENSG00000260364	AC009055.1	7.00
ENSG00000247416	AP000802.1	6.97
ENSG00000275894	AL021578.1	6.97
ENSG00000255008	AP000442.1	6.85
ENSG00000278716	AC133540.1	6.74
ENSG00000267275	AC020911.2	6.47

Ensembl ID	lncRNA	Mean Expression
ENSG00000274213	AC015912.3	6.44
ENSG00000245651	AC083805.1	6.35
ENSG00000254109	RBPMS-AS1	6.26
ENSG00000283945	LINC00032	6.26
ENSG00000239263	RBM43P1	6.15
ENSG00000251314	AC104123.1	6.15
ENSG00000225096	AL445250.1	6.09
ENSG00000242986	RPL21P99	6.09
ENSG00000248896	AC105001.1	6.06
ENSG00000257398	AC126177.3	6.06
ENSG00000287059	AC090004.2	6.06
ENSG00000257277	AC092652.2	6.03
ENSG00000271538	LINC02427	6.03
ENSG00000245384	CXXC4-AS1	5.97
ENSG00000287129	AC097500.1	5.97
ENSG00000255399	TBX5-AS1	5.94
ENSG00000262223	AC110285.1	5.94
ENSG00000236047	AC073410.1	5.91

3

Supplementary Table 4 (partially) – LncRNAs exclusively expressed in hip OA subchondral bone.
The top 50 lncRNAs with highest expression levels exclusively in hip OA subchondral bone are shown here, the rest of the table can be found in the online supplement: https://doi.org/10.1093/rheumatology/keab826

Ensembl ID	lncRNA	Mean Expression
ENSG00000285783	AC098588.2	892.00
ENSG00000285144	AL359555.3	378.90
ENSG00000275527	AC100835.2	183.80
ENSG00000271736	AL138900.2	138.40
ENSG00000268119	AC010615.2	112.00
ENSG00000264066	AC024267.1	109.30
ENSG00000254006	AC104232.1	96.80
ENSG00000136315	AL355922.1	71.40
ENSG00000268734	AC245128.3	59.10
ENSG00000268833	AC243967.2	58.40
ENSG00000223629	DEFA8P	50.70
ENSG00000260592	AC130456.3	48.30
ENSG00000225345	SNX18P3	46.60
ENSG00000273812	BX640514.2	45.00
ENSG00000255929	AP000943.3	41.10
ENSG00000260188	AC002464.1	40.50
ENSG00000226281	AL031123.1	39.90
ENSG00000259986	AC103876.1	38.20
ENSG00000286342	AC073210.3	36.90
ENSG00000268658	LINC00664	31.40
ENSG00000284138	ATP6V0CP4	30.50
ENSG00000283839	AC096667.1	30.30
ENSG00000251002	AC244502.1	29.70
ENSG00000224177	LINC00570	28.00
ENSG00000238160	AC116366.2	27.60
ENSG00000250155	AC008957.1	27.60
ENSG00000224429	LINC00539	27.10
ENSG00000239219	AC008040.1	26.60
ENSG00000204860	FAM201A	24.60
ENSG00000175746	C15orf54	24.20
ENSG00000230773	AC092650.1	23.80

Ensembl ID	lncRNA	Mean Expression
ENSG00000185275	CD24P4	23.30
ENSG00000233038	AC011899.2	23.20
ENSG00000285486	AC003043.2	23.20
ENSG00000249684	AC106795.2	22.90
ENSG00000255571	MIR9-3HG	22.80
ENSG00000267751	AC009005.1	22.40
ENSG00000269243	AC008894.2	21.80
ENSG00000286419	AC097637.3	21.50
ENSG00000287497	AL031123.4	21.30
ENSG00000286602	AC021660.4	20.80
ENSG00000229140	CCDC26	20.70
ENSG00000261218	AC099524.1	20.60
ENSG00000237803	LINC00211	20.10
ENSG00000255733	IFNG-AS1	19.90
ENSG00000236525	AC007278.2	19.60
ENSG00000261804	AC007342.4	19.60
ENSG00000236304	AP001189.1	19.20
ENSG00000242082	SLC5A4-AS1	18.70

3

Supplementary Table 5 (partially) – LncRNAs being differentially expressed between cluster 1 (containing knee samples) and cluster 2 (containing hip samples).
With cluster 1 set as a reference. The top 50 most significantly differentially expressed lncRNAs are shown here, the rest of the table can be found in the online supplement: https://doi.org/10.1093/rheumatology/keab826

Ensembl ID	lncRNA	Base Mean	P-value	FDR	Log 2 Fold Change	Fold Change
ENSG00000274536	AL034397.3	1246.27	4.33E-233	8.90E-230	7.30	157.82
ENSG00000283646	LINC02009	83.94	4.47E-148	4.60E-145	6.48	89.21
ENSG00000265206	AC004687.1	32.76	4.48E-95	3.07E-92	4.03	16.30
ENSG00000288046	AL031123.5	21.51	3.54E-87	1.82E-84	4.19	18.29
ENSG00000187951	AC091057.1	26.80	2.81E-86	1.16E-83	3.99	15.90
ENSG00000180539	C9orf139	27.20	1.05E-84	3.60E-82	3.99	15.93
ENSG00000283743	Z84466.1	183.04	2.49E-73	7.32E-71	4.45	21.89
ENSG00000285117	AC068724.4	178.42	6.32E-64	1.62E-61	7.31	158.87
ENSG00000274272	AC069281.2	140.81	5.85E-63	1.34E-60	1.80	3.48
ENSG00000286646	AL121933.1	31.18	1.23E-59	2.52E-57	3.36	10.24
ENSG00000228340	MIR646HG	55.03	5.15E-59	9.64E-57	2.91	7.50
ENSG00000213373	LINC00671	16.10	5.97E-57	1.02E-54	3.74	13.39
ENSG00000276570	AC010327.6	76.51	3.49E-55	5.53E-53	2.15	4.43
ENSG00000213468	FIRRE	20.35	4.95E-54	7.28E-52	2.72	6.61
ENSG00000282907	Z98883.1	130.83	4.51E-51	6.18E-49	2.43	5.38
ENSG00000228794	LINC01128	139.02	1.83E-50	2.35E-48	1.56	2.95
ENSG00000238164	TNFRSF14-AS1	38.04	4.47E-50	5.41E-48	1.92	3.79
ENSG00000257167	TMPO-AS1	21.19	8.44E-48	9.65E-46	2.90	7.47
ENSG00000261997	AC007336.1	16.62	6.97E-47	7.54E-45	2.83	7.09
ENSG00000260401	AP002761.4	21.68	6.12E-46	6.29E-44	3.77	13.63
ENSG00000267121	AC008105.3	27.31	1.20E-45	1.18E-43	2.24	4.74
ENSG00000281344	HELLPAR	20.97	4.67E-45	4.37E-43	2.67	6.38
ENSG00000204282	TNRC6C-AS1	77.20	1.67E-43	1.50E-41	2.39	5.24
ENSG00000248774	AC097534.1	10.78	3.15E-43	2.70E-41	2.88	7.34
ENSG00000257698	GIHCG	51.37	6.35E-43	5.22E-41	1.93	3.81
ENSG00000227039	ITGB2-AS1	62.32	2.09E-42	1.65E-40	2.42	5.36
ENSG00000215908	CROCCP2	282.00	4.18E-42	3.18E-40	1.89	3.71
ENSG00000248323	LUCAT1	34.22	1.58E-41	1.16E-39	3.08	8.45
ENSG00000270956	AC009948.3	12.22	1.18E-40	8.35E-39	2.67	6.38
ENSG00000259343	TMC3-AS1	22.94	9.95E-40	6.82E-38	2.48	5.57

Ensembl ID	lncRNA	Base Mean	P-value	FDR	Log 2 Fold Change	Fold Change
ENSG00000284948	AC107959.4	34.17	4.90E-39	3.25E-37	3.47	11.06
ENSG00000238113	LINC01410	21.17	9.21E-39	5.92E-37	4.00	15.98
ENSG00000247982	LINC00926	23.33	5.29E-38	3.29E-36	2.20	4.58
ENSG00000237298	TTN-AS1	498.13	1.93E-37	1.17E-35	1.71	3.28
ENSG00000261008	LINC01572	19.89	2.58E-36	1.52E-34	2.40	5.27
ENSG00000270277	AC009948.2	39.54	4.95E-36	2.83E-34	2.30	4.92
ENSG00000265148	TSPOAP1-AS1	29.37	6.73E-36	3.74E-34	1.90	3.73
ENSG00000237943	PRKCQ-AS1	22.55	6.23E-35	3.37E-33	2.50	5.64
ENSG00000260641	AC114811.2	12.18	1.17E-34	6.15E-33	3.56	11.83
ENSG00000260528	FAM157C	26.15	1.35E-34	6.93E-33	3.47	11.10
ENSG00000224152	AC009506.1	36.54	1.32E-32	6.60E-31	1.80	3.48
ENSG00000267174	AC011472.2	21.03	3.64E-32	1.78E-30	2.82	7.06
ENSG00000235499	AC073046.1	15.92	5.16E-32	2.47E-30	2.07	4.18
ENSG00000286488	AC103858.3	13.44	5.67E-32	2.65E-30	2.78	6.88
ENSG00000246695	RASSF8-AS1	91.07	1.21E-31	5.52E-30	-1.36	0.39
ENSG00000276649	AL117335.1	17.54	1.50E-31	6.69E-30	2.27	4.84
ENSG00000285952	AC020663.4	65.56	6.43E-31	2.81E-29	2.33	5.03
ENSG00000286288	AL109809.5	9.22	1.31E-30	5.63E-29	2.60	6.04
ENSG00000282164	PEG13	19.88	4.19E-30	1.76E-28	2.47	5.55

3

Supplementary Table 6 – Differentially expressed lncRNAs in OA subchondral bone

Ensembl ID	lncRNA	Base Mean	P-value	FDR	Log 2 Fold Change	Fold Change
ENSG00000249306	LINC01411	6.19	7.02E-12	2.20E-08	2.89	7.39
ENSG00000249378	LINC01060	32.03	7.29E-05	1.66E-02	1.42	2.67
ENSG00000232044	SILC1	19.66	9.87E-07	1.03E-03	1.13	2.20
ENSG00000230148	HOXB-AS1	10.88	2.26E-05	7.64E-03	1.05	2.07
ENSG00000285906	AC083855.2	13.94	3.05E-04	4.56E-02	0.82	1.77
ENSG00000264672	SEPT4-AS1	15.08	2.50E-04	4.14E-02	0.66	1.58
ENSG00000249859	PVT1	58.59	9.89E-05	2.07E-02	0.60	1.52
ENSG00000242125	SNHG3	1648.02	7.76E-06	6.09E-03	0.52	1.44
ENSG00000284707	AC079781.5	82.01	2.43E-05	7.64E-03	0.44	1.35
ENSG00000284697	AC006511.5	124.06	1.52E-05	7.64E-03	0.39	1.31
ENSG00000276232	AC006064.5	1694.57	2.38E-05	7.64E-03	0.38	1.30
ENSG00000264772	AC016876.2	3402.26	1.30E-04	2.43E-02	0.34	1.26
ENSG00000258210	AC144548.1	290.80	7.40E-05	1.66E-02	0.32	1.25
ENSG00000175061	SNHG29	1471.34	6.98E-05	1.66E-02	0.28	1.22
ENSG00000234741	GAS5	525.86	7.11E-05	1.66E-02	0.28	1.21
ENSG00000284803	AC245033.4	2375.02	2.27E-04	3.95E-02	0.28	1.21
ENSG00000244398	AC116533.1	299.55	2.83E-04	4.44E-02	0.25	1.19
ENSG00000272668	AL590560.2	52.11	1.32E-04	2.43E-02	-0.37	0.77
ENSG00000271880	AGAP11	32.92	1.16E-05	7.25E-03	-0.56	0.68
ENSG00000223561	AC005165.1	17.97	1.51E-09	2.37E-06	-1.17	0.44
ENSG00000229847	EMX2OS	28.30	2.43E-05	7.64E-03	-1.29	0.41

Supplementary Table 7 – Differentially expressed lncRNAs in knee OA subchondral bone

Ensembl ID	lncRNA	Base Mean	P-value	FDR	Log 2 Fold Change	Fold Change
ENSG00000249306	LINC01411	8.07	5.00E-11	1.59E-07	2.94	7.67
ENSG00000249378	LINC01060	39.92	3.18E-05	1.25E-02	1.63	3.10
ENSG00000230148	HOXB-AS1	12.26	7.67E-06	4.07E-03	1.27	2.42
ENSG00000232044	SILC1	25.66	1.25E-07	9.92E-05	1.22	2.33
ENSG00000249859	PVT1	44.52	5.34E-06	3.40E-03	0.82	1.76
ENSG00000264672	SEPT4-AS1	17.32	4.83E-05	1.41E-02	0.82	1.76
ENSG00000285622	AL135926.1	468.53	1.22E-07	9.92E-05	0.76	1.70
ENSG00000272168	CASC15	68.73	1.01E-04	2.67E-02	0.57	1.48
ENSG00000242125	SNHG3	1188.28	1.55E-04	3.53E-02	0.48	1.40
ENSG00000284707	AC079781.5	79.77	2.19E-04	4.64E-02	0.48	1.39
ENSG00000284697	AC006511.5	117.42	3.54E-05	1.25E-02	0.44	1.36
ENSG00000264772	AC016876.2	3501.60	1.21E-04	2.97E-02	0.41	1.32
ENSG00000271880	AGAP11	40.72	4.87E-05	1.41E-02	-0.56	0.68
ENSG00000223561	AC005165.1	22.29	2.06E-08	3.28E-05	-1.15	0.45
ENSG00000229847	EMX2OS	36.04	1.07E-05	4.85E-03	-1.48	0.36

3

Supplementary Table 8 – Validation and replication of selection of identified lncRNAs

lncRNA	RNA-seq		techincal validation		biological replication		techinical and biological replicates together	
	FC	Padj	FC	Pvalue	FC	Pvalue	FC	Pvalue
LINC01411	7.39	2.20E-08	33.12	1.27E-02	9.60	2.69E-03	17.84	5.80E-04
GAS5	1.21	1.66E-02	3.12	8.64E-01	1.11	6.92E-01	1.61	8.44E-01
EMX2OS	0.41	7.64E-03	0.99	1.06E-01	1.23	2.88E-01	1.14	2.60E-02
PVT1	1.52	2.07E-02	2.76	2.41E-02	1.83	8.51E-02	2.14	2.03E-02
LINC01060	2.67	1.66E-02	2.15	3.13E-01	3.01	9.74E-03	2.89	3.56E-03
SILC1	2.20	9.87E-07	2.41	5.00E-06	1.79	1.88E-10	2.05	1.12E-15
AC005165.1	0.44	2.37E-06	-	-	0.49	4.83E-03	-	-

3

Supplementary Table 9 (partially) – Significant correlations between differentially expressed protein-coding mRNAs and differentially expressed lncRNAs in bone of the same patients (N=22 paired samples).
The top 50 highest correlations between lncRNAs and mRNAs are shown here, the rest of the table can be found in the online supplement: https://doi.org/10.1093/rheumatology/keab826

lncRNA	lncRNA Ensembl ID	mRNA	mRNA Ensembl ID	rho	P-value	FDR
AC006511.5	ENSG00000284697	SMARCC2	ENSG00000139613	-0.89	4.44E-16	3.78E-13
AC016876.2	ENSG00000264772	GLB1	ENSG00000170266	0.90	2.22E-16	2.26E-16
AC016876.2	ENSG00000264772	ATP6V0B	ENSG00000117410	0.91	2.22E-16	2.26E-16
AC083855.2	ENSG00000285906	ACKR3	ENSG00000144476	-0.89	1.33E-15	8.26E-13
AC083855.2	ENSG00000285906	FST	ENSG00000134363	-0.89	1.33E-15	8.26E-13
AC083855.2	ENSG00000285906	ENTPD7	ENSG00000198018	0.89	4.44E-16	3.78E-13
AC116533.1	ENSG00000244398	RPLP0	ENSG00000089157	0.89	4.44E-16	3.78E-13
AC116533.1	ENSG00000244398	RPS8	ENSG00000142937	0.89	4.44E-16	3.78E-13
AC144548.1	ENSG00000258210	CHD6	ENSG00000124177	-0.91	2.22E-16	2.26E-16
AC144548.1	ENSG00000258210	ABRACL	ENSG00000146386	0.89	8.88E-16	5.87E-13
AC144548.1	ENSG00000258210	RAB32	ENSG00000118508	0.89	6.66E-16	5.22E-13
AC144548.1	ENSG00000258210	CKS2	ENSG00000123975	0.89	4.44E-16	3.78E-13
AC144548.1	ENSG00000258210	C14orf119	ENSG00000179933	0.90	2.22E-16	2.75E-13
AC144548.1	ENSG00000258210	TOR1A	ENSG00000136827	0.90	2.22E-16	2.75E-13
AC144548.1	ENSG00000258210	PCNA	ENSG00000132646	0.90	2.22E-16	2.75E-13
AC144548.1	ENSG00000258210	ARPC3	ENSG00000111229	0.90	2.22E-16	2.26E-16
AC144548.1	ENSG00000258210	CAP1	ENSG00000131236	0.90	2.22E-16	2.26E-16
AC144548.1	ENSG00000258210	CLTC	ENSG00000141367	0.91	2.22E-16	2.26E-16

lncRNA	lncRNA Ensembl ID	mRNA	mRNA Ensembl ID	rho	P-value	FDR
AC144548.1	ENSG00000258210	ILF2	ENSG00000143621	0.92	2.22E-16	2.26E-16
AC245033.4	ENSG00000284803	RPL7A	ENSG00000148303	0.89	6.66E-16	5.22E-13
AC245033.4	ENSG00000284803	RPS29	ENSG00000213741	0.89	4.44E-16	3.78E-13
AC245033.4	ENSG00000284803	RPLP0	ENSG00000089157	0.91	2.22E-16	2.26E-16
AC245033.4	ENSG00000284803	RPS7	ENSG00000171863	0.91	2.22E-16	2.26E-16
AC245033.4	ENSG00000284803	RPS12	ENSG00000112306	0.91	2.22E-16	2.26E-16
AC245033.4	ENSG00000284803	RPS17	ENSG00000182774	0.92	2.22E-16	2.26E-16
AC245033.4	ENSG00000284803	RPS8	ENSG00000142937	0.92	2.22E-16	2.26E-16
LINC01060	ENSG00000249378	GNG4	ENSG00000168243	0.89	8.88E-16	5.87E-13
LINC01060	ENSG00000249378	PRSS35	ENSG00000146250	0.89	4.44E-16	3.78E-13
PVT1	ENSG00000249859	PPP1R16B	ENSG00000101445	-0.90	2.22E-16	2.26E-16
PVT1	ENSG00000249859	ABCC4	ENSG00000125257	0.89	2.22E-16	2.75E-13
SNHG29	ENSG00000175061	PTPRM	ENSG00000173482	-0.89	4.44E-16	3.78E-13
SNHG29	ENSG00000175061	CHD6	ENSG00000124177	-0.89	4.44E-16	3.78E-13
SNHG29	ENSG00000175061	UBE2J1	ENSG00000198833	0.89	8.88E-16	5.87E-13
SNHG29	ENSG00000175061	MGAT2	ENSG00000168282	0.89	8.88E-16	5.87E-13
SNHG29	ENSG00000175061	PCNA	ENSG00000132646	0.89	8.88E-16	5.87E-13
SNHG29	ENSG00000175061	PTDSS1	ENSG00000156471	0.90	2.26E-16	2.26E-16
SNHG3	ENSG00000242125	PTPRM	ENSG00000173482	-0.92	2.22E-16	2.26E-16
SNHG3	ENSG00000242125	AHNAK	ENSG00000124942	-0.90	2.22E-16	2.26E-16
SNHG3	ENSG00000242125	SYT12	ENSG00000173227	-0.90	2.22E-16	2.75E-13

3

lncRNA	lncRNA Ensembl ID	mRNA	mRNA Ensembl ID	rho	P-value	FDR
SNHG3	ENSG00000242125	SPATA6	ENSG00000132122	-0.90	2.22E-16	2.75E-13
SNHG3	ENSG00000242125	PLEKHM3	ENSG00000178385	-0.89	4.44E-16	3.78E-13
SNHG3	ENSG00000242125	LDHD	ENSG00000166816	-0.89	1.11E-15	7.18E-13
SNHG3	ENSG00000242125	UTRN	ENSG00000152818	-0.88	1.78E-15	1.04E-12
SNHG3	ENSG00000242125	UGGT1	ENSG00000136731	0.89	8.88E-16	5.87E-13
SNHG3	ENSG00000242125	BID	ENSG00000015475	0.89	8.88E-16	5.87E-13
SNHG3	ENSG00000242125	ABCC4	ENSG00000125257	0.89	6.66E-16	5.22E-13
SNHG3	ENSG00000242125	RGS19	ENSG00000171700	0.89	4.44E-16	3.78E-13
SNHG3	ENSG00000242125	CKS2	ENSG00000123975	0.90	2.22E-16	2.26E-16
SNHG3	ENSG00000242125	JPT1	ENSG00000189159	0.91	2.22E-16	2.26E-16

Supplementary Table 10 (partially) – Gene enrichment analysis of correlating genes.
The most significantly enriched GO-term for each lncRNA are shown here, the rest of the table can be found in the online supplement: https://doi.org/10.1093/rheumatology/keab826

lncRNA	Term	Count	%	FDR	Genes
AC006511.5	GO:0070062~extracellular exosome	28	38.89	3.67E-04	SLC25A5, PSMA4, NSF, ATP6V1D, GLA, ARPC3, TARS, GNB4, ATP6V1A, CAP1, RAN, PCNA, TXN, STXBP1, PSMA5, CCT6A, ATP6V1B2, GSTO1, ARPC2, CCT3, CCT2, IGF2, GLB1, INSR, PPIA, IARS, CLIC1, PSMB3
AC116533.1	GO:0006614~SRP-dependent cotranslational protein targeting to membrane	8	26.67	1.90E-07	RPLP0, RPS12, RPL27, RPS8, RPL7A, RPL27A, RPS7, RPS17
AC144548.1	GO:0043209~myelin sheath	8	7.27	2.02E-02	SLC25A5, GDI2, NSF, HSPA8, ATP5PB, CLTC, CCT2, UQCRFS1
AC245033.4	GO:0006614~SRP-dependent cotranslational protein targeting to membrane	18	45.00	8.01E-25	RPL6, RPLP0, RPS13, RPS12, RPL5, RPL23, RPL27, RPS6, RPS24, RPS8, RPL7A, RPL27A, RPS7, RPL4, RPS17, RPL12, RPL10A, RPL39
GAS5	GO:0006614~SRP-dependent cotranslational protein targeting to membrane	12	85.71	1.00E-20	RPL6, RPS13, RPS12, RPL5, RPL23, RPS8, RPL7A, RPS7, RPL4, RPS17, RPL35A, RPL10A
LINC01060	GO:0016021~integral component of membrane	11	78.57	4.97E-03	SLC8A3, SLC9A2, RARRES1, IGSF3, RHBDL2, SGMS2, CDH2, ANO5, LRRC15, GXYLT2, SLC36A2
SILC1	GO:0005578~proteinaceous extracellular matrix	7	25.00	1.07E-04	CCN4, SPARC, OMD, POSTN, CTHRC1, MAMDC2, COL5A2
SNHG29	GO:0018279~protein N-linked glycosylation via asparagine	7	7.29	8.87E-05	UGGT1, ST6GAL2, STT3B, RPN1, MGAT2, UBE2J1, DDOST
SNHG3	GO:0051082~unfolded protein binding	8	4.60	4.40E-02	DNAJB11, CRYAB, HSPA8, UGGT1, CCT6A, CCT3, CCT2, CALR

Supplementary Table 11 (partially) – LncRNAs exclusively expressed in bone, lncRNAs exclusively expressed in cartilage, and lncRNAs expressed in both tissues (N=10 paired samples, preserved and lesioned cartilage and bone).
The top 10 highest expressed lncRNAs exclusively in subchondral bone, the top 10 highest expressed lncRNAs exclusively in articular cartilage and the top 10 highest expressed lncRNAs in both tissues are shown here, the rest of the table can be found in the online supplement: https://doi.org/10.1093/rheumatology/keab826

Tissue	lncRNA	lncRNA Ensembl ID	Mean Expression in bone	Mean expresion in cartilage
Bone	AL627171.2	ENSG00000282885	387446.35	-
Bone	FP236383.3	ENSG00000281181	3240.85	-
Bone	SNHG10	ENSG00000247092	1483.60	-
Bone	FP236383.2	ENSG00000280614	605.90	-
Bone	AL034397.3	ENSG00000274536	507.35	-
Bone	TRHDE-AS1	ENSG00000236333	376.95	-
Bone	HLA-DRB6	ENSG00000229391	276.30	-
Bone	LINC02328	ENSG00000258733	234.10	-
Bone	AC244205.1	ENSG00000240040	229.85	-
Bone	AC242426.2	ENSG00000237188	228.35	-
Cartilage	PART1	ENSG00000152931	-	274.50
Cartilage	SSTR5-AS1	ENSG00000261713	-	137.10
Cartilage	AC087521.3	ENSG00000254409	-	119.90
Cartilage	AL009174.1	ENSG00000227008	-	118.10
Cartilage	MT1P3	ENSG00000229230	-	83.20
Cartilage	AC107075.1	ENSG00000277998	-	82.70
Cartilage	RPL22P2	ENSG00000241081	-	63.70
Cartilage	AL139220.2	ENSG00000230615	-	62.50
Cartilage	LINC01411	ENSG00000249306	-	61.45
Cartilage	AC245060.4	ENSG00000272779	-	47.75
Overlap	AL355075.4	ENSG00000259001	51930.45	32608.05
Overlap	RMRP	ENSG00000269900	46300.60	14252.65
Overlap	MALAT1	ENSG00000251562	45942.75	16241.35
Overlap	XIST	ENSG00000229807	8808.60	4236.35
Overlap	NEAT1	ENSG00000245532	7120.70	2880.80
Overlap	NORAD	ENSG00000260032	4529.90	3223.20
Overlap	AL356488.2	ENSG00000270066	3691.15	1526.30
Overlap	AC016876.2	ENSG00000264772	3800.45	1328.90
Overlap	AC245033.4	ENSG00000284803	2655.90	1237.80
Overlap	AC093010.3	ENSG00000259976	2357.90	1228.40

Supplementary Table 12 – Significantly differentially expressed lncRNAs overlapping between articular cartilage and subchondral bone

lncRNA	Base mean in bone	FC in bone	FDR in bone	Base mean in cartilage	FC in cartilage	FDR in cartilage
AC005165.1	17.97	0.44	2.37E-06	47.47	0.47	1.33E-03
AC079781.5	82.01	1.35	7.64E-03	86.37	1.30	3.08E-02
AL590560.1	52.11	0.77	2.43E-02	69.60	0.65	8.74E-03
LINC01411	6.19	7.39	2.20E-08	50.68	4.48	2.58E-06
SILC1	19.66	2.20	1.03E-03	88.54	2.17	6.39E-07

3
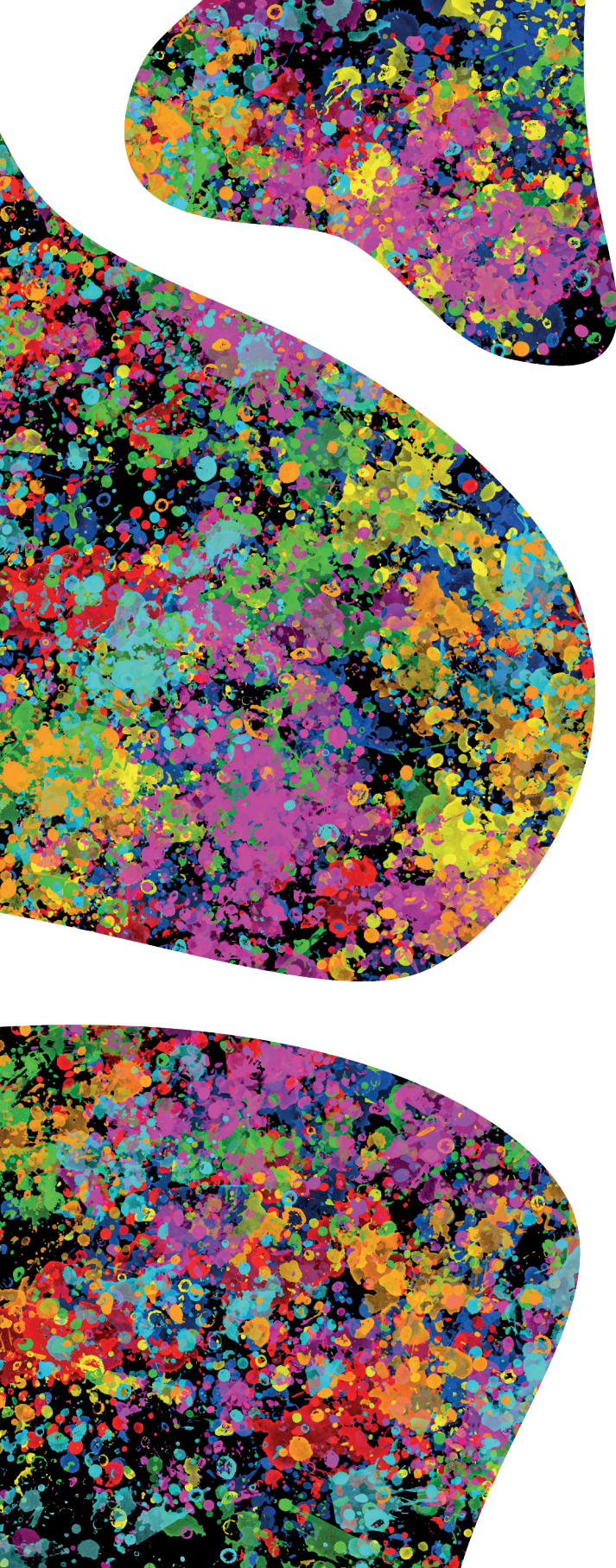
CHAPTER 4

Identification of circulating microRNAs predicting osteoarthritis molecular endotypes and matching druggable targets

Margo Tuerlings[1], Ilja Boone[1], H. Eka D. Suchiman[1], Nico Lakenberg[1], Robert J.P. van der Wal[2], Rob G.H.H. Nelissen[2], Yolande F.M. Ramos[1], Rodrigo Coutinho de Almeida[1], Ingrid Meulenbelt[1]

[1] Dept. of Biomedical Data Sciences, Leiden University Medical Center, Leiden, The Netherlands.
[2] Dept. Orthopaedics Leiden University Medical Center, Leiden, The Netherlands.

Abstract

Objective: To identify circulating micro RNAs (miRNAs) that could serve as biomarkers allowing for effective personalized treatment strategies.

Methods: Previously generated datasets of articular cartilage (mRNA-sequencing, N=56 patients) and plasma (miRNA-sequencing, N=56 patients) were integrated (N=20 patients of whom both cartilage mRNA-seq and plasma miRNA-seq were available). Generalized estimating equations and LASSO regression were applied to identify miRNAs and mRNAs marking previously identified OA endotype A and B. To identify potential druggable targets for OA molecular endotypes, we combined previously reported differentially expressed (DE) genes between preserved and lesioned OA cartilage exclusive for endotype A or B, recent GWAS data and the drug-gene interaction database.

Results: We identified miR-6804-5p, miR-182-3p, let-7e-3p, and miR-3179 expressed in plasma that together with sex and age were able to distinguish OA molecular endotype A and B. To validate predictive capacity of these four miRNAs for molecular endotype, we first identified mRNAs expressed in cartilage marking OA endotypes. Combining plasma miRNA-seq data and articular cartilage mRNA RT-qPCR data showed that prediction of OA endotypes coincided for 86% of additional patients. To match OA endotypes to druggable targets, we filtered exclusive DE genes for each endotype on OA risk genes. We identified MAP2K6 and HLA-DPA1 as druggable targets specific for endotype A and B, respectively.

Conclusion: We here showed that plasma expression levels of miR-6804-5p, miR-182-3p, let-7e-3p, and miR-3179 might be used to distinguish OA endotype A and B, which then could be used to treat patients in an OA endotype specific manner. Use of circulating miRNAs as biomarkers provides a window of opportunities for effective personalized OA treatment strategies.

Introduction

Osteoarthritis (OA) represents multiple subtypes of a degenerative joint disease, in which progressive and irreversible degeneration of the articular cartilage, structural changes in the subchondral bone, inflammation, and loss of joint space is seen [1, 2]. With total joint replacement surgery and pain relief treatment being the only treatment options for OA, there is an unmet desire for disease modifying treatments that target underlying pathophysiological processes [3]. Failure of disease modifying drug development, so far, is partly caused by the fact that it has followed a "one-drug-fits-all-patients" approach, in which OA heterogeneity is ignored [4, 5]. To address heterogeneity in OA pathophysiology, multiple studies have focused on the identification of OA molecular endotypes based on gene expression cluster analysis [6]. To this end, Soul et al. [7] identified two cluster analysis-based OA endotypes using RNA-seq data of knee articular cartilage. These two molecular endotypes were associated to changes in inflammasome activation and innate immune responses, and changes from chondrogenic to a more osteogenic phenotype, respectively. Recently, we also reported on the identification of two OA molecular endotypes in hip and knee articular cartilage in an independent dataset [8]. These endotypes represented similar pathways as reported by Soul et al. [7], indicating their consistency and robustness. Moreover, we showed that these patients showed clinical phenotypic differences. Endotype B patients, having an inflammatory driven disease process, showed increased joint space narrowing comparing to endotype A patients, having a hypertrophy driven disease process [8]. Together these data confirmed that OA may be amenable to tailored treatments targeting these unique molecular endotypes. Nonetheless, to enable molecular endotype-based stratification of patients before treatment in clinical practice, easily accessible and non-invasive biomarkers are required reflecting ongoing processes in articular cartilage. Hereto, Soul et al. [7] reported a set of proteins which were predicted to be secreted in the synovial fluid and could potentially serve as a biomarker for OA endotype. However, collecting synovial fluid is still an invasive procedure and therefore not optimal. For that matter, studies implicate circulating microRNAs (miRNAs) as novel promising biomarkers in numerous diseases, as they are stable in plasma and serum and relatively easily accessible [9-11]. More related to OA, Beyer et al. [12] found let-7e as a negative dose-dependent predictor for severe OA and Ntoumou et al. [13] identified circulating miRNAs predicted to regulate metabolic processes and could serve as biomarker for OA. Likewise, Murata et al. [14] identified miR-132 predictive for rheumatoid arthritis and OA. Recently, we showed for the first time that circulating miRNAs were able to mark disease related mRNA expression patterns in articular cartilage with early OA [15]. To our knowledge, however, there are no studies yet identifying circulating miRNAs as biomarker for OA molecular endotypes.

In the current study, we used our previously described circulating miRNA-seq dataset of plasma [15] and mRNA-seq dataset of OA articular cartilage [16] (N=20 overlapping patients), to identify miRNAs that could serve as biomarkers for our previously reported OA molecular endotypes A and B [8]. Moreover, to identify OA endotype specific potential druggable targets, we combined our previously reported differentially expressed genes between macroscopically preserved and lesioned OA articular cartilage exclusive for either endotype A or endotype B with recent largest GWAS meta-analysis so far [17].

Methods

Sample description

The current study includes 68 patients, who underwent a joint replacement surgery due to OA, as part of the RAAK study (**Supplementary Table 1**). Macroscopically preserved OA cartilage was collected from all joints as described previously [18]. Plasma was collected from 56 patients. Informed consent was obtained from all participants and ethical approval for the RAAK study was given by the medical ethics committee of the Leiden University Medical Center (P08.239/P19.013).

miRNA and mRNA sequencing

miRNA and mRNA sequencing were performed on Illumina HiSeq 2500 and HiSeq 2000/4000, respectively, as described previously [15, 16]. More information on alignment, mapping and quality control is available in **supplementary methods**.

Principal component analysis

As described previously, we selected the 1000 genes with highest coefficient of variation (COV) [8]. Then, we performed principal component analysis (PCA) on the samples selected for these 1000 genes using the FactoMineR 1.42 [19] package in R. The threshold of 0.45 was set based on the average factor loading score of two samples with the smallest difference in PC1. More information is available in **supplementary methods**.

Prediction models

Spearman correlations between factor loading scores and expression levels of either miRNA or mRNA were calculated using the Hmisc 4.2-0 package in R. Both generalized estimating equations and elastic net regularization were performed. The model showing the highest number of correct predictions with the least number of variables was selected. Additional information is available in **supplementary methods**.

RT-qPCR

RT-qPCR was performed to quantitatively determine the mRNA expression levels. The

relative gene expression was evaluated by the -ΔCT values, using *LRRC41* and *U2AF2* as internal controls.

Results

Identification of plasma miRNAs predicting OA molecular endotype

To identify blood-based miRNAs able to distinguish between previously identified OA molecular endotype A (hypertrophy pathway) and B (immune response) [8], we integrated previously generated datasets of plasma (miRNA-sequencing, dataset 1, **Figure 1**) and articular cartilage (mRNA-sequencing, dataset 2, **Figure 1**), which were partially overlapping (N=20 patients, subset 1, **Figure 1**) [15, 16]. Since these 20 overlapping patients were unevenly distributed over OA endotype A (N=17) and B (N=3), we converted binominal "endotype A" and "endotype B" back to a quantitative contribution per patient to either endotype A or B by using principal component analysis (PCA) (**Supplementary Figure 1**), as reported previously [7]. Patients characteristics of the data- and the subsets are listed in **Supplementary Table 1**. To identify readily detectable miRNAs in plasma (dataset 1), we selected for highest quartile of expression levels (N=663 miRNAs out of 2652 miRNAs expressed in total). Subsequently, to find plasma miRNAs that mark OA molecular endotype, we correlated these 663 miRNAs to quantitative factor loading scores of OA endotypes of subset 1 patients (N= 20 patients with complete data, **Figure 1**). In total 21 significant correlating miRNAs were detected. Among the highest correlating miRNAs, we found miR-195-5p (ρ=-0.61), miR-182-3p (ρ=0.60) and miR-4665-5p (ρ=0.60) (**Supplementary Table 2**). Subsequently, to identify the minimal number of miRNAs with highest predictive value for OA endotype, we used miRNAs with a correlation of $|\rho|>0.5$ (N=9 miRNAs) and performed generalized estimating equations (GEE) with quantitative factor loading scores of OA endotypes as dependent variable and miRNAs as covariates while adjusting for age and sex. Upon selecting for significant variables, we found that miR-6804-5p, miR-182-3p, let-7e-3p,
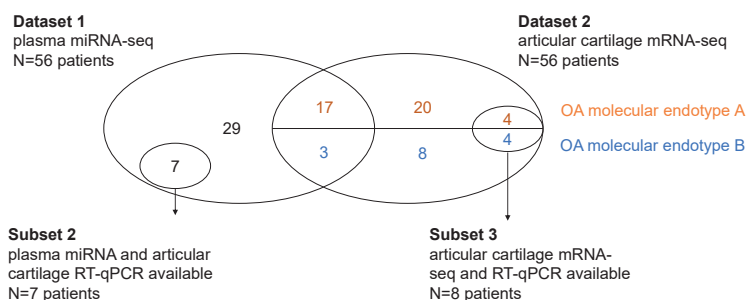
4
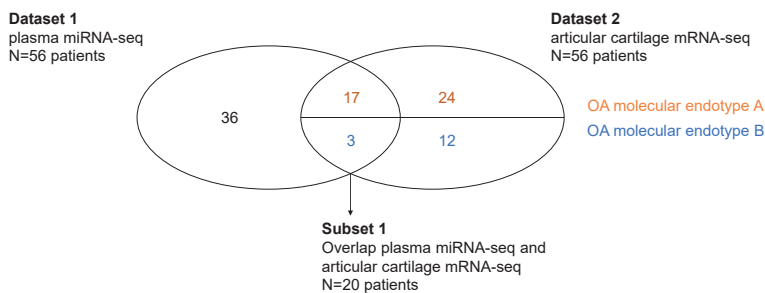
Figure 1 – Venn diagram of samples used in this study.
Dataset 1 consists of 56 patients of whom miRNA-seq of plasma was available and dataset 2 consists of 56 patients of whom mRNA-seq of cartilage was available. Subset 1 refers to the overlap between plasma miRNA-seq data and articular cartilage mRNA-seq data.

and miR-3179 together explained quantitative OA molecular endotypes of patients of subset 1 (**Equation 1, Supplementary Table 3, Supplementary Figure 2**).

Equation 1

Quantitative factor loading scores of OA molecular endotypes =– 0.45 * miR_6804_5p + 0.52 * miR_182_3p – 0.50 * let_7e_3p + 0.16 * miR_3179 + 0.04 * age – 0.56 * sex - 1.95

Confirmation of OA molecular endotype predicting plasma miRNAs

To allow validation of the capability of the four identified miRNAs in plasma to predict OA endotypes using **Equation 1** in an independent dataset, we had available subset 2 (**Figure 2**). Subset 2 consisted of 7 patients of whom plasma miRNA-seq and articular cartilage cDNA to measure limited number of genes by RT-qPCR, but no information on OA endotype data was available. Therefore, we first set out to identify mRNA markers in articular cartilage that together enable prediction of OA endotype of patients in subset 1 (**Figure 1**). These markers eventually allow delineation of OA endotypes based on cartilage mRNA expression levels in subset 2 (**Figure 2**).

Figure 2 – Venn diagram of samples used in this study.
Dataset 1 consists of 56 patients of whom miRNA-seq of plasma was available and dataset 2 consists of 56 patients of whom mRNA-seq of cartilage was available. Subset 2 refers to the patients of whom we had plasma miRNA-seq data available and articular cartilage cDNA available to perform RT-qPCR. Subset 3 refers to the patients of whom we had articular cartilage mRNA-seq available and articular cartilage cDNA available to perform RT-qPCR.

To predict OA endotype of patients based on mRNA-seq data of articular cartilage in subset 1, we selected for previously reported FDR significantly differentially expressed genes between endotype A and B (N=2967 genes) [8]. To select for genes that are readily detectable, we further stratified for genes that were among the two highest expression level quartiles in articular cartilage (N=500 genes). Subsequently, we performed Spearman correlation between expression levels of these 500 genes and quantitative factor loading scores of OA endotypes (**Supplementary Table 4**). To identify the minimal number of genes with highest predictive value for OA endotype,

we selected genes highly correlating to OA endotypes ($|\rho|>0.9$, N=13 genes) and we performed LASSO regression. We found that expression levels of *MMP19, SLCO2B1* and *CDH11* in articular cartilage together could predict OA endotype (**Equation 2**), with 97.5% accuracy in the 36 non-overlapping samples (dataset 2, **Supplementary Figure 3B**). Together, these data confirm that mRNA expression levels of specified three genes in cartilage are highly predictive of OA molecular endotypes.

Equation 2
Predicted factor loading score= 0.31 * MMP19 + 0.20 * SLCO2B1 + 0.0047 * CDH11 -3.13

Being able to predict OA endotype based on mRNA levels in cartilage, allowed us to perform validation of predictive values of the four miRNAs in the independent subset 2 as articular cartilage RT-qPCR data and plasma miRNA-seq was available herein. However, prior to this analyses we needed to address conversion of RNA-seq to RT-qPCR derived mRNA expression data. Therefore we used subset 3 (**Figure 2**), consisting of 8 patients of whom RNA-seq data and articular cartilage cDNA was available. The RT-qPCR threshold was set based on the average difference between normalized read counts (VST) and -ΔCT values. Using this threshold, all 8 patients were assigned correctly to their OA endotype (**Figure 3**).

4

● Prediction based on VST values of mRNA in articular cartilage (RNA-seq)

■ Prediction based on -ΔCT values of mRNA in articular cartilage (RT-qPCR)
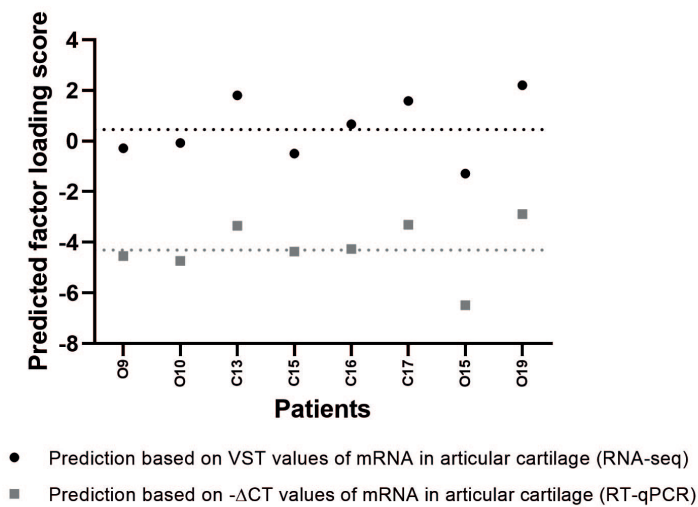
Figure 3 – Prediction of OA molecular endotype using VST expression levels of articular cartilage mRNA (RNA-sequencing data) and prediction of OA molecular endotype using -ΔCT values of articular cartilage mRNA (RT-qPCR) in 8 patients.
Threshold of RNA-seq prediction: 0.45. Threshold of RT-qPCR prediction: -4.31. Patients indicated with O: patients of whom we have plasma miRNA-seq data and articular cartilage mRNA-seq data. Patients indicated with C: patients of whom we only have articular cartilage mRNA data.

Next, we used subset 2 (**Figure 2**), to assign patients to either OA endotype A or B based on plasma miRNA-seq data by applying **Equation 1** or based on articular cartilage RT-qPCR data by applying **Equation 2**. As shown in **Figure 4**, all patients were assigned to the same OA molecular endotype by both prediction methods, except for P6 (86% accuracy).
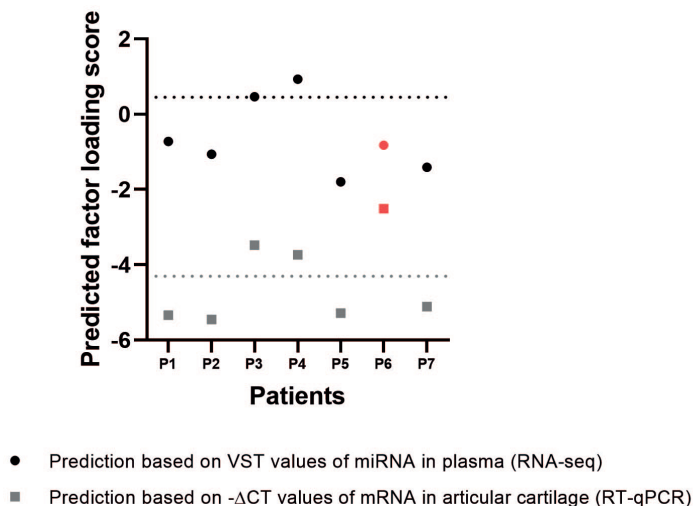

Figure 4 – Prediction based on VST expression levels of plasma miRNA (RNA sequencing data) and prediction based on -ΔCT values of articular cartilage mRNA (RT-qPCR) in 7 patients.
Patients indicated with P: patients of whom we have plasma miRNA-seq data and articular cartilage RT-qPCR data.

Potential therapeutics for OA molecular endotype
Now that we have identified biomarkers that enable stratification of patients based on their OA molecular endotype, the next step was to identify potential druggable targets able to specifically treat endotype A or B patients. In this regard, we used our previously reported differentially expressed genes between macroscopically preserved and lesioned OA articular cartilage unique for endotype A (N=1114 genes) or B (N=72 genes) [8]. To select for genes that were most likely causal to OA pathophysiology and therefore could target underlying OA pathophysiological process, we filtered these differentially expressed genes for genes with SNPs that were recently identified in the largest genome-wide meta-analysis so far [17]. In doing so, we identified *POLD3, ERG, MAP2K6*, and *MN1* as differentially expressed OA risk genes with unique expression patterns in endotype A patients, making these four genes attractive potential druggable targets for patients with endotype A OA (**Supplementary Table 5A**). Similarly, we identified *HLA-DPA1* as attractive potential druggable target for patients with endotype B OA (**Supplementary Table 5B**). Subsequently, we used our previous studies on allelic

imbalanced expression (AIE) in articular cartilage and subchondral bone to identify the direction of effect of these five potential targets [20, 21]. We found SNPs located in *MAP2K6* and *HLA-DPA1* showing AIE, which were in high LD (R^2 = 0.84 and R^2= 0.71, respectively) with the identified OA risk SNPs. Based on this AIE we could make a firm hypothesis that increased levels of *MAP2K6* and *HLA-DPA1* confer risk to OA, suggesting that inhibiting these genes could be a potential treatment strategy. To explore whether there are already approved drugs available to target these genes, we used the online drug gene interaction database (DGIdb 4.0)[22]. In total we found 11 drug-gene interactions for OA molecular endotype A, including 3 drug-gene interactions of *MAP2K6,* while we did not find any drug-gene interactions for endotype B (**Supplementary Table 5**).

Discussion

The aim of the current study was to identify non-invasive biomarkers able to classify patients according to previously identified robust OA molecular endotypes in articular cartilage. By combining miRNA-seq data of plasma and mRNA-seq data of articular cartilage of the same patients, we identified four miRNAs (miR-6804-5p, miR-182-3p, let-7e-3p, and miR-3179) expressed in plasma that were able to classify our previously reported OA molecular endotypes in articular cartilage. In an additional dataset of patients without previously assessed OA endotype, we showed that prediction of OA molecular endotypes coincided using miRNA-seq data of plasma and mRNA RT-qPCR data of articular cartilage in 86% of patients. Moreover, we identified *MAP2K6* and *HLA-DPA1* as potential druggable targets for specific treatment endotype A or B patients, respectively. Therefore, we advocate that expression levels of these four miRNAs in plasma could be used to stratify patients into OA molecular endotypes prior to treatment during clinical trials for more effective treatment response. Hypothetically, to limit failure of clinical trials, patients with inflammatory-driven OA (endotype B) should be enriched in clinical trials using anti-inflammatory drugs or treatment with *MAP2K6* inhibitors, while patients with hypertrophy-driven OA (endotype A) should be enriched in clinical trials using *HLA-DPA1* inhibitors. To our knowledge, we here showed for the first time that circulating miRNAs can be used as biomarker for OA molecular endotypes, as such providing a novel window of opportunities for effective personalized OA treatment strategies.

Mitogen-activated protein kinase kinase 6, encoded by *MAP2K6,* is an intracellular signaling protein which is activated by stress signals and inflammation [23]. Map kinases are known to regulate, amongst others, pain mediators and cartilage degrading enzymes such as matrix metalloproteinases and are therefore formerly suggested as therapeutic targets for OA [24]. Based on allelic imbalanced expression in articular cartilage of allele rs1133228-A [20], located in *MAP2K6* and in high LD with the identified OA risk SNP

rs2716212 [17], we hypothesize that increased expression of *MAP2K6* confers risk to OA. Therefore, inhibiting *MAP2K6* expression in patients with OA endotype A might be a potential therapeutic strategy. *HLA-DPA1*, encoding major histocompatibility complex class II DP alpha 1, plays a role in the immune system and is upregulated in rheumatoid arthritis [25]. Allelic imbalanced expression in subchondral bone of rs1126506-T [21], located in *HLA-DPA1* and in high LD with OA risk SNP rs2856821, we hypothesize that increased expression confers risk to OA. Based on this hypothesis inhibition of *HLA-DPA1* expression could by a therapeutic strategy specific for patients with OA endotype B. Functional studies investigating underlying biological mechanisms of both genes are necessary to confirm their potential as druggable target.

To find the minimal number of miRNAs and mRNAs with highest predictive value for OA endotypes, we performed both LASSO regression and generalized estimating equations. We selected the method that showed the lowest number of variables with highest predicting capacity. In doing so, four circulating miRNAs were identified of which the expression levels together were able to predict OA molecular endotype with 86% accuracy in replication. Nonetheless, given the relatively small sample size, replication in a larger dataset would be required to confirm. To our knowledge, these four miRNAs in plasma were not previously linked to OA pathophysiology, except for let-7e. Beyer et al. showed that expression levels of let-7e were significantly different between plasma of OA patients and healthy controls [12]. Moreover, it has been shown that let-7e could be used as a negative dose dependent predictor of OA [26]. In our dataset, let-7e-3p was shown to negatively correlate with quantitative factor loading scores of OA endotypes (ρ=-0.55), with let-7e-3p being higher expressed in OA endotype A representing chondrocyte hypertrophy. MiR-182-3p expression was previously shown to have a potential regulatory role in osteosarcoma [27] and plasma levels of miR-182 were previously associated to various other types of cancer [28, 29]. Plasma exosome levels of miR-3179 were previously shown to be associated with low bone mineral density in postmenopausal women [30]. To our knowledge, associations between miR-6804 and the musculoskeletal system have not yet been reported.

Although sample sizes of our discovery and validation datasets were relatively small (N=20 overlapping patients, subset 1), the large consistent and robust differences between the two OA molecular endotypes allowed for the detection of four predicting miRNAs. Notably, miR-195-5p and miR-4665-5p were among the highest correlating miRNAs to factor loading score (ρ=-0.61 and ρ=0.60, respectively), while these miRNAs were not included in the final predicting model.

Altogether, we here showed that miRNA expression levels in plasma could reflect

ongoing processes in articular cartilage, making them attractive, easily accessible, non-invasive biomarkers which could further advance the development of personalized medicine of OA and could lead to a higher clinical trial success rate.

Declarations

Disclosures

The authors have declared no conflicts of interest.

4

References

1. Kean, W.F., R. Kean, and W.W. Buchanan, *Osteoarthritis: symptoms, signs and source of pain.* Inflammopharmacology, 2004. **12**(1): p. 3-31.
2. Loeser, R.F., et al., *Osteoarthritis: a disease of the joint as an organ.* Arthritis Rheum, 2012. **64**(6): p. 1697-707.
3. Ghouri, A. and P.G. Conaghan, *Update on novel pharmacological therapies for osteoarthritis.* Ther Adv Musculoskelet Dis, 2019. **11**: p. 1759720x19864492.
4. Grässel, S. and D. Muschter, *Recent advances in the treatment of osteoarthritis.* F1000Research, 2020. **9**: p. F1000 Faculty Rev-325.
5. Angelini, F., et al., *Osteoarthritis endotype discovery via clustering of biochemical marker data.* Annals of the Rheumatic Diseases, 2022. **81**(5): p. 666-675.
6. Yuan, C., et al., *Classification of four distinct osteoarthritis subtypes with a knee joint tissue transcriptome atlas.* Bone Research, 2020. **8**(1): p. 38.
7. Soul, J., et al., *Stratification of knee osteoarthritis: two major patient subgroups identified by genome-wide expression analysis of articular cartilage.* Ann Rheum Dis, 2018. **77**(3): p. 423.
8. Coutinho de Almeida, R., et al., *Identification and characterization of two consistent osteoarthritis subtypes by transcriptome and clinical data integration.* Rheumatology (Oxford), 2020.
9. Cruz, M.S., et al., *miRNAs emerge as circulating biomarkers of post-myocardial infarction heart failure.* Heart Failure Reviews, 2020. **25**(2): p. 321-329.
10. Vanhie, A., et al., *Plasma miRNAs as biomarkers for endometriosis.* Hum Reprod, 2019. **34**(9): p. 1650-1660.
11. Bouvy, C., et al., *Circulating MicroRNAs as Biomarkers in Diffuse Large B-cell Lymphoma: A Pilot Prospective Longitudinal Clinical Study.* Biomark Cancer, 2018. **10**: p. 1179299x18781095.
12. Beyer, C., et al., *Signature of circulating microRNAs in osteoarthritis.* Ann Rheum Dis, 2015. **74**(3): p. e18.
13. Ntoumou, E., et al., *Serum microRNA array analysis identifies miR-140-3p, miR-33b-3p and miR-671-3p as potential osteoarthritis biomarkers involved in metabolic processes.* Clin Epigenetics, 2017. **9**: p. 127.
14. Murata, K., et al., *Plasma and synovial fluid microRNAs as potential biomarkers of rheumatoid arthritis and osteoarthritis.* Arthritis Res Ther, 2010. **12**(3): p. R86.
15. Ramos, Y.F.M., et al., *Circulating MicroRNAs Highly Correlate to Expression of Cartilage Genes Potentially Reflecting OA Susceptibility-Towards Identification of Applicable Early OA Biomarkers.* Biomolecules, 2021. **11**(9): p. 1356.

16. Coutinho de Almeida, R., et al., *RNA sequencing data integration reveals an miRNA interactome of osteoarthritis cartilage.* Ann Rheum Dis, 2019. **78**(2): p. 270-277.
17. Boer, C.G., et al., *Deciphering osteoarthritis genetics across 826,690 individuals from 9 populations.* Cell, 2021.
18. Ramos, Y.F., et al., *Genes involved in the osteoarthritis process identified through genome wide expression analysis in articular cartilage; the RAAK study.* PLoS One, 2014. **9**(7): p. e103056.
19. Lê, S., J. Josse, and F. Husson, *FactoMineR: An R Package for Multivariate Analysis.* Journal of Statistical Software, 2008. **25**(1): p. 1 - 18.
20. den Hollander, W., et al., *Annotating Transcriptional Effects of Genetic Variants in Disease-Relevant Tissue: Transcriptome-Wide Allelic Imbalance in Osteoarthritic Cartilage.* Arthritis Rheumatol, 2019. **71**(4): p. 561-570.
21. Coutinho de Almeida, R., et al., *Allelic expression imbalance in articular cartilage and subchondral bone refined genome-wide association signals in osteoarthritis.* medRxiv, 2022: p. 2022.04.07.22273552.
22. Freshour, S.L., et al., *Integration of the Drug–Gene Interaction Database (DGIdb 4.0) with open crowdsource efforts.* Nucleic Acids Research, 2020. **49**(D1): p. D1144-D1151.
23. Jia, Z. and Q.J. Wei, *CircRNA-MSR Regulates LPS-Induced C28/I2 Chondrocyte Injury through miR-643/MAP2K6 Signaling Pathway.* Cartilage, 2021. **13**(2_suppl): p. 785s-795s.
24. Loeser, R.F., E.A. Erickson, and D.L. Long, *Mitogen-activated protein kinases as therapeutic targets in osteoarthritis.* Current opinion in rheumatology, 2008. **20**(5): p. 581-586.
25. Li, X., et al., *Promising targets and drugs in rheumatoid arthritis.* Bone & Joint Research, 2020. **9**(8): p. 501-514.
26. Feng, L., et al., *Circulating microRNA let-7e is decreased in knee osteoarthritis, accompanied by elevated apoptosis and reduced autophagy.* Int J Mol Med, 2020. **45**(5): p. 1464-1476.
27. Chen, G., et al., *Potential Regulatory Effects of miR-182-3p in Osteosarcoma via Targeting EBF2.* BioMed Research International, 2019. **2019**: p. 4897905.
28. Liu, X., et al., *Elevated circulating miR-182 acts as a diagnostic biomarker for early colorectal cancer.* Cancer Manag Res, 2018. **10**: p. 857-865.
29. Song, C., et al., *High expression of microRNA-183/182/96 cluster as a prognostic biomarker for breast cancer.* Scientific Reports, 2016. **6**(1): p. 24502.
30. Kong, D., et al., *Comparative profile of exosomal microRNAs in postmenopausal women with various bone mineral densities by small RNA sequencing.* Genomics, 2021. **113**(3): p. 1514-1521.

4

Supplementary data

Supplementary methods

miRNA sequencing

Small RNAs were isolated from 200 ul plasma using the Qiagen miRNAeasy Serum/ Plasma Kit (Qiagen, Germany). The TruSeq rapid SBS kit (Illumnia, USA) was used to generate small RNA sequencing libraries and RNAs were separated on 4-20% SDS-PAGE. Sequencing was performed on the Illumina HiSeq2500. Alignment to GRCh37/ hg19 reference genome was done using Bowtie [1]. HTseq count v0.11.1 [2] was used to estimate the read abundances per sample and were assigned to miRbase v21 [3]. In total, 2652 miRNAs were mapped. Since miRNAs generally show low expression levels and in the current study we were aiming to identify biomarkers, we selected the upper expression quartile for further analysis (N=663 miRNAs), to only include miRNAs that are readily measurable.

mRNA sequencing

Total RNA was isolated from preserved OA articular cartilage using Qiagen RNeasy Mini Kit (Qiagen, GmbH, Hilden, Germany). Paired-end 2×100 bp RNA-sequencing (Illumina TruSeq RNA Library Prep Kit, Illumina HiSeq2000 and Illumina HiSeq4000) was performed. Strand specific RNA-seq libraries were generated which yielded a mean of 20 million reads per sample. Data from both Illumina platforms were integrated and analyzed with the same in-house pipeline. RNA-seq reads were aligned using GSNAP [4] against GRCh37/hg19 using default parameters. Read abundances per sample was estimated using HTSeq count v0.11.1 [2]. Only uniquely mapping reads were used for estimating expression. The quality of raw reads was checked using MultiQC v1.7 [5]. The adaptors were clipped using Cutadapt v1.1 [6] applying default settings (min overlap 3, min length).

Define previously assigned subtypes

Since the N=20 overlapping patients were unevenly distributed over subtype A (N=17 patients) and subtype B (N=3 patients) and a binominal prediction requires at least five observations per group, we converted binomial variables subtype A and subtype B to a continuous variable. First, we selected the 1000 genes with highest coefficient of variation (COV) as described previously [7]. Then, we performed principal component analysis (PCA) on the samples selected for these 1000 genes using the FactoMineR 1.42 [8] package in R. To validate the assignment of subtype A and B using the factor loading scores, we performed hierarchical clustering on the PCA map, using the FactoMineR package. Subsequently, the factor loading scores of the patients were used as continuous variable for further analysis. The threshold of 0.45 was set based on the average factor

loading score of two samples with the smallest difference in PC1.

Generalized Estimating Equations

Generalized Estimating equations (GEE) was performed using IBM SPSS statistics v25. A linear model was applied and an independent structure was used. The factor loading score was set as the dependent variable and mRNAs, miRNAs, sex and/or age were set as covariates. For prediction of factor loading scores using miRNAs in plasma, only miRNAs showing correlation of $|\rho|>0.5$ with factor loading score were included as covariate. For prediction of factor loading score using mRNAs in articular cartilage, only mRNAs showing correlation of $|\rho|>0.9$ with factor loading score were included as covariate.

Elastic net regularization

Elastic net regularization was performed using the glmnet 4.1 [9] package in R, with 80% of the dataset as training dataset and 20% of the dataset as test dataset. The lambda resulting in the minimum mean cross-validated error was selected (miRNAs in plasma: lambda = 0.1133088, mRNAs in articular cartilage: lambda = 0.2766053). The alpha was selected based on the mean squared error (as low as possible), the minimum number of variables included in the model, and the highest correlation between predicted factor loading score and actual factor loading score (alpha =1, for both miRNAs in plasma and mRNAs in articular cartilage).

RT-qPCR

RNA was isolated from the cartilage as described above. cDNA synthesis was done using Transcriptor First Strand cDNA Synthesis Kit (Roche, Switzerland), using 100 ng of RNA. RT-qPCR was performed to quantitatively determine the mRNA expression levels. The relative gene expression was evaluated by the -ΔCT values, using LRRC41 and U2AF2 as internal controls. The housekeeping genes were identified by selecting for low coefficient of variance across all patients and by selecting for minimal difference in expression level between subtype A and subtype B (*LRRC41*: FC=0.983, *U2AF2*: FC=1.019).

References supplementary methods
1. Langmead, B., et al., Ultrafast and memory-efficient alignment of short DNA sequences to the human genome. Genome Biology, 2009. 10(3): p. R25.
2. Anders, S., P.T. Pyl, and W. Huber, HTSeq--a Python framework to work with high-throughput sequencing data. Bioinformatics, 2015. 31(2): p. 166-9.
3. Kozomara, A. and S. Griffiths-Jones, miRBase: annotating high confidence microRNAs using deep sequencing data. Nucleic Acids Res, 2014. 42(Database issue): p. D68-73.
4. Wu, T.D. and C.K. Watanabe, GMAP: a genomic mapping and alignment program for mRNA and EST sequences. Bioinformatics, 2005. 21(9): p. 1859-75.
5. Ewels, P., et al., MultiQC: summarize analysis results for multiple tools and samples in a single report. Bioinformatics, 2016. 32(19): p. 3047-8.
6. Martin, M., Cutadapt removes adapter sequences from high-throughput sequencing reads. 2011, 2011. 17(1): p. 3 %J EMBnet.journal.
7. Coutinho de Almeida, R., et al., Identification and characterization of two consistent osteoarthritis subtypes by

transcriptome and clinical data integration. Rheumatology (Oxford), 2020.

8. Lê, S., J. Josse, and F. Husson, FactoMineR: An R Package for Multivariate Analysis. Journal of Statistical Software, 2008. 25(1): p. 1 - 18.

9. Friedman, J.H., T. Hastie, and R. Tibshirani, Regularization Paths for Generalized Linear Models via Coordinate Descent. Journal of Statistical Software, 2010. 33(1): p. 1 - 22.

10. Coutinho de Almeida, R., et al., Allelic expression imbalance in articular cartilage and subchondral bone refined genome-wide association signals in osteoarthritis. 2022: p. 2022.04.07.22273552.
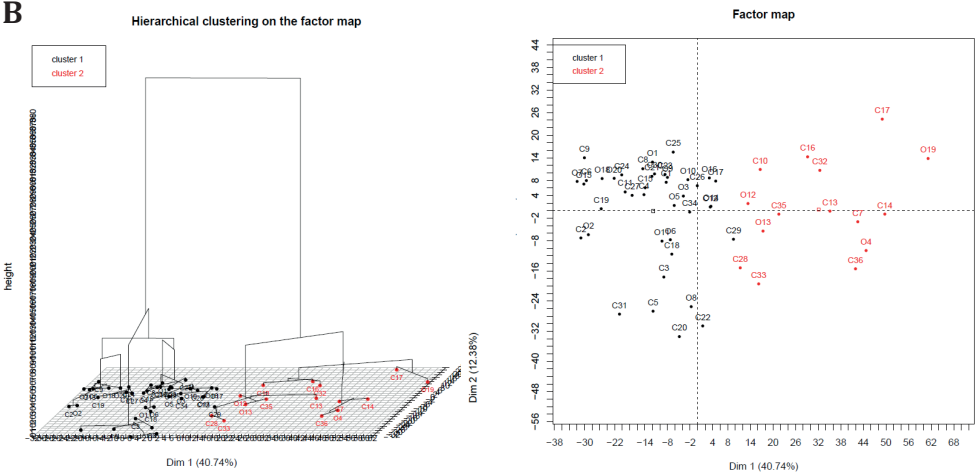
11. den Hollander, W., et al., Annotating Transcriptional Effects of Genetic Variants in Disease-Relevant Tissue: Transcriptome-Wide Allelic Imbalance in Osteoarthritic Cartilage. Arthritis Rheumatol, 2019. 71(4): p. 561-570.
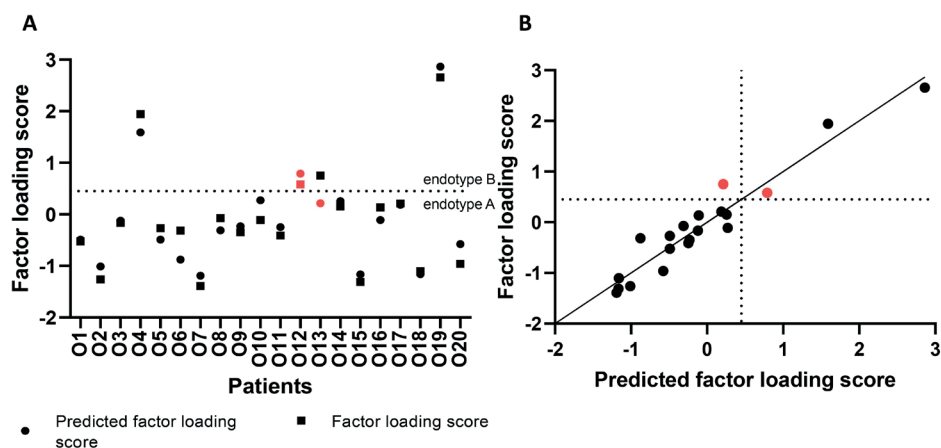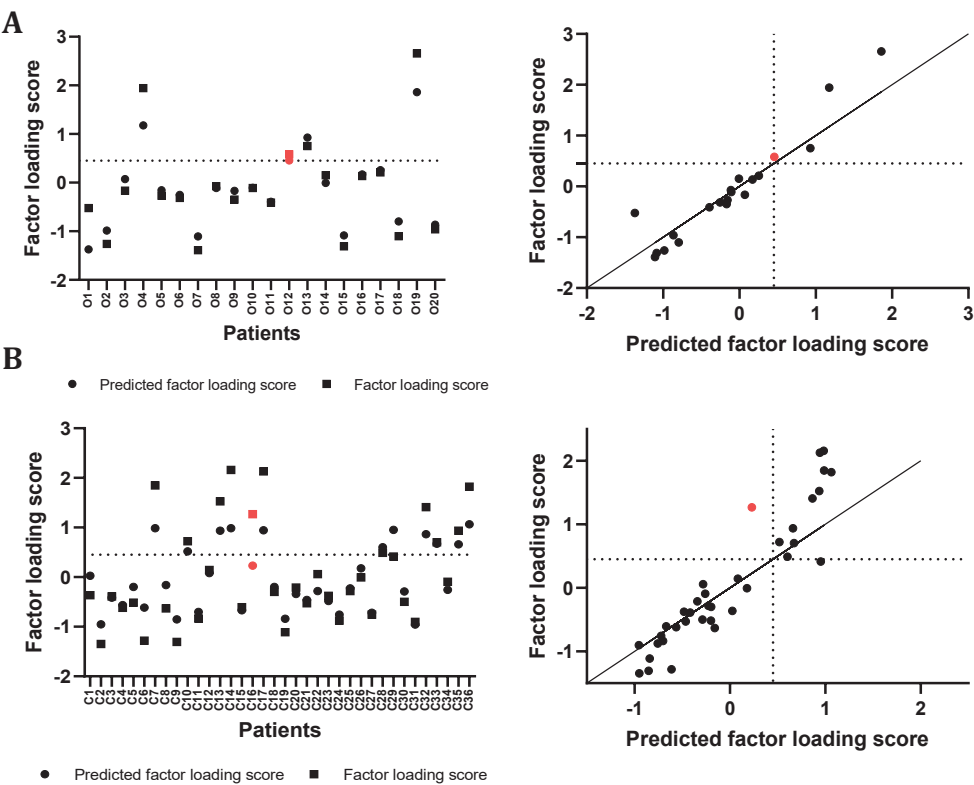
Supplementary figures

A
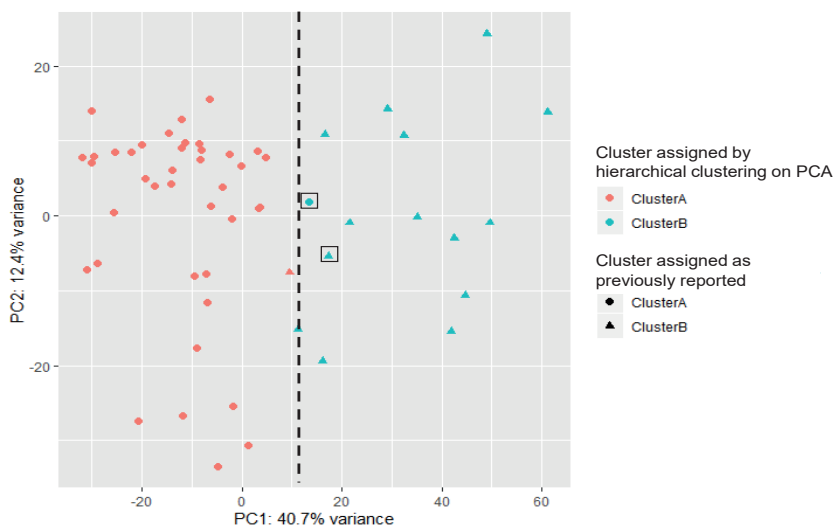
B

Supplementary Figure 1- Visualisation of cluster analysis.
(A) PCA on the samples using the 1000 genes showing the highest COV showing the separation of the clusters mainly described in PC1. The shapes represent OA subtypes as reported previously, while the colors represent OA subtype based on hierarchical clustering on the PCA. Patient O12 and C29 were not assigned similarly by the two clustering methods. The dotted line represents the threshold of separation, corresponding to a factor loading score of 0.45. (B) Hierarchical clustering on the PCA factor map to confirm whether patients are correctly assigned to an OA subtype.

Supplementary Figure 2 – Factor loading scores and predicited factor loading scores.
(A) Factor loading score vs. Predicted factor loading score. (B) Correlation between factor loading score and predicted factor loading score (ρ= 0.92) (right). In red the patients are shown that are incorrectly predicted. The dotted line represents the factor loading score threshold of 0.45. Patients indicated with O: patients of whom we have miRNA in plasma data and mRNA in articular cartilage data.

4

Supplementary Figure 2 – Factor loading score vs. Predicted factor loading score (left) and correlation between factor loading score and predicted factor loading score (ρ= 0.96 and ρ= 0.93, respectively) (right).
(A) Predictions are based on mRNA in articular cartilage and shown for the 20 overlapping patients and (B) 36 non-overlapping patients. In red patients are shown that are incorrectly predicted. The dotted line represents the factor loading score threshold of 0.45, i.e. patients with factor loading score above 0.45 are assigned to subtype B, while patients with factor loading scores below 0.45 are assigned to subtype A. Patients indicated with O: patients of whom we have miRNA in plasma data and mRNA in articular cartilage data. Patients indicated with C: patients of whom we only have mRNA in articular cartilage data.

Supplementary tables

Supplementary Table 1 – Information on samples used in this study
Supplementary Table 1A - Distribution of patients over datasets

	dataset 1	dataset 2
Goal	1. Define quantitative mRNA regression scores marking contribution of patient to OA subtype 2. Define mRNAs in articular cartilage that mark OA subtype	Define miRNAs in plasma that mark OA subtype
Number of patients	N=56	N=56
Cartilage mRNA data	N=56	N=20
Plasma miRNA data	N=20	N=56
OA subtype	N=56	N=20
Subtype A	N=41	N=17
Subtype B	N=15	N=3

Supplementary Table 1B - Sample characteristics

	Cartilage samples in cluster analysis (N=56)	Overlap between cartilage and miRNA samples (N=20)	Additional dataset for replication (N=7)
mean age (stdev)	68.0 (8.4)	72.8 (6.1)	67.9 (9.8)
female (male)	45 (11)	16 (4)	6 (6)
knees (hips)	35 (21)	15 (5)	8 (4)

4

Supplementary Table 2 (partially) - Spearman correlations between top 25% highest expressed miRNA in plasma (N=663 miRNAs) and factor loading score.
The top 50 highest correlations between miRNAs and factor loading scores are shown here.

miRNA	ρ	|ρ|	Pval	Padj
hsa-miR-195-5p	-0.61	0.61	4.13E-03	9.97E-01
hsa-miR-182-3p	0.60	0.60	4.89E-03	9.97E-01
hsa-miR-4665-5p	0.60	0.60	5.60E-03	9.97E-01
hsa-miR-3179	-0.58	0.58	7.90E-03	9.97E-01
hsa-miR-1307-3p	0.57	0.57	8.28E-03	9.97E-01
hsa-let-7e-3p	-0.55	0.55	1.15E-02	9.97E-01
hsa-miR-193b-3p	-0.55	0.55	1.26E-02	9.97E-01
hsa-miR-195-3p	-0.54	0.54	1.43E-02	9.97E-01
hsa-miR-6804-5p	-0.53	0.53	1.67E-02	9.97E-01
hsa-miR-500b-3p	-0.49	0.49	2.76E-02	9.97E-01
hsa-miR-378e	0.49	0.49	2.78E-02	9.97E-01
hsa-miR-1270	-0.49	0.49	2.81E-02	9.97E-01
hsa-miR-1343-3p	0.48	0.48	3.05E-02	9.97E-01
hsa-miR-11401	0.48	0.48	3.11E-02	9.97E-01
hsa-miR-4504	-0.48	0.48	3.20E-02	9.97E-01
hsa-miR-296-3p	0.47	0.47	3.68E-02	9.97E-01
hsa-miR-6810-5p	0.46	0.46	4.26E-02	9.97E-01
hsa-miR-301b-3p	-0.45	0.45	4.49E-02	9.97E-01
hsa-miR-132-5p	-0.45	0.45	4.51E-02	9.97E-01
hsa-miR-671-5p	0.45	0.45	4.66E-02	9.97E-01
hsa-miR-6767-5p	-0.45	0.45	4.74E-02	9.97E-01
hsa-miR-4651	0.44	0.44	5.04E-02	9.97E-01
hsa-miR-3909	-0.43	0.43	5.61E-02	9.97E-01
hsa-miR-4510	-0.42	0.42	6.28E-02	9.97E-01
hsa-miR-5698	-0.42	0.42	6.29E-02	9.97E-01
hsa-miR-4661-5p	0.42	0.42	6.39E-02	9.97E-01
hsa-miR-1227-3p	-0.42	0.42	6.62E-02	9.97E-01
hsa-miR-4646-5p	0.42	0.42	6.77E-02	9.97E-01
hsa-miR-4755-5p	-0.41	0.41	6.95E-02	9.97E-01
hsa-miR-548j-3p	-0.41	0.41	7.20E-02	9.97E-01
hsa-miR-1-3p	-0.41	0.41	7.33E-02	9.97E-01
hsa-miR-4473	-0.40	0.40	8.01E-02	9.97E-01
hsa-miR-1255b-5p	-0.40	0.40	8.06E-02	9.97E-01

miRNA	ρ	|ρ|	Pval	Padj
hsa-miR-6813-5p	0.40	0.40	8.44E-02	9.97E-01
hsa-miR-4488	0.40	0.40	8.44E-02	9.97E-01
hsa-miR-450b-5p	-0.39	0.39	8.56E-02	9.97E-01
hsa-miR-574-5p	-0.39	0.39	8.78E-02	9.97E-01
hsa-miR-190b-5p	0.39	0.39	8.83E-02	9.97E-01
hsa-miR-339-5p	0.39	0.39	8.83E-02	9.97E-01
hsa-miR-1296-5p	-0.39	0.39	8.88E-02	9.97E-01
hsa-miR-320c	0.39	0.39	9.10E-02	9.97E-01
hsa-miR-30c-1-3p	0.39	0.39	9.23E-02	9.97E-01
hsa-miR-500a-3p	-0.38	0.38	9.37E-02	9.97E-01
hsa-miR-410-3p	0.38	0.38	9.86E-02	9.97E-01
hsa-miR-532-3p	0.38	0.38	9.94E-02	9.97E-01
hsa-miR-129-5p	-0.38	0.38	1.01E-01	9.97E-01
hsa-miR-6726-3p	-0.38	0.38	1.02E-01	9.97E-01
hsa-miR-6812-3p	-0.37	0.37	1.08E-01	9.97E-01
hsa-miR-411-5p	0.37	0.37	1.08E-01	9.97E-01

4

Supplementary Table 3 - GEE, with factor loading score as dependent variable and age, sex and correlating miRNAs as covariates

Parameter	B	Std. Error	95% Wald Confidence Interval		Hypothesis Test		
			Lower	Upper	Wald Chi-Square	df	Sig.
(Intercept)	-1.95	0.74	-3.39	-0.50	6.95	1	8.37E-03
Age	0.04	0.01	0.02	0.06	16.20	1	5.70E-05
Sex	-0.56	0.21	-0.97	-0.15	7.20	1	7.31E-03
hsa_miR_6804_5p	-0.45	0.06	-0.55	-0.34	65.14	1	6.99E-16
hsa_miR_182_3p	0.52	0.05	0.42	0.62	105.91	1	0.00E+00
hsa_let_7e_3p	-0.50	0.08	-0.65	-0.34	41.59	1	1.12E-10
hsa_miR_3179	0.16	0.04	0.08	0.24	16.03	1	6.25E-05

Supplementary Table 4 (partially) - Correlations between well-expressed (highest two expression quartiles) FDR significantly differentially expressed mRNAs between cluster A and B in articular cartilage and the factor loading score.
The top 50 highest correlations between mRNAs and factor loading scores are shown here.

Ensembl ID	Gene name	ρ	|ρ|	Pval	Padj
ENSG00000101347	SAMHD1	0.94	0.94	5.32E-10	2.66E-07
ENSG00000140937	CDH11	0.92	0.92	9.20E-09	1.95E-06
ENSG00000123342	MMP19	0.91	0.91	1.80E-08	1.95E-06
ENSG00000172061	LRRC15	0.91	0.91	2.01E-08	1.95E-06
ENSG00000177575	CD163	0.91	0.91	2.01E-08	1.95E-06
ENSG00000144810	COL8A1	0.91	0.91	2.34E-08	1.95E-06
ENSG00000196735	HLA-DQA1	0.91	0.91	2.81E-08	1.95E-06
ENSG00000150687	PRSS23	0.91	0.91	3.12E-08	1.95E-06
ENSG00000159189	C1QC	0.91	0.91	3.59E-08	1.99E-06
ENSG00000154096	THY1	0.90	0.90	4.72E-08	2.15E-06
ENSG00000160255	ITGB2	0.90	0.90	4.72E-08	2.15E-06
ENSG00000137491	SLCO2B1	0.90	0.90	5.40E-08	2.25E-06
ENSG00000158710	TAGLN2	0.90	0.90	6.16E-08	2.37E-06
ENSG00000187653	TMSB4XP8	0.90	0.90	8.25E-08	2.95E-06
ENSG00000122861	PLAU	0.90	0.90	9.35E-08	3.12E-06
ENSG00000162745	OLFML2B	0.89	0.89	1.16E-07	3.61E-06
ENSG00000162511	LAPTM5	0.89	0.89	1.47E-07	4.31E-06
ENSG00000155659	VSIG4	0.88	0.88	2.59E-07	7.19E-06
ENSG00000196126	HLA-DRB1	0.88	0.88	3.57E-07	9.40E-06
ENSG00000128294	TPST2	0.88	0.88	3.97E-07	9.92E-06
ENSG00000100292	HMOX1	0.88	0.88	4.40E-07	1.03E-05
ENSG00000107438	PDLIM1	0.87	0.87	4.53E-07	1.03E-05
ENSG00000011600	TYROBP	0.87	0.87	4.87E-07	1.06E-05
ENSG00000159713	TPPP3	0.87	0.87	5.39E-07	1.12E-05
ENSG00000204287	HLA-DRA	0.87	0.87	5.95E-07	1.19E-05
ENSG00000075223	SEMA3C	0.87	0.87	7.24E-07	1.39E-05
ENSG00000143320	CRABP2	0.87	0.87	8.19E-07	1.52E-05
ENSG00000141480	ARRB2	0.86	0.86	1.06E-06	1.75E-05
ENSG00000137507	LRRC32	0.86	0.86	1.08E-06	1.75E-05
ENSG00000019582	CD74	0.86	0.86	1.16E-06	1.75E-05
ENSG00000121281	ADCY7	0.86	0.86	1.16E-06	1.75E-05
ENSG00000166825	ANPEP	0.86	0.86	1.16E-06	1.75E-05
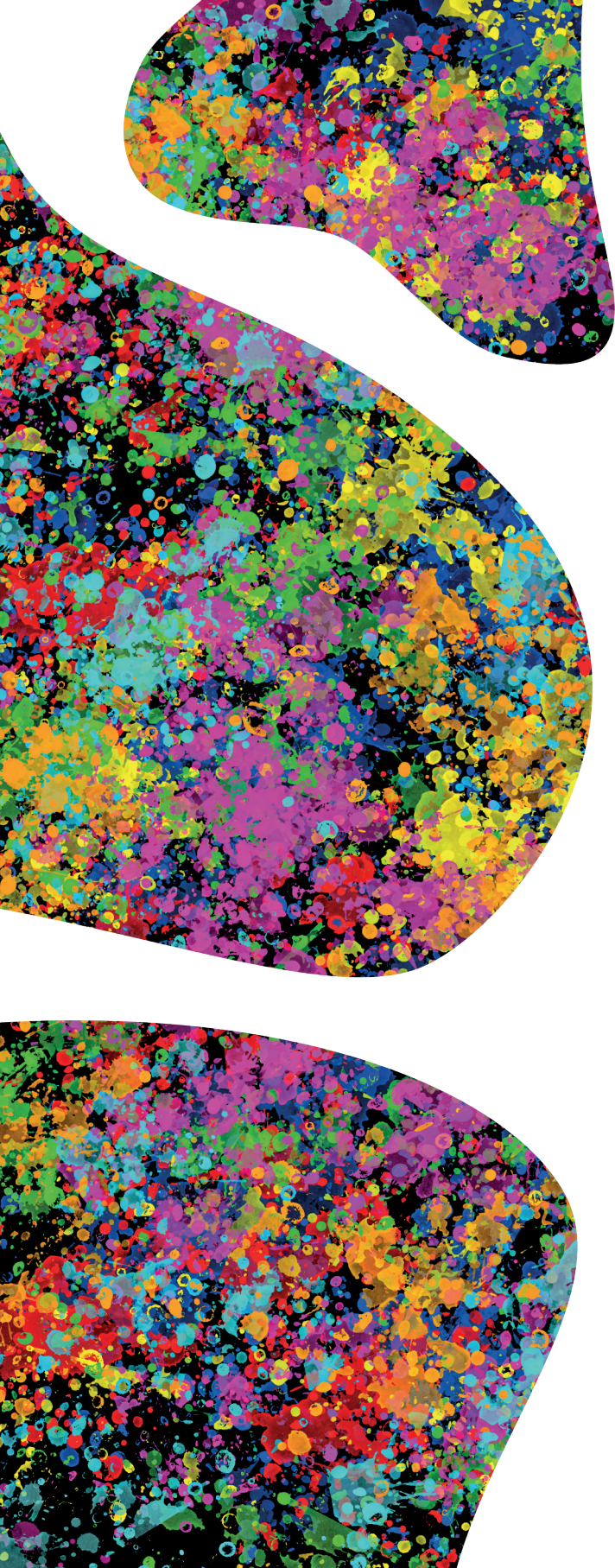
Ensembl ID	Gene name	ρ	|ρ|	Pval	Padj
ENSG00000186340	THBS2	0.86	0.86	1.16E-06	1.75E-05
ENSG00000203747	FCGR3A	0.86	0.86	1.42E-06	2.09E-05
ENSG00000108821	COL1A1	0.85	0.85	1.65E-06	2.34E-05
ENSG00000133110	POSTN	0.85	0.85	1.80E-06	2.34E-05
ENSG00000136167	LCP1	0.85	0.85	1.80E-06	2.34E-05
ENSG00000168398	BDKRB2	0.85	0.85	1.80E-06	2.34E-05
ENSG00000074410	CA12	0.85	0.85	1.82E-06	2.34E-05
ENSG00000116741	RGS2	0.85	0.85	1.96E-06	2.39E-05
ENSG00000173369	C1QB	0.85	0.85	1.96E-06	2.39E-05
ENSG00000157613	CREB3L1	0.85	0.85	2.13E-06	2.48E-05
ENSG00000183160	TMEM119	0.85	0.85	2.13E-06	2.48E-05
ENSG00000261371	PECAM1	0.85	0.85	2.52E-06	2.87E-05
ENSG00000167460	TPM4	0.85	0.85	2.74E-06	3.04E-05
ENSG00000136235	GPNMB	0.84	0.84	3.48E-06	3.77E-05
ENSG00000205403	CFI	0.84	0.84	3.56E-06	3.77E-05
ENSG00000099953	MMP11	0.84	0.84	3.77E-06	3.77E-05
ENSG00000129038	LOXL1	0.84	0.84	3.77E-06	3.77E-05

4

Supplementary Table 5 - OA risk genes differentially expressed between preserved and lesioned OA articular cartilage in either molecular endotype A or endotype B.

Supplementary Table 5A - OA risk genes differentially expressed between preserved and lesioned OA tissue of patients with OA molecular endotype A

Gene	Fold change[7]	P-value[7]	Padj[7]	Previously reported allelic imbalance	OA susceptibility based on AI	Potential therapeutics
POLD3	0.85	6.28E-03	4.18E-02	-	-	-
ERG	0.82	1.27E-03	1.25E-02	-	-	Sotalol hydrochloride (inhibitor), Amiodarone hydrochloride (inhibitor), Dofetilide (inhibitor), Idarubicin hydrochloride, Medroxyprogesterone acetate, Daunorubicin hydrochloride, Guanidine hydrochloride (inhibitor), Dalfampridine (inhibitor)
MAP2K6	0.70	6.51E-03	4.28E-02	cartilage [20]	Increased expression	Cobimetinib (inhibitor), Binimetinib (inhibitor), Trametinib (inhibitor)
MN1	0.69	2.28E-03	1.96E-02	-	-	-

Supplementary Table 5B - OA risk genes differentially expressed between preserved and lesioned OA tissue of patients with OA molecular endotype B

Gene	Fold change[7]	P-value[7]	Padj[7]	Previously reported allelic imbalance	OA susceptibility based on AI	Potential therapeutics
HLA-DPA1	0.33	1.05E-06	4.55E-04	subchondral bone [21]	Increased expression	-

4

CHAPTER 5

Characterization of underlying subchondral bone of identified OA molecular endotypes in articular cartilage

Margo Tuerlings[1], Ilja Boone[1], H. Eka D. Suchiman[1], Nico Lakenberg[1], Robert J.P. van der Wal[2], Rob G.H.H. Nelissen[2], Yolande F.M. Ramos[1], Rodrigo Coutinho de Almeida[1], Ingrid Meulenbelt[1]

[1] Dept. of Biomedical Data Sciences, Leiden University Medical Center, Leiden, The Netherlands.
[2] Dept. Orthopaedics Leiden University Medical Center, Leiden, The Netherlands.

Abstract

Objective: To characterize the underlying subchondral bone transcriptomic profile of previously identified OA molecular endotypes in OA articular cartilage.

Methods: Previously generated mRNA-seq datasets of articular cartilage (N=56 patients) and subchondral bone (N=24 patients) were combined (N=14 patients of whom both articular cartilage and subchondral bone mRNA-seq data were available) to characterize the underlying subchondral bone of molecular endotype A and B previously identified in articular cartilage. Differential expression analysis between subchondral bone of endotype A and B patients was performed. Moreover, differential expression analysis between preserved and lesioned OA subchondral bone stratified for OA molecular endotype was performed. Generalized estimating equations (GEE) was applied to find association between genes that mark OA endotype in bone and radiographic phenotype joint space narrowing (JSN) scores.

Results: Upon comparing gene expression levels of the underlying subchondral bone between OA molecular endotype A and B, we found 543 genes being FDR significantly differentially expressed. Similar to articular cartilage, these 543 differentially expressed genes in subchondral bone were enriched for processes such as immune response (GO:0006955), characterized by expression of *IL1B* (FD=3.98, FDR=4.11x10^{-3})*, TNFSF14* (FD=7.48, FDR=1.44x10^{-2})*,* and *OSM* (FD=6.31 FDR=1.19x10^{-4}), with higher expression of these genes in molecular endotype B compared to A. Upon calculating association beteween gene expression levels and radiographic phenotypes, we found *RSP7P1* and *NSA2* being positively associated to JSN and these genes were higher expressed in endotype B compared to endotype A patients. On the other hand, we found *ZFP41* and *NOTCH4* being negatively associated to JSN and these genes showed higher expression in endotype A compared to endotype B patients. The latter confirms the association between endotype B and increased JSN, which is also observed in articular cartilage.

Conclusion: Altogether, we here showed that underlying bone of OA endotypes identified in articular cartilage is significantly different between OA molecular endotypes. We showed that OA endotype B was associated with excessive bone formation, in line with increased joint space narrowing. Moreover, OA endotype A was associated with increased expression of neuronal markers, suggesting these patients might experience pain in an earlier OA stage compared to endotype B OA patients.

Introduction

Osteoarthritis (OA) is a highly prevalent heterogeneous disease of the whole joint, characterized by, amongst others, articular cartilage degeneration and subchondral bone remodeling [1, 2]. OA has a considerable genetic component and previous comprehensive genome wide association studies (GWAS) have identified OA risk genes, such as *WNT10B, TNFSF11,* and *IL11,* that are involved in maintenance processes in both articular cartilage and subchondral bone, indicating that both tissues are involved in initiation and progression of OA pathophysiology [3-7]. Prevalence of OA is increased among elderly and pain and stiffness are hallmark symptoms of OA. As such, OA is known to cause substantial effects on quality of life. Yet, no treatment options are available to prevent, slow down, or cure OA, except for total joint replacement surgery at end-stage OA [8]. Failure in development of OA disease modifying treatments might be due to OA heterogeneity, that does not accommodate the one-drug-fits-all-patients design applied thus far [9]. In this respect, Soul et al [10] reported on the identification of two OA molecular endotypes using RNA-sequencing (RNA-seq) of articular cartilage, which we confirmed in an independent dataset [11]. The two identified endotypes represented chondrocyte hypertrophy pathway and immune response pathway, respectively. Moreover, we showed that joint space width was significantly lower (increased joint space narrowing (JSN)) in endotype B compared to endotype A patients [11]. Subsequently, to make these OA molecular endotypes more applicable to clinical practice, we focused on identification of circulating miRNAs that can be used to stratify patients into OA endotype before a potential treatment strategy starts (**Chapter 4**). Moreover, we proposed potential therapeutic targets for both endotypes by combining differential expression analysis data with GWAS and allelic imbalance data. As such, we identified *MAP2K6* as potential druggable target for endotype A patients and *HLA-DPA1* as potential druggable target for endotype B patients. Although effort has been made to identify and characterize these OA endotypes in articular cartilage and find biomarkers in blood plasma, the underlying subchondral bone remains unexplored. This despite the fact that subchondral bone contributes to onset and progression of OA as shown by genetic studies [7], indicating that these differences, and hence optimal treatment options, can also originate from subchondral bone. Therefore, in the current study we set out to characterize OA molecular cartilage endotypes in the underlying subchondral bone by using our previously described RNA-seq datasets [12, 13].

5

Methods

Sample description

This study includes 66 patient of the RAAK study, who underwent a joint replacement surgery due to OA. Macroscopically preserved and lesioned OA articular cartilage and its underlying subchondral bone were collected as described previously [14]. Informed consent was obtained from all participants and ethical approval for the RAAK study was given by the medical ethics committee of the Leiden University Medical Center (P08.239/P19.013).

mRNA sequencing

Total RNA was isolated from articular cartilage and subchondral bone using Qiagen RNeasy Mini Kit (Qiagen, GmbH, Hilden, Germany). Paired-end 2×100 bp RNA-sequencing (Illumina TruSeq RNA Library Prep Kit, Illumina HiSeq2000 and Illumina HiSeq4000) was performed. Strand specific RNA-seq libraries were generated which yielded a mean of 20 million reads per sample. Data from both Illumina platforms were integrated and analyzed with the same in-house pipeline. RNA-seq reads were aligned using GSNAP [15] against GRCh37 (articular cartilage or GRCh38 (subchondral bone) using default parameters. Read abundances per sample was estimated using HTSeq count v0.11.1 [16]. Only uniquely mapping reads were used for estimating expression. The quality of raw reads was checked using MultiQC v1.7 [17]. The adaptors were clipped using Cutadapt v1.1 [18] applying default settings (min overlap 3, min length).

Differential expression analysis

Differential expression analysis was performed between OA endotype A and B and between preserved and lesioned subchondral bone using the DESeq2 R package, version 1.24.0 [19]. Endotype A or preserved tissue were set as the reference and to correct for multiple testing Benjamini-Hochberg method was used, as indicated by the false discovery rate (FDR), with a significance cutoff value of 0.05.

Spearman correlation

First, gene expression levels were normalized by performing variance-stabilizing transformation using DESeq2 R package. Subsequently, Spearman correlations between gene expression levels and previously reported factor loading scores were calculated using Hmisc R package. Again Benjamini-Hochberg method was used to correct for multiple testing, as indicated by FDR.

Association between radiographic phenotypes and gene expression levels

Generalized estimation equation was performed in SPSS v25 to calculate association, with gene expression as dependent variable and sex, age, joint site and BMI as covariates.

Scoring of radiographic phenotypes joint space narrowing and osteophyte scores were described previously [11].

Results

Sample characteristics

The current study includes mRNA-seq data of 66 patients (N=56 articular cartilage samples, N=24 subchondral bone samples) who underwent a total joint replacement surgery due to OA (RAAK-study). As shown in **Figure 1**, of 14 patients both articular cartilage and subchondral bone mRNA-seq data were available. Of these 14 patients, 11 patients were assigned to OA endotype A, representing chondrocyte hypertrophy pathway while 3 patients were assigned to OA endotype B, representing immune response pathway and being associated to increased joint space narrowing in our previous study [11]. Data of these 14 patients were used to characterize the subchondral bone. Patients characteristics are shown in **Supplementary Table 1**.

Dataset 1
Articular cartilage preserved
N=56 patients

Molecular endotype A   30   11   10

Molecular endotype B   12   3

Dataset 2
Subchondral bone preserved
N=24 patients

Subset 1
Preserved articular cartilage and
subchondral bone data available
N=14 patients

5
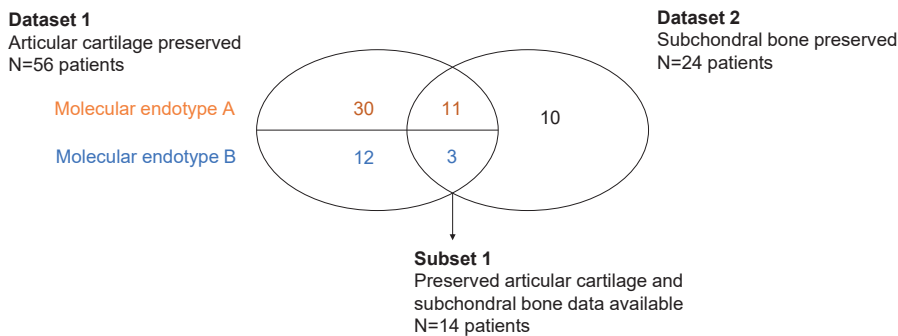
Figure 1 – Venn diagram of datasets used in this study.
Dataset 1 consists of preserved OA articular cartilage mRNA-seq data of 56 patients of whom endotypes were determined previously. Dataset 2 consists of preserved OA subchondral bone mRNA-seq data of 24 patients. Of 14 patients both articular cartilage and subchondral bone mRNA-seq data was available, indicated with subset 1.

Differential expression analysis between OA molecular endotype A and B subchondral bone

To evaluate whether the underlying subchondral bone showed differences between molecular endotype A and B identified in cartilage, we first compared transcriptomic profiles of macroscopically preserved subchondral bone between these endotypes (N=11 and N=3 paired samples for endotype A and B, respectively. **Subset 1, Figure 1**). Upon performing differential expression analysis, we identified 543 FDR significantly differentially expressed genes (**Supplementary Table 2**), of which 363 genes showed an absolute fold difference of 2 or higher. The most significantly upregulated gene in

endotype A relative to endotype B was *CHRDL2* (FD= 34.84, FDR= 3.37×10^{-2}), while the most significantly upregulated gene in endotype B relative to endotype A was *BCL2L15* (FD= 22.17, FDR= $4,65 \times 10^{-3}$). To see whether these differentially expressed genes were involved in particular pathways or processes, we performed gene enrichment analysis. Among the 94 genes upregulated in endotype A relative to endotype B, we only found significant enrichment for positive regulation of transcription from RNA polymerase II promoter (GO:0045944, 16 genes, FDR=1.21×10^{-2}), characterized by *NFAT5* (FD=1.67, FDR=4.23×10^{-3}) and *KLF15* (FD=2.98, FDR=3.28×10^{-2}) (**Supplementary Table 3A**). Among the 449 genes upregulated in endotype B relative to endotype A subchondral bone, we found significant enrichment for 32 processes, including immune response (GO:0006955, 34 genes, FDR=5.30×10^{-6}), characterized by expression of *IL1B* (FD=3.98, FDR=4.11×10^{-3})*, TNFSF14* (FD=7.48, FDR=1.44×10^{-2})*,* and *OSM* (FD=6.31 FDR=1.19×10^{-4}), and positive regulation of interleukin-6 production (GO:0032755, 16 genes, FDR=2.19×10^{-5}), characterized by expression of *IL1B* (FD=3.98, FDR=4.11×10^{-3}), *TNFSF4* (FD=2.37, FDR=4.04×10^{-2})*,* and *AIF1* (FD=2.53, FDR=6.22×10^{-3}), both processes also enriched among genes differentially expressed between OA endotypes in articular cartilage (**Supplementary Table 3B**).

Endotype A and B exclusive genes with OA pathophysiology in subchondral bone
Next, we explored the OA pathophysiological process in both OA molecular endotypes by comparing gene expression levels of macroscopically preserved and lesioned OA subchondral bone. Upon performing differential expression analysis between preserved and lesioned subchondral bone samples of patients with endotype A OA, we identified 107 genes FDR significantly differentially expressed (**Supplementary Table 4**). Of these genes, 15 genes showed an absolute foldchange of 2 or higher, including neuronal markers *STMN2* (FC=24.40 FDR=1.52×10^{-2})*, FGF14* (FC=0.32, FDR=7.73×10^{-4}), and *CNTNAP2* (FC=2.60, FDR=1.50×10^{-2}). We did not find significantly enriched processes among the differentially expressed genes. Differential expression analysis between preserved and lesioned subchondral bone of patients with endotype B OA resulted in identification of 11 genes being FDR significantly differentially expressed, of which 7 showed an absolute foldchange of 2 or higher (**Supplementary Table 5**). These differentially expressed genes included *COL1A1* (FC=2.26, FDR=6.52×10^{-4})*, GDF6* (FC=16.69, FDR=2.27×10^{-2})*,* and *CXCL9* (FC=0.30, FDR=8.56×10^{-4}). Gene enrichment analysis on these 11 differentially expressed genes showed significant enrichment for extracellular region and collagen type 1 trimer.

As shown in **Figure 2**, we identified 30 genes being exclusive for OA endotype A, i.e. not differentially expressed in OA endotype B nor in the total dataset [13], including *MYOC* (FC=0.15, FDR=1.93×10^{-2})*, CNTFR* (FC=0.51, .FDR=1.31×10^{-2})*,* and *CIC* (FC=0.74, FDR=3.84×10^{-2}). Moreover, we identified 7 genes exclusive for OA endotype B, i.e. not

differentially expressed in OA endotype A nor in the total dataset, including *COL1A1* (FC=2.26, FDR=6.52x10^{-4}), *COL1A2* (FC=1.89, FDR=3.46x10^{-2}), and *GDF6* (FC=16.69, FDR=2.27x10^{-2}).
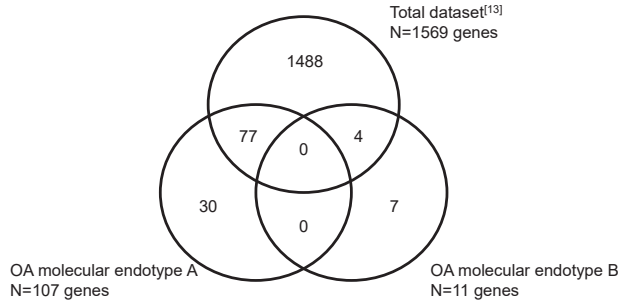

Figure 2 – Venn diagram of genes differentially expressed between preserved and lesioned OA subchondral bone in the total dataset, OA endotype A, and OA endotype B.
We identified 30 genes being exclusively differentially expressed in OA endotype A and 7 genes being exclusively differentially expressed in OA endotype B.

Markers for OA molecular endotype in subchondral bone

To find genes expressed in subchondral bone that mark OA endotype A or B, we calculated Spearman correlations between gene expression levels of the here identified genes differentially expressed between endotype A and B and previously reported quantitative factor loading scores representing contribution of each patient to either endotype A or B (N=14 patients, of whom RNA-seq data of subchondral bone and factor loading scores were available). Albeit not FDR significant, we found 36 genes correlating to these factor loading scores (|ρ|>0.6, P-value <0.05, **Table 1**).

Since radiographic OA feature joint space narrowing was previously shown to be higher in endotype B compared to endotype A patients, we calculated association between the 36 correlating genes and these radiographic phenotype scores (N=24 patients of whom RNA-seq data and radiographic phenotypes were available). As shown in **Table 1**, *RSP7P1, NSA2,* and *AC023090.2* were positively associated to joint space narrowing score, while *ZFP41* and *NOTCH4* were negatively associated to joint space narrowing score. All positively associated genes were higher expressed in endotype B, except for *AC023090.2*, while all negatively associated genes were lower expressed in endotype B compared to endotype A. This again confirms endotype B being associated to increased joint space narrowing. Together, these results show that high expression levels of *RSP7P1* and *NSA2* and low expression of *ZFP41* and *NOTCH4* characterize endotype B OA in subchondral bone.

Comparison subchondral bone and articular cartilage
To find genes that mark OA molecular endotypes A and B in both articular cartilage and subchondral bone, we compared the results of subchondral bone presented here with our previously reported results on articular cartilage [11]. Upon comparing genes that were differently expressed between endotype A and B in both tissues, we found 185 genes overlapping, of which 180 genes showed similar directions of effect, including *PLAUR, CHRDL2,* and *NOTCH4* (**Supplementary Figure 1A, Supplementary Table 6**). These 180 genes were significantly enriched for 46 processes (**Supplementary Table 7**). Of these 46 processes, 45 were involved in processes regarding immune response, represented by genes such as *IL1B, OSM,* and *CD38*.
Upon comparing the exclusively molecular endotype A and B differentially expressed genes between preserved and lesioned subchondral bone and articular cartilage, we found 3 genes exclusively differentially expressed in molecular endotype A in both subchondral bone and articular cartilage (**Supplementary Figure 1B, Supplementary Table 8**). We did not find any overlapping genes between bone and cartilage in molecular endotype B exclusive genes (**Supplementary Figure 1C**).

Discussion
In the current study, we characterized the underlying bone of previously identified consistent OA molecular endotypes (endotype A and endotype B) in articular cartilage. Upon comparing gene expression levels of the underlying subchondral bone between the molecular endotypes identified in articular cartilage, we found 543 genes being FDR significantly differentially expressed. Compared to findings in articular cartilage, these 543 differentially expressed genes were enriched for similar processes, including immune response (GO:0006955) and signal transduction (GO:0007165). Subsequently, upon performing differential expression analysis between preserved and lesioned OA subchondral bone stratified for OA molecular endotype, we identified 30 FDR significantly differently expressed genes exclusively for endotype A and 7 FDR significantly differentially expressed genes exclusively for endotype B.

Although OA molecular endotype A and B robustly identified in articular cartilage were not previously identified in subchondral bone, we here showed that underlying subchondral bone is different between OA endotypes. Upon performing differential expression analysis between preserved and lesioned OA subchondral bone stratified for OA endotype, we identified 107 genes FDR significantly differentially expressed for endotype A. Among these genes we found neuronal markers *CNTNAP2* and *STMN2,* which were both increased in lesioned OA subchondral bone (FC=2.60 and FC=24.40, respectively) [20-23]. This could suggest that new neuronal structures are formed with OA in patients with endotype A OA, resulting in more pain compared to patients with

Table 1 – association between genes marking endotype A and B OA in subchondral bone and radiographic phenotype joint space narrowing.

RSP7P1, *NSA2*, and *AC023090.2* showed positive association to JSN scores and were higher expressed in endotype B compared to endotype A patients, except for *AC023090.2*. *ZFP41* and *NOTCH4* were negatively associated to JSN and were higher expressed in endotype A compared to endotype B OA patients. Correlation between gene expression and FLS was calculated using data of 14 patients and association between gene expression and joint space narrowing scores was calculated using data of 24 patients.

Gene	Joint space narrowing score				Correlation FLS		Fold difference B vs A
	b	lower	upper	p-value	ρ	p-value	
SVBP	-0.03	-0.12	0.05	3.99E-01	0.72	3.78E-03	1.61
RIT1	-0.01	-0.06	0.04	7.19E-01	0.71	4.45E-03	1.41
ELOF1	0.01	-0.04	0.06	6.89E-01	0.71	4.82E-03	1.50
RPS24P8	0.03	0.00	0.07	6.13E-02	0.70	5.63E-03	1.51
LYSMD2	0.02	-0.04	0.08	4.87E-01	0.68	7.04E-03	1.50
IL1B	0.10	-0.02	0.22	9.32E-02	0.68	7.56E-03	3.98
AC004453.1	0.06	-0.02	0.14	1.43E-01	0.67	8.70E-03	1.44
CYREN	0.02	-0.04	0.08	5.65E-01	0.67	8.70E-03	1.49
AL450405.1	-0.04	-0.11	0.04	3.54E-01	0.67	9.32E-03	1.41
RPS7P1	**0.04**	**0.00**	**0.08**	**4.54E-02**	**0.65**	1.21E-02	**1.49**
TNFSF4	0.04	-0.04	0.11	3.37E-01	0.64	1.29E-02	2.37
ID2	0.03	-0.09	0.15	6.23E-01	0.63	1.56E-02	1.35
TUBAP2	0.01	-0.06	0.07	8.67E-01	0.63	1.56E-02	2.42
OST4	-0.04	-0.09	0.00	8.08E-02	0.63	1.65E-02	1.48
ANAPC11	-0.03	-0.08	0.02	2.13E-01	0.62	1.76E-02	1.51
TUBA1C	0.00	-0.08	0.07	9.79E-01	0.62	1.76E-02	2.09
CENPK	0.00	-0.07	0.07	9.29E-01	0.62	1.86E-02	3.65
NSA2	**0.06**	**0.02**	**0.10**	**6.10E-03**	**0.61**	1.97E-02	**1.47**
GAPDHP1	-0.07	-0.15	0.01	8.25E-02	0.61	2.09E-02	1.87
TMEM9B	-0.01	-0.04	0.02	5.29E-01	0.61	2.09E-02	1.48
EEF1B2	0.06	-0.01	0.12	8.25E-02	0.60	2.21E-02	1.74
AL590999.1	0.05	-0.01	0.11	1.12E-01	-0.60	2.21E-02	0.32
AC068587.4	0.02	-0.22	0.27	8.53E-01	-0.61	2.09E-02	0.25
ZFP41	**-0.08**	**-0.14**	**-0.02**	**1.23E-02**	**-0.62**	1.86E-02	**0.46**
FAM214A	0.02	-0.03	0.08	3.98E-01	-0.62	1.76E-02	0.65
NALT1	-0.06	-0.19	0.07	3.77E-01	-0.63	1.56E-02	0.20
ZNF580	-0.04	-0.10	0.03	2.49E-01	-0.63	1.56E-02	0.56
TTC28	-0.03	-0.13	0.06	4.70E-01	-0.64	1.47E-02	0.51
KIAA1217	-0.05	-0.16	0.06	3.63E-01	-0.65	1.14E-02	0.49
KAT2A	-0.03	-0.09	0.04	3.98E-01	-0.66	1.07E-02	0.66
USP31	0.00	-0.05	0.05	9.16E-01	-0.66	9.98E-03	0.63
ZNF703	-0.06	-0.19	0.06	2.91E-01	-0.67	9.32E-03	0.35

5

AC023090.2	**0.05**	**0.01**	**0.08**	**1.58E-02**	**-0.67**	8.70E-03	**0.21**
NOTCH4	**-0.14**	**-0.22**	**-0.07**	**1.33E-04**	**-0.69**	6.07E-03	**0.54**
KLF15	0.07	-0.02	0.16	1.27E-01	-0.75	1.84E-03	0.34
CNTN2	-0.03	-0.15	0.10	6.84E-01	-0.83	2.51E-04	0.18

endotype B OA, which is in line with the fact that patients of endotype A have wide joint spaces, hence cartilage, at the moment of their total joint replacement surgery. Upon comparing preserved and lesioned OA subchondral bone in endotype B OA, we identified 11 FDR significant differentially expressed genes. Among these 11 genes we identified *COL1A1* (FC=2.26) , *COL1A2* (FC=1.88), *CXCL9* (FC=0.30)*,* and *GDF6* (FC=16.69). *CXCL9*, encoding C-X-C motif chemokine ligand 9, was previously shown to inhibit bone formation and promoting bone resorption, resulting in bone loss [24]. *GDF6,* encoding growth differentiation factor 6, is required for normal formation of joints and bone [25, 26]. Upregulation of *COL1A1, COL1A2,* and *GDF6,* together with downregulation of *CXCL9* suggests capacity of bone formation with ongoing OA in endotype B patients, which is in line with observed increased joint space narrowing. It is tempting to speculate that this bone forming capacity prevents pain sensation in these endotype B patients.

In our previous study in which we performed cluster analysis based on top 1000 most variable genes expressed in subchondral bone, we identified clusters based on joint site but no clustering similar to identified OA molecular endotype A and B in articular cartilage [13]. This suggests that the difference between hip and knee subchondral bone is probably larger than the difference between OA endotypes. Therefore, a larger dataset is required to be able to identify OA endotypes in subchondral bone. Moreover, optimizing the number of variable genes included in the cluster analysis could also result in identification of these OA endotypes. As such, the main drawback of current study is the relatively low sample size and small overlap between subchondral bone and articular cartilage samples (N=14 patients: N=11 endotype A, N=3 endotype B). Nevertheless, despite this low sample size we were able to identify FDR significantly differentially expressed genes, indicating their consistency in expression. Increasing sample size and overlap between articular cartilage and subchondral bone might result in the identification of more genes and pathways and therefore better characterization. Validation of the results reported here in an independent dataset is necessary.

Altogether, we here showed that underlying bone of OA endotypes identified in articular cartilage is significantly different between endotypes. We showed that OA endotype B was associated with bone formation capacity, in line with increased joint space narrowing. Moreover, OA endotype A was associated with increased expression

of neuronal markers, suggesting these patients might experience pain in an earlier OA stage compared to endotype B OA patients.

Declarations

5

Disclosures

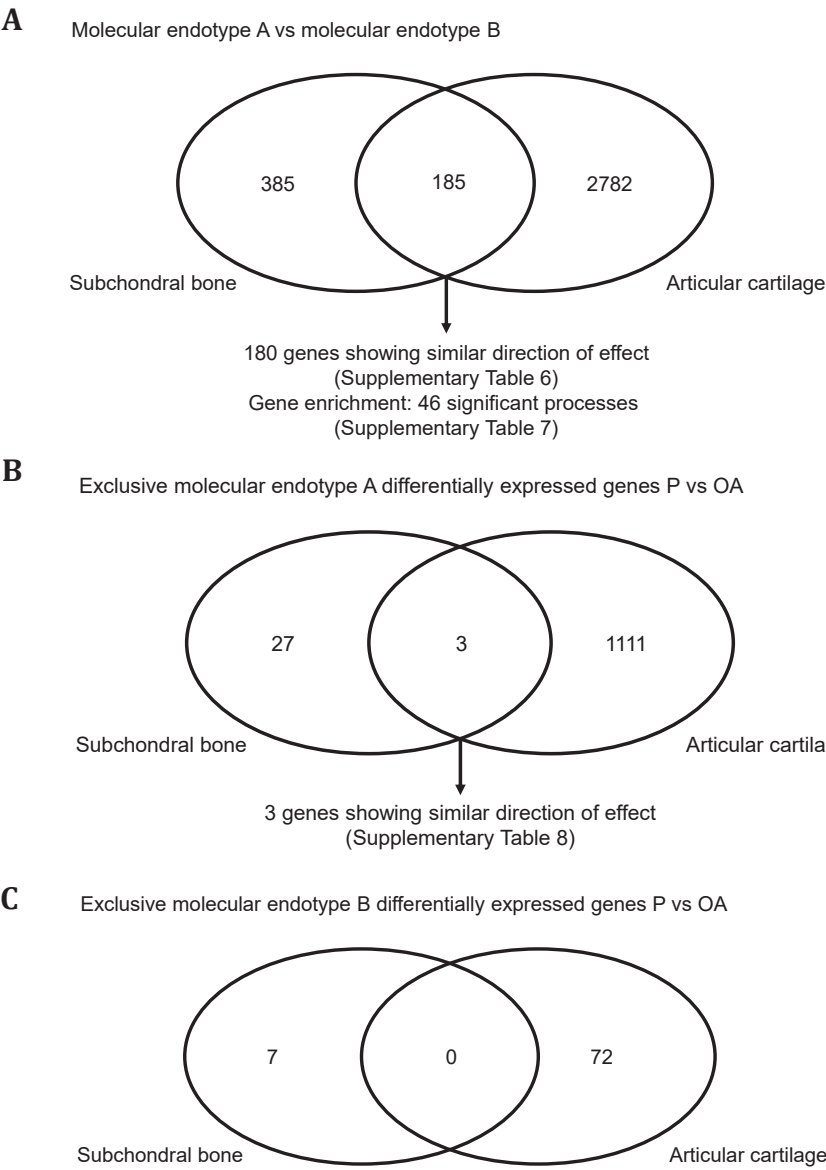The authors have declared no conflicts of interest.

References

1. Li, G., et al., *Subchondral bone in osteoarthritis: insight into risk factors and microstructural changes.* Arthritis Research & Therapy, 2013. **15**(6): p. 223.
2. Glyn-Jones, S., et al., *Osteoarthritis.* Lancet, 2015. **386**(9991): p. 376-87.
3. Fellows, C.R., C. Matta, and A. Mobasheri, *Applying Proteomics to Study Crosstalk at the Cartilage-Subchondral Bone Interface in Osteoarthritis: Current Status and Future Directions.* EBioMedicine, 2016. **11**: p. 2-4.
4. Goldring, S.R. and M.B. Goldring, *Changes in the osteochondral unit during osteoarthritis: structure, function and cartilage-bone crosstalk.* Nat Rev Rheumatol, 2016. **12**(11): p. 632-644.
5. Funck-Brentano, T. and M. Cohen-Solal, *Crosstalk between cartilage and bone: when bone cytokines matter.* Cytokine Growth Factor Rev, 2011. **22**(2): p. 91-7.
6. Pan, J., et al., *Elevated cross-talk between subchondral bone and cartilage in osteoarthritic joints.* Bone, 2012. **51**(2): p. 212-7.
7. Boer, C.G., et al., *Deciphering osteoarthritis genetics across 826,690 individuals from 9 populations.* Cell, 2021.
8. Ghouri, A. and P.G. Conaghan, *Update on novel pharmacological therapies for osteoarthritis.* Ther Adv Musculoskelet Dis, 2019. **11**: p. 1759720x19864492.
9. Grässel, S. and D. Muschter, *Recent advances in the treatment of osteoarthritis.* F1000Research, 2020. **9**: p. F1000 Faculty Rev-325.
10. Soul, J., et al., *Stratification of knee osteoarthritis: two major patient subgroups identified by genome-wide expression analysis of articular cartilage.* Ann Rheum Dis, 2018. **77**(3): p. 423.
11. Coutinho de Almeida, R., et al., *Identification and characterization of two consistent osteoarthritis subtypes by transcriptome and clinical data integration.* Rheumatology (Oxford), 2020.
12. Coutinho de Almeida, R., et al., *RNA sequencing data integration reveals an miRNA interactome of osteoarthritis cartilage.* Ann Rheum Dis, 2019. **78**(2): p. 270-277.
13. Tuerlings, M., et al., *RNA sequencing reveals interacting key determinants of osteoarthritis acting in subchondral bone and articular cartilage.* Arthritis Rheumatol, 2020.
14. Ramos, Y.F., et al., *Genes involved in the osteoarthritis process identified through genome wide expression analysis in articular cartilage; the RAAK study.* PLoS One, 2014. **9**(7): p. e103056.
15. Wu, T.D. and C.K. Watanabe, *GMAP: a genomic mapping and alignment program for mRNA and EST sequences.* Bioinformatics, 2005. **21**(9): p. 1859-75.
16. Anders, S., P.T. Pyl, and W. Huber, *HTSeq--a Python framework to work with high-throughput sequencing data.* Bioinformatics, 2015. **31**(2): p. 166-9.
17. Ewels, P., et al., *MultiQC: summarize analysis results for multiple tools and samples in a single report.* Bioinformatics, 2016.

32(19): p. 3047-8.

18. Martin, M., *Cutadapt removes adapter sequences from high-throughput sequencing reads.* 2011, 2011. **17**(1): p. 3 %J EMBnet.journal.

19. Love, M.I., W. Huber, and S. Anders, *Moderated estimation of fold change and dispersion for RNA-seq data with DESeq2.* Genome Biology, 2014. **15**(12): p. 550.

20. Lu, Z., et al., *Molecular Architecture of Contactin-associated Protein-like 2 (CNTNAP2) and Its Interaction with Contactin 2 (CNTN2).* J Biol Chem, 2016. **291**(46): p. 24133-24147.

21. Rodenas-Cuadrado, P., J. Ho, and S.C. Vernes, *Shining a light on CNTNAP2: complex functions to complex disorders.* Eur J Hum Genet, 2014. **22**(2): p. 171-8.

22. Chiellini, C., et al., *Stathmin-like 2, a developmentally-associated neuronal marker, is expressed and modulated during osteogenesis of human mesenchymal stem cells.* Biochem Biophys Res Commun, 2008. **374**(1): p. 64-8.

23. Kuttapitiya, A., et al., *Microarray analysis of bone marrow lesions in osteoarthritis demonstrates upregulation of genes implicated in osteochondral turnover, neurogenesis and inflammation.* Ann Rheum Dis, 2017. **76**(10): p. 1764-1773.

24. Liu, Z., et al., *Increased Osteoblastic Cxcl9 Contributes to the Uncoupled Bone Formation and Resorption in Postmenopausal Osteoporosis.* Clinical interventions in aging, 2020. **15**: p. 1201-1212.

25. Deng, P., et al., *Growth differentiation factor 6, a repressive target of EZH2, promotes the commitment of human embryonic stem cells to mesenchymal stem cells.* Bone Research, 2020. **8**(1): p. 39.

26. Settle, S.H., Jr., et al., *Multiple joint and skeletal patterning defects caused by single and double mutations in the mouse Gdf6 and Gdf5 genes.* Dev Biol, 2003. **254**(1): p. 116-30.

5

Supplementary files

Supplementary figures

A   Molecular endotype A vs molecular endotype B

385   185   2782

Subchondral bone   Articular cartilage

180 genes showing similar direction of effect
(Supplementary Table 6)
Gene enrichment: 46 significant processes
(Supplementary Table 7)

B   Exclusive molecular endotype A differentially expressed genes P vs OA

27   3   1111

Subchondral bone   Articular cartilage

3 genes showing similar direction of effect
(Supplementary Table 8)

C   Exclusive molecular endotype B differentially expressed genes P vs OA

7   0   72

Subchondral bone   Articular cartilage

Supplementary Figure 1 – Venn diagrams representing overlapping genes between subchondral bone and articular cartilage.
(A) Overlapping genes differentially expressed between OA molecular endotype A and B in articular cartilage and subchondral bone. (B) Overlapping differentially expressed genes between preserved and lesioned articular cartilage and subchondral bone exclusive for molecular endotype A. (C) Overlapping differentially expressed genes between preserved and lesioned articular cartilage and subchondral bone exclusive for molecular endotype B.

Supplementary tables

Supplementary Table 1 – patient characteristics

	Cartilage samples (N=56)	Bone samples (N=24)	Overlap cartilage and bone (N=14)
mean age (stdev)	68.0 (8.4)	66.2 (8.6)	67 (8.9)
female (male)	45 (11)	22 (2)	12 (2)
knees (hips)	35 (21)	18 (6)	12 (2)

5

Supplementary Table 2 (partially) - Differentially expressed genes in macroscopically preserved subchondral bone between OA endotype A and B.
Subtype A is set as a reference. The top 50 most significant differentially expressed genes between OA endotype A and B are shown here.

Ensembl ID	Gene Name	Base mean	Log 2 fold change	Fold change	P-value	FDR
ENSG00000198829	SUCNR1	68.00	2.61	6.10	1.31E-08	1.19E-04
ENSG00000099985	OSM	13.00	2.66	6.31	1.39E-08	1.19E-04
ENSG00000101916	TLR8	87.89	2.19	4.57	6.80E-08	3.88E-04
ENSG00000204482	LST1	145.88	2.64	6.24	4.06E-07	1.60E-03
ENSG00000100427	MLC1	64.30	4.29	19.51	4.68E-07	1.60E-03
ENSG00000118640	VAMP8	136.50	1.57	2.97	1.22E-06	3.28E-03
ENSG00000087586	AURKA	50.22	3.21	9.26	1.61E-06	3.28E-03
ENSG00000173391	OLR1	55.34	3.95	15.45	1.72E-06	3.28E-03
ENSG00000131355	ADGRE3	25.53	4.17	18.01	1.45E-06	3.28E-03
ENSG00000111639	MRPL51	216.99	0.61	1.53	3.46E-06	3.49E-03
ENSG00000274210	RF00003	80.59	1.71	3.28	2.69E-06	3.49E-03
ENSG00000116701	NCF2	397.12	2.04	4.10	2.93E-06	3.49E-03
ENSG00000146285	SCML4	13.29	2.16	4.47	2.83E-06	3.49E-03
ENSG00000150681	RGS18	110.25	2.50	5.65	2.62E-06	3.49E-03
ENSG00000105374	NKG7	128.09	2.98	7.88	3.30E-06	3.49E-03
ENSG00000214212	C19orf38	48.88	3.15	8.89	3.36E-06	3.49E-03
ENSG00000163563	MNDA	423.31	3.47	11.10	2.40E-06	3.49E-03
ENSG00000090382	LYZ	3397.50	4.02	16.19	3.72E-06	3.54E-03
ENSG00000123329	ARHGAP9	160.76	2.32	5.00	4.10E-06	3.70E-03
ENSG00000116586	LAMTOR2	99.12	0.68	1.60	4.86E-06	4.11E-03
ENSG00000125538	IL1B	14.23	1.99	3.98	5.04E-06	4.11E-03
ENSG00000149328	GLB1L2	136.66	-1.92	0.26	5.91E-06	4.23E-03
ENSG00000102908	NFAT5	1401.35	-0.74	0.60	6.17E-06	4.23E-03
ENSG00000120280	CXorf21	48.52	1.89	3.70	6.01E-06	4.23E-03
ENSG00000072274	TFRC	1625.28	3.00	7.98	6.14E-06	4.23E-03
ENSG00000111348	ARHGDIB	1126.50	2.10	4.30	6.83E-06	4.50E-03
ENSG00000224578	HNRNPA1P48	204.31	0.89	1.85	7.26E-06	4.60E-03
ENSG00000160883	HK3	197.06	3.62	12.26	7.53E-06	4.61E-03
ENSG00000188761	BCL2L15	20.18	4.47	22.17	7.87E-06	4.65E-03
ENSG00000151725	CENPU	49.02	3.14	8.81	8.39E-06	4.79E-03
ENSG00000187116	LILRA5	44.28	3.33	10.04	9.45E-06	5.22E-03

Ensembl ID	Gene Name	Base mean	Log 2 fold change	Fold change	P-value	FDR
ENSG00000170312	CDK1	83.29	2.68	6.41	9.94E-06	5.32E-03
ENSG00000145569	OTULINL	155.75	1.31	2.47	1.15E-05	5.78E-03
ENSG00000132965	ALOX5AP	197.85	2.71	6.55	1.15E-05	5.78E-03
ENSG00000169429	CXCL8	47.25	2.49	5.60	1.19E-05	5.83E-03
ENSG00000138160	KIF11	98.56	3.48	11.19	1.26E-05	5.99E-03
ENSG00000102445	RUBCNL	70.34	1.13	2.19	1.31E-05	6.08E-03
ENSG00000175348	TMEM9B	208.68	0.57	1.48	1.49E-05	6.22E-03
ENSG00000213261	EEF1B2P6	21.33	1.13	2.18	1.47E-05	6.22E-03
ENSG00000204472	AIF1	219.86	1.34	2.53	1.48E-05	6.22E-03
ENSG00000174837	ADGRE1	22.89	2.95	7.71	1.47E-05	6.22E-03
ENSG00000105383	CD33	112.33	1.23	2.35	1.79E-05	6.27E-03
ENSG00000155629	PIK3AP1	471.28	1.28	2.43	1.74E-05	6.27E-03
ENSG00000163154	TNFAIP8L2	48.58	1.85	3.61	1.70E-05	6.27E-03
ENSG00000165168	CYBB	1795.73	1.94	3.83	1.78E-05	6.27E-03
ENSG00000111679	PTPN6	297.26	1.95	3.87	1.68E-05	6.27E-03
ENSG00000100365	NCF4	239.96	2.04	4.12	1.64E-05	6.27E-03
ENSG00000166501	PRKCB	214.73	2.28	4.86	1.75E-05	6.27E-03
ENSG00000084110	HAL	32.42	3.23	9.40	1.76E-05	6.27E-03
ENSG00000158321	AUTS2	242.66	-1.12	0.46	1.87E-05	6.28E-03

5

Supplementary Table 3 – Gene enrichment on genes differentially expressed between OA molecular endotype A and B.
Supplementary Table 3A- Gene enrichment of genes upregulated in endotype A relative to endotype B subchondral bone

GO-Term	Count	%	P-value	FDR	Genes
GO:0045944~positive regulation of transcription from RNA polymerase II promoter	16	20	2.22E-05	1.21E-02	ZFP64, SALL4, NFAT5, GLI3, ZMIZ1, KAT2A, ZBTB16, LPIN3, CRTC3, ZFHX3, NFIC, AUTS2, KLF15, ATF7, TNKS, ZNF580

Supplementary Table 3B- Gene enrichment of genes upregulated in endotype B relative to endotype A subchondral bone

GO-Term	Count	%	P-value	FDR	Genes
GO:0005886~plasma membrane	169	39	1.12E-12	4.72E-10	M6PR, CD38, LAMP2, BTK, PLAUR, TYROBP, ACPP, WAS, DEF6, CYBA, SLC2A3, GNA15, YBX1, DAPP1, CDC42, TFRC, ANKRD13A, ICAM3, STXBP2, PTPRC, FYB1, PILRA, LAT2, SRPK1, CYTH4, GRAP2, CSF2RB, MLC1, RASSF2, SIRPB1, HCK, TLR8, RP2, CORO1A, AQP9, CD37, LILRB1, ICAM4, NKG7, CD33, PIK3CG, BIN2, CLEC4A, TREML2, ITGA4, GCA, IL18RAP, PLEK, LAMTOR2, RAB29, TNFSF4, LRMP, VAMP8, ADCY7, CCRL2, CD244, ARL4A, CLTA, NCKAP1L, PTGER2, OPRL1, TNFSF14, VASP, HCST, CFP, YWHAH, RAC2, LRRC4, ATP8B3, MPP1, LILRB2, SH3BGRL, CAP1, ADGRE3, CD180, DOCK2, USP15, PLXNC1, LCP1, MYO1G, GYPC, CASP1, GPR84, GPR65, PSTPIP1, IGSF6, ARRB2, VAV1, MYO1F, SIGLEC10, SLC2A5, EFHD2, CD53, RIT1, RALB, PAK1, LAMTOR1, RGS18, ADAM8, ARL11, PSTPIP2, PIP4P2, PIK3AP1, CD1C, FCER1G, JAML, FCGR3B, CXCR1, CIP2A, CD200R1, PLB1, F2RL1, SYK, CYBB, MELK, PRKCB, CLEC4D, STX3, NOD2, SNX20, CD300A, RGS14, SLC50A1, PTAFR, CD52, REPS2, UBB, EMB, OSCAR, CEACAM3, FPR1, RGS19, HDAC3, RAB37, OLR1, TNFRSF10C, TLR1, ADGRE1, TBC1D10C, KCNE3, P2RY2, GAPT, CRLF3, CD300LB, ZNRF2, CXCR2, EVI2B, CD300LF, CD300E, HYAL3, LILRA5, SELL, SEMA4A, SIRPB2, C5AR1, SLC28A3, MBP, SUCNR1, CHML, LST1, LILRB3, IGLV1-40, IGLV3-21, GPSM3, UBA52, LTB, NFAM1, LILRA6, LYN
GO:0006955~immune response	34	8	2.34E-09	5.30E-06	WAS, LCP2, FYB1, OSM, TLR8, PIK3CG, CLEC4A, IL18RAP, TNFSF4, CCRL2, IL1B, TNFSF14, CFP, LILRB2, GPR65, IGSF6, VAV1, CD1C, FCGR3B, CTSS, CXCR1, CLEC4D, PTAFR, CXCL8, CTSW, TLR1, CXCR2, C5AR1, MBP, LST1, IGLV1-40, IGLV3-21, GPSM3, LTB
GO:0030667~secretory granule membrane	17	4	9.93E-09	1.49E-06	CD38, TYROBP, SLC2A3, RAB27A, PTPRC, SIRPB1, VAMP8, NCKAP1L, ADGRE3, FCGR3B, CXCR1, PTAFR, FPR1, CXCR2, SELL, C5AR1, LILRB3

5

GO-Term	Count	%	P-value	FDR	Genes
GO:0070821~tertiary granule membrane	15	3	1.06E-08	1.49E-06	CYBA, SLC2A3, CD33, LAMTOR2, VAMP8, LILRB2, GPR84, CD53, ADAM8, FCER1G, CYBB, CLEC4D, CD300A, PTAFR, OLR1
GO:0032755~positive regulation of interleukin-6 production	16	4	2.77E-08	2.19E-05	BTK, TYROBP, CYBA, TLR8, PYCARD, TNFSF4, IL1B, LILRB2, F2RL1, SYK, NOD2, PTAFR, TLR1, LILRA5, MBP, AIF1
GO:0006954~inflammatory response	31	7	2.90E-08	2.19E-05	CYBA, LYZ, NLRC4, HCK, TLR8, PYCARD, NKG7, PIK3CG, IL18RAP, TNFSF4, CCRL2, PTGER2, IL1B, CD180, PSTPIP1, ADAM8, GBP5, PROK2, F2RL1, CYBB, AD0008864.1, PTAFR, CXCL8, FPR1, OLR1, TLR1, CXCR2, HYAL3, C5AR1, AIF1, NFAM1
GO:0035579~specific granule membrane	16	4	7.12E-08	7.53E-06	PLAUR, CYBA, SLC2A3, CD33, LAMTOR2, VAMP8, GPR84, SLC2A5, CD53, LAMTOR1, ADAM8, CYBB, CLEC4D, CEACAM3, RAB37, OLR1
GO:0101003~ficolin-1-rich granule membrane	12	3	6.29E-07	5.32E-05	LAMP2, SLC2A3, NCKAP1L, LILRB2, ADGRE3, LAMTOR1, ADAM8, FCER1G, CLEC4D, CD300A, FPR1, TBC1D10C
GO:0007165~signal transduction	56	13	8.67E-07	4.91E-04	CD38, PLAUR, TYROBP, GDI2, DAPP1, ARHGAP1, PILRA, ARHGAP4, GRAP2, CSF2RB, RASSF2, SIRPB1, PYCARD, LILRB1, CD33, TNFSF4, STMN1, RPS6KA1, CD244, ARHGAP9, IL1B, TNFSF14, YWHAH, RAC2, GMFG, MPP1, LILRB2, CAP1, OSTF1, STAM, CASP1, PSTPIP1, CMTM2, COPS3, ARRB2, CD53, RIT1, RALB, RACGAP1, ARHGAP25, CD200R1, TAGAP, PRKCB, CXCL8, CEACAM3, FPR1, MOB1B, TLR1, ERFE, CXCR2, ARHGAP30, C5AR1, LTB, NFAM1, LYN, RASSF5
GO:0030593~neutrophil chemotaxis	11	3	3.68E-06	1.67E-03	PIK3CG, NCKAP1L, IL1B, VAV1, FCER1G, JAML, CXCR1, SYK, CXCL8, CXCR2, C5AR1
GO:0050790~regulation of catalytic activity	27	6	1.06E-05	4.00E-03	BTK, WAS, DEF6, GDI2, ACAP1, ARHGAP4, CYTH4, NCF4, SEC23B, RP2, ARHGDIB, EEF1B2, LAMTOR2, NCF2, PSD4, RAC2, ALOX5AP, DOCK2, BMP2K, SAE1, LAMTOR1, RGS18, RACGAP1, TAGAP, ARHGAP30, CHML, GPSM3

GO-Term	Count	%	P-value	FDR	Genes
GO:0005887~integral component of plasma membrane	51	12	1.73E-05	1.22E-03	M6PR, PLAUR, TYROBP, SLC2A3, TFRC, ICAM3, PTPRC, CSF2RB, SIRPB1, AQP9, CD37, ICAM4, NKG7, CD33, CLEC4A, TNFSF4, LRMP, ADCY7, CCRL2, NCKAP1L, PTGER2, OPRL1, LILRB2, ADGRE3, PLXNC1, GYPC, GPR84, GPR65, IGSF6, SLC2A5, CD53, ADAM8, CD1C, FCER1G, FCGR3B, F2RL1, CYBB, PTAFR, EMB, OLR1, TLR1, ADGRE1, P2RY2, CXCR2, EVI2B, SELL, SEMA4A, C5AR1, SLC28A3, CHML, LILRB3
GO:0070062~extracellular exosome	84	20	2.04E-05	1.23E-03	CD38, LAMP2, ACPP, WAS, GDI2, SLC2A3, YBX1, RAB27A, CDC42, TFRC, ICAM3, STXBP2, VDAC3, PTPRC, PILRA, LAT2, LYZ, RP2, GLA, CORO1A, CD37, BLVRA, LTA4H, ARPC3, ARHGDIB, PTPN6, SNX3, ACTR3, ITGA4, GCA, QPCT, CAPZA1, RAB29, STMN1, VAMP8, GOT1, GLIPR2, NCKAP1L, VASP, YWHAH, RAC2, ARPC1B, SH3BGRL, CAP1, PCNA, DOCK2, LCP1, MYO1G, TXN, TOR1A, SLC2A5, CD53, TPM3, RALB, LAMTOR1, FAM49B, RACGAP1, ARPC5, FCGR3B, ARPC2, MNDA, TKT, H2AFZ, PRKCB, STX3, CD300A, CDK1, UBB, OSCAR, LRG1, CFL1, MOB1B, B3GNT8, GBA, ALYREF, HIST2H2BE, TUBB4B, HIST1H4J, SUCNR1, IGLV3-21, UBA52, LYN, HIST1H4K, PSMB3
GO:0050766~positive regulation of phagocytosis	9	2	2.14E-05	6.68E-03	BTK, CYBA, RAB27A, SIRPB1, PYCARD, IL1B, DOCK2, FCER1G, NOD2
GO:0032731~positive regulation of interleukin-1 beta production	10	2	2.36E-05	6.68E-03	TYROBP, NLRC4, TLR8, PYCARD, CASP1, GBP5, MNDA, F2RL1, NOD2, LILRA5
GO:0005102~receptor binding	22	5	4.09E-05	1.65E-02	PLAUR, TYROBP, ICAM3, PTPRC, FYB1, FCN1, HCK, GLA, TNFSF4, TNFSF14, HCST, MPP1, TESPA1, PLXNC1, CNPY3, ARRB2, PIK3AP1, F2RL1, SYK, GBA, LTB, LYN
GO:0032396~inhibitory MHC class I receptor activity	5	1	5.34E-05	1.65E-02	LILRB1, LILRB2, LILRA5, LILRB3, LILRA6
GO:0032757~positive regulation of interleukin-8 production	10	2	5.91E-05	1.49E-02	FCN1, TLR8, PYCARD, CD244, IL1B, LAMTOR5, F2RL1, SYK, NOD2, TLR1
GO:0045730~respiratory burst	6	1	6.55E-05	1.49E-02	CYBA, NCF4, NCF2, RAC2, CYBB, CD52

5

GO-Term	Count	%	P-value	FDR	Genes
GO:0006935~chemotaxis	12	3	8.45E-05	1.74E-02	PLAUR, CCRL2, NCKAP1L, RAC2, DOCK2, CMTM2, PROK2, PTAFR, CXCL8, FPR1, CXCR2, C5AR1
GO:0005576~extracellular region	62	14	1.00E-04	4.73E-03	PLAUR, ALOX5, GDI2, YBX1, RAB27A, TFRC, STXBP2, FCN1, LYZ, OSM, GLA, PYCARD, LILRB1, ICAM4, BIN2, LTA4H, ACRBP, PTPN6, GCA, QPCT, PLEK, CAP2A1, PLBD1, GLIPR2, ARHGAP9, IL1B, CFP, GMFG, CAP1, ADGRE3, DOCK2, OSTF1, AOAH, TXN, CASP1, SIGLEC10, FAM49B, HK3, ARPC5, FCGR3B, CTSS, PROK2, MNDA, CD200R1, GYG1, CXCL8, CD52, OSCAR, LRG1, CTSW, HPSE, OLR1, SVBP, ERFE, HYAL3, LILRA5, TUBB4B, HIST1H4J, TMSB4X, IGLV1-40, IGLV3-21, HIST1H4K
GO:0005885~Arp2/3 protein complex	5	1	1.01E-04	4.73E-03	ARPC3, ACTR3, ARPC1B, ARPC5, ARPC2
GO:0031623~receptor internalization	9	2	1.19E-04	1.96E-02	TFRC, LILRB1, ARRB2, RALB, FCER1G, CXCR1, SYK, CXCL8, CXCR2
GO:0002250~adaptive immune response	19	4	1.24E-04	1.96E-02	BTK, LAT2, LILRB1, PIK3CG, CLEC4A, CD244, LILRB2, SIGLEC10, CD1C, CTSS, SYK, PRKCB, CLEC4D, ADGRE1, LILRB3, IGLV1-40, IGLV3-21, LILRA6, LYN
GO:0032760~positive regulation of tumor necrosis factor production	12	3	1.27E-04	1.96E-02	BTK, TYROBP, CYBA, PTPRC, PYCARD, SASH3, SYK, CYBB, NOD2, PTAFR, TLR1, LILRA5
GO:0032729~positive regulation of interferon-gamma production	10	2	1.32E-04	1.96E-02	TLR8, PYCARD, LILRB1, TNFSF4, SASH3, CD244, IL1B, PTPN22, FAM49B, F2RL1
GO:0042102~positive regulation of T cell proliferation	9	2	1.38E-04	1.96E-02	TFRC, PTPRC, CORO1A, TNFSF4, SASH3, NCKAP1L, IL1B, LILRB2, AIF1
GO:0007186~G-protein coupled receptor signaling pathway	22	5	1.96E-04	2.62E-02	FCN1, PIK3CG, PTPN6, CCRL2, PTGER2, RAC2, ADGRE3, GPR65, VAV1, RGS18, PROK2, CXCR1, F2RL1, RGS14, PTAFR, CXCL8, FPR1, RGS19, ADGRE1, P2RY2, SUCNR1, CHML
GO:0045087~innate immune response	28	7	2.13E-04	2.67E-02	BTK, CYBA, NLRC4, SRPK1, HCK, RIOK3, TLR8, CORO1A, PYCARD, PIK3CG, CLEC4A, NCF2, CXorf21, CD244, CD180, CNPY3, PSTPIP1, SIGLEC10, FCER1G, TNFAIP8L2, F2RL1, SYK, CYBB, NOD2, TLR1, APOBEC3B, LILRA5, LYN
GO:0032733~positive regulation of interleukin-10 production	7	2	2.24E-04	2.67E-02	PYCARD, TNFSF4, SASH3, F2RL1, SYK, NOD2, LILRA5

5

GO-Term	Count	%	P-value	FDR	Genes
GO:0043020~NADPH oxidase complex	5	1	2.51E-04	1.06E-02	CYBA, NCF4, NCF2, RAC2, CYBB
GO:0038096~Fc-gamma receptor signaling pathway involved in phagocytosis	6	1	2.97E-04	3.37E-02	HCK, MYO1G, VAV1, PAK1, SYK, LYN

Supplementary Table 4 (partially) - Differentially expressed genes between macroscopically preserved and lesioned OA subchondral bone of patients with molecular endotype A OA.
The top 50 most significant differentially expressed genes between preserved and lesioned subchondral bone are shown here.

Ensembl ID	Gene name	Base mean	Log 2 fold change	Fold change	P-value	FDR
ENSG00000054938	CHRDL2	71.69	-3.88	0.07	2.98E-08	4.63E-04
ENSG00000102466	FGF14	19.50	-1.66	0.32	1.99E-07	7.73E-04
ENSG00000139718	SETD1B	260.38	-0.54	0.69	1.08E-07	7.73E-04
ENSG00000159307	SCUBE1	1579.37	-0.96	0.52	1.90E-07	7.73E-04
ENSG00000146830	GIGYF1	473.12	-0.31	0.80	3.88E-07	1.20E-03
ENSG00000252835	SCARNA21	607.24	0.43	1.35	4.69E-07	1.21E-03
ENSG00000153064	BANK1	90.61	-0.99	0.50	9.09E-07	2.01E-03
ENSG00000113594	LIFR	4351.68	0.38	1.30	1.61E-06	2.50E-03
ENSG00000134014	ELP3	389.12	0.26	1.20	1.56E-06	2.50E-03
ENSG00000167548	KMT2D	1048.61	-0.43	0.74	1.39E-06	2.50E-03
ENSG00000162998	FRZB	1002.99	-0.91	0.53	1.97E-06	2.77E-03
ENSG00000175573	C11orf68	132.68	-0.44	0.74	2.60E-06	3.36E-03
ENSG00000272333	KMT2B	289.54	-0.43	0.74	4.82E-06	5.75E-03
ENSG00000132359	RAP1GAP2	86.98	-0.65	0.64	6.46E-06	6.98E-03
ENSG00000167978	SRRM2	3172.15	-0.37	0.78	6.75E-06	6.98E-03
ENSG00000111676	ATN1	485.50	-0.47	0.72	9.92E-06	9.07E-03
ENSG00000270547	LINC01235	36.38	-1.95	0.26	9.94E-06	9.07E-03
ENSG00000196498	NCOR2	732.58	-0.52	0.70	1.33E-05	1.15E-02
ENSG00000129351	ILF3	903.85	-0.23	0.85	1.44E-05	1.18E-02
ENSG00000116698	SMG7	346.59	-0.31	0.81	1.67E-05	1.20E-02
ENSG00000122824	NUDT10	41.46	0.68	1.60	1.78E-05	1.20E-02
ENSG00000168488	ATXN2L	341.24	-0.38	0.77	1.77E-05	1.20E-02
ENSG00000179399	GPC5	29.20	-1.42	0.37	1.64E-05	1.20E-02
ENSG00000122756	CNTFR	51.10	-0.97	0.51	2.05E-05	1.31E-02
ENSG00000166925	TSC22D4	200.82	-0.44	0.74	2.18E-05	1.31E-02
ENSG00000182095	TNRC18	1076.27	-0.42	0.75	2.19E-05	1.31E-02
ENSG00000140443	IGF1R	653.60	-0.46	0.72	2.33E-05	1.34E-02
ENSG00000140416	TPM1	1974.72	0.42	1.33	2.75E-05	1.46E-02
ENSG00000177303	CASKIN2	363.75	-0.51	0.70	2.77E-05	1.46E-02
ENSG00000196104	SPOCK3	29.16	-2.50	0.18	2.83E-05	1.46E-02
ENSG00000187595	ZNF385C	17.57	-1.41	0.38	2.99E-05	1.49E-02

Ensembl ID	Gene name	Base mean	Log 2 fold change	Fold change	P-value	FDR
ENSG00000174469	CNTNAP2	99.27	1.38	2.60	3.13E-05	1.50E-02
ENSG00000204469	PRRC2A	1193.92	-0.41	0.75	3.20E-05	1.50E-02
ENSG00000104435	STMN2	76.11	4.61	24.40	3.37E-05	1.52E-02
ENSG00000110237	ARHGEF17	1030.01	-0.39	0.76	3.43E-05	1.52E-02
ENSG00000110046	ATG2A	216.72	-0.41	0.75	3.53E-05	1.52E-02
ENSG00000005339	CREBBP	1049.29	-0.38	0.77	4.36E-05	1.65E-02
ENSG00000074181	NOTCH3	3487.44	-0.62	0.65	4.47E-05	1.65E-02
ENSG00000115616	SLC9A2	17.72	1.41	2.66	4.27E-05	1.65E-02
ENSG00000116285	ERRFI1	749.87	0.62	1.54	4.39E-05	1.65E-02
ENSG00000175727	MLXIP	529.48	-0.30	0.81	4.19E-05	1.65E-02
ENSG00000184634	MED12	476.66	-0.31	0.80	4.23E-05	1.65E-02
ENSG00000187535	IFT140	157.77	-0.34	0.79	5.01E-05	1.81E-02
ENSG00000068697	LAPTM4A	1625.75	0.20	1.15	5.43E-05	1.88E-02
ENSG00000108175	ZMIZ1	1108.34	-0.44	0.74	5.93E-05	1.88E-02
ENSG00000108509	CAMTA2	206.76	-0.43	0.74	5.84E-05	1.88E-02
ENSG00000112584	FAM120B	348.12	-0.26	0.84	5.69E-05	1.88E-02
ENSG00000132024	CC2D1A	196.05	-0.33	0.79	5.70E-05	1.88E-02
ENSG00000148400	NOTCH1	964.62	-0.64	0.64	5.93E-05	1.88E-02
ENSG00000126461	SCAF1	211.18	-0.62	0.65	6.17E-05	1.91E-02

5

Supplementary Table 5 - Differentially expressed genes between macroscopically preserved and lesioned OA subchondral bone of patients with molecular endotype B OA.

Ensembl ID	Gene name	Base mean	Log 2 fold change	Fold change	P-value	FDR
ENSG00000108821	COL1A1	1.00E5	1.18	2.26	4.83E-08	6.52E-04
ENSG00000138755	CXCL9	123.45	-1.73	0.30	1.30E-07	8.56E-04
ENSG00000164694	FNDC1	574.56	1.07	2.10	1.90E-07	8.56E-04
ENSG00000156466	GDF6	64.10	4.06	16.69	6.71E-06	2.27E-02
ENSG00000006016	CRLF1	100.99	1.68	3.21	1.56E-05	2.77E-02
ENSG00000011028	AC080038.1	3290.14	0.81	1.75	1.64E-05	2.77E-02
ENSG00000107249	GLIS3	144.94	1.30	2.46	1.40E-05	2.77E-02
ENSG00000166741	NNMT	1482.53	0.77	1.71	1.53E-05	2.77E-02
ENSG00000100626	GALNT16	78.39	2.15	4.44	2.15E-05	3.23E-02
ENSG00000164692	COL1A2	1.09E5	0.91	1.88	2.56E-05	3.46E-02
ENSG00000211677	IGLC2	3393.08	0.97	1.96	3.71E-05	4.55E-02

Supplementary Table 6 (Partially) - Genes differentially expressed between molecular endotype A and B in both articular cartilage and subchondral bone. With endotype A as reference, i.e. FC>1 means higher expressed in endotype B relative to endotype A. Top 50 most significant genes are shown here.

Ensembl ID	Gene name	Base mean cartilage	FDR cartilage	FD cartilage	Base mean bone	FDR bone	FD bone	Direction
ENSG00000105383	CD33	8.37	4.84E-16	11.08	112.33	6.27E-03	2.35	Similar
ENSG00000111679	PTPN6	49.75	1.04E-14	2.19	297.26	6.27E-03	3.87	Similar
ENSG00000204472	AIF1	33.67	6.91E-13	8.94	219.86	6.22E-03	2.53	Similar
ENSG00000120280	CXorf21	2.58	1.02E-11	12.05	48.52	4.23E-03	3.70	Similar
ENSG00000155629	PIK3AP1	22.27	7.14E-13	4.87	471.28	6.27E-03	2.43	Similar
ENSG00000151651	ADAM8	40.30	5.76E-13	4.58	137.70	7.59E-03	6.22	Similar
ENSG00000165025	SYK	26.65	1.70E-15	5.14	523.66	8.56E-03	3.13	Similar
ENSG00000204482	LST1	11.77	2.91E-10	7.78	145.88	1.60E-03	6.24	Similar
ENSG00000136167	LCP1	62.80	1.99E-11	5.79	1825.07	8.48E-03	4.37	Similar
ENSG00000158869	FCER1G	40.98	3.61E-14	8.16	255.04	1.12E-02	2.66	Similar
ENSG00000060558	GNA15	12.08	1.72E-11	7.55	97.03	8.56E-03	2.23	Similar
ENSG00000142347	MYO1F	33.38	3.52E-12	4.59	394.20	9.12E-03	4.43	Similar
ENSG00000169403	PTAFR	19.60	7.60E-12	7.37	145.17	9.28E-03	3.15	Similar
ENSG00000160883	HK3	16.58	2.71E-09	7.20	197.06	4.61E-03	12.26	Similar
ENSG00000100365	NCF4	15.45	1.85E-09	7.57	239.96	6.27E-03	4.12	Similar
ENSG00000089820	ARHGAP4	47.90	1.02E-15	4.04	315.67	1.84E-02	2.32	Similar
ENSG00000085514	PILRA	19.85	2.47E-09	3.13	68.17	6.39E-03	2.74	Similar
ENSG00000010671	BTK	8.88	3.08E-10	6.75	120.02	8.56E-03	3.81	Similar
ENSG00000132965	ALOX5AP	28.57	1.87E-08	6.07	197.85	5.78E-03	6.55	Similar

5

Ensembl ID	Gene name	Base mean cartilage	FDR cartilage	FD cartilage	Base mean bone	FDR bone	FD bone	Direction
ENSG00000086730	LAT2	17.34	3.81E-16	4.27	131.52	1.99E-02	3.02	Similar
ENSG00000126264	HCST	8.73	2.81E-10	3.42	91.28	8.91E-03	3.64	Similar
ENSG00000138756	BMP2K	74.66	3.50E-11	2.57	848.56	1.41E-02	1.94	Similar
ENSG00000163154	TNFAIP8L2	4.99	1.35E-08	6.12	48.58	6.27E-03	3.61	Similar
ENSG00000123338	NCKAP1L	40.87	4.38E-14	3.62	684.80	1.80E-02	2.28	Similar
ENSG00000169429	CXCL8	36.05	2.92E-08	10.74	47.25	5.83E-03	5.60	Similar
ENSG00000120549	KIAA1217	77.62	3.20E-11	4.93	460.17	1.58E-02	0.49	Opposite
ENSG00000170571	EMB	25.80	2.22E-08	6.00	559.88	6.28E-03	5.28	Similar
ENSG00000101336	HCK	26.39	3.93E-10	7.15	249.75	1.08E-02	3.26	Similar
ENSG00000100055	CYTH4	39.40	4.26E-15	8.65	377.78	2.11E-02	1.74	Similar
ENSG00000116701	NCF2	23.04	8.71E-07	3.52	397.12	3.49E-03	4.10	Similar
ENSG00000141968	VAV1	9.67	7.91E-12	6.29	174.37	1.92E-02	2.80	Similar
ENSG00000012779	ALOX5	21.79	5.99E-11	6.54	202.71	1.70E-02	5.38	Similar
ENSG00000198829	SUCNR1	2.58	9.85E-06	4.27	68.00	1.19E-04	6.10	Similar
ENSG00000186407	CD300E	8.23	8.49E-08	6.75	30.77	6.28E-03	4.01	Similar
ENSG00000163131	CTSS	127.88	2.42E-10	3.12	1064.78	1.48E-02	2.80	Similar
ENSG00000141480	ARRB2	73.74	2.30E-16	2.87	326.59	2.59E-02	2.25	Similar
ENSG00000075884	ARHGAP15	4.13	1.94E-10	10.16	127.68	1.63E-02	3.99	Similar
ENSG00000187116	LILRA5	1.98	5.11E-06	5.20	44.28	5.22E-03	10.04	Similar
ENSG00000003400	CASP10	9.96	8.34E-16	7.75	222.04	2.62E-02	1.72	Similar
ENSG00000140030	GPR65	2.80	5.29E-07	6.32	63.10	6.28E-03	2.76	Similar

Ensembl ID	Gene name	Base mean cartilage	FDR cartilage	FD cartilage	Base mean bone	FDR bone	FD bone	Direction
ENSG00000101916	TLR8	4.96	3.12E-05	4.82	87.89	3.88E-04	4.57	Similar
ENSG00000167851	CD300A	22.72	2.30E-12	3.40	94.05	2.52E-02	2.51	Similar
ENSG00000110934	BIN2	9.60	5.75E-09	5.40	192.87	1.30E-02	5.50	Similar
ENSG00000131042	LILRB2	14.83	3.32E-11	7.03	98.72	2.11E-02	2.83	Similar
ENSG00000081237	PTPRC	38.54	4.93E-09	5.10	964.12	1.44E-02	3.20	Similar
ENSG00000115232	ITGA4	10.82	5.55E-10	6.87	319.18	1.77E-02	4.62	Similar
ENSG00000128340	RAC2	26.03	1.85E-06	5.37	341.80	6.39E-03	6.85	Similar
ENSG00000123329	ARHGAP9	24.44	4.17E-05	2.96	160.76	3.70E-03	5.00	Similar
ENSG00000115956	PLEK	35.29	3.46E-08	4.23	613.11	1.12E-02	3.73	Similar
ENSG00000244482	LILRA6	8.79	2.15E-08	5.31	36.32	1.37E-02	4.14	Similar

5

Supplementary Table 7 - Gene enrichment on genes differentially expressed between endotype A and B in both articular cartilage and subchondral bone, with similar directions of effect.

GO-Term	Count	%	P-value	FDR	Genes
GO:0005886~plasma membrane	91	52	4.59E-16	1.06E-13	CD38, BTK, PLAUR, TYROBP, ACPP, WAS, GNA15, DAPP1, STXBP2, PTPRC, PILRA, LAT2, CYTH4, GRAP2, NCF4, CSF2RB, RASSF2, HCK, TLR8, CORO1A, LILRB1, CD33, PIK3CG, ZBTB16, BIN2, CLEC4A, TREML2, ITGA4, PLEK, NCF2, LRMP, VAMP8, ADCY7, CCRL2, ARL4A, CNTFR, NCKAP1L, HCST, CFP, RAC2, LRRC4, ATP8B3, LILRB2, CD180, DOCK2, PLXNC1, LCP1, MYO1G, GYPC, CASP1, GPR84, GPR65, ARRB2, VAV1, MYO1F, SIGLEC10, SLC2A5, EFHD2, CD53, RGS18, ADAM8, ARL11, PIK3AP1, CD1C, FCER1G, JAML, CD200R1, SYK, CYBB, MELK, NOD2, SNX20, CD300A, PTAFR, EMB, FPR1, RGS19, CD300LB, CD300LF, CD300E, LILRA5, SIRPB2, C5AR1, SLC28A3, SUCNR1, LST1, LILRB3, IGLV1-40, IGLV3-21, GPSM3, LILRA6
GO:0006955~immune response	22	13	8.09E-10	1.05E-06	WAS, LCP2, OSM, TLR8, PIK3CG, CLEC4A, CCRL2, IL1B, CFP, LILRB2, GPR65, IGSF6, VAV1, CD1C, CTSS, PTAFR, CXCL8, C5AR1, LST1, IGLV1-40, IGLV3-21, GPSM3
GO:0070821~tertiary granule membrane	10	6	8.78E-08	1.01E-05	CD33, VAMP8, LILRB2, GPR84, CD53, ADAM8, FCER1G, CYBB, CD300A, PTAFR
GO:0030593~neutrophil chemotaxis	9	5	3.04E-07	1.97E-04	PIK3CG, NCKAP1L, IL1B, VAV1, FCER1G, JAML, SYK, CXCL8, C5AR1
GO:0032755~positive regulation of interleukin-6 production	10	6	7.86E-07	3.39E-04	BTK, TYROBP, TLR8, IL1B, LILRB2, SYK, NOD2, PTAFR, LILRA5, AIF1
GO:0032396~inhibitory MHC class I receptor activity	5	3	1.16E-06	4.03E-04	LILRB1, LILRB2, LILRA5, LILRB3, LILRA6
GO:0002250~adaptive immune response	14	8	1.99E-06	6.45E-04	BTK, LAT2, LILRB1, PIK3CG, CLEC4A, LILRB2, SIGLEC10, CD1C, CTSS, SYK, LILRB3, IGLV1-40, IGLV3-21, LILRA6
GO:0030667~secretory granule membrane	9	5	1.27E-05	7.69E-04	CD38, TYROBP, PTPRC, VAMP8, NCKAP1L, PTAFR, FPR1, C5AR1, LILRB3
GO:0001891~phagocytic cup	6	3	1.33E-05	7.69E-04	CORO1A, BIN2, LCP1, MYO1G, ARHGAP25, AIF1

GO-Term	Count	%	P-value	FDR	Genes
GO:0032731~positive regulation of interleukin-1 beta production	8	5	2.98E-06	7.71E-04	TYROBP, NLRC4, TLR8, CASP1, GBP5, MNDA, NOD2, LILRA5
GO:0006954~inflammatory response	16	9	6.49E-06	1.40E-03	LYZ, NLRC4, HCK, TLR8, PIK3CG, CCRL2, IL1B, CD180, ADAM8, GBP5, CYBB, PTAFR, CXCL8, FPR1, C5AR1, AIF1
GO:0019221~cytokine-mediated signaling pathway	10	6	8.75E-06	1.62E-03	CSF2RB, HCK, LILRB1, PTPN6, CNTFR, IL1B, LILRB2, LILRA5, LILRB3, LILRA6
GO:0045087~innate immune response	18	10	1.31E-05	2.12E-03	BTK, NLRC4, HCK, TLR8, CORO1A, PIK3CG, CLEC4A, NCF2, CXorf21, CD180, SIGLEC10, FCER1G, TNFAIP8L2, SYK, CYBB, NOD2, APOBEC3B, LILRA5
GO:0006935~chemotaxis	9	5	1.66E-05	2.15E-03	PLAUR, CCRL2, NCKAP1L, RAC2, DOCK2, PTAFR, CXCL8, FPR1, C5AR1
GO:0032760~positive regulation of tumor necrosis factor production	9	5	1.66E-05	2.15E-03	BTK, TYROBP, PTPRC, SASH3, SYK, CYBB, NOD2, PTAFR, LILRA5
GO:0005887~integral component of plasma membrane	28	16	4.94E-05	2.28E-03	PLAUR, TYROBP, PTPRC, CSF2RB, CD33, CLEC4A, LRMP, ADCY7, CCRL2, NCKAP1L, LILRB2, PLXNC1, GYPC, GPR84, GPR65, IGSF6, SLC2A5, CD53, ADAM8, CD1C, FCER1G, CYBB, PTAFR, EMB, EVI2B, C5AR1, SLC28A3, LILRB3
GO:0002376~immune system process	7	4	2.18E-05	2.35E-03	NLRC4, LRMP, NOD2, CD300A, CD300LB, CD300LF, CD300E
GO:0007165~signal transduction	28	16	2.18E-05	2.35E-03	CD38, PLAUR, TYROBP, DAPP1, ARHGAP15, PILRA, ARHGAP4, GRAP2, CSF2RB, RASSF2, LILRB1, CD33, STMN1, CNTFR, ARHGAP9, IL1B, RAC2, GMFG, LILRB2, CASP1, ARRB2, CD53, ARHGAP25, CD200R1, CXCL8, FPR1, ARHGAP30, C5AR1
GO:0035579~specific granule membrane	8	5	7.98E-05	3.07E-03	PLAUR, CD33, VAMP8, GPR84, SLC2A5, CD53, ADAM8, CYBB
GO:0042102~positive regulation of T cell proliferation	7	4	3.44E-05	3.43E-03	PTPRC, CORO1A, SASH3, NCKAP1L, IL1B, LILRB2, AIF1
GO:0032695~negative regulation of interleukin-12 production	5	3	4.90E-05	4.53E-03	TLR8, LILRB1, ARRB2, NOD2, LILRA5

5

GO-Term	Count	%	P-value	FDR	Genes
GO:0050853~B cell receptor signaling pathway	8	5	1.09E-04	9.38E-03	CD38, BTK, PTPRC, LAT2, PTPN6, NCKAP1L, MNDA, SYK
GO:0002675~positive regulation of acute inflammatory response	4	2	1.79E-04	1.44E-02	OSM, PIK3CG, ALOX5AP, ADAM8
GO:0101003~ficolin-1-rich granule membrane	6	3	4.41E-04	1.45E-02	NCKAP1L, LILRB2, ADAM8, FCER1G, CD300A, FPR1
GO:0043020~NADPH oxidase complex	4	2	5.15E-04	1.49E-02	NCF4, NCF2, RAC2, CYBB
GO:0045089~positive regulation of innate immune response	5	3	2.22E-04	1.69E-02	TLR8, CXorf21, ADAM8, GBP5, NOD2
GO:0035580~specific granule lumen	6	3	6.60E-04	1.69E-02	LYZ, PTPN6, QPCT, CFP, DOCK2, HPSE
GO:0050727~regulation of inflammatory response	7	4	2.82E-04	2.03E-02	ALOX5, HCK, CASP1, PIK3AP1, NOD2, TMSB4X, GPSM3
GO:0009986~cell surface	16	9	1.01E-03	2.33E-02	CD38, PLAUR, TYROBP, PTPRC, CD33, TREML2, ITGA4, HCST, LILRB2, CD53, ADAM8, FCER1G, CD200R1, NOD2, LILRA5, C5AR1
GO:0005576~extracellular region	30	17	1.24E-03	2.54E-02	PLAUR, ALOX5, STXBP2, LYZ, OSM, LILRB1, BIN2, ACRBP, PTPN6, QPCT, PLEK, GLIPR2, ARHGAP9, IL1B, CFP, GMFG, DOCK2, AOAH, CASP1, SIGLEC10, HK3, CTSS, MNDA, CD200R1, CXCL8, HPSE, LILRA5, TMSB4X, IGLV1-40, IGLV3-21
GO:0032010~phagolysosome	3	2	1.32E-03	2.54E-02	NCF4, NCF2, ADAM8
GO:0032720~negative regulation of tumor necrosis factor production	6	3	4.51E-04	3.07E-02	LILRB1, CD33, PTPN6, CLEC4A, ARRB2, NOD2
GO:0009897~external side of plasma membrane	12	7	1.83E-03	3.25E-02	PTPRC, CSF2RB, TLR8, LILRB1, CD33, CLEC4A, ITGA4, CCRL2, CNTFR, CD1C, FCER1G, CD200R1
GO:0050729~positive regulation of inflammatory response	7	4	7.35E-04	4.35E-02	NLRC4, OSM, IL1B, CASP1, LILRA5, SUCNR1, GPSM3

GO-Term	Count	%	P-value	FDR	Genes
GO:0035556~intracellular signal transduction	14	8	7.37E-04	4.35E-02	BTK, TYROBP, LCP2, LAT2, PTPN6, ECT2, STMN1, ADCY7, PLCL2, CD200R1, SYK, MELK, NOD2, CXCL8
GO:0050790~regulation of catalytic activity	13	7	7.43E-04	4.35E-02	BTK, WAS, ARHGAP4, CYTH4, NCF4, NCF2, RAC2, ALOX5AP, DOCK2, BMP2K, RGS18, ARHGAP30, GPSM3
GO:0045730~respiratory burst	4	2	7.92E-04	4.35E-02	NCF4, NCF2, RAC2, CYBB
GO:0038156~interleukin-3-mediated signaling pathway	3	2	8.07E-04	4.35E-02	CSF2RB, FCER1G, SYK
GO:0030889~negative regulation of B cell proliferation	4	2	9.53E-04	4.55E-02	BTK, TYROBP, MNDA, CD300A
GO:0030890~positive regulation of B cell proliferation	5	3	9.85E-04	4.55E-02	CD38, BTK, PTPRC, SASH3, NCKAP1L
GO:0042098~T cell proliferation	5	3	9.85E-04	4.55E-02	PTPRC, CORO1A, PIK3CG, PTPN6, SASH3
GO:0006968~cellular defense response	5	3	9.85E-04	4.55E-02	TYROBP, NCF2, LILRB2, MNDA, C5AR1
GO:1904813~ficolin-1-rich granule lumen	7	4	2.93E-03	4.83E-02	ALOX5, BIN2, QPCT, GMFG, HK3, CTSS, MNDA
GO:0005884~actin filament	6	3	3.14E-03	4.83E-02	WAS, HCK, CORO1A, RAC2, LCP1, AIF1
GO:1904724~tertiary granule lumen	5	3	3.35E-03	4.83E-02	LYZ, PTPN6, QPCT, CFP, CTSS
GO:0031663~lipopolysaccharide-mediated signaling pathway	5	3	1.09E-03	4.85E-02	SPI1, HCK, IL1B, CD180, PTAFR

5

Supplementary Table 8 - Genes differentially expressed between preserved and lesioned OA articular cartilage and subchondral bone exclusively for molecular endotype A.

Ensembl ID	Gene name	Base mean cartilage	FDR cartilage	FD cartilage	Base mean bone	FDR bone	FD bone	Direction
ENSG00000008441	NFIX	1462.89	4.66E-02	0.74	690.67	1.96E-02	0.69	Similar
ENSG00000125430	HS3ST3B1	81.50	2.71E-02	0.68	24.82	2.47E-02	0.49	Similar
ENSG00000129351	ILF3	805.88	2.57E-02	0.92	903.85	1.18E-02	0.85	Similar

5
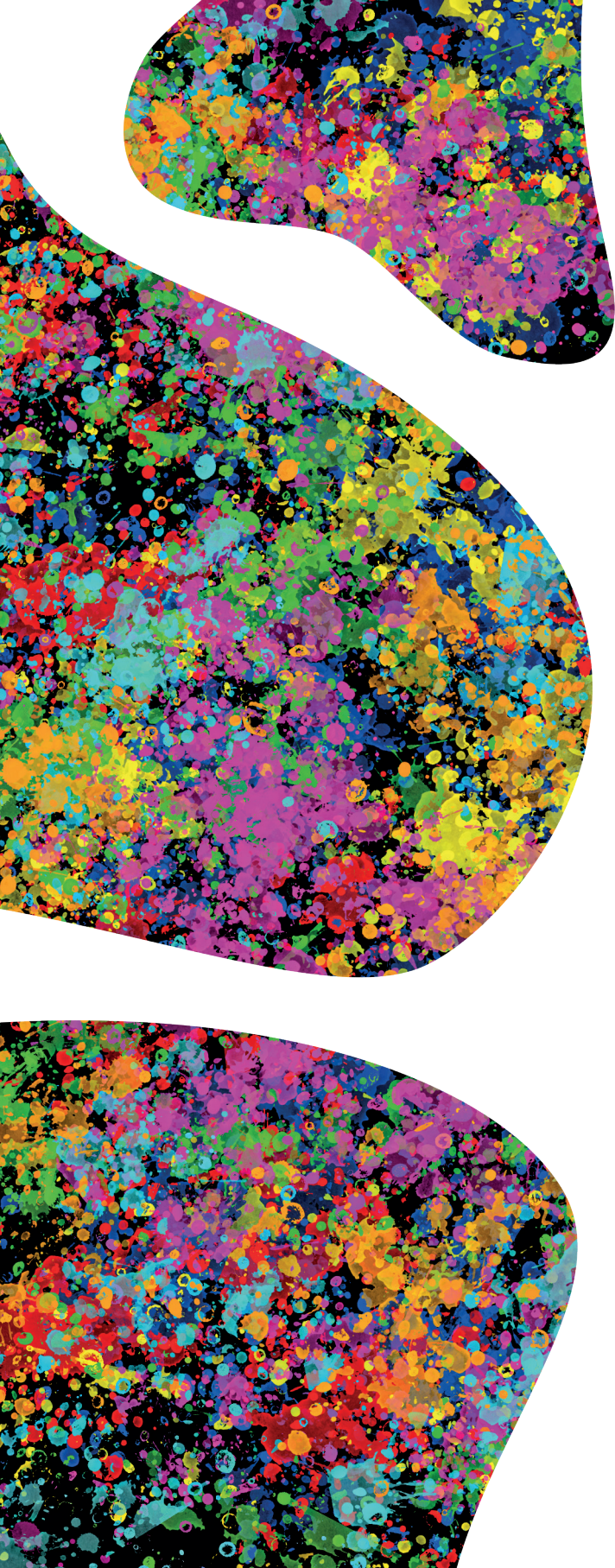
CHAPTER 6

WWP2 confers risk to osteoarthritis by affecting cartilage matrix deposition via hypoxia associated genes

Margo Tuerlings[1], George M.C. Janssen[2], Ilja Boone[1], Marcella van Hoolwerff[1], Alejandro Rodriguez Ruiz[1], Evelyn Houtman[1], H. Eka D. Suchiman[1], Robert J.P. van der Wal [3], Rob G.H.H. Nelissen[3], Rodrigo Coutinho de Almeida[1], Peter A. van Veelen[2], Yolande F.M. Ramos[1], Ingrid Meulenbelt[1]

[1] Dept. of Biomedical Data Sciences, Leiden University Medical Center, Leiden, The Netherlands.
[2] Center for proteomics and metabolomics , Leiden University Medical Center, Leiden, The Netherlands
[3] Dept. Orthopaedics Leiden University Medical Center, Leiden, The Netherlands.

Abstract

Objective: To explore the co-expression network of the osteoarthritis (OA) risk gene *WWP2* in articular cartilage and study cartilage characteristics when mimicking the effect of OA risk allele rs1052429-A on *WWP2* expression in a human 3D *in vitro* model of cartilage.

Method: Co-expression behavior of *WWP2* with genes expressed in lesioned OA articular cartilage (N=35 samples) was explored. By applying lentiviral particle mediated *WWP2* upregulation in 3D *in vitro* pellet cultures of human primary chondrocytes (N=8 donors) the effects of upregulation on cartilage matrix deposition was evaluated. Finally, we transfected primary chondrocytes with miR-140 mimics to evaluate whether miR-140 and WWP2 are involved in similar pathways.

Results: Upon performing Spearman correlations in lesioned OA cartilage, 98 highly correlating genes ($|\rho|>0.7$) were identified. Among these genes, we identified *GJA1*, *GDF10*, *STC2*, *WDR1*, and *WNK4.* Subsequent upregulation of WWP2 on 3D chondrocyte pellet cultures resulted in a decreased expression of *COL2A1* and *ACAN* and an increase in *EPAS1* expression. Additionally, we observed a decreased expression of *GDF10, STC2,* and *GJA1*. Proteomics analysis identified 42 proteins being differentially expressed with WWP2 upregulation, which were enriched for ubiquitin conjugating enzyme activity. Finally, upregulation of miR-140 in 2D chondrocytes resulted in significant upregulation of *WWP2* and *WDR1*.

Conclusion: Mimicking the effect of OA risk allele rs1052429-A on *WWP2* expression initiates detrimental processes in the cartilage shown by a response in hypoxia associated genes *EPAS1,GDF10,* and *GJA1* and a decrease in anabolic markers, *COL2A1* and *ACAN*.

Introduction

Globally, osteoarthritis (OA) is a highly prevalent and disabling joint disease which confers high social and economic burden to society. Risk factors for OA include sex, abnormal joint loading, obesity, metabolic diseases, and genetic factors [1]. To discover genes and underlying disease pathways, large genome wide association meta-analyses have been performed and multiple robust single nucleotide polymorphisms (SNPs) were identified significantly conferring risk to initiation and progression of OA [2-4]. Similar to other complex traits, these risk alleles have subsequently been found to affect expression of positional genes *in cis* in disease relevant tissues, also known as allelic imbalance (AI)[5 ,6]. Founded by this mechanism, we previously used RNA sequencing data of OA articular cartilage to report on genome-wide AI expression of SNPs in cartilage specific genes, as such, providing an AI expression database to *in silico* check functional aspects of identified and/or future OA risk SNPs [7]. One of the top findings was SNP rs1052429 located in the 3'UTR of the *WWP2* gene showing highly significant AI, with risk allele rs1052429-A marking higher expression of *WWP2* relative to rs1052429-G. Among the OA risk SNPs identified in a large genome-wide meta-analysis of Icelandic and UK knee OA patients was rs34195470, located in *WWP2* gene and a proxy of our AI SNP rs1052429 (r^2=0.6) [2]. Recently, rs34195470 was confirmed being OA risk SNP in the largest genome-wide meta-analysis so far, including individuals from 9 populations [4]. Based on these data, we could make a firm hypothesis that *WWP2,* with risk alleles rs34195470-G and rs1052429-A, confers robust risk to human OA which is marked by increased expression of *WWP2*. We also previously identified transcription of *WWP2* in cartilage being epigenetically regulated [8], as well as being responsive in the OA pathophysiological process [9]. Moreover, *WWP2* was previously shown to be a marker for hypertrophic chondrocytes in OA knee joints [10].

WWP2 is a member of the Nedd4 superfamily, a small group within the E3 ubiquitin ligase enzymes and is involved in post-translational modifications. The WWP2 protein contains four double tryptophan (WW) domains, which allow specific protein-protein interactions and it is expressed in multiple organs throughout the body [11]. More specifically to cartilage, Nakamura et al. [12] showed that WWP2 interacts with SOX9 to form a complex that facilitates nuclear translocation of SOX9, as such enabling SOX9 transcriptional activity. Despite the association between the risk allele and higher expression levels of *WWP2* in human cartilage, the effect of *WWP2* knockout (KO) in mice with age-related and surgically induced models of OA showed that lack of *WWP2* expression resulted in increased expression of catabolic cartilage markers *RUNX2* and *ADAMTS5* [13]*.* In a different context, *WWP2* was found to be a host gene for microRNA-140 (miR-140), a miRNA highly expressed in cartilage and shown to be differentially expressed between preserved and lesioned OA cartilage [9]. As such, it

was suggested that expression of miR-140 and the C-terminal transcript of *WWP2* (*WWP2-C*, also called *WWP2* isoform 2) are co-regulated [14 ,15].

In the current study, we set out to explore how increased levels of *WWP2*, conferring risk to OA, affect cartilage matrix. To get gain insight in the *WWP2* pathway, we started with exploring a *WWP2* co-expression network in our previous whole-transcriptome OA cartilage dataset [9]. Moreover, to study the effect of the genetic risk allele (increased levels of *WWP2*), we functionally assessed the effect of lentiviral-mediated upregulation of *WWP2* in a 3D *in vitro* model using primary human chondrocytes. Apart from conventional anabolic and catabolic cartilage markers, genes identified in the *WWP2* co-expression network were used as a read-out to evaluate the effect of *WWP2* upregulation. Since WWP2 is involved in post-translational modifications, we explored the effect of *WWP2* upregulation on protein level by performing proteomic analysis. Finally, we explored the effects of upregulation of miR-140 in primary chondrocytes by transfection with miR-140 mimics.

Methods

Sample description

All material included in this study is obtained as part of the Research Arthritis and Articular Cartilage (RAAK) study. The RAAK-study is aimed at biobanking of joint materials of patients who underwent a total joint replacement surgery due to OA. Classification of macroscopically preserved and lesioned OA cartilage was done as described previously [16]. For all sample characteristics see **Supplementary Table 1**. The RAAK-study is approved by the medical ethics committee of the Leiden University Medical Center (P08.239/P19.013).

RNA-sequencing

Lesioned OA cartilage was collected from hip and knee joints (N=35 samples), snap frozen in liquid nitrogen, pulverized and homogenized in TRIzol (Invitrogen), and RNA was isolated using Qiagen RNeasy Mini Kit (Qiagen). Paired-end 2×100 bp RNA-sequencing (Illumina HiSeq2000 and Illumina HiSeq4000) was performed. Data from both Illumina platforms were integrated and analyzed with the same in-house pipeline. Additional details are described in **Supplementary methods.**

Creating a co-expression network

We explored co-expression behavior of WWP2 with progression of OA by correlating (Spearman correlation) *WWP2* expression levels in our RNA sequencing dataset with expression levels of all genes expressed in OA articular cartilage (N=20048 genes) [9]. To correct for multiple testing, the Benjamini-Hochberg method was used, as

indicated by the false discovery rate (FDR), with a significance cutoff value of 0.05. To include the most informative genes a threshold of $|\rho|>0.7$ and FDR<0.05 were selected, corresponding to approximately the top 1% of the total significant correlations.

Lentiviral transduction

The full length WWP2 plasmid was digested and inserted into the XhoI/XbaI sites of the pLV-CMV-IRES-eGFP lentiviral backbone (kindly provided by Prof. Dr. Hoeben). The pLV-CMV-IRES-eGFP lentiviral backbone without the WWP2 insert was used as a control. Additional details are available in the **Supplementary methods**.

In vitro 3D pellet cultures

3D pellet cultures were formed by adding 2.5x105 cells in their expansion medium to a 15 ml Falcon tube and subsequently expose them to centrifugal forces (1200 rpm, 4 minutes). Chondrogenesis was initiated in serum-free chondrogenic differentiation medium. Additional details are available in the **Supplementary methods**.

RT-qPCR

RNA was isolated from the samples using the RNeasy Mini Kit (Qiagen). cDNA synthesis was performed using the First Strand cDNA Synthesis Kit (Roche Applied Science). Subsequently, RT-qPCR was performed adjusting for housekeeping genes GAPDH and SDHA. Additional details are available in the **Supplementary methods**.

Quantitative Proteomics Using TMT Labeling

Lysis, digestion, TMT labeling and mass spectrometry analysis was essentially performed as described previously [8]. All searches and subsequent data analysis, including Percolator and abundance ratio calculation, were performed using Proteome Discoverer 2.4 (Thermo Scientific). Additional details are available in the **Supplementary methods**.

Histochemistry

Sections of the 3D chondrocyte pellet culutes were stained for glycosaminoglycan (GAG) deposition using the Alcian Blue staining. The staining was quantified using Fiji. Additional details are available in **Supplementary methods**.

Transfection with miR-140 mimics

Primary chondrocytes were transfected with hsa-miR-3p mimic (Invitrogen) or a control mimic at 5 nM final concentration using Opti-MEM (Gibco) and Lipofectamine RNAiMax Transfection reagent (Invitrogen) according to manufacturer's protocol. Additional details are available in **Supplementary methods.**

6

An overview of the applied strategy can be seen in **Figure 1**. The RNA sequencing data of the articular cartilage is deposited at ArrayExpress (E-MTAB-7313). Further data generated and used in this study is not openly available due to reasons of sensitivity and are available from the corresponding author upon reasonable request.

Results

Co-expression network of WWP2

To identify genes that are regulated by, or co-expressed with, *WWP2* in OA cartilage, we used RNA sequencing data of lesioned OA cartilage (N=35 samples, **Supplementary Table 1A**) to perform Spearman correlation between expression levels of *WWP2* and genes expressed in cartilage (N=20048 genes, **Supplementary Table 2, Figure 1A**). We identified 98 genes highly correlating ($|\rho|>0.7$) to *WWP2*. These 98 genes were significantly enriched for, amongst others, GO-terms Extracellular exosome (GO:0070062, 36 genes), characterized by expression of *GJA1* (encoding gap junction alpha 1)*, SMO* (encoding smoothened frizzled class receptor)*,* and *WDR1* (encoding WD repeat domain 1), and Myelin sheath (GO:0043209, 10 genes), characterized by expression of *WDR1, RALA* (encoding RAS like proto-oncogene A), and *CCT5* (encoding chaperonin containing TCP1 subunit 5) (**Supplementary Table 3**). As shown in **Supplementary Figure 1**, genes highly correlating to *WWP2* (N=98) formed a highly interconnected network, i.e. genes that are all highly correlating with each other. In this network we identified direct and indirect relations with *WWP2*, including *GJA1* (ρ=-0.81, 70 connections, i.e. highly correlating to 70 genes in the network), *WNK4* (encoding WNK lysine deficient protein kinase 4, ρ=0.81*,* 37 connections), *ACAN* (encoding aggrecan, ρ=0.78, 16 connections), and *STC2* (encoding stanniocalcin 2, ρ=0.77, 17 connections).

Lentiviral particle-mediated upregulation of WWP2

The effect of upregulation of *WWP2* was studied on cartilaginous matrix deposition in *in vitro* 3D chondrocyte pellet cultures, by creating a lentiviral particle mediated upregulation of *WWP2*. 3D pellet cultures were harvested after three or seven days of culturing and gene (N=16 pellet cultures of N=8 donors) and protein (N=16 pellet cultures of N=4 donors) expression levels were measured (**Supplementary Table 1B**). First, we confirmed whether *WWP2* upregulation was successful by measuring both gene and protein expression levels at day zero of the 3D chondrocyte pellet culture, and we observed a significant increase in *WWP2* gene expression levels (P=1.0x10^{-5}, **Supplementary Figure 2A and supplementary Figure 2B**), which was confirmed on protein level (P=3.2x10^{-6}, **Supplementary Figure 2C**).

Effect of WWP2 upregulation on cartilage matrix deposition

Next, we evaluated effect of *WWP2* upregulation on expression levels of conventional

Figure 1 – Schematic overview of applied strategy.
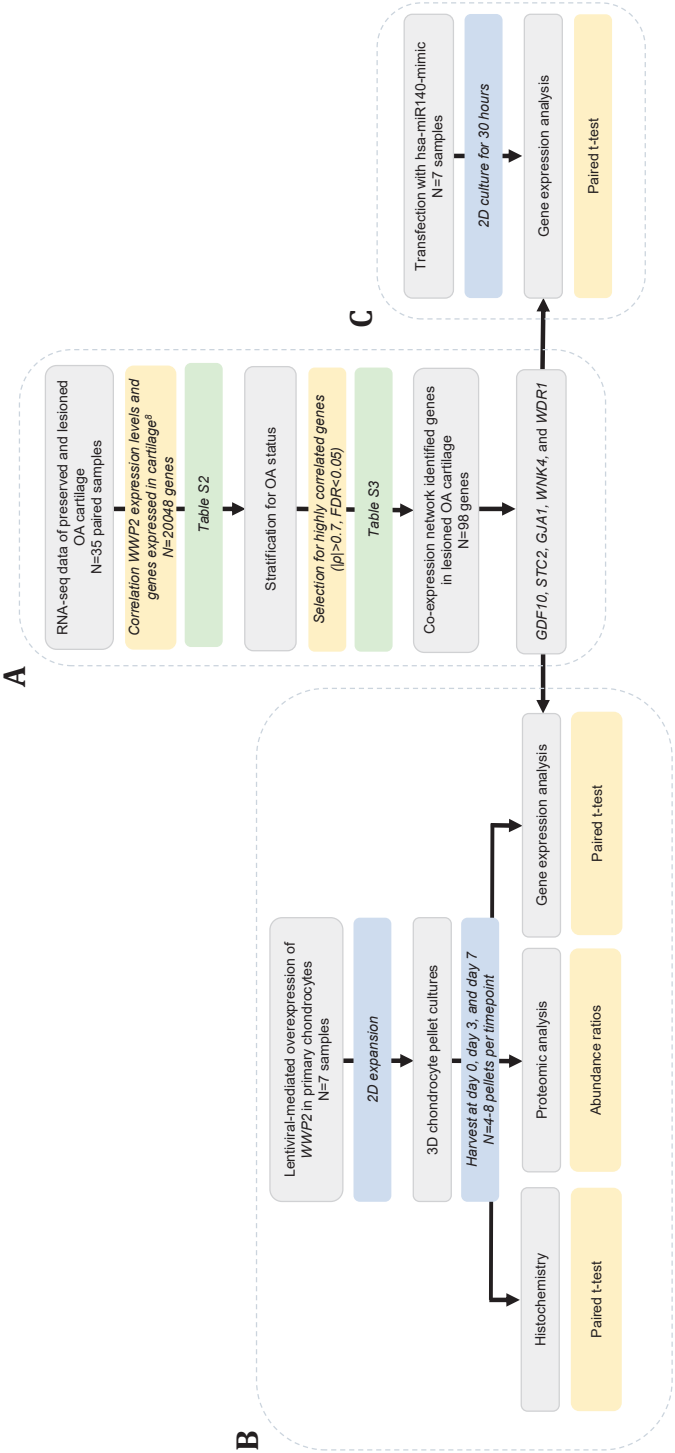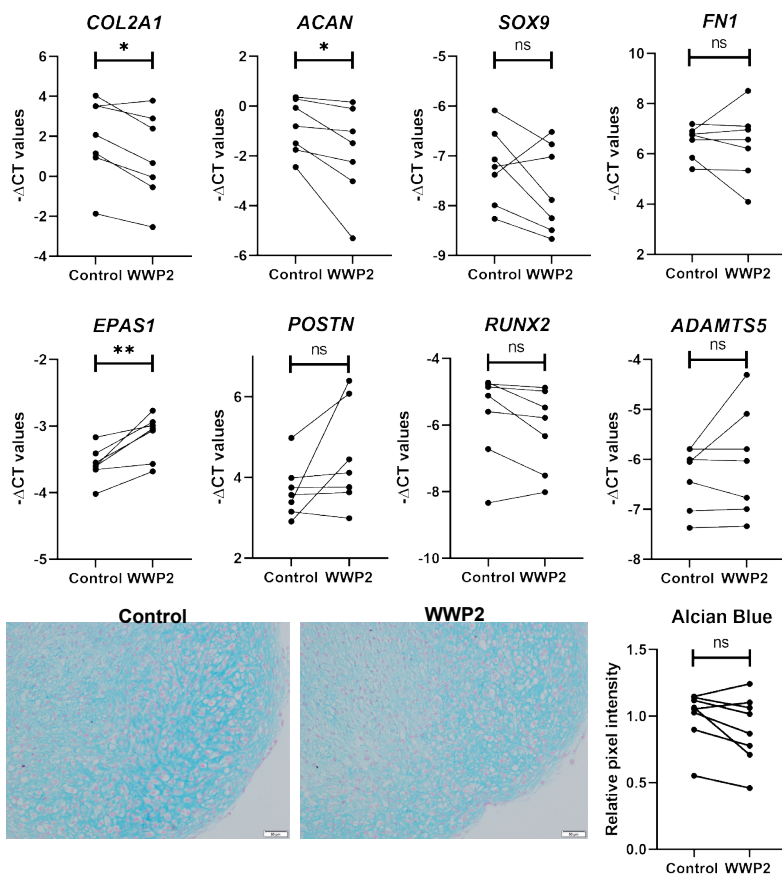
Figure 2 – mRNA expression levels of cartilage matrix markers (A) and cartilage degeneration markers (B) for pellets with WWP2 upregulation and their controls at day 7 (N=11-12 pellet cultures, N=7 donors). (C) Alcian Blue staining visualizing GAGs deposition in WWP2 overexpressed pellets and their controls after 7 days of culturing (N= 26 pellet cultures, N=8 donors).
The scale bar indicates 50 um. Ns: not significant. *P<0.05, ** P<0.005 upon performing a Paired sample t-test.

cartilage genes during 3D pellet culture of seven days (**Figure 1B**). As shown in **Figure 2A**, we found significant reduced gene expression of *ACAN* (FC=0.80, *P*=0.04) and *COL2A1* (encoding collagen type 2 alpha chain 1, FC=0.77, *P*=0.01), in *WWP2* upregulated pellets compared to their controls at day seven (**Supplementary Table 4**). Moreover, we showed significant increased gene expression of degeneration markers *EPAS1* (encoding endothelial PAS domain protein 1, FC=1.56, *P*=0.004) (**Figure 2B**). Notably, *SOX9*, *ADAMTS5*, and *RUNX2*, which were previously linked to WWP2 function, were not consistently changed upon WWP2 upregulation. Moreover, we stained 3D pellet cultures for presence of glycosaminoglycans (GAGs) using Alcian Blue staining, and observed a trend towards decreased Alcian Blue intensity when comparing *WWP2*

upregulated pellets with controls (**Figure 2C**).

Effect of WWP2 upregulation on genes correlated to WWP2

To investigate functional relationships between *WWP2* and identified correlating and highly interconnected genes, we selected *GDF10* (encoding growth differentiation factor 10, ρ=0.72, 18 connections), *STC2* (ρ=0.77, 17 connections), *GJA1* (ρ=-0.81, 70 connections), *WDR1* (encoding WD repeat-containing protein 1, ρ=-0.70, 5 connections), and *WNK4 (*ρ=0.81, 37 connections) from the network (**Supplementary Figure 1**) to use as read-out of WWP2 upregulation in 3D chondrocyte pellet cultures (**Figure 1B**). As shown in **Figure 3**, we observed significant decreased gene expression of *GDF10* (FC=0.62, *P*=0.002) and *STC2* (FC=0.73, *P*=0.04) with upregulation of *WWP2*. Albeit not significant, gene expression of *GJA1* (FC=0.76, *P*=0.08) was also consistently lower in *WWP2* upregulated pellets. Together, these data suggest that *GDF10*, *STC2*, and *GJA1* are downstream of *WWP2* either by direct or indirect activity. In contrast, *WNK4* and *WDR1* did not show consistent changes in expression with upregulation of *WWP2*, suggesting *WNK4* and *WDR1* are rather upstream in the pathway of *WWP2.*
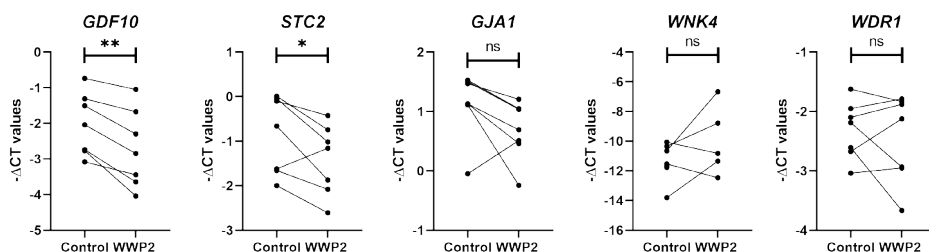
Figure 3 – mRNA expression levels of genes correlating with WWP2 in WWP2 upregulated 3D chondrocyte pellet cultures compared to their controls after 7 days of culturing (N=6-12 pellet cultures, N=7 donors).
Ns: not significant, * P<0.05, ** P<0.05 upon performing a Paired sample t-test.

Proteomics

To study the extent to which gene expression levels translate to protein levels, we performed proteomics analysis. Prior to differential expression analysis of pellet cultures with and without WWP2 upregulation, we explored protein expression levels of cartilage markers in our control pellet cultures at day three and day seven of 3D pellet culture. Upon comparing day three and day seven with day zero of control pellets, we observed increased protein expression of cartilage markers COL2A1 (FC=2.68 and FC=32.94, respectively), ACAN (FC=5.28 and FC=13.75, respectively), COMP (cartilage oligomeric matrix protein, FC=5.31 and FC=20.25, respectively), and FN1 (fibronectin, FC=2.12 and FC=3.51, respectively) (**Supplementary Table 5, Supplementary Figure**

3). Moreover, mesenchymal markers CD44 (FC=0.83 and FC=0.46, respectively) and CD166 (FC=0.79 and FC=0.62, respectively) and IGFBP3 (insulin growth factor binding protein 3, FC=0.10 and FC=0.10, respectively) were downregulated on both days. Together, this indicates that cartilage-like matrix is produced by chondrocytes already at day three, but is increasing towards day seven. Notably, SOX9 was not detected in the proteomics analysis.
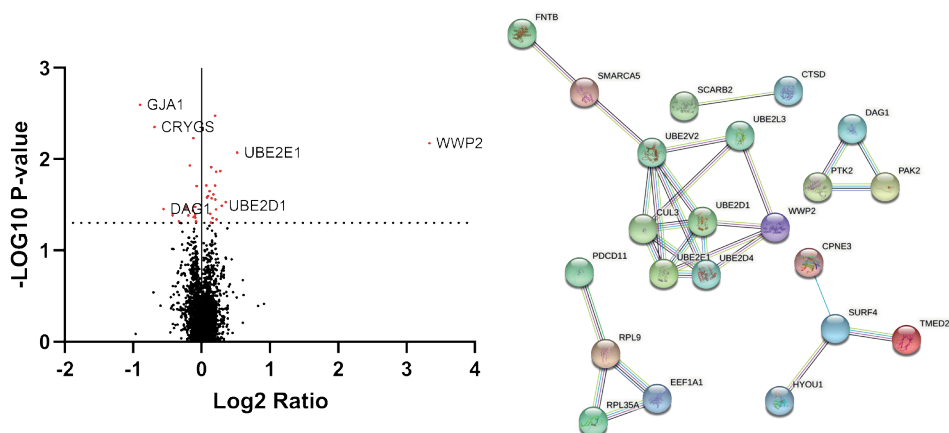
Figure 4 – Results of proteomics comparing WWP2 transduced 3D pellet cultures and their controls. (A) Volcano plot of proteins differentially expressed between WWP2 transduced 3D pellet cultures and their controls at day three and day seven together (N=16 pellets, N=4 donors). The red dots indicate the significantly differentially expressed proteins. (B) Protein-protein interaction network in STRING.

Next, we evaluated the effect of WWP2 upregulation on cartilage matrix deposition on protein level (**Figure 1B**). Since we observed increased protein expression of cartilage markers in control pellet cultures already on day three (**Supplementary Figure 3A**), we pooled day three and day seven for further analysis to increase power. Upon comparing pellet cultures with and without WWP2 upregulation, we found WWP2 still being significantly upregulated after three and seven days of culturing. Furthermore, we found 42 proteins significantly differentially expressed (**Figure 4A, Supplementary Table 6**), of which GJA1 (FC=0.54) was most significantly downregulated in WWP2 upregulated pellet cultures, confirming the downregulation observed on gene expression level (FC=0.76). Oppositely, the observed changes in *ACAN, COL2A1, FN1,* and *POSTN* gene expression levels were not confirmed on protein level. Proteins encoded by *SOX9, EPAS1, RUNX2,* and *ADAMTS5* were either not identified or did not show unique peptides. Upon performing enrichment analysis on the 42 differentially expressed proteins, we found significant enrichment for ubiquitin conjugating enzyme activity (5 proteins, FDR=0.002) and ubiquitin-protein transferase activity (6 proteins, FDR=0.03), both terms characterized by expression of, amongst others, UBE2D4, UBE2L3, and UBE2D1. Furthermore, these 42 proteins showed significant protein-protein interactions

(P=0.02, **Figure 4B**), also representing ubiquitin conjugating enzyme activity.

miR-140-3p and WWP2

Since it has been suggested that *WWP2* and miR-140 are co-expressed [14 ,15], we transfected primary chondrocytes with miR-140-3p mimics, to assess whether this miRNA regulates *WWP2* expression or similar genes as involved in the *WWP2* co-expression network (N=7, **Supplementary Table 1B**, **Figure 1C**). To investigate whether miR-140-3p regulates *WWP2,* we first evaluated the effects of miR-140-3p mimic on expression levels of *WWP2* full length and *WWP2* splice variants isoform 2, isoform 4, and isoform 6 (**Supplementary Figure 4**)*.* MiR-140 is suggested to be co-
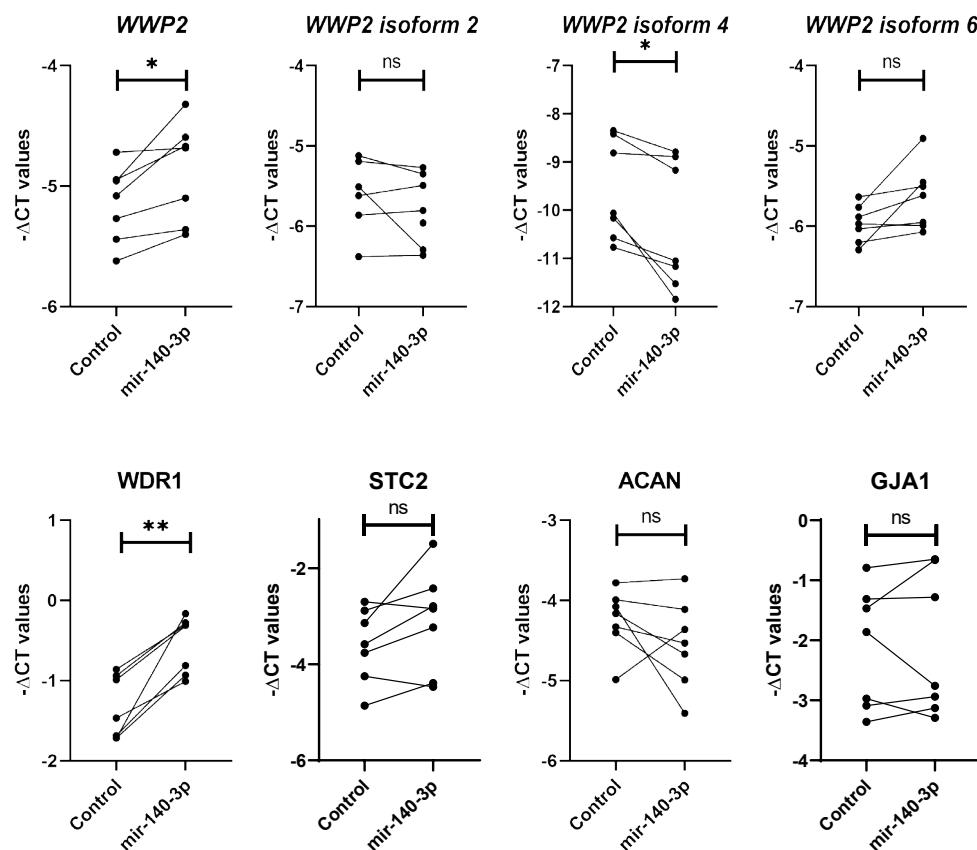
Figure 5 – mRNA expression levels upon transfection with miR-140-3p.
(A) expression levels of WWP2 and its isoforms. (B) Expression levels of genes correlated to WWP2 (N=8 wells, N=4 donors). Ns: not significant, * p<0.05, ** p<0.005 upon performing a Paired sample t-test.

expressed with splice variant *WWP2* isoform 2*,* also called *WWP2-C,* as they share the promotor [15]. Isoform 4 is also known as *WWP2-N* and is a transcript that does not contain miR-140 (**Supplementary Figure 4**). As shown in **Figure 5A**, we observed significant increased expression levels of *WWP2* (FC=1.22, *P*=0.02) with upregulation of miR-140-3p. Moreover*,* we observed consistent increased expression of *WWP2* isoform 6 (FC=1.29, *P*=0.06), while significant decreased expression of isoform 4 (FC=0.63, *P*=0.02) (**Supplementary Table 7**). Notably, we did not see effect on expression levels of *WWP2* isoform 2, also called *WWP2-C*. With respect to highly correlated genes, we observed increased expression of *WDR1* (FC=1.79, *P*=1.00×10^{-3}), one of the genes that was not consistently changed with *WWP2* upregulation (**Figure 5B**). Albeit not significant, we observed an increased expression of *STC2* (FC=1.55, *P*=0.08), which is also contradictory to the effects of *WWP2* upregulation. Moreover, we did not observe consistent effects on *GJA1* expression levels.

Discussion

By combining a genome-wide screen for cartilage specific allelic imbalance [7] and large scale GWAS [2 ,4], we hypothesized that upregulated expression of *WWP2* confers robust risk to OA. Here, we set out to functionally investigate the role of *WWP2* in cartilage by exploring the *WWP2* co-expression network in a previously assessed RNA sequencing dataset [9]. Moreover, lentiviral-mediated upregulation of *WWP2* was shown to have detrimental effects on cartilage matrix deposition, as shown by downregulation of *COL2A1* and *ACAN* and upregulation of *EPAS1*. Apart from conventional anabolic and catabolic cartilage markers, genes identified in the *WWP2* co-expression network were used as read-out, showing *GDF10*, *STC2*, and *GJA1* being responsive to *WWP2* upregulation. Furthermore, to explore effects of miR-140-3p, that was suggested to be co-regulated with *WWP2,* we transfected primary chondrocytes with miR-140-3p mimics.

Based on AI expression of the OA risk SNP rs1052429, we hypothesized that *WWP2* confers risk to OA onset by upregulated expression, whereas *WWP2* exhibited FDR significantly lower expression in lesioned compared to preserved cartilage (FC=0.78, FDR=5.3×10^{-3}), together suggesting that lower expression levels of *WWP2* in lesioned OA cartilage are rather an attempt of chondrocytes to reverse the OA state than a cause to the OA process [23 ,24]. Concomitantly, co-expression network analyses showed 98 highly and significantly ($|\rho|>0.7$, FDR<0.05) correlating genes to *WWP2*, including *GJA1* (ρ=-0.81), *WNK4* (ρ=0.81), *ACAN* (ρ=0.78), and *STC2* (ρ=0.77) (**Supplementary Table 2**). Previously, it was shown that WWP2 interacts with SOX9 and that it regulates SOX9 transcriptional activity [12]. Although *SOX9* is highly expressed in cartilage, *SOX9* was not among the high and significant correlations (ρ=0.5). On the other hand, *SOX9* was

previously shown to regulate the expression of, amongst others *ACAN* [25 ,26], which was here shown to be highly correlated to *WWP2* (ρ=0.78).

Upon studying the effect of upregulation of *WWP2*, we found *EPAS1* and *GDF10* being genes that had most consistent and significant changed levels of gene expression. *EPAS1*, encoding hypoxia-inducible factor 2 alpha, is known for its role in endochondral ossification and is a known cartilage degradation marker in OA [27 ,28]. *GDF10*, also known as bone morphogenic protein 3, is involved in osteogenesis as it inhibits osteoblast differentiation via *SMAD2* and *SMAD3 [24 ,29]*. The latter also being previously identified as OA susceptibility gene [2]. Furthermore, lower expression level of *GDF10* was associated with OA severity in both bone and cartilage [30]. Interestingly, *GDF10* was shown to be a hypoxia inducible gene, like *EPAS1*, which is regulated by SOX9 and was identified as marker for differentiated chondrocytes as it inhibits adipogenesis and osteogenesis [31]. Both *EPAS1* and *GDF10* were not in the proteomics analysis, either because they were not measured (EPAS1) or they did not show unique peptides (GDF10). Additionally, we observed a decrease in *STC2* and *GJA1* expression. Downregulation of *GJA1* did not reach statistical significance on gene expression level, while on protein level GJA1 was the most significantly downregulated protein. STC2 is a glycoprotein and upregulation of *STC2* in mice has been shown to delay endochondral ossification [32 ,33]. Moreover, it was shown that *STC2* was higher expressed in healthy cartilage compared to osteophytic cartilage [34], suggesting its potential role in initiation and progression of OA in presence of higher *WWP2* expression. GJA1, also known as connexin 43, is a major protein of functional gap junctions which allows for cell-cell communication. More specific to cartilage, connexin 43 is essential in mechanotransduction [35]. Alterations in connexin 43 expression and localization affects this cell-cell communication, by which homeostasis to maintain cartilage tissue gets disturbed [36]. Notably, like EPAS1 and GDF10, the function of connexin 43 is regulated by oxygen levels [37]. Upregulation of *EPAS1* and downregulation of *GDF10*, *STC2* and *GJA1* suggests that increased level of WWP2 has detrimental effects on cartilage matrix deposition, which acts via hypoxia associated chondrocyte dedifferentiation. This is in line with decreased gene expression levels of *COL2A1* and *ACAN,* two major cartilage markers.

To evaluate the effects of WWP2 upregulation on cartilage matrix deposition on protein level, we performed proteomics analysis. We did confirm upregulation of WWP2 on day zero, which was still present at day three and seven (**Figure 4, Supplementary Figure 2,**). Moreover, we found 42 significantly differentially expressed proteins upon comparing pellet cultures with and without WWP2 upregulation, of which GJA1 was most significantly differentially expressed and showing the highest fold change (FC=0.49). We were not able to confirm differences we observed in gene expression

6

levels of *COL2A1, ACAN, FN1,* and *POSTN* on protein level (**Supplementary Table 6**), which might be due to the relatively low sample size (N=4 donors) or due to suboptimal timepoint chosen to evaluate the effect of WWP2 on either gene or protein expression level. Since WWP2 is a E3 ubiquitin ligase and the differentially expressed proteins were significantly enriched for ubiquitin conjugating enzyme activity and ubiquitin-protein transferase activity, upregulation of WWP2 could also affect proteins cellular location, activity, and protein-protein interactions without changing expression levels itself, which is not captured by our read-outs. Moreover, it should be noted that the here observed fold differences were relatively low and additional validation and replication are necessary.

Since it has been suggested that miR-140 is co-expressed with *WWP2-C* [14], *WWP2* isoform 2, we generated upregulation of miR-140 in 2D primary chondrocytes to explore whether *WWP2* and miR-140 are involved in similar pathways. In the miR-140 upregulated cells, we observed significant increased expression levels of *WWP2,* indicating miR-140 indeed targets *WWP2*. Nonetheless, given the predicted *WWP2* target site of miR-140 (3'UTR of *WWP2* isoform 6 [38]) and the absence of SNPs in this region in linkage disequilibrium with the OA risk SNP rs1052429, the genetic *WWP2* risk nor the allelic imbalance is brought about via an aberrant miR-140 binding to *WWP2*. The fact that we did not observe consistent changes in expression levels of *WWP2* isoform 2, suggests that *WWP2* isoform 2 and miR-140 indeed share the intron 10 (*WWP2* full length) promotor as hypothesized previously by Rice at al. [15]. Additional research is required to fully understand the role of miR-140 in the *WWP2* pathway and in OA pathophysiology in general.

Although lower expression of *WWP2* was observed in lesioned compared to preserved cartilage in our previous study [9], genetic evidence suggests that higher expression of *WWP2* predisposes to development of OA, indicating that downregulation in OA pathophysiology is merely a response to the pathophysiological process and a beneficial attempt of chondrocytes to reverse the OA state [7]. The latter shows that genes identified being differentially expressed between preserved and lesioned OA articular cartilage are a response to the OA pathophysiological process and not necessarily causal to the OA pathophysiological process. To identify genes causal to OA, genetic studies have to be performed. To our surprise, Styrkarsdottir et al. [2] reported on *WWP2* expression in adipose tissue as function of SNP rs4985453-G, a proxy of their identified OA risk allele rs34195470-G (R^2=0.79) and our AI SNP rs1052429-A (R^2=0.77), highlighting the OA risk allele being associated with lower expression levels of *WWP2*. Upon investigating the GTEx eQTL data of *WWP2* with the highlighted SNPs [39], we found only data showing consistently higher expression of *WWP2* as function of OA risk alleles of the

respective SNPs across multiple tissues (**Supplementary Figure 5**), underscoring the aberrant effects observed here with *WWP2* upregulation. Although Mokuda et al. [13] showed that lack of *WWP2* expression in mice resulted in increased expression of *RUNX2* and *ADAMTS5*, we here did not observe consistent changes in expression of *RUNX2* or *ADAMTS5* upon upregulation of *WWP2* in our human chondrocyte pellet cultures and culturing for seven days. This difference could be due to translational limitations from mice to humans. Alternatively, we here create neocartilage, and the effect on *RUNX2* and *ADAMTS5* may be a temporal or time-dependent effect, which we do not observe at day seven of culturing.

In conclusion, our data provide support to our hypothesis that high levels of *WWP2* have detrimental effects on cartilage homeostasis. We identified *EPAS1, GJA1, GDF10,* and *STC2*, all genes involved in chondrocyte dedifferentiation, to be involved in the *WWP2* pathway. Moreover, we showed that miR-140 is likely involved in similar pathways as *WWP2* and miR-140 might play a role in regulating *WWP2* expression. Together these data contribute to a better understanding of how *WWP2* confers risk to OA and is a step towards translation from bench to bedside.

Declarations

6

Chapter 6

Disclosures

The authors have no relevant financial or non-financial interests to disclose.

References

1. Vina ER, Kwoh CK. Epidemiology of osteoarthritis: literature update. *Curr Opin Rheumatol* 2018;30(2):160-67. doi: 10.1097/bor.0000000000000479 [published Online First: 2017/12/12]
2. Styrkarsdottir U, Lund SH, Thorleifsson G, Zink F, Stefansson OA, Sigurdsson JK, et al. Meta-analysis of Icelandic and UK data sets identifies missense variants in SMO, IL11, COL11A1 and 13 more new loci associated with osteoarthritis. *Nat Genet* 2018;50(12):1681-87. doi: 10.1038/s41588-018-0247-0 [published Online First: 2018/10/31]
3. Zengini E, Hatzikotoulas K, Tachmazidou I, Steinberg J, Hartwig FP, Southam L, et al. Genome-wide analyses using UK Biobank data provide insights into the genetic architecture of osteoarthritis. *Nat Genet* 2018;50(4):549-58. doi: 10.1038/s41588-018-0079-y [published Online First: 2018/03/22]
4. Boer CG, Hatzikotoulas K, Southam L, Stefánsdóttir L, Zhang Y, Coutinho de Almeida R, et al. Deciphering osteoarthritis genetics across 826,690 individuals from 9 populations. *Cell* 2021 doi: 10.1016/j.cell.2021.07.038 [published Online First: 2021/08/28]
5. Gee F, Clubbs CF, Raine EV, Reynard LN, Loughlin J. Allelic expression analysis of the osteoarthritis susceptibility locus that maps to chromosome 3p21 reveals cis-acting eQTLs at GNL3 and SPCS1. *BMC Med Genet* 2014;15:53. doi: 10.1186/1471-2350-15-53 [published Online First: 2014/06/03]
6. Raine EV, Dodd AW, Reynard LN, Loughlin J. Allelic expression analysis of the osteoarthritis susceptibility gene COL11A1 in human joint tissues. *BMC Musculoskelet Disord* 2013;14:85. doi: 10.1186/1471-2474-14-85 [published Online First: 2013/03/19]
7. den Hollander W, Pulyakhina I, Boer C, Bomer N, van der Breggen R, Arindrarto W, et al. Annotating Transcriptional Effects of Genetic Variants in Disease-Relevant Tissue: Transcriptome-Wide Allelic Imbalance in Osteoarthritic Cartilage. *Arthritis Rheumatol* 2019;71(4):561-70. doi: 10.1002/art.40748 [published Online First: 2018/10/10]
8. den Hollander W, Ramos YF, Bomer N, Elzinga S, van der Breggen R, Lakenberg N, et al. Transcriptional associations of osteoarthritis-mediated loss of epigenetic control in articular cartilage. *Arthritis Rheumatol* 2015;67(8):2108-16. doi: 10.1002/art.39162 [published Online First: 2015/04/22]
9. Coutinho de Almeida R, Ramos YFM, Mahfouz A, den Hollander W, Lakenberg N, Houtman E, et al. RNA sequencing data integration reveals an miRNA interactome of osteoarthritis cartilage. *Annals of the rheumatic diseases* 2019;78(2):270-77. doi: 10.1136/annrheumdis-2018-213882 [published Online First: 2018/12/07]
10. Ji Q, Zheng Y, Zhang G, Hu Y, Fan X, Hou Y, et al. Single-cell RNA-seq analysis reveals the progression of human osteoarthritis. 2019;78(1):100-10. doi: 10.1136/annrheumdis-2017-212863 %J Annals of the Rheumatic Diseases
11. Chantry A. WWP2 ubiquitin ligase and its isoforms: new biological insight and promising disease targets. *Cell Cycle* 2011;10(15):2437-9. doi: 10.4161/cc.10.15.16874 [published Online First: 2011/07/14]
12. Nakamura Y, Yamamoto K, He X, Otsuki B, Kim Y, Murao H, et al. Wwp2 is essential for palatogenesis mediated by the interaction between Sox9 and mediator subunit 25. *Nat Commun* 2011;2:251. doi: 10.1038/ncomms1242 [published Online First: 2011/03/24]
13. Mokuda S, Nakamichi R, Matsuzaki T, Ito Y, Sato T, Miyata K, et al. Wwp2 maintains cartilage homeostasis through regulation of Adamts5. *Nature Communications* 2019;10(1):2429. doi: 10.1038/s41467-019-10177-1
14. Yang J, Qin S, Yi C, Ma G, Zhu H, Zhou W, et al. MiR-140 is co-expressed with Wwp2-C transcript and activated by Sox9 to target Sp1 in maintaining the chondrocyte proliferation. *FEBS Lett* 2011;585(19):2992-7. doi: 10.1016/j.febslet.2011.08.013 [published Online First: 2011/08/30]
15. Rice SJ, Beier F, Young DA, Loughlin J. Interplay between genetics and epigenetics in osteoarthritis. *Nature Reviews Rheumatology* 2020;16(5):268-81. doi: 10.1038/s41584-020-0407-3
16. Ramos YF, den Hollander W, Bovee JV, Bomer N, van der Breggen R, Lakenberg N, et al. Genes involved in the osteoarthritis process identified through genome wide expression analysis in articular cartilage; the RAAK study. *PloS one* 2014;9(7):e103056. doi: 10.1371/journal.pone.0103056 [published Online First: 2014/07/24]
17. Wu TD, Watanabe CK. GMAP: a genomic mapping and alignment program for mRNA and EST sequences. *Bioinformatics* 2005;21(9):1859-75. doi: 10.1093/bioinformatics/bti310 [published Online First: 2005/02/25]
18. Anders S, Pyl PT, Huber W. HTSeq--a Python framework to work with high-throughput sequencing data. *Bioinformatics* 2015;31(2):166-9. doi: 10.1093/bioinformatics/btu638 [published Online First: 2014/09/28]
19. Ewels P, Magnusson M, Lundin S, Kaller M. MultiQC: summarize analysis results for multiple tools and samples in a single report. *Bioinformatics* 2016;32(19):3047-8. doi: 10.1093/bioinformatics/btw354 [published Online First: 2016/06/18]
20. Love MI, Huber W, Anders S. Moderated estimation of fold change and dispersion for RNA-seq data with DESeq2. *Genome Biology* 2014;15(12):550. doi: 10.1186/s13059-014-0550-8
21. Bomer N, den Hollander W, Ramos YF, Bos SD, van der Breggen R, Lakenberg N, et al. Underlying molecular mechanisms of DIO2 susceptibility in symptomatic osteoarthritis. *Annals of the rheumatic diseases* 2015;74(8):1571-9. doi: 10.1136/annrheumdis-2013-204739 [published Online First: 2014/04/04]
22. Pirro M, Mohammed Y, van Vliet SJ, Rombouts Y, Sciacca A, de Ru AH, et al. N-Glycoproteins Have a Major Role in MGL Binding to Colorectal Cancer Cell Lines: Associations with Overall Proteome Diversity. *Int J Mol Sci* 2020;21(15) doi: 10.3390/ijms21155522 [published Online First: 2020/08/06]
23. Reynard LN. Analysis of genetics and DNA methylation in osteoarthritis: What have we learnt about the disease? *Semin Cell Dev Biol* 2017;62:57-66. doi: 10.1016/j.semcdb.2016.04.017 [published Online First: 2016/05/01]
24. Rice SJ, Cheung K, Reynard LN, Loughlin J. Discovery and analysis of methylation quantitative trait loci (mQTLs) mapping to novel osteoarthritis genetic risk signals. *Osteoarthritis Cartilage* 2019;27(10):1545-56. doi: 10.1016/j.joca.2019.05.017 [published Online First: 2019/06/08]
25. Sekiya I, Tsuji K, Koopman P, Watanabe H, Yamada Y, Shinomiya K, et al. SOX9 enhances aggrecan gene promoter/enhancer activity and is up-regulated by retinoic acid in a cartilage-derived cell line, TC6. *J Biol Chem* 2000;275(15):10738-44. doi: 10.1074/jbc.275.15.10738 [published Online First: 2001/02/07]
26. Nishimura R, Hata K, Takahata Y, Murakami T, Nakamura E, Yagi H. Regulation of Cartilage Development and Diseases by Transcription Factors. *J Bone Metab* 2017;24(3):147-53. doi: 10.11005/jbm.2017.24.3.147 [published Online First: 2017/09/29]
27. Yang S, Kim J, Ryu JH, Oh H, Chun CH, Kim BJ, et al. Hypoxia-inducible factor-2alpha is a catabolic regulator of osteoarthritic cartilage destruction. *Nat Med* 2010;16(6):687-93. doi: 10.1038/nm.2153 [published Online First: 2010/05/25]

28. Saito T, Fukai A, Mabuchi A, Ikeda T, Yano F, Ohba S, et al. Transcriptional regulation of endochondral ossification by HIF-2alpha during skeletal growth and osteoarthritis development. *Nat Med* 2010;16(6):678-86. doi: 10.1038/nm.2146 [published Online First: 2010/05/25]

29. Matsumoto Y, Otsuka F, Hino J, Miyoshi T, Takano M, Miyazato M, et al. Bone morphogenetic protein-3b (BMP-3b) inhibits osteoblast differentiation via Smad2/3 pathway by counteracting Smad1/5/8 signaling. *Mol Cell Endocrinol* 2012;350(1):78-86. doi: 10.1016/j.mce.2011.11.023 [published Online First: 2011/12/14]

30. Chou CH, Lee CH, Lu LS, Song IW, Chuang HP, Kuo SY, et al. Direct assessment of articular cartilage and underlying subchondral bone reveals a progressive gene expression change in human osteoarthritic knees. *Osteoarthritis Cartilage* 2013;21(3):450-61. doi: 10.1016/j.joca.2012.11.016 [published Online First: 2012/12/12]

31. Lafont JE, Talma S, Hopfgarten C, Murphy CL. Hypoxia promotes the differentiated human articular chondrocyte phenotype through SOX9-dependent and -independent pathways. *J Biol Chem* 2008;283(8):4778-86. doi: 10.1074/jbc.M707729200 [published Online First: 2007/12/14]

32. Gagliardi AD, Kuo EY, Raulic S, Wagner GF, DiMattia GE. Human stanniocalcin-2 exhibits potent growth-suppressive properties in transgenic mice independently of growth hormone and IGFs. *Am J Physiol Endocrinol Metab* 2005;288(1):E92-105. doi: 10.1152/ajpendo.00268.2004 [published Online First: 2004/09/16]

33. Chang AC, Hook J, Lemckert FA, McDonald MM, Nguyen MA, Hardeman EC, et al. The murine stanniocalcin 2 gene is a negative regulator of postnatal growth. *Endocrinology* 2008;149(5):2403-10. doi: 10.1210/en.2007-1219 [published Online First: 2008/02/09]

34. Gelse K, Ekici AB, Cipa F, Swoboda B, Carl HD, Olk A, et al. Molecular differentiation between osteophytic and articular cartilage--clues for a transient and permanent chondrocyte phenotype. *Osteoarthritis Cartilage* 2012;20(2):162-71. doi: 10.1016/j.joca.2011.12.004 [published Online First: 2012/01/03]

35. Gago-Fuentes R, Bechberger JF, Varela-Eirin M, Varela-Vazquez A, Acea B, Fonseca E, et al. The C-terminal domain of connexin43 modulates cartilage structure via chondrocyte phenotypic changes. *Oncotarget* 2016;7(45):73055-67. doi: 10.18632/oncotarget.12197 [published Online First: 2016/09/30]

36. Mayan MD, Gago-Fuentes R, Carpintero-Fernandez P, Fernandez-Puente P, Filgueira-Fernandez P, Goyanes N, et al. Articular chondrocyte network mediated by gap junctions: role in metabolic cartilage homeostasis. *Annals of the rheumatic diseases* 2015;74(1):275-84. doi: 10.1136/annrheumdis-2013-204244 [published Online First: 2013/11/15]

37. Knight MM, McGlashan SR, Garcia M, Jensen CG, Poole CA. Articular chondrocytes express connexin 43 hemichannels and P2 receptors - a putative mechanoreceptor complex involving the primary cilium? *J Anat* 2009;214(2):275-83. doi: 10.1111/j.1469-7580.2008.01021.x [published Online First: 2009/02/12]

38. Agarwal V, Bell GW, Nam J-W, Bartel DP. Predicting effective microRNA target sites in mammalian mRNAs. *eLife* 2015;4:e05005. doi: 10.7554/eLife.05005

39. The Genotype-Tissue Expression (GTEx) project. *Nat Genet* 2013;45(6):580-5. doi: 10.1038/ng.2653 [published Online First: 2013/05/30]

6

Supplementary files
Supplementary methods

RNA-sequencing
Lesioned OA cartilage was collected from macroscopically lesioned areas (based on color of the articular cartilage, surface integrity, and depth of the cartilage upon sampling with scalpel) of hip and knee joints and snap frozen in liquid nitrogen. Subsequently, the cartilage was pulverized and homogenized in TRIzol reagent (Invitrogen) using mixer mill 200 (Retsch). RNA was isolated from the articular cartilage using Qiagen RNeasy Mini Kit (Qiagen, GmbH, Hilden, Germany). Paired-end 2×100 bp RNA-sequencing (Illumina TruSeq RNA Library Prep Kit, Illumina HiSeq2000 and Illumina HiSeq4000) was performed. Strand specific RNA-seq libraries were generated which yielded a mean of 20 million reads per sample. Data from both Illumina platforms were integrated and analyzed with the same in-house pipeline. RNA-seq reads were aligned using GSNAP [2] against GRCh38 using default parameters. Read abundances per sample was estimated using HTSeq count v0.11.1 [3]. Only uniquely mapping reads were used for estimating expression. The quality of the raw reads for RNA-sequencing was checked using MultiQC v1.7. [4]. To identify outliers, principal component analysis (PCA) was applied. The DESeq2 package [5] was used to normalize the RNA-seq data, as a variance-stabilizing transformation was performed.

Lentiviral transduction
The full length WWP2 plasmid (NM_001270454.1) was ordered in pcDNA3.1 with XhoI/XbaI cloning sites (Genscript Biotech). The plasmid was digested and inserted into the XhoI/XbaI sites of the pLV-CMV-IRES-eGFP lentiviral backbone (kindly provided by Prof. Dr. Hoeben, Dept. of Molecular Cell Biology, Leiden University Medical Center). Lentiviral production was performed in HEK 293T cells, using Lenti-vpak Lentiviral Packaging Kit (Origene Technologies, Inc.). The HEK 293T cells were expanded in DMEM (high glucose; Gibco) supplemented with 10% fetal calf serum (FBS, Gibco) and 100 U/ml penicillin and 100 ug/ml streptomycin (Gibco). The pLV-CMV-IRES-eGFP lentiviral backbone without the WWP2 insert was used as a control. Primary chondrocytes were isolated from the articular cartilage of human joints and expanded in DMEM (high glucose; Gibco) supplemented with 10% FBS (Gibco), 100 U/ml penicillin and 100 ug/ml streptomycin (Gibco), and 0.5 ng/ml FGF-2 (PeproTech), as described previously [7]. After expansion, the chondrocytes were seeded in a density of 3.5x105 cells per 10 cm culture dish (passage 2) and left overnight. Then, the lentivirus was added in a MOI of 1 in addition of 15 ug/ml Polybrene (Sigma-Aldrich). After incubation of approximately 16 hours, the lentiviral solution was replaced by normal culture medium. The chondrocytes were passaged and expanded afterwards.

In vitro 3D pellet cultures
Primary chondrocytes were isolated from macroscopically preserved cartilage of OA hip and knee joints by incubating the cartilage overnight in expansion medium (DMEM (high glucose; Gibco), supplemented with 10% fetal bovine serum (FBS; Gibco), 100 U/ml penicillin and 100 ug/ml streptomycin (Gibco), 0.5 ng/ml FGF-2 (PeproTech)) in addition of 2 mg/ml collagenase type I. To remove undigested cartilage fragments, the primary chondrocytes were then resuspended, filtered through a 100 μm mesh and plated in a culture dish with expansion medium. 3D pellet cultures were formed by adding 2.5x105 cells in their expansion medium to a 15 ml Falcon tube and subsequently expose them to centrifugal forces (1200 rpm, 4 minutes). After 24 hours, the expansion medium was replaced by chondrogenic differentiation medium (DMEM (high glucose; Gibco), supplemented with Ascorbic acid (50 μg/ml; Sigma-Aldrich), L-Proline (40 μg/ml; Sigma-Aldrich), Sodium Puryvate (100 μg/ml; Sigma-Aldrich), Dexamethasone (0.1 μM; Sigma-Aldrich), ITS+, 100 U/ml penicillin and 100 ug/ml streptomycin (Gibco) and TGF-β1 (10 ng/ml; PeproTech)), as described previously [7]. Medium was refreshed every 3-4 days and the caps of the Falcon tubes were open for the first 7 days to allow oxygen entering the tubes. The pellets were harvested at different timepoints; after 24 hours (day 0) and after 7 days. The harvested materials were lysed using RNABee (Bioconnect) and stored at -80oC until further processing.

RT-qPCR
RNA was isolated from the samples using the RNeasy Mini Kit (Qiagen). cDNA synthesis was performed using the First Strand cDNA Synthesis Kit (Roche Applied Science). Subsequently, RT-qPCR was performed with the Biomark™ 96.96 Dynamic Arrays (Fluidigm) according to the manufacturer's protocol. Additional RT-qPCR was performed using SYBR Green without the ROX reference dye (Roche Applied Science) and the QuantStudio 6 Real-Time PCR system (Applied Biosystems). In both methods, GAPDH and SDHA were used as housekeeping genes. The measured gene expression levels were corrected for the housekeeping genes GAPDH and SDHA, and the fold changes were calculated using the 2-ΔΔCT method. All values were calculated relative to the control groups. The paired sample t-test was used to calculate significance ($P<0.05$).

Quantitative Proteomics Using TMT Labeling
Lysis, digestion, TMT labeling and mass spectrometry analysis was essentially performed as described [8]. In short, 3D pellet cultures were washed with PBS, extracted with 100 ul 5% SDS, 100 mM Tris HCl pH 7.6 each, sonicated twice for 10 min and incubated for 20 min at 95°C. Insoluble material was removed by centrifugation for 2 minutes at 15,000 rpm in an Eppendorf centrifuge. Proteins were reduced, alkylated, subjected to chloroform methanol precipitation and digested with trypsin as described earlier [8].
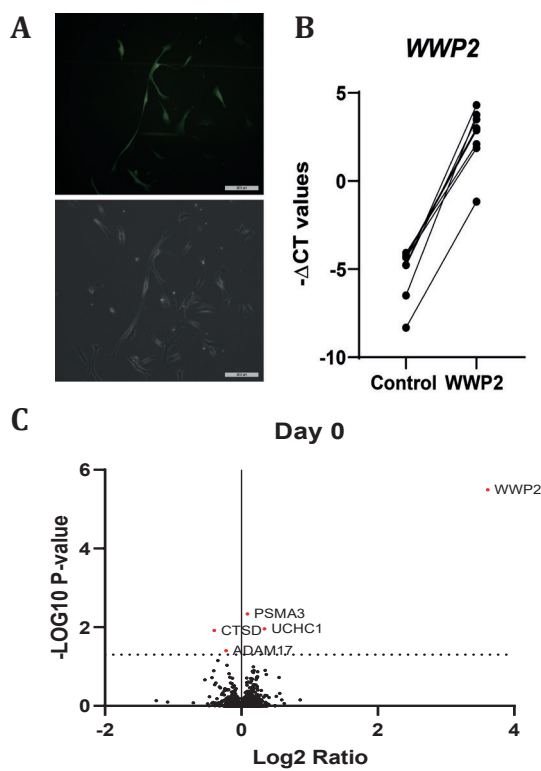
Peptide concentration was determined by BCA Gold protein assay (Pierce) and 10ug of the peptide was labeled using TMT10plex reagent (Thermo). Three separate TMT10 sets were prepared with a common reference sample consisting of a mixture of all peptide samples. TMT-labeled peptides were dissolved in 0.1% formic acid and subsequently analyzed by online C18 nano-HPLC MS/MS with a system consisting of an Easy nLC 1200 gradient HPLC system (Thermo, Bremen, Germany), and an Orbitrap Fusion LUMOS mass spectrometer in synchronous precursor selection (Thermo). For peptide identification, MS/MS spectra were searched against the human database (20596 entries) using Mascot Version 2.2.07 (Matrix Science) with the following settings: 10 ppm and 0.6 Da deviation for precursor and fragment masses, respectively. Trypsin was set as enzyme and two missed cleavages were allowed. Carbamidomethyl on cysteines and TMT6plex on Lys and N-term were set as fixed modifications. Variable modifications were oxidation (on Met and Pro) and acetylation on the protein N-terminus. All searches and subsequent data analysis, including Percolator and abundance ratio calculation, were performed using Proteome Discoverer 2.4 (Thermo Scientific). Peptide-spectrum matches were adjusted to a 1% FDR. Proteins were filtered on a minimal unique peptide count of 2. Since the sample size was rather small and we did observe significant increased expression of cartilage markers already at day three of pellet culture, we pooled the data of day 3 and day 7 for further analysis.

Histochemistry

The 3D chondrocyte pellet cultures were fixed with 4% formaldehyde and subsequently embedded in paraffin. The sections were stained for glycosaminoglycan (GAG) deposition using the Alcian Blue staining. The staining was quantified by loading the images in Fiji and splitting the color channels. Subsequently, the grey values were measured and corrected for the grey value of the background and for the number of cells present. The paired sample t-test was again used to calculate significance.

Transfection with miR-140 mimics

Primary chondrocytes were passaged in a concentration of 4.0×10^4 cells per well. After 24 hours, the cells were transfected with hsa-miR-140-3p mimic (Invitrogen) or a control mimic at 5 nM final concentration using Opti-MEM (Gibco) and Lipofectamine RNAiMax Transfection reagent (Invitrogen) according to manufacturer's protocol. These miRNA mimics are chemically modified double-stranded RNA molecules that mimic endogenous miRNAs, in this case miR-140-3p. The control mimic consists of a random miRNA sequence that does not have an effect in human tissues. Approximately 16 hours after transfection, the cells were lysed using TRizol (Thermo Fisher Scientific) for RNA isolation and stored at -80oC until further processing.

References

1. Rmos YF, den Hollander W, Bovee JV, Bomer N, van der Breggen R, Lakenberg N, et al. Genes involved in the osteoarthritis process identified through genome wide expression analysis in articular cartilage; the RAAK study. PloS one 2014;9(7):e103056. doi: 10.1371/journal.pone.0103056 [published Online First: 2014/07/24]
2. Wu TD, Watanabe CK. GMAP: a genomic mapping and alignment program for mRNA and EST sequences. Bioinformatics 2005;21(9):1859-75. doi: 10.1093/bioinformatics/bti310 [published Online First: 2005/02/25]
3. Anders S, Pyl PT, Huber W. HTSeq--a Python framework to work with high-throughput sequencing data. Bioinformatics 2015;31(2):166-9. doi: 10.1093/bioinformatics/btu638 [published Online First: 2014/09/28]
4. Ewels P, Magnusson M, Lundin S, Kaller M. MultiQC: summarize analysis results for multiple tools and samples in a single report. Bioinformatics 2016;32(19):3047-8. doi: 10.1093/bioinformatics/btw354 [published Online First: 2016/06/18]
5. Love MI, Huber W, Anders S. Moderated estimation of fold change and dispersion for RNA-seq data with DESeq2. Genome Biology 2014;15(12):550. doi: 10.1186/s13059-014-0550-8
6. Coutinho de Almeida R, Ramos YFM, Mahfouz A, den Hollander W, Lakenberg N, Houtman E, et al. RNA sequencing data integration reveals an miRNA interactome of osteoarthritis cartilage. Annals of the rheumatic diseases 2019;78(2):270-77. doi: 10.1136/annrheumdis-2018-213882 [published Online First: 2018/12/07]
7. Bomer N, den Hollander W, Ramos YF, Bos SD, van der Breggen R, Lakenberg N, et al. Underlying molecular mechanisms of DIO2 susceptibility in symptomatic osteoarthritis. Annals of the rheumatic diseases 2015;74(8):1571-9. doi: 10.1136/annrheumdis-2013-204739 [published Online First: 2014/04/04]
8. Pirro M, Mohammed Y, van Vliet SJ, Rombouts Y, Sciacca A, de Ru AH, et al. N-Glycoproteins Have a Major Role in MGL Binding to Colorectal Cancer Cell Lines: Associations with Overall Proteome Diversity. Int J Mol Sci 2020;21(15) doi: 10.3390/ijms21155522 [published Online First: 2020/08/06]

Supplementary figures

Supplementary Figure 1 - Interconnected network of genes highly correlating (|ρ|>0.7, FDR<0.05) to WWP2 in lesioned OA articular cartilage.
The positive correlations are shown in green and the negative correlations are shown in orange. The size of the nodes in the network indicate the number of connections.

6

A

B *WWP2*

C Day 0

Supplementary Figure 2 – Overexpression of WWP2.
(A) Monolayer of chondrocytes 3 days after transduction. (B) -ΔCT values of WWP2 overexpressed pellets and their controls at day 0 of the 3D pellet culture. (C) Volcano plot of proteomics analysis at day 0 showing WWP2 being upregulated.

A day 3 vs. day 0

B day 7 vs. day 0

Supplementary Figure 3 – Volcano plot of proteins differentially expressed between day three and day zero (A) and day seven and day zero (B) of pellet culture in the control pellets (N=16 pellet cultures, N=4 donors)
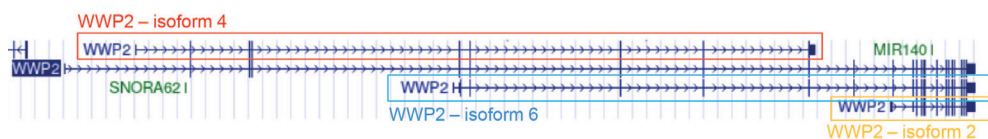
Supplementary Figure 4 – Overview of WWP2 transcripts as shown by UCSC genome browser.
WWP2 isoform 2, also called WWP2-C, is suggested to be co-expressed with miR-140, while WWP2 isoform 4, also called WWP2-N, does not contain miR-140.
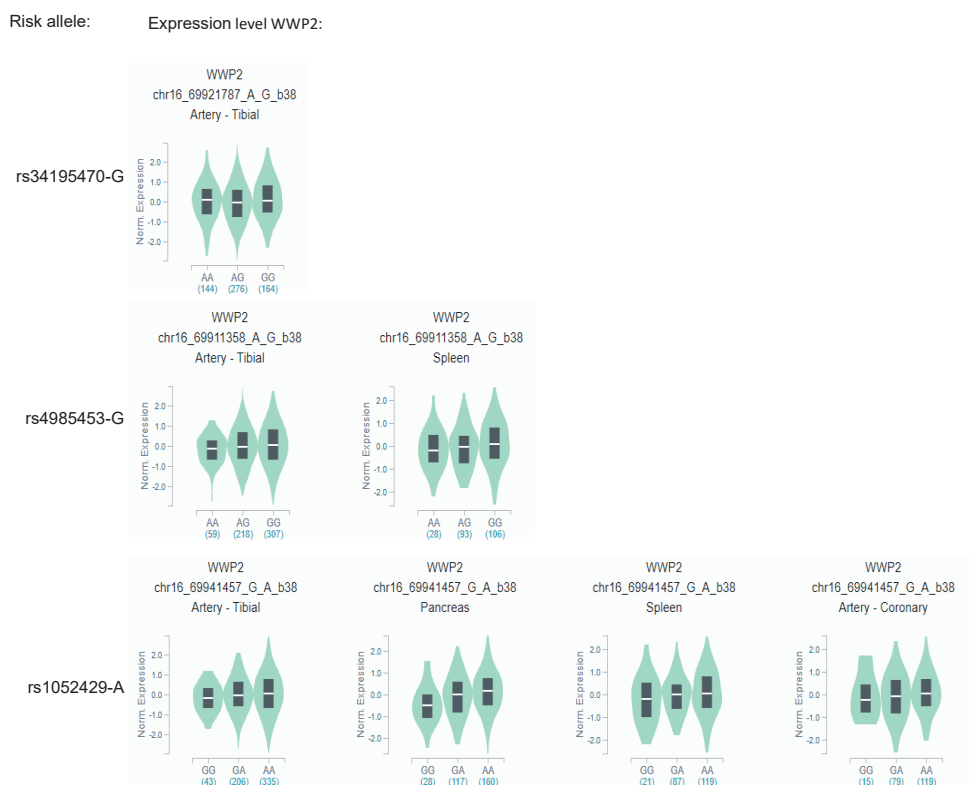
Supplementary Figure 5 – GTEx violin plots of WWP2 expression as function of the three OA susceptibility alleles.
In all three cases, the OA risk allele is associated to higher expression levels of WWP2 across multiple tissues.

Supplementary tables

Supplementary Table 1 – Baseline characteristics of material included in the current study
Supplementary Table 1A – Sample characteristics of RNA-seq data for correlation

	RNA-seq data (N=35)
Participants	35
Age (SD)	68,6 (9,0)
BMI (SD)*	28,3 (3,4)
Knees (Hips)	28 (7)
Females (Males)	27 (7)
* Available for 21 out of 35 patients.	

Supplementary Table 1B – Sample characteristics of functional experiments

	Lentiviral particle mediated overexpression of WWP2 (Gene expression, N=8)	Lentiviral particle mediated overexpression of WWP2 (proteomics, N=4)	Transfection miR-140 (N=7)
Age (SD)	71.1 (9.2)	75.5 (11.6)	71.6 (9.8)
Knees (Hips)	8 (0)	4 (0)	7 (0)
Females (Males)	5(3)	2 (2)	5(2)

Supplementary Table 2 (partially) - Spearman correlations between expression levels of WWP2 and genes expressed in articular cartilage (N=20048 genes) in lesioned OA cartilage samples.
The top 50 highest absolute correlations are shown here, the rest of the table can be found in the online supplement: https://doi.org/10.1016/j.joca.2022.09.009

Ensembl ID	Gene Name	ρ	P-value	FDR
ENSG00000256321	AC087235.2	0.84	3.26E-10	6.54E-06
ENSG00000152661	GJA1	-0.81	2.93E-09	2.93E-05
ENSG00000126562	WNK4	0.81	4.56E-09	3.04E-05
ENSG00000196715	VKORC1L1	-0.80	6.71E-09	3.36E-05
ENSG00000100744	GSKIP	-0.79	1.59E-08	5.64E-05
ENSG00000138107	ACTR1A	-0.79	1.75E-08	5.64E-05
ENSG00000269113	TRABD2B	0.79	1.97E-08	5.64E-05
ENSG00000112208	BAG2	-0.79	2.30E-08	5.76E-05
ENSG00000128602	SMO	0.78	2.89E-08	6.44E-05
ENSG00000112742	TTK	-0.78	4.36E-08	8.58E-05
ENSG00000182481	KPNA2	-0.77	4.95E-08	8.58E-05
ENSG00000089775	ZBTB25	0.77	5.13E-08	8.58E-05
ENSG00000113739	STC2	0.77	6.96E-08	1.01E-04
ENSG00000154767	XPC	0.77	7.08E-08	1.01E-04
ENSG00000150753	CCT5	-0.76	9.05E-08	1.19E-04
ENSG00000157766	ACAN	0.76	9.53E-08	1.19E-04
ENSG00000257337	AC068888.1	0.76	1.08E-07	1.22E-04
ENSG00000174013	FBXO45	-0.76	1.09E-07	1.22E-04
ENSG00000131747	TOP2A	-0.76	1.21E-07	1.24E-04
ENSG00000164626	KCNK5	0.76	1.30E-07	1.24E-04
ENSG00000256995	AC084816.1	0.76	1.30E-07	1.24E-04
ENSG00000141527	CARD14	0.76	1.36E-07	1.24E-04
ENSG00000111450	STX2	-0.75	1.66E-07	1.45E-04
ENSG00000131236	CAP1	-0.75	1.90E-07	1.52E-04
ENSG00000167037	SGSM1	0.75	1.90E-07	1.52E-04
ENSG00000147010	SH3KBP1	-0.75	2.13E-07	1.59E-04
ENSG00000158710	TAGLN2	-0.75	2.27E-07	1.59E-04
ENSG00000226696	LENG8-AS1	0.75	2.27E-07	1.59E-04
ENSG00000056558	TRAF1	0.75	2.31E-07	1.59E-04
ENSG00000166226	CCT2	-0.75	2.58E-07	1.70E-04
ENSG00000136457	CHAD	0.75	2.75E-07	1.70E-04
ENSG00000170312	CDK1	-0.75	2.75E-07	1.70E-04
ENSG00000183726	TMEM50A	-0.74	2.88E-07	1.70E-04

Ensembl ID	Gene Name	ρ	P-value	FDR
ENSG00000091317	CMTM6	-0.74	2.93E-07	1.70E-04
ENSG00000124209	RAB22A	-0.74	2.97E-07	1.70E-04
ENSG00000136108	CKAP2	-0.74	3.22E-07	1.72E-04
ENSG00000172349	IL16	0.74	3.22E-07	1.72E-04
ENSG00000150687	PRSS23	-0.74	3.27E-07	1.72E-04
ENSG00000148672	GLUD1	-0.74	3.59E-07	1.85E-04
ENSG00000184009	ACTG1	-0.74	3.76E-07	1.88E-04
ENSG00000186350	RXRA	0.74	3.88E-07	1.90E-04
ENSG00000132849	PATJ	0.74	4.06E-07	1.94E-04
ENSG00000276791	AC092117.1	0.74	4.45E-07	2.01E-04
ENSG00000104660	LEPROTL1	-0.74	4.52E-07	2.01E-04
ENSG00000116741	RGS2	-0.74	4.52E-07	2.01E-04
ENSG00000224963	U82695.1	0.74	4.66E-07	2.03E-04
ENSG00000144908	ALDH1L1	0.74	4.95E-07	2.07E-04
ENSG00000167552	TUBA1A	-0.74	4.95E-07	2.07E-04
ENSG00000006451	RALA	-0.73	5.50E-07	2.25E-04
ENSG00000163466	ARPC2	-0.73	6.48E-07	2.60E-04

Supplementary Table 3 - Significant gene enrichment of 98 genes correlating to WWP2

GO-term	Count	P-value	FDR	Genes
GO:0070062~extracellular exosome	36	1.94E-07	2.26E-05	RALA, SCIN, CDC42, WDR1, CMTM6, MYL12A, CHCHD3, LIPA, HSPA8, STX2, RAB23, CD58, TGFBI, RAB22A, SMO, CAP1, PAT J, ACTR1A, TPM3, ALDH1L1, ATP6V1B2, PRSS23, CCT5, GJA1, XPC, TAGLN2, SPTBN4, ARPC2, YWHAZ, CCT2, YWHAB, TUBA1A, CDK1, ACTG1, AKR1C3, TRABD2B
GO:0043209~myelin sheath	10	2.43E-07	2.26E-05	RALA, CDC42, WDR1, HSPA8, ACTR1A, ATP6V1B2, CCT5, CCT2, TUBA1A, ACTG1
GO:0005829~cytosol	35	2.56E-04	1.59E-02	TSPOAP1, TRAF1, CDC42, WDR1, TPX2, MYL12A, HSPA8, BAG2, RGS2, CENPF, HIF3A, WNK4, ACTR1A, TPM3, ALDH1L1, SH3KBP1, ATP6V1B2, CCT5, GJA1, OBSCN, SPTBN4, ARPC2, YWHAZ, WNK2, CCT2, YWHAB, SGSM1, TUBA1A, CDK1, PFKFB3, IL16, KPNA2, ACTG1, AKR1C3, ARHGAP11A
GO:0005925~focal adhesion	10	6.46E-04	3.00E-02	RALA, CDC42, HSPA8, CAP1, SH3KBP1, GJA1, ARPC2, YWHAZ, YWHAB, ACTG1

6

Supplementary Table 4 - Gene expression level differences upon upregulation of WWP2.

Category	Gene	Fold change	P-value
Cartilage markers	COL2A1	0.6	1.05E-02
	ACAN	0.8	3.45E-02
	SOX9	0.77	1.84E-01
	FN1	0.93	8.22E-01
Cartilage degeneration markers	EPAS1	1.56	4.19E-03
	POSTN	1.25	1.12E-01
	RUNX2	0.8	8.70E-02
	ADAMTS5	1.15	2.57E-01
Genes correlating to WWP2	GDF10	0.62	2.21E-03
	STC2	0.73	3.63E-02
	GJA1	0.76	8.28E-02
	WNK4	2.61	2.52E-01
	WDR1	0.98	5.36E-01

Supplementary Table 5 (partially) - Differential protein expression on day three and day seven relative to day zero of pellet culture in our 3D chondrocyte pellet cultures.
The top 50 proteins with highest abundance ratio da7/day0 are shown here, the rest of the table can be found in the online supplement: https://doi.org/10.1016/j.joca.2022.09.009

Accession	Name	# Peptides	# Unique Peptides	Abundance Ratio: day3/day0	Abundance Ratio: day7/day0
P27658	COL8A1	6	6	13.27	40.19
P02458	COL2A1	67	61	2.68	32.94
P22914	CRYGS	9	9	12.54	31.15
P02461	COL3A1	109	108	11.89	27.14
Q06828	FMOD	8	8	7.68	25.00
Q02388	COL7A1	7	7	6.74	23.52
P02452	COL1A1	109	105	7.03	22.97
P49747	COMP	21	21	5.31	20.25
Q07507	DPT	5	5	6.86	16.10
P08123	COL1A2	94	93	4.99	14.41
P16112	ACAN	43	43	5.28	13.75
Q15063	POSTN	39	39	4.31	12.43
O00339	MATN2	22	22	5.10	11.95
P12107	COL11A1	35	28	3.11	10.84
Q15782	CHI3L2	9	9	9.03	10.04
P51888	PRELP	12	12	4.07	9.67
P55001	MFAP2	4	4	5.28	9.44
P05090	APOD	7	7	5.83	9.43
P21810	BGN	12	11	3.73	9.34
Q8IUX7	AEBP1	38	37	3.90	8.02
P05997	COL5A2	50	48	3.61	7.87
P13611	VCAN	27	27	2.80	7.65
P20908	COL5A1	37	30	3.23	6.27
P07996	THBS1	34	33	3.19	6.06
P24821	TNC	106	106	3.45	5.86
P14555	PLA2G2A	4	4	1.90	5.79
Q07092	COL16A1	17	17	2.71	5.78
Q5JTB6	PLAC9	4	4	4.54	5.75
Q16790	CA9	6	6	4.47	5.54
Q8TF66	LRRC15	7	7	1.26	4.89
P10915	HAPLN1	15	15	2.86	4.39
P35555	FBN1	101	95	2.79	4.38

6

Accession	Name	# Peptides	# Unique Peptides	Abundance Ratio: day3/day0	Abundance Ratio: day7/day0
P02462	COL4A1	9	9	3.42	4.29
Q15582	TGFBI	33	33	3.30	4.17
Q6UX71	PLXDC2	7	7	2.61	4.16
P09486	SPARC	12	12	1.93	4.06
Q9Y6C2	EMILIN1	38	38	3.09	3.88
Q92954	PRG4	57	57	1.67	3.71
Q15113	PCOLCE	16	16	2.55	3.69
Q92743	HTRA1	10	10	2.69	3.53
P02751	FN1	98	98	2.12	3.51
P02795	MT2A	4	1	1.90	3.49
Q658P3	STEAP3	7	7	2.36	3.38
P35556	FBN2	17	11	3.00	3.34
Q14112	NID2	33	32	2.94	3.32
P02792	FTL	10	10	3.43	3.31
P12111	COL6A3	165	165	2.53	3.10
Q76M96	CCDC80	13	13	1.59	3.04
Q13451	FKBP5	21	20	2.77	3.02
Q14767	LTBP2	23	23	1.29	2.99

Supplementary Table 6 (partially) - Differential protein expression between chondrocyte pellet cultures with and without upregulation of WWP2.
The top 50 proteins with highest abundance ratio WWP2/control are shown here, the rest of the table can be found in the online supplement: https://doi.org/10.1016/j.joca.2022.09.009

Accession	Name	# Peptides	# Unique Peptides	Abundance Ratio: WWP2/control
O00308	WWP2	31	28	10.10
P09914	IFIT1	2	1	1.89
P26022	PTX3	2	2	1.78
Q16832	DDR2	2	2	1.53
Q96LR5	UBE2E2	4	2	1.52
P33897	ABCD1	2	2	1.52
P51965	UBE2E1	3	1	1.44
P28300	LOX	3	3	1.43
Q96B36	AKT1S1	2	2	1.38
Q9P2K8	EIF2AK4	3	3	1.37
Q969T4	UBE2E3	3	1	1.36
Q9UBX5	FBLN5	5	5	1.33
P54652	HSPA2	27	14	1.32
Q01780	EXOSC10	2	2	1.32
P21741	MDK	3	3	1.31
Q96GY0	ZC2HC1A	2	2	1.31
Q9Y4K4	MAP4K5	2	2	1.31
Q92541	RTF1	3	3	1.30
P05161	ISG15	3	3	1.30
P47974	ZFP36L2	2	1	1.30
P25205	MCM3	2	2	1.30
P61077	UBE2D3	3	2	1.30
P62837	UBE2D2	3	2	1.30
Q9Y4F5	CEP170B	2	2	1.30
Q13613	MTMR1	3	3	1.30
Q9H7D7	WDR26	2	2	1.29
O00148	DDX39A	14	3	1.29
Q5RI15	COX20	2	2	1.28
Q13586	STIM1	2	2	1.28
Q9Y625	GPC6	6	6	1.28
P55290	CDH13	6	6	1.27
Q9HA77	CARS2	4	4	1.26

Accession	Name	# Peptides	# Unique Peptides	Abundance Ratio: WWP2/control
Q9H6T3	RPAP3	2	2	1.26
Q9H2K8	TAOK3	3	2	1.26
Q5T9L3	WLS	2	2	1.26
Q5RKV6	EXOSC6	3	3	1.26
Q8IVF2	AHNAK2	15	13	1.26
Q8IWT0	ZBTB8OS	2	2	1.25
Q05655	PRKCD	3	2	1.25
O94804	STK10	7	6	1.25
Q96RK0	CIC	2	2	1.25
P83111	LACTB	4	4	1.25
Q9UM22	EPDR1	2	2	1.25
Q9BQE4	SELENOS	2	2	1.25
Q9HAV7	GRPEL1	2	2	1.25
P28845	HSD11B1	3	3	1.25
P29373	CRABP2	3	3	1.25
Q93062	RBPMS	2	2	1.24
Q5VWZ2	LYPLAL1	2	2	1.24
O43172	PRPF4	4	4	1.24

Supplementary Table 7 - Gene expression level differences upon upregulation of miR-140-3p.

Category	Gene	Fold change	P-value
WWP2 transcripts	*WWP2-FL*	1.22	1.63E-02
	WWP2-isoform2	0.92	3.29E-01
	WWP2-isoform4	0.63	1.63E-02
	WWP2-isoform6	1.29	5.67E-02
Genes correlating to *WWP2*	*WDR1*	1.79	1.19E-03
	STC2	1.55	7.51E-02
	GJA1	1.07	9.24E-01
	ACAN	0.88	2.44E-01

6

CHAPTER 7

Exploring the therapeutic effect of IL11 on lesioned OA human osteochondral explants

Margo Tuerlings[1], Ilja Boone[1], Janneke E. Simon[1], Maurice W. de Haan[1], Evelyn Houtman[1], H. Eka D. Suchiman[1], Robert J.P. van der Wal[2], Rob G.H.H. Nelissen[2], Rachid Mahdad[3], Yolande F.M. Ramos[1], Ingrid Meulenbelt[1]

[1] Dept. of Biomedical Data Sciences, Leiden University Medical Center, Leiden, The Netherlands.
[2] Center for proteomics and metabolomics , Leiden University Medical Center, Leiden, The Netherlands
[3] Dept. Orthopaedics, Alrijne hospital, Leiderdorp, The Netherlands

Abstract

Objective: To explore osteoarthritis (OA) risk gene IL11 co-expression profiles in our previously reported RNA-sequencing datasets of OA articular cartilage and subchondral bone and investigate the potential therapeutic effect of hrIL11 in a biomimetic aged human osteochondral explant model of OA.

Methods: We used RNA-sequencing datasets of macroscopically preserved and lesioned OA articular cartilage (N=35 patients) and subchondral bone (N=24 patients). Spearman correlations were calculated between IL11 expression levels and genes expressed in cartilage (N=20048 genes) or subchondral bone (N=15809 genes). Osteochondral explants were isolated from macroscopically lesioned areas of the joint and were kept in culture for two weeks, with or without exposure to 200ng/ml hrIL11.

Results: We identified more genes being correlated in the lesioned (N=203 and N=198, respectively) compared to preserved (N=106 and N=0, respectively) articular cartilage and subchondral bone. The genes correlated to *IL11* in lesioned cartilage and bone were significantly enriched for processes regarding extracellular space and endoplasmic reticulum, respectively. Exposure of *ex vivo* osteochondral explants to hrIL11 showed minimal effects. In articular cartilage we only observed significant upregulation of *SPP1* and downregulation of *WNT16*, together suggesting a more hypertrophic chondrocyte phenotype upon hrIL11 exposure. In the underlying subchondral bone we only observed significant downregulation of *PTGES* and *IL11RA*, suggesting reduced osteoclast activity. Notably, we observed a different response between patients in terms of intrinsic *IL11* expression levels upon exposure to hrIL11.

Conclusion: The current study shows the importance of functionally investigating OA risk genes, as we here showed that treating the whole joint with hrIL11 as suggested does not necessarily have a beneficial outcome. Based on our results, treatment of OA articular cartilage with hrIL11 shows unbeneficial effects, while treatment of OA subchondral bone with hrIL11 might be positive for both subchondral bone and articular cartilage.

Introduction

Osteoarthritis (OA) is an age-related joint disease in which progressive degeneration of articular cartilage and remodeling of subchondral bone are seen. Therapeutic strategies mainly consist of pain relief treatment, often leading to total joint replacement surgery at end-stage OA. To allow development of new therapeutic strategies, identification of key determinants in OA onset and progression is essential. To discover such key determinants, genome-wide association studies (GWAS) have focused on identification of robust single nucleotide polymorphisms (SNPs) significantly conferring risk to OA [1-4]. In a large genome-wide meta-analysis including data of Icelandic and UK OA patients, rs4252548-T was identified, a SNP in the coding region of interleukin 11 (IL11), being associated to OA [4]. Most recently, this SNP was confirmed in the largest genome-wide meta-analysis so far, including individuals from 9 populations [1]. The identified risk allele, rs4252548-T, is a missense mutation (p.Arg112His) resulting in a thermally unstable protein. As such, it is hypothesized that rs4252548-T confers risk to OA via reduced availability of IL11 protein, whereas, administration of human recombinant IL11 (hrIL11) protein, an approved drug for thrombocytopenia [5], was put forward as a potential therapeutic strategy for OA. Counterintuitively, however, *IL11* gene expression is among the highest upregulated genes both in macroscopically lesioned articular cartilage [6] and subchondral bone [7] compared to preserved tissue. Such high potency of joint tissue cells to upregulate *IL11* is not directly brought into line with the effect of the OA risk missense mutation, unless translation to IL11 protein or receptor signaling with OA is abrogated.

IL11, for that matter, is a member of the interleukin-6 (IL6) cytokine family and can signal via binding to a specific heterodimeric membrane bound complex containing IL11RA and GP130, known as classic signaling, or via binding to soluble IL11RA and a dimeric membrane bound complex of GP130, known as trans signaling [8, 9]. While GP130 is ubiquitously expressed across different cell types, IL11RA is expressed by specific cell types including chondrocytes, osteoblasts, osteocytes, and osteoclasts, indicating an essential, as of yet unclear, role for IL11 in these joint tissues [10-12]. Deletion of IL11 signaling in mice by knocking out IL11RA resulted in increased trabecular bone mass and reduced osteoclast differentiation [13]. Moreover, administration of IL11 in a rheumatoid arthritis murine model resulted in decreased level of synovitis, suggesting IL11 also has anti-inflammatory effects [14].

To obtain more insight into the *IL11* co-expression profiles in articular cartilage and subchondral bone, we used our previously reported RNA-sequencing (RNA-seq) datasets to create co-expression networks [6, 7]. Moreover, to investigate the potential therapeutic effect of hrIL11 on articular cartilage and subchondral bone we exposed

our previously established biomimetic aged human osteochondral explant model of OA to hrIL11 [15].

Methods

Sample characteristics

RNA-sequencing data of macroscopically preserved and lesioned OA articular cartilage (N=35 patients, RAAK-study) and OA subchondral bone (N=24 patients, RAAK-study) was included in the current study. Moreover, preserved and lesioned osteochondral explants were isolated from knee joints of 8 additional patients. Patients characteristics are shown in **Supplementary Table 1**. Classification of macroscopically preserved and lesioned areas of the joint was done as described previously [14]. Ethical approval for the RAAK study was supplied by the medical ethics committee of the Leiden University Medical Centre (P08.239/P19.013).

RNA-sequencing

RNA was isolated from the articular cartilage using Qiagen RNeasy Mini Kit (Qiagen, GmbH, Hilden, Germany). Paired-end 2×100 bp RNA-sequencing (Illumina TruSeq RNA Library Prep Kit, Illumina HiSeq2000 and Illumina HiSeq4000) was performed. Strand specific RNA-seq libraries were generated which yielded a mean of 20 million reads per sample. Data from both Illumina platforms were integrated and analyzed with the same in-house pipeline. RNA-seq reads were aligned using GSNAP [15] against GRCh38 using default parameters. Read abundances per sample was estimated using HTSeq count v0.11.1 [16]. Only uniquely mapping reads were used for estimating expression. The quality of the raw reads for RNA-sequencing was checked using MultiQC v1.7. [17]. The DESeq2 package [18] was used to normalize the RNA-seq data, as a variance-stabilizing transformation was performed. Data of subchondral bone is available at the European Genome-Phenome Archive (EGAS00001004476) and data of articular cartilage is available at ArrayExpress (E-MTAB-7313).

IL11 co-expression

Spearman correlations were calculated between *IL11* and genes expressed in articular cartilage (N=20048 genes) or subchondral bone (N=15809 genes) using R package Hmisc v.4.2-0. Benjamini-Hochberg method was used to correct for multiple testing. Genes were considered significantly correlating with $|\rho| > 0.6$ and False Discovery Rate (FDR) < 0.05.

Osteochondral explants

Osteochondral explants were isolated from macroscopically preserved and lesioned areas of OA knee joints within 3 hours of joint replacement surgery. Osteochondral

explants containing both subchondral bone and articular cartilage (diameter = 8mm) were cultured as described previously [19]. In short, explants were washed in sterile PBS and taken into culture in chondrogenic differentiation medium (CDM) in a 5% CO_2 incubator at 37°C. On day 3 of culture, hrIL11 protein was added to the culture medium (200ng/ml, PeproTech). The medium containing hrIL11 was refreshed on day 6 and day 10 of culture. After a total culture period of 14 days, cartilage and bone were harvested separately, snap-frozen in liquid nitrogen, and stored in the freezer (-80°C) for further analysis.

RT-qPCR
Articular cartilage and subchondral bone were pulverized separately and homogenized using TRIzol reagent (Invitrogen). RNA was extracted from the samples using RNeasy Mini Kit (Qiagen) and cDNA synthesis was performed using the First Strand cDNA Synthesis Kit (Roche Applied Science) according to manufacturer's protocols. Subsequently, RT-qPCR was performed with the Biomark™ 96.96 Dynamic Arrays (Fluidigm) according to the manufacturer's protocol. Additional RT-qPCR was performed with QuantStudio 6 Real-Time PCR system (Applied Biosystems) using Fast Start SYBR Green Master mix (Roche Applied Science). Gene expression levels were corrected for housekeeping gene *SDHA.* Fold changes were calculated using the $2^{-\Delta\Delta CT}$ method. All values were calculated relative to the control group. Paired generalized estimating equations were applied using SPSS version 25.

(Immuno-) histochemistry
Explants were fixed in 4% formaldehyde overnight, decalcified using EDTA (12.5%, pH=7.4) and embedded in paraffin. Tissue sections were made of 5 um. Subsequently, slides were deparaffinated and rehydrated with Histoclear and ethanol (100-50%). Sections were stained with haematoxylin and eosin (HE staining), toloidine blue (Sigma-Aldrich), or antibody staining was performed. For antibody staining endogenous peroxidase activity was blocked by MeOH/0.3% H_2O_2. Subsequently, antigen retrieval was performed with Proteinase K (25ug/ml) followed by hyaluronidase (5mg/mL). Sections were blocked with 5% non-fat dry milk in PBS and incubated overnight at 4°C with the primary antibody (anti-IL11 Rabbit, 1:50, Thermo Fischer Scientific). The next day, the sections were incubated with Powervision-Poly/HRP (ImmunoLogic), followed by incubation with DAB (Sigma). Sections were dehydrated with ethanol (50-100%) and Histoclear and mounted with Pertex.

Results
IL11 co-expression in articular cartilage and subchondral bone
To identify genes that are regulated by or co-expressed with *IL11* with ongoing

OA, we first performed Spearman correlations between expression levels of *IL11* and genes expressed in articular cartilage (N=20048 genes). As shown in **Figure 1A** and **Figure 1B**, 106 genes were significantly correlating to *IL11* in preserved OA articular cartilage, while 203 genes were correlated to *IL11* in lesioned OA articular cartilage (**Supplementary Table 2**). Only 21 genes were correlated to *IL11* in both preserved and lesioned articular cartilage. This relatively small overlap in correlating genes suggests distinct functions for *IL11* between preserved and lesioned cartilage. However, upon gene enrichment analysis, we identified similar processes for preserved and lesioned cartilage, including extracellular space (GO:0005615) and extracellular region (GO:0005576), characterized by different genes (**Supplementary Table 3**). Among the overlapping genes we identified *PLAUR* ($\rho_{preserved}$=0.60 and $\rho_{lesioned}$=0.77) and *CLCF1* ($\rho_{preserved}$=0.64 and $\rho_{lesioned}$=0.75), both genes showing higher correlations in lesioned articular cartilage. With respect to IL11 receptors, we did not find significant correlations between *IL11* and *IL11RA* and *gp130* expression levels in either preserved
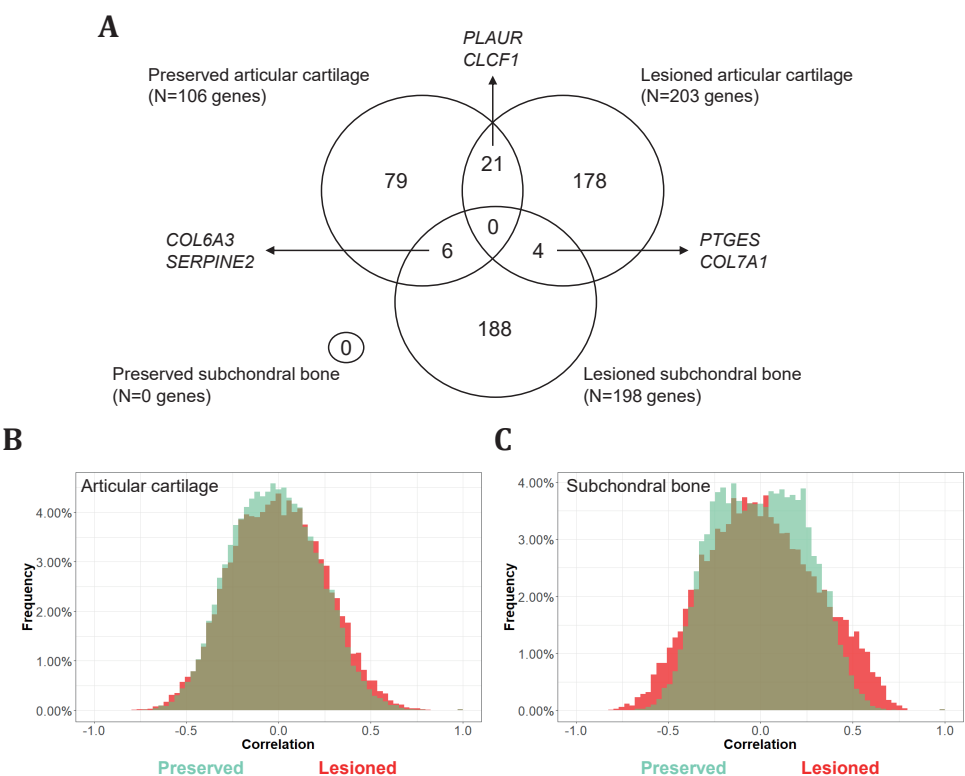
Figure 1 – Spearman correlations between expression levels IL11 and genes expressed in articular cartilage or subchondral bone.
(A) Overlap in significantly correlating genes. Genes with |ρ|>0.6 and FDR<0.05 are considered significantly correlating. (B) Distribution of correlations in subchondral bone. (C) Distribution of correlations in articular cartilage.

cartilage (ρ=0.04 and ρ=-0.21, respectively) or lesioned cartilage (ρ=0.06 and ρ=-0.17, respectively) (**Supplementary Table 4**).

Upon performing Spearman correlations between expression levels of *IL11* and genes expressed in subchondral bone (N=15809 genes) we did not observe any correlations between *IL11* and genes expressed in preserved subchondral bone. In lesioned subchondral bone, we identified 198 genes that significantly correlated to *IL11* expression levels (**Figure 1A** and **Figure 1C, Supplementary Table 5**). Among the highest correlations we found *ELOVL5* (ρ=-0.88) and *WNT16* (ρ=0.81). Gene enrichment analysis including these 198 genes showed significant enrichment for endoplasmic reticulum (GO:0005783) and golgi apparatus (GO:005794) (**Supplementary Table 6**). Moreover, as shown in **Figure 1A,** of these 198 genes correlating to *IL11* in lesioned subchondral bone, 6 genes were also correlating to *IL11* in preserved articular cartilage, including *COL6A3* and *SERPINE2*, and 4 genes were also correlating to *IL11* in lesioned articular cartilage. The increased number of significant correlations in lesioned compared to preserved cartilage and bone tissue suggest that *IL11* plays a role mainly in lesioned OA tissue. With respect to IL11 receptors in subchondral bone, we did not find significant correlations between *IL11* and *IL11RA* and *gp130* expression levels in either preserved (ρ=0.31 and ρ=0.28, respectively) or lesioned (ρ=-0.05 and ρ=-0.14, respectively) tissue (**Supplementary Table 4**).

Table 1 - Gene expression differences in lesioned OA osteochondral explants upon exposure to hrIL11. The genes selected as read-out were cartilage/bone markers (ACAN, COL2A1, SPP1, and RUNX2), genes involved in IL11 pathway (IL11, IL11RA, GP130, and IL6), and genes correlating to IL11 (WNT16, PLAUR, PTGES, and SDC1). Paired GEE was performed to calculate significance.

	Articular cartilage		Subchondral bone	
gene	**FC**	**P-value**	**FC**	**P-value**
ACAN	1,39	9,02E-02	0,94	1,44E-01
COL2A1	1,43	5,46E-01	1,65	3,01E-01
SPP1	**1,87**	**1,59E-02**	1,09	6,43E-01
RUNX2	1,86	4,75E-01	1,05	9,41E-01
IL11	1,00	4,38E-01	1,35	9,84E-02
IL11RA	1,68	1,89E-01	**0,87**	**3,73E-02**
GP130	1,54	8,00E-02	1,00	5,21E-01
WNT16	**0,63**	**6,15E-03**	1,16	1,46E-01
PLAUR	1,31	4,48E-01	1,14	8,60E-01
PTGES	1,89	1,10E-01	**0,79**	**4,12E-02**
SDC1	1,40	6,33E-01	0,87	1,97E-01

7
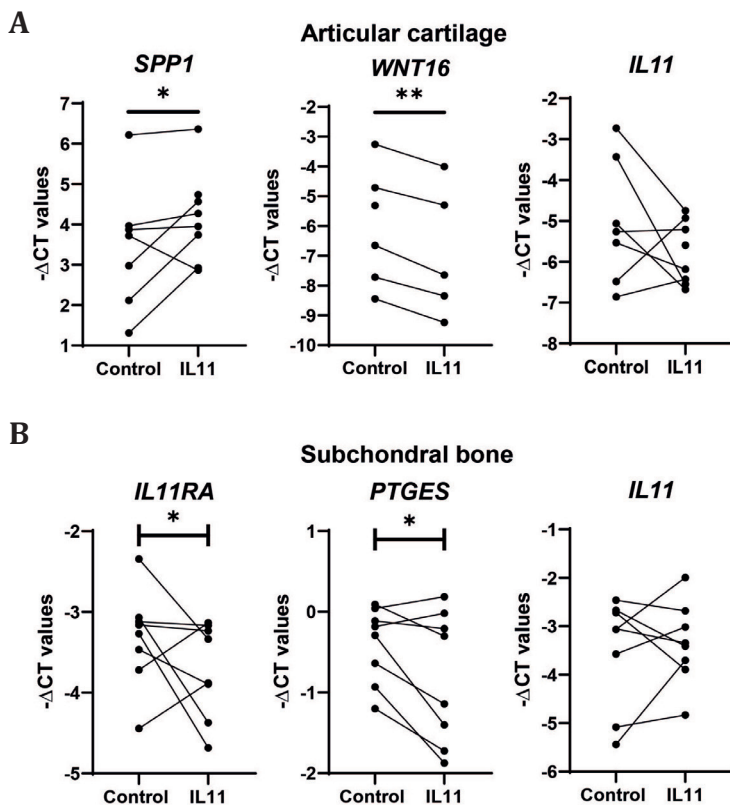
Figure 2 – Gene expression differences in lesioned OA osteochondral explants upon exposure to hrIL11.
(A) Gene expression differences in articular cartilage. (B) Gene expression differences in subchondral bone. Paired GEE was performed to calculate significance. * P<0.05, ** P<0.01, *** P<0.005.

Effects of hrIL11 on lesioned articular cartilage and subchondral bone

Since addition of hrIL11 is previously proposed as therapeutic strategy for OA, we added hrIL11 to the culture medium of macroscopically lesioned osteochondral explants from day 3 onwards and evaluated effects of hrIL11 on cartilage and bone matrix deposition. We used gene expression levels of *ACAN* and *COL2A1* as anabolic cartilage and *SPP1* and *RUNX2* as anabolic bone markers. Moreover, to study *IL11* signaling we used gene expression levels of *IL11, IL11RA,* and *GP130* marking IL11 receptors. Finally, we selected *WNT16, PLAUR, PTGES,* and *SDC1* as genes correlating to *IL11* in joint tissues. To our surprise, the effects of hrIL11 exposure to lesioned osteochondral explants were minimal (**Table 1**). In lesioned cartilage we only observed significant increased expression levels of bone marker *SPP1* (FC=1.87, Pval=1.59×10^{-2}) and decreased expression of *IL11* correlating gene *WNT16* (FC=0.63, Pval= $6,15 \times 10^{-3}$) (**Figure 2A**). In lesioned subchondral bone we only observed significant downregulation of *IL11RA* (FC=0.87, Pval=3.73×10^{-2}) and *PTGES* (FC=0.79, Pval=4.12×10^{-2}) (**Figure 2B**). Notably,
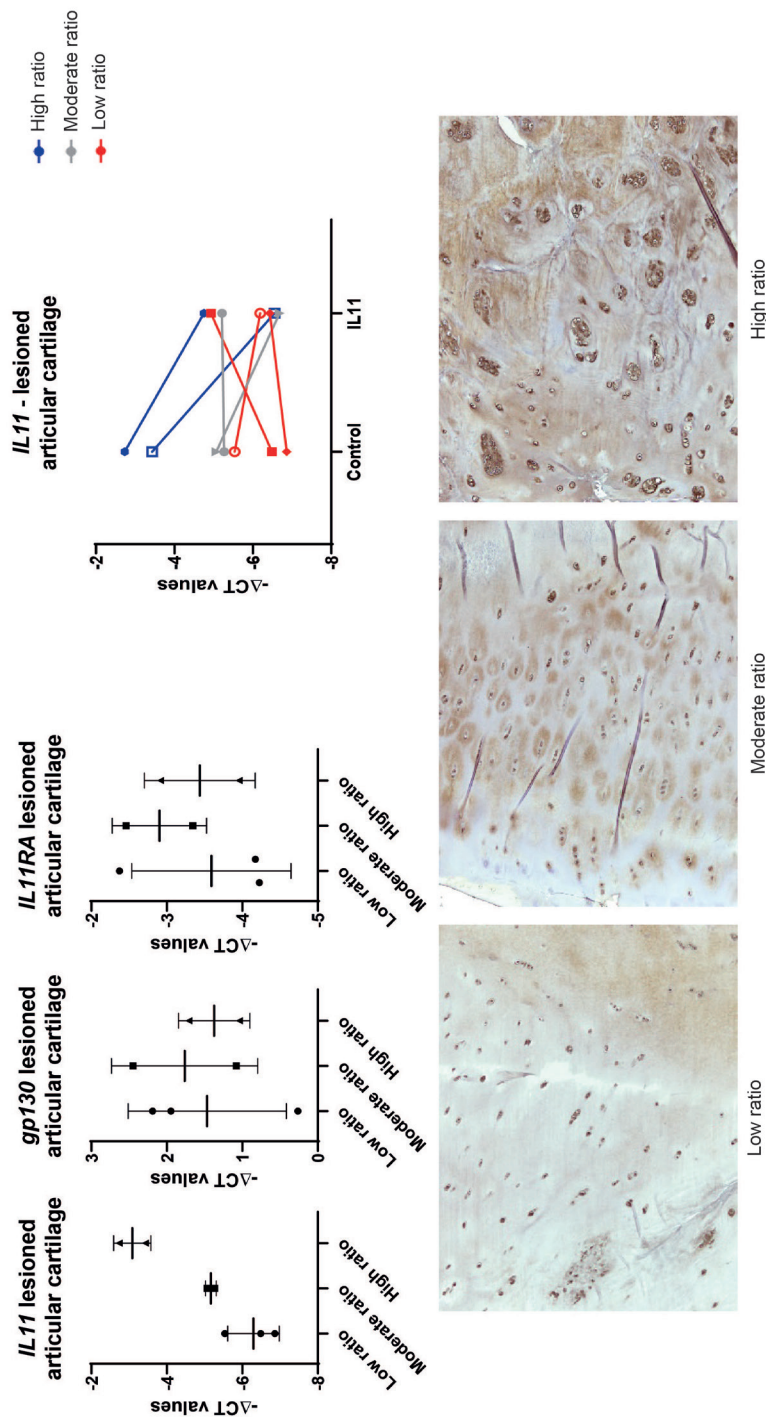
Figure 3 – Expression patterns in lesioned articular cartilage while stratifying for low, moderate, and high IL11:receptors ratio. (A) Expression of IL11, IL11RA, and GP130 in articular cartilage. (B) Response of IL11 gene expression to hrIL11 exposure. (C) Protein expression levels of IL11 in articular cartilage of control osteochondral explants.

intrinsic *IL11* expression did not consistently change upon hrIL11 exposure in lesioned cartilage nor subchondral bone, suggesting lack of signal transduction.

Difference in response to hrIL11 between patients

Exposing lesioned OA osteochondral explants to hrIL11 showed minimal effects as indicated by the low number of significantly differentially expressed genes (**Table 1**). Moreover, we observed considerable donor variation in terms of *IL11* gene expression upon hrIL11 exposure particularly in articular cartilage, suggesting differences in IL11 signaling between patients (**Figure 2A**). Therefore, we explored whether intrinsic gene expression levels of *IL11* and IL11 receptors *IL11RA* and *GP130* could determine the response to hrIL11 in articular cartilage. To this end, we calculated the percentage of *IL11* expression relative to expression of *IL11, IL11RA*, and *GP130* together. Subsequently, we ranked the patients based on this percentage and we stratified the patients in patients with low ratio, i.e. low levels of *IL11* relative to levels of receptors*,* patients with moderate ratio, and patients with high ratio and plotted *IL11, IL11RA,* and *GP130* expression levels. As shown in **Figure 3A**, the difference in ratio was mainly explained by differences in *IL11* expression levels. Hereto, we evaluated whether these ratios explained the observed variation in response of *IL11* expression levels in articular cartilage upon exposing lesioned osteochondral explants to hrIL11. As shown in **Figure 3B**, patients with high ratios, i.e. high *IL11* expression relative to IL11 receptors, showed consistent downregulation of *IL11* expression upon hrIL11 exposure. Upon performing immunohistochemistry to assess whether intrinsic IL11 protein is being produced in these patients, we observed more staining in cartilage samples of patients with high ratios, confirming that *IL11* is translated into protein (**Figure 3C**). Based on these results, we hypothesize that the downregulation, and thus response, in intrinsic *IL11* observed upon exposure to hrIL11 in patient with high ratio might be due to either less efficient binding of intrinsic IL11 protein binding to its receptor compared to hrIL11 or due to restoration of the balance between trans and classic signaling by addition of hrIL11.

Ratios in RNA-seq dataset of lesioned articular cartilage

Since the sample size of osteochondral explants was relatively low (N=7 donors), we next evaluated whether similar differences in *IL11* gene expression levels were observed in our RNA-seq dataset of articular cartilage. As shown in **Figure 4**, the different ratios were also present in RNA-seq data and the differences between the ratios was mainly described by *IL11* expression levels, similar as we observed in the osteochondral explants.

IL11 lesioned articular cartilage
gp130 lesioned articular cartilage
IL11RA lesioned articular cartilage
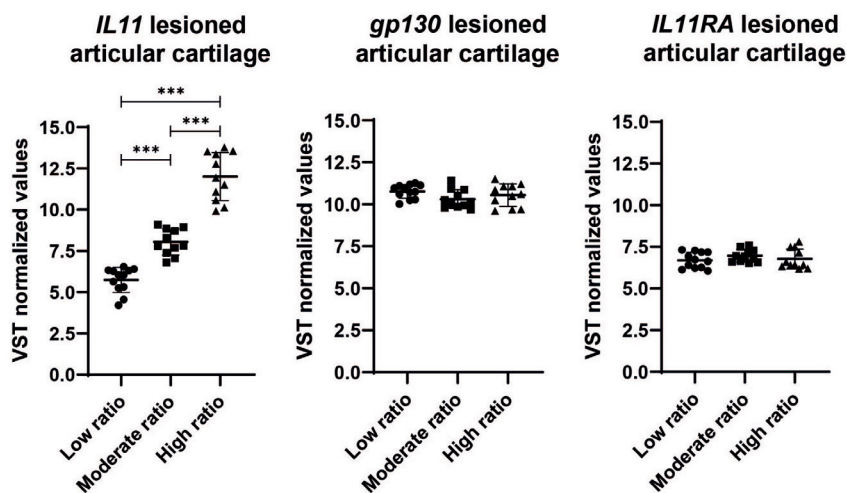
Figure 4 – Expression patterns in lesioned autologous articular cartilage while stratifying for low, moderate, and high IL11:receptors ratio in RNA-seq data.

Discussion

In the current study, we set out to functionally investigate the effect of hrIL11 as potential therapeutic strategy by exposing our previously established biomimetic aged human osteochondral explant model of OA to hrIL11 [15]. Although the effect of hrIL11 exposure on osteochondral explants was generally minimal as reflected by the low number of responsive genes in both tissues (**Table 1**), we did observe significant upregulation of bone marker *SPP1* and downregulation of *WNT16* in articular cartilage, suggesting a more hypertrophic chondrocyte phenotype. Exposure to hrIL11 on subchondral bone only showed significant decreased expression of *IL11RA* and *PTGES,* which potentially is a beneficial response as both genes are known to be involved in osteoclastogenesis and could thus contribute to OA associated bone turnover [13, 21]. Notably, we observed heterogeneity in the response to hrIL11 exposure on articular cartilage between patients, as patients with high *IL11*:receptors ratio in lesioned articular cartilage responded differently compared to patients with low *IL11*:receptors ratio in terms of intrinsic *IL11* gene expression levels. Together, the data presented in this study show that treatment of the whole joint with hrIL11 does not necessarily result in a beneficial response and that heterogeneity between patients should be considered in future studies.

Upon addition of hrIL11 to osteochondral explants, gene expression levels of *SPP1* and *WNT16* were significantly changed in articular cartilage. *WNT16* was previously shown to protect cartilage from degradation and it contributes to cartilage homeostasis by inhibiting canonical WNT signaling [22, 23]. Therefore, the observed significant

7

downregulation in *WNT16,* together with the increased expression of bone marker *SPP1*, indicates towards an unbeneficial response upon treatment of OA articular cartilage with hrIL11. In subchondral bone of explants exposed to hrIL11, we observed significant downregulation of *PTGES* and *IL11RA*. PGES-1, encoded by *PTGES*, is a protein that converts PGH_2 to PGE_2, a major mediator of inflammation and known to stimulate osteoclastogenesis [24]. Moreover, PGE_2 was shown to enhance bone-resorbing activity of mature osteoclasts [21]. The observed significant decreased expression levels of *IL11RA* suggest a negative feedback loop reducing IL11 signaling. In previous studies it was shown that deletion of IL11 signaling by knocking out IL11RA in mice showed reduced osteoclast differentiation [13]. Together these data suggest that treatment of lesioned OA subchondral bone with hrIL11 results in reduced bone resorption by suppressing osteoclastogenesis and activity of mature osteoclasts. Since it is suggested that excessive subchondral bone remodeling seen with osteoarthritis is due to increased osteoclast activity [25] and multiple studies have shown that osteoclasts activation could also result in cartilage degradation [26-28], the potentially reduced oteoclastogenesis could be a beneficial response for both OA subchondral bone and articular cartilage. The potential unbeneficial response in articular cartilage and beneficial response in subchondral bone together suggest that risk allele rs4252548-T might confer risk to OA via subchondral bone. However, more research is necessary to confirm this including a larger sample size.

We observed variation upon hrIL11 exposure in both articular cartilage and subchondral bone, as indicated by the low number of genes being significantly differentially expressed. One reason for the low number of significantly differentially expressed genes upon hrIL11 exposure could be the relatively low sample size (N=8 patients, N=6-28 osteochondral explants) combined with high donor variation seen with osteochondral explant cultures [15]. Another explanation could be heterogeneity between patients as reflected by a difference in response to hrIL11 due to intrinsic expression levels of *IL11* and its receptors *IL11RA* and *GP130,* as shown in **Figure 3**. Moreover, in our previous study in which we identified two OA molecular endotypes, we observed a different response in terms of *IL11* expression with ongoing OA between these two molecular endotypes (FC=19 and FC=60 between macroscopically preserved and lesioned articular cartilage, respectively) [29]. These molecular endotypes did correspond with the low, moderate, and high ratios reported here, i.e. molecular endotype B was mainly represented among the high ratio patients (**Supplementary Figure 1**). Notably, the frequency of the identified risk SNP is low, which makes it unlikely that there are carriers among the 8 patients that were included, therefore more general effect is expected. Additional research is needed to further elucidate differences between patients based on intrinsic *IL11* expression levels and differences in *IL11* response

to OA pathophysiology. Moreover, identification of non-invasive biomarkers, such as circulating miRNAs, that reflect these intrinsic *IL11* expression level differences might be of added value to enable intrinsic *IL11*-based stratification before starting treatment for example with hrIL11.

On another level, differences on IL11 trans- and classic signaling have been reported and are not captured by the current study [30, 31]. For IL6 it has been suggested that classic signaling, i.e. binding of IL6 to membrane anchored IL6R and gp130, has beneficial effects on cartilage as inhibits metalloproteinases and slightly stimulates proteoglycan production [32, 33]. On the other hand, trans signaling, i.e. binding of IL6 to soluble IL6R and membrane bound gp130, is mostly described being detrimental for cartilage. Moreover, trans signaling is known to be involved in bone resorption, by promoting osteoclastogenesis, and bone formation [32]. Of note is that contradictory results on both classic and trans signaling have also been reported [34]. Similar to IL6 signaling, different effects of classic and trans signaling might occur for IL11 signaling and should be further investigated in future studies.

Next to increasing sample size, culture conditions such as hrIL11 dose, culture period, and culture media composition could still be optimized to obtain more conclusive effects. Of note is that our culture media contains dexamethasone, which is an anti-inflammatory component and could potentially interfere with hrIL11 effects.

Based on genetics it was hypothesized that low levels of IL11 confer risk to OA and administration of hrIL11 protein was suggested as potential treatment for OA. Although previous studies have estimated that drug targets founded by genetic evidence have at least two fold increased success rates [35, 36], we here showed the importance of functionally investigating OA risk genes, as we showed that treating the whole joint with hrIL11 as suggested does not necessarily have a beneficial outcome. Based on our results, treatment of OA articular cartilage with hrIL11 shows unbeneficial effects, while treatment of OA subchondral bone with hrIL11 might be positive for both subchondral bone and articular cartilage. The latter suggest that risk allele rs4252548-T confers risk to OA via subchondral bone.

Declarations

Acknowledgements

7

Disclosures

The authors have no relevant financial or non-financial interests to disclose.

References

1   Boer, C.G., et al., Deciphering osteoarthritis genetics across 826,690 individuals from 9 populations. Cell, 2021.
2. Styrkarsdottir, U., et al., Whole-genome sequencing identifies rare genotypes in COMP and CHADL associated with high risk of hip osteoarthritis. Nat Genet, 2017. 49(5): p. 801-805.
3. Zengini, E., et al., Genome-wide analyses using UK Biobank data provide insights into the genetic architecture of osteoarthritis. Nat Genet, 2018. 50(4): p. 549-558.
4. Styrkarsdottir, U., et al., Meta-analysis of Icelandic and UK data sets identifies missense variants in SMO, IL11, COL11A1 and 13 more new loci associated with osteoarthritis. Nat Genet, 2018. 50(12): p. 1681-1687.
5. Tachmazidou, I., et al., Identification of new therapeutic targets for osteoarthritis through genome-wide analyses of UK Biobank data. Nat Genet, 2019. 51(2): p. 230-236.
6. Coutinho de Almeida, R., et al., RNA sequencing data integration reveals an miRNA interactome of osteoarthritis cartilage. Ann Rheum Dis, 2019. 78(2): p. 270-277.
7. Tuerlings, M., et al., RNA sequencing reveals interacting key determinants of osteoarthritis acting in subchondral bone and articular cartilage. Arthritis Rheumatol, 2020.
8. Nguyen, P.M., S.M. Abdirahman, and T.L. Putoczki, Emerging roles for Interleukin-11 in disease. Growth Factors, 2019. 37(1-2): p. 1-11.
9. Jones, S.A. and B.J. Jenkins, Recent insights into targeting the IL-6 cytokine family in inflammatory diseases and cancer. Nature Reviews Immunology, 2018. 18(12): p. 773-789.
10. Fung, K.Y., et al., Emerging roles for IL-11 in inflammatory diseases. Cytokine, 2022. 149: p. 155750.
11. Kespohl, B., et al., The cytokine interleukin-11 crucially links bone formation, remodeling and resorption. Cytokine & Growth Factor Reviews, 2021. 60: p. 18-27.
12. Sims, N.A., Cell-specific paracrine actions of IL-6 family cytokines from bone, marrow and muscle that control bone formation and resorption. Int J Biochem Cell Biol, 2016. 79: p. 14-23.
13. Sims, N.A., et al., Interleukin-11 Receptor Signaling Is Required for Normal Bone Remodeling. Journal of Bone and Mineral Research, 2005. 20(7): p. 1093-1102.
14. Walmsley, M., et al., An anti-inflammatory role for interleukin-11 in established murine collagen-induced arthritis. Immunology, 1998. 95(1): p. 31.
15. Houtman, E., et al., Human Osteochondral Explants: Reliable Biomimetic Models to Investigate Disease Mechanisms and Develop Personalized Treatments for Osteoarthritis. Rheumatology and Therapy, 2021. 8(1): p. 499-515.
16. Ramos, Y.F., et al., Genes involved in the osteoarthritis process identified through genome wide expression analysis in articular cartilage; the RAAK study. PLoS One, 2014. 9(7): p. e103056.
17. Wu, T.D. and C.K. Watanabe, GMAP: a genomic mapping and alignment program for mRNA and EST sequences. Bioinformatics, 2005. 21(9): p. 1859-75.
18. Anders, S., P.T. Pyl, and W. Huber, HTSeq--a Python framework to work with high-throughput sequencing data. Bioinformatics, 2015. 31(2): p. 166-9.
19. Ewels, P., et al., MultiQC: summarize analysis results for multiple tools and samples in a single report. Bioinformatics, 2016. 32(19): p. 3047-8.
20. Love, M.I., W. Huber, and S. Anders, Moderated estimation of fold change and dispersion for RNA-seq data with DESeq2. Genome Biology, 2014. 15(12): p. 550.
21. Kaji, H., et al., Prostaglandin E2 stimulates osteoclast-like cell formation and bone-resorbing activity via osteoblasts: role of cAMP-dependent protein kinase. J Bone Miner Res, 1996. 11(1): p. 62-71.
22. Nalesso, G., et al., WNT16 antagonises excessive canonical WNT activation and protects cartilage in osteoarthritis. Annals of the Rheumatic Diseases, 2017. 76(1): p. 218-226.
23. Yan, H., et al., Induction of WNT16 via Peptide-mRNA Nanoparticle-Based Delivery Maintains Cartilage Homeostasis. Pharmaceutics, 2020. 12(1): p. 73.
24. Murakami, M., et al., Prostaglandin E synthase. Prostaglandins & Other Lipid Mediators, 2002. 68-69: p. 383-399.
25. Duan, L., et al., Noncoding RNAs in subchondral bone osteoclast function and their therapeutic potential for osteoarthritis. Arthritis Research & Therapy, 2020. 22(1): p. 279.

26. Bertuglia, A., et al., Osteoclasts are recruited to the subchondral bone in naturally occurring post-traumatic equine carpal osteoarthritis and may contribute to cartilage degradation. Osteoarthritis and Cartilage, 2016. 24(3): p. 555-566.
27. Löfvall, H., et al., Osteoclasts degrade bone and cartilage knee joint compartments through different resorption processes. Arthritis Research & Therapy, 2018. 20(1): p. 67.
28. Strassle, B.W., et al., Inhibition of osteoclasts prevents cartilage loss and pain in a rat model of degenerative joint disease. Osteoarthritis and Cartilage, 2010. 18(10): p. 1319-1328.
29. Coutinho de Almeida, R., et al., Identification and characterization of two consistent osteoarthritis subtypes by transcriptome and clinical data integration. Rheumatology (Oxford), 2020.
30. Lokau, J., M. Agthe, and C. Garbers, Generation of Soluble Interleukin-11 and Interleukin-6 Receptors: A Crucial Function for Proteases during Inflammation. Mediators Inflamm, 2016. 2016: p. 1785021.
31. Lokau, J., et al., Proteolytic Cleavage Governs Interleukin-11 Trans-signaling. Cell Reports, 2016. 14(7): p. 1761-1773.
32. Wiegertjes, R., F.A.J. van de Loo, and E.N. Blaney Davidson, A roadmap to target interleukin-6 in osteoarthritis. Rheumatology (Oxford), 2020. 59(10): p. 2681-2694.
33. Tsuchida, A.I., et al., Interleukin-6 is elevated in synovial fluid of patients with focal cartilage defects and stimulates cartilage matrix production in an in vitro regeneration model. Arthritis Res Ther, 2012. 14(6): p. R262.
34. Ryu, J.H., et al., Interleukin-6 plays an essential role in hypoxia-inducible factor 2α-induced experimental osteoarthritic cartilage destruction in mice. Arthritis Rheum, 2011. 63(9): p. 2732-43.
35. Nelson, M.R., et al., The support of human genetic evidence for approved drug indications. Nat Genet, 2015. 47(8): p. 856-60.
36. King, E.A., J.W. Davis, and J.F. Degner, Are drug targets with genetic support twice as likely to be approved? Revised estimates of the impact of genetic support for drug mechanisms on the probability of drug approval. PLOS Genetics, 2019. 15(12): p. e1008489.

7

Supplementary files

Supplementary figures
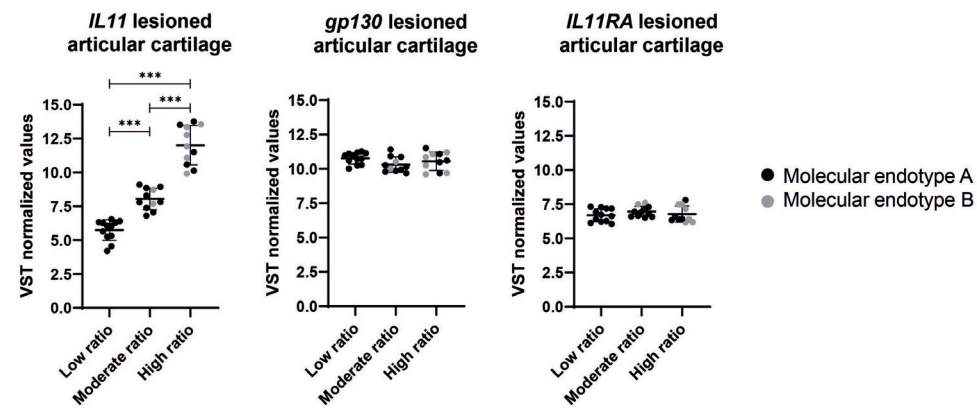
Supplementary Figure 1 - Expression patterns in lesioned autologous articular cartilage while stratifying for low, moderate, and high IL11:receptors ratio in RNA-seq data.
The molecular endotypes A and B are indicated by black and grey dots, respectively.

Supplementary tables

Supplementary Table 1 – Baseline characteristics of material included in the current study.

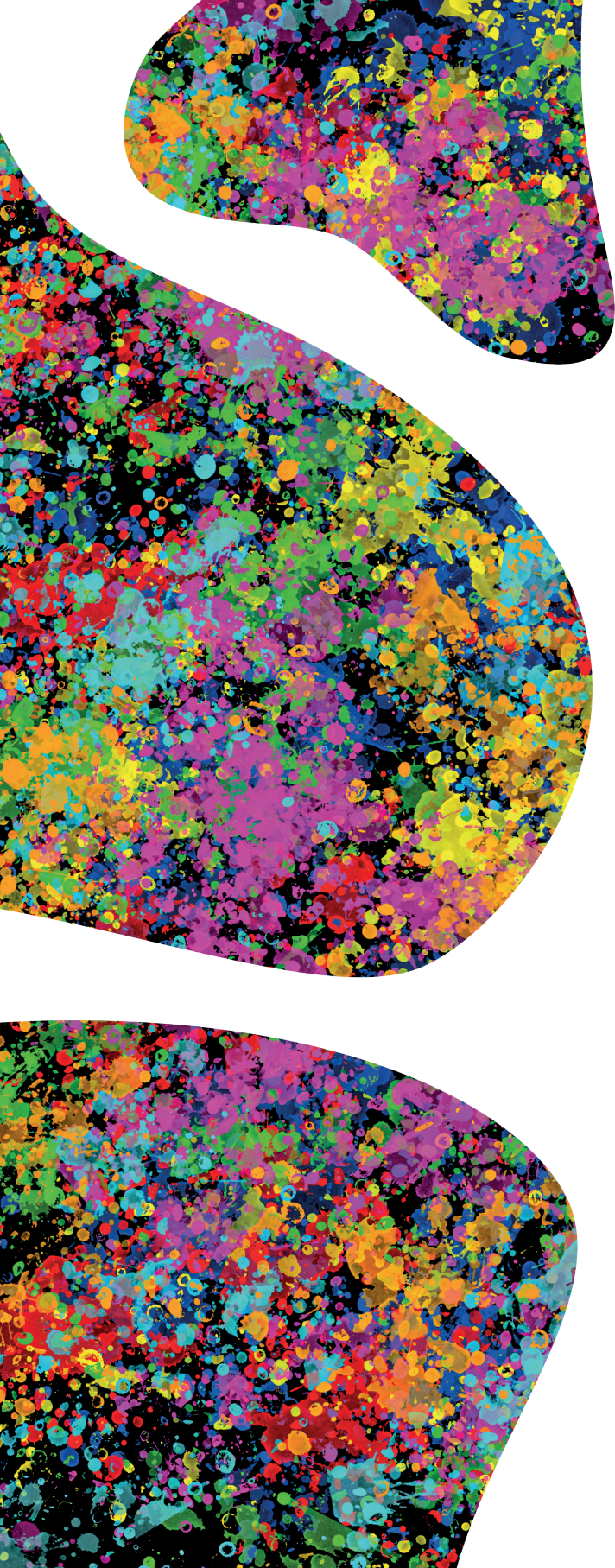|	RNA-seq data articular cartilage (N=35)	RNA-seq data subchondral bone (N=24)	Osteochondral explants (N=8)
Participants	35	24	8
Age (SD)	68,6 (9,0)	66,2 (8,5)	70,3 (10,9)
Knees (Hips)	28 (7)	18 (6)	8 (0)
Females (Males)	27 (7)	22 (2)	6 (2)

Supplementary Table 2 (partially) – Significant correlations in articular cartilage (|ρ|>0.6 and FDR<0.05).
The top 25 highest absolute correlations between genes expressed in articular cartilage and IL11 in preserved and in lesioned articular cartilage are shown here.

Gene	Ensembl ID	ρ	P-value	FDR	Tissue status
LIF	ENSG00000128342	0.88	3.83E-12	7.68E-08	Lesioned
DRGX	ENSG00000165606	0.81	8.57E-09	6.36E-05	Lesioned
BMP1	ENSG00000168487	0.80	1.08E-08	6.36E-05	Lesioned
WNT7B	ENSG00000188064	0.80	1.27E-08	6.36E-05	Lesioned
S100A2	ENSG00000196754	0.79	2.81E-08	9.60E-05	Lesioned
AP001528.3	ENSG00000280339	-0.79	2.87E-08	9.60E-05	Lesioned
CYTL1	ENSG00000170891	-0.78	6.83E-08	1.96E-04	Lesioned
PLAUR	ENSG00000011422	0.77	7.97E-08	2.00E-04	Lesioned
SPINK1	ENSG00000164266	0.77	9.28E-08	2.01E-04	Lesioned
NGF	ENSG00000134259	0.77	1.00E-07	2.01E-04	Lesioned
KBTBD12	ENSG00000187715	-0.76	1.53E-07	2.80E-04	Lesioned
TPRG1	ENSG00000188001	-0.76	2.01E-07	3.36E-04	Lesioned
SCGB1D2	ENSG00000124935	0.75	2.60E-07	3.40E-04	Lesioned
TNFRSF12A	ENSG00000006327	0.75	2.62E-07	3.40E-04	Lesioned
TNP1	ENSG00000118245	0.75	2.70E-07	3.40E-04	Lesioned
CLCF1	ENSG00000175505	0.75	2.71E-07	3.40E-04	Lesioned
DUSP4	ENSG00000120875	0.75	3.83E-07	4.11E-04	Lesioned
LAMB3	ENSG00000196878	0.75	3.83E-07	4.11E-04	Lesioned
NDRG2	ENSG00000165795	-0.75	3.89E-07	4.11E-04	Lesioned
POMGNT1	ENSG00000085998	0.74	4.60E-07	4.41E-04	Lesioned
ADAMTS14	ENSG00000138316	0.74	4.68E-07	4.41E-04	Lesioned
LINC01711	ENSG00000268941	0.74	4.84E-07	4.41E-04	Lesioned
MPPED1	ENSG00000186732	-0.74	5.80E-07	5.05E-04	Lesioned
PIK3IP1	ENSG00000100100	-0.73	7.63E-07	6.37E-04	Lesioned
RPSAP52	ENSG00000241749	0.73	8.25E-07	6.62E-04	Lesioned
MTHFD2L	ENSG00000163738	-0.78	5.25E-08	7.21E-04	Preserved
COL5A1	ENSG00000130635	0.77	8.30E-08	7.21E-04	Preserved
LINC01711	ENSG00000268941	0.77	1.08E-07	7.21E-04	Preserved
LOXL2	ENSG00000134013	0.76	2.41E-07	1.21E-03	Preserved
ERFE	ENSG00000178752	0.74	4.50E-07	1.80E-03	Preserved
SERPINE1	ENSG00000106366	0.74	6.41E-07	2.14E-03	Preserved
TNC	ENSG00000041982	0.73	1.12E-06	3.22E-03	Preserved

7

Gene	Ensembl ID	ρ	P-value	FDR	Tissue status
SERPINE2	ENSG00000135919	0.72	1.39E-06	3.49E-03	Preserved
CPM	ENSG00000135678	-0.72	1.57E-06	3.50E-03	Preserved
HERC5	ENSG00000138646	-0.71	2.08E-06	3.91E-03	Preserved
P3H2	ENSG00000090530	0.71	2.14E-06	3.91E-03	Preserved
COL15A1	ENSG00000204291	0.71	2.50E-06	4.17E-03	Preserved
FAM149A	ENSG00000109794	-0.70	4.38E-06	6.45E-03	Preserved
HTRA1	ENSG00000166033	0.70	4.51E-06	6.45E-03	Preserved
IGFBP3	ENSG00000146674	0.69	6.97E-06	9.22E-03	Preserved
NOTUM	ENSG00000185269	0.69	7.36E-06	9.22E-03	Preserved
BMP6	ENSG00000153162	0.68	8.26E-06	9.74E-03	Preserved
GFRA2	ENSG00000168546	0.68	9.16E-06	1.00E-02	Preserved
CRTC3	ENSG00000140577	-0.68	9.52E-06	1.00E-02	Preserved
DNER	ENSG00000187957	0.68	1.12E-05	1.11E-02	Preserved
RPARP-AS1	ENSG00000269609	-0.68	1.16E-05	1.11E-02	Preserved
STK32A	ENSG00000169302	-0.67	1.29E-05	1.17E-02	Preserved
ACADL	ENSG00000115361	-0.67	1.39E-05	1.17E-02	Preserved
DIRAS1	ENSG00000176490	0.67	1.40E-05	1.17E-02	Preserved
SLC39A11	ENSG00000133195	-0.67	1.48E-05	1.17E-02	Preserved

Supplementary Table 3 - gene enrichment of genes correlating to IL11 in articular cartilage.

Supplementary Table 3A - Gene enrichment of genes correlating to IL11 in preserved articular cartilage.

GO-term	Count	%	P-value	FDR	Genes
GO:0005576~extracellular region	28	27.2	3.14E-09	4.48E-07	PLAUR, TNC, DKK3, FSTL3, SERPINE1, AEBP1, LOXL3, TNFSF11, TGFBI, DNAI1, ADM2, COL5A1, CPM, SERPINE2, WNT9A, IGFBP3, BMP6, COL6A3, HTRA1, CLCF1, ERFE, ARSI, NOTUM, NTF3, WNT7B, APOD, LAMB3, COL15A1
GO:0005615~extracellular space	24	23.3	4.48E-08	3.20E-06	TNC, DKK3, FSTL3, SERPINE1, PRKAG2, AEBP1, LOXL3, TNFSF11, TGFBI, COL5A1, LOXL2, CPM, SERPINE2, WNT9A, IGFBP3, BMP6, COL6A3, HTRA1, CLCF1, ERFE, NTF3, WNT7B, APOD, COL15A1
GO:0005788~endoplasmic reticulum lumen	11	10.7	2.51E-06	1.20E-04	PLAUR, TNC, FSTL3, P3H2, COL5A1, IGFBP3, COL6A3, ARSI, NOTUM, WNT7B, COL15A1
GO:0005604~basement membrane	5	4.9	1.36E-03	4.85E-02	TNC, P3H2, TGFBI, COL5A1, LOXL2

Supplementary Table 3B - Gene enrichment of genes correlating to IL11 in lesioned articular cartilage.

GO-term	Count	%	P-value	FDR	Genes
GO:0005615~extracellular space	37	19.5	1.33E-08	3.24E-06	CFH, MYOC, TGFBR3, FSTL3, ASIP, TIMP1, TFPI2, COL7A1, CCL20, FNDC4, IGFBP5, RARRES1, TGFBI, INHBA, PTGIS, SCGB1D2, WNT1, BMP2, LIF, C1QL1, LOXL2, NGF, SEMA7A, HAPLN3, IGFBP4, UCN2, IGFBP1, CPAMD8, FRZB, ANGPTL4, BMP1, CYTL1, CLCF1, GPC5, PAPPA, WNT7B, PDGFA
GO:0005576~extracellular region	40	21.1	4.60E-08	5.61E-06	CFH, PLAUR, TGFBR3, FSTL3, ISM2, TIMP1, TFPI2, COL7A1, CCL20, FNDC4, IGFBP5, NRP2, TGFBI, INHBA, TREM1, WNT1, BMP2, LIF, NGF, CRB1, ADAMTS14, HAPLN3, IGFBP4, UCN2, IGFBP1, ADAMTS1, CPAMD8, FRZB, ANGPTL4, BMP1, ENHO, OSCAR, CLCF1, GPC5, PAPPA, NOTUM, WNT7B, LAMB3, PDGFA, PNP

7

Supplementary Table 4 - Correlations between IL11 and IL11RA and GP130 expression levels

Tissue	Receptor	ρ	Pval	Padj
Preserved bone	gp130	0.28	1.94E-01	6.83E-01
Preserved bone	IL11RA	0.31	1.56E-01	6.63E-01
Lesioned bone	gp130	-0.14	5.35E-01	7.97E-01
Lesioned bone	IL11RA	-0.05	8.23E-01	9.35E-01
Preserved cartilage	gp130	-0.21	2.34E-01	5.85E-01
Preserved cartilage	IL11RA	0.04	8.06E-01	9.33E-01
Lesioned cartilage	gp130	-0.17	3.41E-01	6.42E-01
Lesioned cartilage	IL11RA	0.06	7.57E-01	9.01E-01

Supplementary Table 5 (partially) - Significant correlations in subchondral bone (|ρ|>0.6 and FDR<0.05).
The top 25 highest absolute correlations between genes expressed in subchondral bone and IL11 in lesioned subchondral bone are shown here.

Gene	Ensembl ID	ρ	Pval	Padj	Tissue status
ELOVL5	ENSG00000012660	-0.88	2.56E-08	4.05E-04	Lesioned
GALK1	ENSG00000108479	0.84	4.20E-07	3.32E-03	Lesioned
CD302	ENSG00000241399	-0.82	1.34E-06	7.06E-03	Lesioned
WNT16	ENSG00000002745	0.81	2.75E-06	1.09E-02	Lesioned
NCOA7	ENSG00000111912	-0.80	4.31E-06	1.36E-02	Lesioned
SDC1	ENSG00000115884	0.79	7.84E-06	1.50E-02	Lesioned
RCHY1	ENSG00000163743	-0.79	8.56E-06	1.50E-02	Lesioned
CUEDC2	ENSG00000107874	0.79	8.56E-06	1.50E-02	Lesioned
CDK2AP1	ENSG00000111328	0.79	8.56E-06	1.50E-02	Lesioned
DICER1	ENSG00000100697	-0.78	1.11E-05	1.66E-02	Lesioned
CHST10	ENSG00000115526	0.78	1.16E-05	1.66E-02	Lesioned
NCOA1	ENSG00000084676	-0.78	1.37E-05	1.80E-02	Lesioned
SORT1	ENSG00000134243	-0.77	1.68E-05	1.84E-02	Lesioned
DNAJC1	ENSG00000136770	0.77	1.68E-05	1.84E-02	Lesioned
SDF4	ENSG00000078808	0.77	1.75E-05	1.84E-02	Lesioned
YIPF2	ENSG00000130733	0.77	1.90E-05	1.87E-02	Lesioned
IFI27L2	ENSG00000119632	0.76	2.22E-05	1.91E-02	Lesioned
KIAA1755	ENSG00000149633	0.76	2.80E-05	1.91E-02	Lesioned
HSDL2	ENSG00000119471	-0.76	2.91E-05	1.91E-02	Lesioned
MME	ENSG00000196549	-0.76	2.91E-05	1.91E-02	Lesioned
AGFG1	ENSG00000173744	-0.75	3.14E-05	1.91E-02	Lesioned
COL7A1	ENSG00000114270	0.75	3.14E-05	1.91E-02	Lesioned
EMC10	ENSG00000161671	0.75	3.14E-05	1.91E-02	Lesioned
PHPT1	ENSG00000054148	0.75	3.26E-05	1.91E-02	Lesioned
YIF1A	ENSG00000174851	0.75	3.26E-05	1.91E-02	Lesioned

7

Supplementary Table 6 - Gene enrichment of genes correlating to IL11 in lesioned subchondral bone

GO- Term	Count	%	P-value	FDR	Genes
GO:0005783~endoplasmic reticulum	32	16.2	4.28E-06	1.20E-03	ELOVL5, SEC61A1, PDIA5, P4HA2, SDF4, P3H2, CRAT, EEF1D, OGN, MAN1A1, SLC39A7, COL4A3BP, THBS4, P3H1, RRBP1, ERGIC3, OS9, DNAJC1, P3H4, POU2F1, TENM2, DIAPH2, PDE3B, PDIA4, EMC10, ATP1A1, FAM57A, MAP2K1, FKBP2, SULF2, UVRAG, SLC35B4
GO:0005794~Golgi apparatus	30	15.2	5.83E-05	8.16E-03	XYLT2, B4GALT7, ST6GALNAC2, SDF4, P3H2, VTI1B, RABAC1, AP1S1, MAN1A1, SLC39A7, COL4A3BP, CHST10, STK25, B4GALT2, SMO, YIPF2, SORT1, CD36, TLR4, TENM2, PDE3B, PXYLP1, SLC35B2, ATP1A1, MAP2K1, YIF1A, CHST6, ZDHHC17, SLC35B4, B3GNT9

7

Capturing essential physiological aspects of interacting cartilage and bone tissue with osteoarthritis pathophysiology - a human osteochondral unit-on-a-chip model

Margo Tuerlings[1*], Ilja Boone[1*], Hossein Eslami Amirabadi[2], Michelle A.M. Vis[3], H. Eka D. Suchiman[1], Enrike H.M.J. van der Linden[4], Sandra Hofmann[3], Rob G.H.H. Nelissen[4], Jaap M.J. den Toonder[2‡], Yolande F.M. Ramos[1‡], Ingrid Meulenbelt[1‡]

[1] Dept. of Biomedical Data Sciences, Leiden University Medical Center, Leiden, The Netherlands.
[2] Center for proteomics and metabolomics , Leiden University Medical Center, Leiden, The Netherlands
[3] Dept. Orthopaedics Leiden University Medical Center, Leiden, The Netherlands.

[*] contributed equally to this work
[‡] shared last

Abstract

Given the multi-tissue aspects of osteoarthritis (OA) pathophysiology, translation of OA susceptibility genes towards underlying biological mechanism and eventually drug target discovery requires appropriate human *in vitro* OA models that incorporate both functional bone and cartilage tissue units. Therefore, we developed a microfluidic chip with an integrated fibrous polycaprolactone (PCL) matrix in which neo-bone and cartilage is produced, that could serve as a tailored human *in vitro* disease model of the osteochondral unit of joints. The model enables to evaluate OA related environmental perturbations to (individual) tissue units by controlling environmental cues, for example by adding biochemical agents. After establishing the co-culture in the system, a layer of cartilaginous matrix was deposited in the chondrogenic compartment, while a bone-like matrix appeared to be deposited between the PCL fibers, indicated by both histology and gene expression levels of collagen type 2 (*COL2A1*) and osteopontin (*OPN*), respectively. As proof-of-principle, the bone and cartilaginous tissue were exposed to active thyroid hormone (T3), creating an age-related OA disease model. This resulted in increased expression levels of hypertrophy markers integrin binding sialoprotein (*IBSP)* and alkaline phosphatase (*ALPL)* in both cartilage and bone, as expected. Altogether, this model could contribute to enhanced translation from OA risk genes towards novel OA therapies.

Introduction

Osteoarthritis (OA) is an age-related degenerative joint disease, affecting more than 10% of the population over the age of 60 years [1-3]. The OA pathophysiological process is characterized by structural changes in both cartilage and the subchondral bone, including cartilage degeneration, subchondral bone thickening and osteophyte formation. In absence of effective disease modifying treatments, OA puts high social and economic burden on society [4]. OA has a considerable genetic component and many studies have been performed highlighting involvement of OA susceptibility The function of these genes merely involving maintenance processes in both bone and cartilage, confirm that aberrant molecular crosstalk between articular cartilage and subchondral bone plays an essential role in the initiation and progression of OA [5-8]. Furthermore, by applying molecular profiling of human OA articular cartilage, it has been consistently shown that activated articular chondrocytes with OA pathophysiology lose their healthy maturational arrested state and recapitulated an hypertrophic growth plate morphology with associated debilitating gene expressions [9, 10]. To reliably mimic OA related chondrocyte hypertrophy, we recently showed that active thyroid hormone (Triiodothyronine, T3) could serve as a reliable trigger to induce OA related chondrocyte hypertrophy, marked by increased expression levels of *ALPL*, *RUNX2*, and *COL10A1* [11-13], and eventually to the formation of bone [14, 15].

Given the multi-tissue function, translation of strong OA risk genes towards underlying biological mechanism, and eventually drug target discovery and testing requires appropriate human *in vitro* OA models that incorporate both functional bone and cartilage tissue units [16]. Such multi-tissue models require microfluidic tissue-on-chip systems that allow controllable automated flow in the different tissue compartment i.e. for culturing of chondrocytes and osteogenic cells separately in their preferred medium but in close contact with each other. Moreover, microfluidic chip technology allows OA related environmental perturbations to (individual) tissue units by adding e.g. biochemical cues such as unbeneficial metabolites, cytokines, or factors inducing hypertrophy [13]. Up until now, available microfluidic model systems mimicking osteochondral interaction are, however, hydrogel-based [17-20], while ideally biological extracellular matrix (ECM) can be studied on top of cartilage and subchondral bone gene expression data.

To this end we have developed a dual-tissue microfluidic device, that allows faithful engineering of functional interacting neo-cartilage and neo-bone tissues readily deposited by human primary osteogenic cells and human primary articular chondrocytes (hPACs) from patients that underwent joint replacement surgery due to OA (RAAK-study) [21]. Deposition of ECM by the primary cells was compared to our

8

previously described 3D cell pellet culture model, which is epigenetically highly similar to autologous tissue [22]. As proof-of-principle, we evaluated whether we could mimic the dysfunctional adaptation processes of hypertrophic chondrocytes in our model, by exposing the system to T3. Henceforth, osteochondral unit-on-a-chip model could serve as reliable biomimetic model to study tissue repair and regenerative capacity during OA.

Results

Microfluidic chip design

To allow engineering of functional interacting neo-cartilage and neo-bone tissues, a microfluidic chip was designed consisting of two channels that were separated by an electrospun polycaprolactone (PCL) matrix with a well-like structure on top of it. As shown in **Figure 1A**, the PCL matrix consists of a microfiber layer with thickness 190.1 ± 30.58 μm, fibre diameters of 8.60 ± 0.97 μm, and pore-sizes of 25.51 ± 12.37 μm (**Figure 1B** and **Figure 1C**), and a nanofiber layer, with fibre diameters of 0.74 ± 0.55 μm and pore-sizes of 2.14 ± 1.14 μm (**Figure 1B** and **Figure 1C**). The microfiber layer served as a scaffold to seed and culture primary osteogenic cells, while the nanofiber layer will separate the primary osteogenic cells from the hPACs and prevent their migration to the other compartment. hPACs inherently prone to deposit high-quality cartilaginous tissue were seeded and cultured in high density in the well-like structure. Upon culturing primary osteogenic cells and hPACs for 28 and 21 days (**Supplementary Figure 1**), respectively, we harvested the constructs from the microfluidic chips and performed histology or we separated the two compartments for RT-qPCR. To determine the optimal time between media refreshment of the system to keep the chondro- and osteogenic media separate, we performed diffusion experiments using Dextran. Dextran was injected in the chondrogenic channel and after approximately 60 min fluorescence was measured in the osteogenic channel (**Supplementary Figure 2**).

Gene expression analyses

Quality of chondrogenic and osteogenic matrix deposited in the chip was studied by means of RT-qPCR of cartilage markers *COL2A1* (encoding collagen type 2) and *ACAN* (encoding aggrecan) and bone markers *OPN* (encoding osteopontin), *RUNX2* (encoding RUNX Family Transcription Factor 2), and *COL1A1* (encoding collagen type 1), in comparison to our established 3D *in vitro* pellet culture model [22] of the same donors (N=3-4 donors, **Supplementary Table 1A**). Moreover, we included gene expression data of our previously assessed RNA-sequencing (RNA-seq) datasets of autologous preserved bone and cartilage of patients that underwent a joint replacement surgery due to OA (**Supplementary Table 1B**) [9, 23]. As shown in **Figure 2A**, we observed similar expression levels of *COL2A1* and *ACAN* between the chondrogenic compartment of the
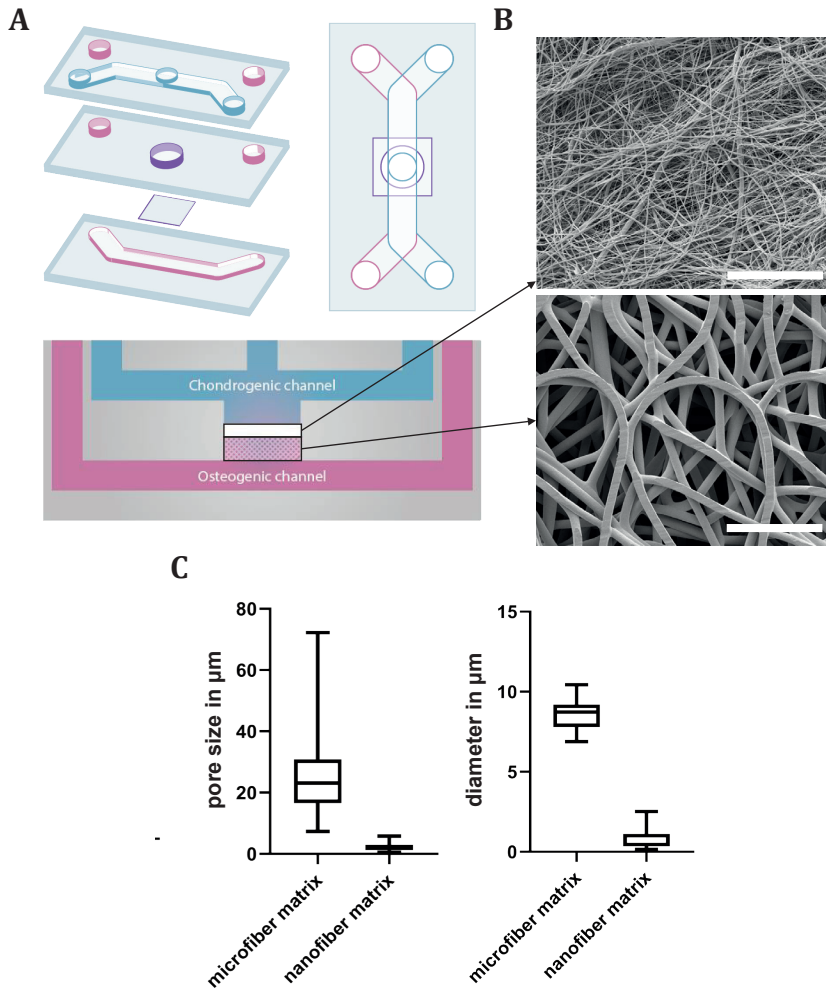
Figure 1 – Osteochondral unit-on-a-chip model system.
(A) Schematic overview of the design of the microfluidic chip (blue: chondrogenic channel, pink: osteogenic channel, purple: co-culture compartment). (B) Scanning electron microscopy pictures of the PCL electrospun matrix, with microfibers (bottom) and nanofibers (top). The white scalebar indicates 100 μm. (C) Quantification of diameters and pore sizes of microfibers and nanofibers using the Quanta 600F ESEM software.

chip and the chondrocyte pellet cultures. Moreover, when comparing the chondrogenic to the osteogenic compartment, we observed higher expression of *COL2A1* (FC=9.0) in the chondrogenic compartment, which was in line with the 3D pellet cultures and RNA-seq data. As shown in **Figure 2B**, we observed similar expression levels of *RUNX2* and *OPN* between the osteogenic compartment of the chip and the osteogenic cell pellet cultures. Upon comparing the osteogenic compartment with the chondrogenic compartment, we observed higher expression of *RUNX2* (FC=3.6) and *OPN* (FC=8.4) (**Figure 2B**). Notably, *COL1A1* did not show similar expression levels between the chip and pellet cultures, as

Figure 2– Gene expression levels of cartilage markers (A) and bone markers (B) measured in the osteochondral unit-on-a-chip model system (left panel), the 3D cell pellet cultures (middle panel), or the RNA-seq datasets of native tissue (right panel).

The chondrogenic compartment/chondrocyte cell pellet cultures are indicated with CH, while the osteogenic compartment and the osteogenic cell pellet cultures are indicated with OB. Paired sample T-test was used for statistical assessment, with * P<0.05, **P<0.005, ***P<0.001.

well as consistent differences between the osteogenic and chondrogenic compartment. These gene expression levels suggest that high-quality neo-bone and neo-cartilage matrix was deposited in our microfluidic model system after 28 days.

Neo-bone and cartilage matrix deposition
As shown in **Figure 3A**, a general Hematoxylin and Eosin (H&E) histological staining of the complete chip indicated the presence of two tissue types in the model system, a dense cartilage-like matrix with a relatively high nuclei count on top of loose bone-like matrix. The matrix deposition in the osteochondral unit-on-a-chip model was assessed using several bone and cartilage stainings. Despite the fact that there was not a significant difference in *ACAN* expression levels between the chondrogenic and osteogenic compartment, we observed more intense Alcian Blue staining in the chondrogenic compartment, indicating higher glycosaminoglycan (GAG) content. The Alizarin Red staining showed calcium deposits at multiple locations of the osteogenic compartment of the chip, but not in the neo-cartilage (**Figure 3C**). This is in line with the more intense staining of bone marker OPN in the osteogenic compartment compared to the chondrogenic compartment (FC=1.48, P=6.6×10^{-2}, **Figure 3D**). Both osteogenic staining suggest inhomogeneous distribution of cells throughout the matrix. Notably, most mineralization took place in the surface area of the bone matrix. As shown in **Figure 3E**, we observed COL2A1 staining in both compartments (FC=1.05, P=1.26×10^{-1}), however, the staining appeared to be more structured (indicated by the arrow) in the chondrogenic compartment. Together, the gene expression findings and histology suggest the formation of two individual layers of cartilage- and bone like-matrix separated by the nanofiber PCL matrix.

Implementation of an age-related disease model
To evaluate whether our biomimetic model can be used to study the effects of OA-related changes, we exposed both the chondrogenic and osteogenic compartments of our microfluidic chip to hypertrophy-inducing thyroid hormone T3, for 5 consecutive days (N=5 donors, **Supplementary Table 1B**). Effects were determined by measuring expression levels of the chondrocyte hypertrophy markers *ALPL* (encoding alkaline phosphatase), *IBSP* (encoding Integrin Binding Sialoprotein), and *RUNX2*. As shown in **Figure 4A**, within the chondrogenic compartments we observed upregulation of hypertrophy markers *IBSP* (FC=5.04, P=2.7×10^{-2}), *ALPL* (FC=2.83), and *RUNX2* (FC=1.93) upon comparing the hypertrophic and control chips, however *ALPL* and *RUNX2* did not reach statistical significance (P=0.172 and P=0.104, respectively). We did not observe consistent changes in the expression level of chondrogenic markers *ACAN* and *COL2A1* (**Supplementary Figure 3**). Within the osteogenic compartments we observed an upregulation of *ALPL* (FC=2.57, P=4.1×10^{-2}) and *IBSP* (FC=2.29) between
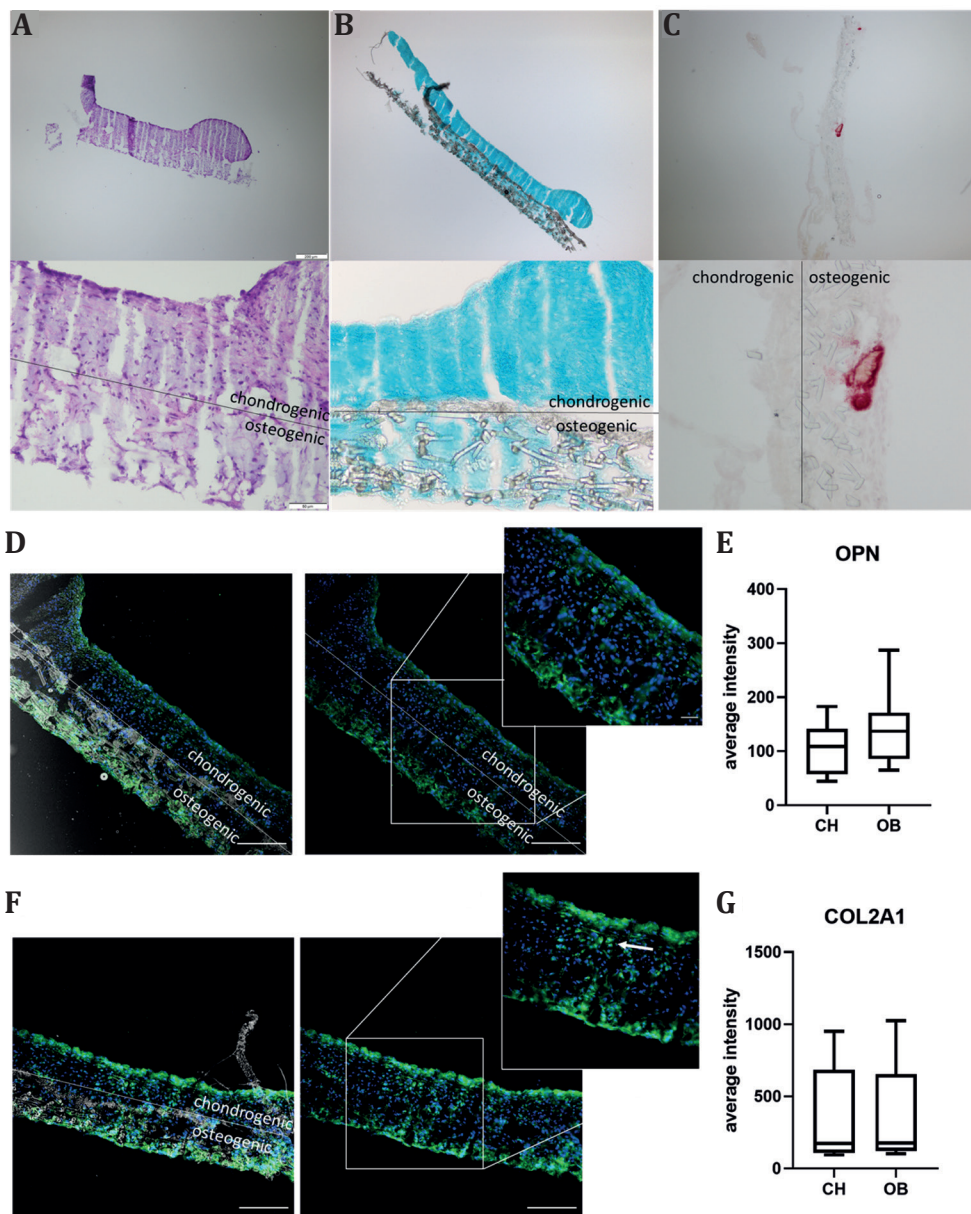
Figure 3 – Representative images of (immuno-)histochemistry on cross sections of the osteochondral unit-on-a-chip system.
(A) Hematoxylin/ Eosin (H&E) staining. (B) Alcian Blue staining. (C) Alizarin red staining. (D) OPN staining (in green) and DAPI staining (in blue) and (E) COL2A1 staining (in green) and DAPI staining (in blue) of both chondrogenic and osteogenic compartment of the chip. Overlap brightfield and fluorescence image (left) and fluorescence image (right). Scalebar in smaller and larger magnification represents 200 µm and 50 µm, respectively.
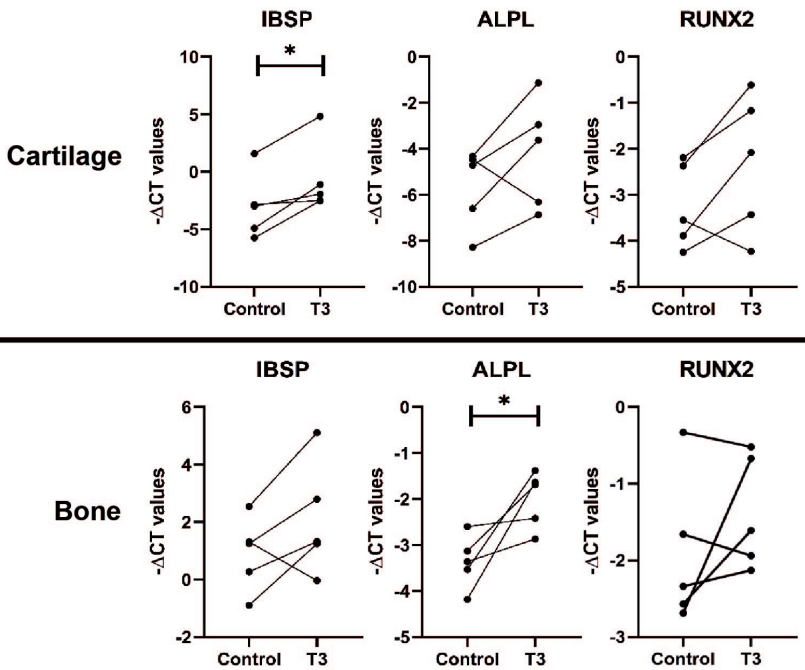
Figure 4 – Gene expression levels of hypertrophy markers in the chondrogenic compartment (A) and in the osteogenic compartment (B) upon exposure to hypertrophy by adding T3.
Paired sample T-test was used for statistical assessment, with * P<0.05, **P<0.005, ***P<0.001

the hypertrophic and control chips, however *IBSP* did not reach statistical significance (P=0.157). Notably, *RUNX2* did not show a consistent direction of effect in the osteogenic compartment (**Figure 4B**). Similar variations in directions of effect were seen in the reference 3D pellet cultures (**Supplementary Figure 4**). These findings suggest that our microfluidic model system can serve as a hypertrophy-induced OA model to study concurrently cartilage and bone changes.

In addition, we collected medium from the system on the day starting the exposure (day 23) and the day of harvesting the osteochondral unit-on-a-chip system (day 28). To examine cartilage breakdown as a consequence of hypertrophy, we measured the sGAG release by performing a dimethylmethylene blue (DMMB) assay on the medium collected from the chondrogenic compartment (N=3 donors). As shown in **Figure 5**, we observed increased sGAG release from day 23 to day 28 in all three hypertrophic samples, while control samples showed variation (two samples decreased and one sample increased) in sGAG release. These results additionally show the possibility to perform multiple measurements on different time points for the same system during culture.

8

Cartilage
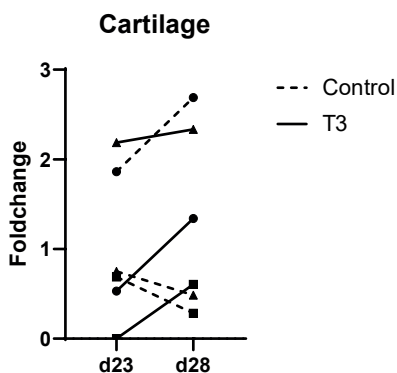
Figure 5 – sGAG measurement in medium collected from the chondrogenic compartment on two different time points, before (day 23) and after (day d28) exposure to hypertrophy by adding T3.

Discussion

Currently, there are no *in vitro* biomimetic OA models available that incorporate functional bone and cartilage tissue units, including biological matrix, in interaction. Here, we introduce a novel dual-tissue microfluidic model system in which interacting neo-cartilage and neo-bone are deposited. The current model allows for in depth investigations of underlying mechanisms of OA risk genes beyond gene expression, towards a reliable biomimetic model of the osteochondral joint unit for tissue repair and regenerative capacity of primary osteogenic cells and hPACs upon OA related perturbations. Moreover, the model system can be used as pre-clinical model for identification of druggable targets and for drug testing.

Upon culturing hPACs and osteogenic cells for 21 and 28 days, respectively, the osteogenic cells deposited osteogenic matrix in their compartment of the microfluidic chip, as indicated by the Alizarin Red and OPN staining (**Figure 3C** and **Figure 3D)**. The osteogenic nature of the matrix was confirmed by RT-qPCR, as bone markers *OPN* and *RUNX2* were highly expressed, while cartilage marker *COL2A1* was lowly expressed in the osteogenic compartment compared to the chondrogenic compartment (**Figure 2**). However, *ACAN* expression levels were relatively high in the osteogenic compartment. This, together with the lack of a calcified zone (**Figure 3A**) and the relatively low mineralization rate (**Figure 3C**), suggests the bone-like matrix in the system is not yet mature and therefore needs to be further optimized, for instance by extending the culture period or by homogenizing the distribution of osteogenic cells over the matrix. Upon culturing the hPACs for 21 days in our dual-tissue model system, we observed a thick layer of cartilaginous matrix deposited on top of the PCL matrix in the well-like structure as shown by the presence of GAGs (**Figure 3B**). Although COL2A1 staining was observed in both compartments (**Figure 3F**), the staining

appeared to be more structured in the chondrogenic compartment. The difference in COL2A1 staining intensity between the chondrogenic and osteogenic compartment was minimal compared to the difference in OPN staining intensity between the two compartments, which confirmed the differences seen in gene expression levels (**Figure 2**). The H&E staining showed little difference in tissue morphology between chondro- and osteogenic compartments, which is partly due to the tears in the osteochondral construct as result of sectioning. In contrast to the osteogenic compartment, we observed high expression levels of *COL2A1,* while low expression levels of *OPN* and *RUNX2* in the chondrogenic compartment, showing similar directions as both the well-established 3D pellet cultures [22] and the RNA-seq of autologous cartilage and bone (**Figure 2**). The differences observed in gene expression levels between the osteogenic and chondrogenic compartments are smaller than the differences observed in the osteogenic and chondrogenic 3D cell pellet cultures, which might be due to the fact that within the chip we have a co-culture while the pellets are purely chondrocytes or osteogenic cells. Notably, *COL1A1* showed relatively high expression levels in both the osteogenic and chondrogenic compartment, while COL1 is known as an abundant protein in bone and is usually not present in healthy articular cartilage. Nonetheless, *COL1A1* is shown to be present in osteoarthritic articular cartilage [24], which we also observe in our RNA-seq data of the autologous macroscopically preserved cartilage from an end-stage OA joint. Therefore, *COL1A1* might not be a suitable bone marker when working with OA tissues.

Upon inducing hypertrophy by exposing the constructs to T3 for five consecutive days, we observed consistently increased expression levels of chondrocyte hypertrophy markers *IBSP*, *ALPL*, and *RUNX2* in the chondrogenic compartment. IBSP is a structural protein of bone matrix and ALP and RUNX2 are both osteoblastic markers. All three markers are known to be expressed by terminal hypertrophic chondrocytes [25-28]. The upregulation of these genes upon exposure to hypertrophy indicates that the gene expression pattern of the chondrogenic compartment changes towards an osteogenic phenotype, similar to OA pathophysiology and similar to the effects we observed in our previous study establishing a hypertrophic OA model [13]. Despite the small sample size of the measurements on the collected medium, we show here the possibility to determine sGAGs at multiple timepoints during culture. The increase in sGAG release in the medium suggests that there was potentially more cartilage breakdown in hypertrophic constructs, which is in line with the OA phenotype. In the osteogenic compartment, *IBSP* and *ALPL* were also consistently upregulated in the hypertrophic compared to the control group, which may indicate increased bone formation upon inducing hypertrophy. This confirms possibility of implementing disease-related perturbations to our chip to mimic pathophysiological processes. Therefore, our model

8

system could serve as a platform for identification of druggable targets and eventually drug testing. Together, this will contribute to cost-efficient preclinical research and reduce, refine, and replace animal experiments.

By introducing a novel dual-tissue microfluidic model system we established, for the first time, an osteochondral model in which interacting neo-cartilage and neo-osteogenic tissues are deposited by the primary cells. This is in contrast to currently available microfluidic model systems representing osteochondral construct based on cells encapsulated in specific hydrogels [17-20]. For example Lin et al. [17] developed an osteochondral system consisting of two separate compartments to create chondrogenic and osteogenic microenvironments. Human bone marrow-derived stem cells were seeded in hydrogels inside this model system and UV was used to cure the hydrogel. Although this model attractively represents an osteochondral co-culture, the use of hydrogels has some disadvantages. The hydrogel requires UV or hydrogen peroxide exposure for its crosslinking, which may negatively influence primary cells by inducing cell senescence and adding potential uncertainty to the model [29]. In addition, hydrogels still fail to accurately mimic the 3D environment and a reoccurring problem is the formation of matrix islands within hydrogels, which occur because of the elastic nature of the material [30]. Moreover, the main disadvantage of the use of hydrogels instead of the formation of neo-tissue is that it limits the study output to only cell signalling and tissue repair upon perturbations is not visible.

Although we here showed that cartilaginous and osteogenic ECM were deposited in our microfluidic model system and that our model system can be used to study the effects of perturbations, further improvements to the model can still be made. In our previous studies [13, 31], we showed that mechanical stress is an important trigger to OA onset and this type of perturbation cannot yet be captured by our model system. Hence, it would be added value to incorporate an actuation chamber to the model system, which can be used to apply mechanical stress to the construct and the cells within. In addition, to fully recapitulate an OA joint, implementation of other cell types such as synoviocytes, adipocytes, and immune cells would be preferable. Nevertheless, the most important hallmarks of OA are degeneration of articular cartilage and remodelling of subchondral bone. Moreover, genetic studies have indicated that aberrant molecular crosstalk between articular cartilage and subchondral bone plays a major role during OA pathophysiological process, which can be studied using the here presented model. In the current study, the model system was cultured under normoxic (20% oxygen) conditions, while it is known that chondrocytes *in vivo* reside under hypoxic conditions (0-5% oxygen). Also, the cells in the subchondral bone are exposed to lower oxygen levels (5-10% oxygen) *in vivo.* Therefore, it might be beneficial to incorporate an oxygen

gradient over the microfluidic chip or to culture the system under reduced oxygen levels. The primary cells used in the presented model system were isolated from end-stage OA joints. Primary cells are a finite cell source and the use of a more stable cell source, in the form of induced pluripotent stem cells (iPSCs), would be desirable. Using iPSCs in our model system would allow us to study, for example, high impact mutations in the interacting joint tissues bone and cartilage, instead of focussing on solely one tissue. Finally, to ensure compatibility with high-throughput screens, of newly developed medication as part of pre-clinical studies and to minimize the amount of reagents required, the model system could even be further miniaturised and upscaled.

In conclusion, with this osteochondral unit-on-a-chip model system we indicate that it is possible to culture functional cartilage and bone tissue *in vitro*. This, together with the implementation of age-related perturbation to this dual-tissue microfluidic chip, further advances the ongoing search for an appropriate multiple tissue interacting 3D-culture for multi-tissue diseases such as OA [32]. While this microfluidic chip is still further advancing, this model could contribute to enhanced translation from OA risk genes towards novel OA therapies.

Methods

Sample description

The current study includes N=24 participants of the RAAK study, who underwent a joint replacement surgery as a consequence of OA. Material of four of these patients was used in the first set of experiments, in which we developed the osteochondral unit-on-a-chip system (**Supplementary Table 1A**). Material of five other participants was used in implementation of an OA-related disease model (**Supplementary Table 1C**). Material of the remaining participants was used for RNA sequencing (**Supplementary Table 1B).** Informed consent was obtained from all participants of the RAAK study and ethical approval for the RAAK study was given by the medical ethics committee of the Leiden University Medical Center (P08.239/P19.013).

Electrospun matrix

The matrix was fabricated by electrospinning polycaprolactone (PCL, Corbion Purac Bopmaterials) as described previously[33]. Briefly, 18% PCL was dissolved in chloroform (anhydrous, amylene stabilized, Merck) for the microfibers and 12% PCL was dissolved in chloroform:methanol (Merck). Electrospinning was done using the EC-CLI electrospinning apparatus (IME Techologies). The obtained matrices were characterized using scanning electron microscopy (SEM, Quanta 600F ESEM, Fei). To increase conductivity of the surface, the matrices were sputter coated with gold prior to visualization. The quantification of the pore sizes was done by measuring the

8

distance between fibers on at least 10 locations in at least six different images. The fiber diameter was measured in a similar way. For both quantifications the Quanta 600F ESEM software was used.

Microfluidic chip
The microfluidic chip was fabricated with a selective curing process as described previously [33]. Concisely, polydimethylsiloxane (PDMS, Dow Corning) without curing agent (PDMS-) was spincoated on a microscope glass slide. Then, the PCL matrix was applied on the spincoated PDMS-. PDMS with curing agent (PDMS+, curing agent: PDMS-1:10) was poured in a petri-dish, degassed, and partially cured at 65°C. The partially cured PDMS was peeled off, cut in pieces with a surface area of approximately 2 cm by 3.5 cm. Subsequently, a hole with a diameter of 4 mm was punched in the PDMS+, creating a well-like structure. Then, the well was aligned with the matrix. PDMS+ was prepared, poured over the mold containing the structures of the microfluidic channels, degassed, and partially cured at 65°C. The partially cured PDMS+ was peeled off, cut, and aligned with the well, after which it was left to completely cure overnight at room temperature. Subsequently, the cured structure was peeled off the glass slide and the holes for the in- and outlets were punched. Again PDMS+ was prepared, poured over the mold containing the channel structures, degassed, partially cured, peeled off, and cut, after which it was aligned with the matrix attached to the already cured structure. The chip was left at 40°C to completely cure. The chip was flushed with isopropyl alcohol to remove the residuals of PDMS- from the matrix. Finally, female luers were attached to the in- and outlets.

Diffusion
Fluorescein isothiocyanate-dextran (Merck) was dissolved in a concentration of 2 mg ml^{-1} and added to the chondrogenic channel of an empty chip. Fluorescent images were obtained of the osteogenic channel every 5 min for 2 h at 37 °C using a fluorescent microscope (Leica, AF6000 LX). The average intensity was measured in these images using ImageJ.

Cell culture
Primary osteogenic cells and hPACs were isolated from human joints as described previously [11, 34]. Isolation of primary osteogenic cells results in a mixture of bone cells, i.e. MSCs, osteoblasts, and osteocytes. Comparison of expression levels of osteogenic and chondrogenic markers of these cells with the expression levels in subchondral bone, showed similar expression profiles [Tuerlings et al., under review]. Subsequently, the osteogenic cells and hPACs were expanded in 2D in osteogenic expansion medium (OBM) consisting of α-MEM + GlutaMAX (Thermofisher, 500 ml) supplemented with

heat-inactivated FCS (10%, Biowest) and penicillin-streptomycin (Gibco, 0.2%, 10000 U ml^{-1}) and chondrogenic expansion medium (MSC medium) consisting of DMEM (Thermofisher, 500 ml) supplemented with FCS (10%, Biowest), penicillin-streptomycin (0.2%, 10000 U ml^{-1}) and FGF-2 (0.5 ng ml^{-1}, PeproTech), respectively.

Prior to seeding the cells in the microfluidic model system, the microfluidic chips were coated with fibronectin (Merck Chemicals), by flushing the system with fibronectin in PBS solution and incubate overnight. Osteogenic cells were seeded at a concentration of 6.0×10^6 cells ml^{-1} into the bottom compartment of the chip. After incubation to allow the cells to attach, the chip was connected to a syringe pump (Nexus 3000, Chemyx), programmed to withdraw medium from the system once every hour, with a flow of 50 µl min^{-1} in every channel. After 24 h, the OBM was replaced with osteogenic differentiation medium (ODM) consisting of α-MEM + GlutaMAX (Thermofisher, 500 ml) supplemented with heat-inactivated FCS (10%, Biowest), dexamethasone (0.1 µm; Sigma-Aldrich), L-ascorbate-2-phosphate (50 µg ml^{-1}, Sigma-Aldrich), and penicillin-streptomycin (0.2%, 10 000 U ml^{-1}).

After 6 days of culturing, hPACs were seeded in the upper compartment of the microfluidic chip via the middle inlet located directly above the matrix (**Figure 1A**) at a concentration of 1.5×10^7 cells ml^{-1}. After incubation to allow the hPACs to attach, the chip was reconnected to the syringe pump. After 24 h, both media reservoirs were refreshed: β-glycerophosphate (5mm; Sigma-Aldrich) was added to the ODM and MSC medium was replaced with chondrogenic differentiation medium consisting of DMEM (Thermofisher) supplemented with L-ascorbate-2-phosphate (50 µg ml^{-1}, Sigma-Aldrich), L-Proline (40 µg ml^{-1}, Sigma-Aldrich), Sodium Puryvate (100 µg ml^{-1}, Sigma-Aldrich), Dexamethasone (0.1 µm, Sigma-Aldrich), ITS+ (Corning), TGF-β1 (10 ng ml^{-1}, PeproTech), and antibiotics. In the T3-induced hypertrophy experiments, 500 ng ml^{-1} T3 was added to both media from day 23 onwards. After 28 days of culture, the chips were harvested for further processing. An overview of the experiment timeline is shown in **Supplementary Figure 1**. 3D pellet cultures were formed by adding 2.5×10^5 cells in their expansion medium to a 15 ml Falcon tube and subsequently exposing them to centrifugal forces. After 24 h, the expansion medium was replaced by either osteogenic differentiation medium or chondrogenic differentiation medium. The medium was refreshed every 3–4 days.

Relative gene expression levels
The two compartments were manually separated and were lysed using Trizol (Invitrogen) and stored at −80 °C until further processing. RNA was isolated from the

8

samples using the RNeasy Mini Kit (Qiagen). cDNA synthesis was performed using the First Strand cDNA Synthesis Kit (Roche Applied Science). Subsequently, RT-qPCR was performed using SYBR Green without the ROX reference dye (Roche Applied Science) and the QuantStudio 6 Real-Time PCR system (Applied Biosystems). GAPDH and SDHA were used as housekeeping genes. The measured gene expression levels were corrected for the housekeeping genes GAPDH and SDHA, and the foldchanges were calculated using the $2^{-\Delta\Delta CT}$ method. All values were calculated relative to the

Histochemistry

For the different types of staining, the harvested materials were fixed with 4% formaldehyde, embedded in Tissue-Tek (Sakura), and sectioned at 25 μm thickness. After rehydration in PBS, Haematoxylin and Eosin staining was performed using the H&E stain Kit (Abcam). In addition, Alcian blue staining was performed using Alcian Blue 8-GX (Sigma) for 30 min and Alizarin red staining with Alizarin Red S (Sigma) for 1 min. All slides were mounted before brightfield imaging on Olympus BX53. Images were made with the Olympus DP26, using 4x and 20x objectives, and processed with Olympus cellSens Dimension 1.18 software. OPN and COL2 were visualized using immunohistochemistry. After rehydration, the tissue was blocked with 5% normal Goat serum (NGS, Sigma), incubated with primary rabbit anti-OPN antibody (HPA027541, Atlas antibodies) or with primary rabbit anti-COL2 antibody (ab34712, Abcam) followed by incubation of goat anti-rabbit Alexa Fluor 488 as the secondary antibody (ab150077, Abcam) and counterstained with DAPI prior to imaging on fluorescent microscope (Leica, AF6000 LX) with objectives HC PL FLUOTAR 10.0 × 0.30 DRY and HCX PL APO CS 20.0 × 0.75 DRY UV. Images were obtained with the Hamamatsu-C9100-02-COM4 camera and LASAF V2.7.4.10100 software and processed using ImageJ 1.53c.

DMMB Assay

sGAG concentration was measured in medium collected over 6 h from the chondrogenic compartment and measurements were done on two different time points, before (day 23) and after (day d28) exposure to hypertrophy by adding T3. Photometric 1.9 dimethylene blue (DMMB, Sigma Aldrich) dye was used to stain sGAGs, with Shark chondroitin sulfate (Sigma Aldrich) in culture medium as a reference. The collected medium from the chondrogenic compartment was diluted 30x, after which DMMB staining was added. Absorbance at 525 and 595 nm was measured using a microplate reader (Synergy HT, BioTek).

Statistical Analysis

For the RT-qPCR data, the minus delta CT values were used to perform the analysis. No outliers were visualized in the RT-qPCR data using boxplots. The RNA sequencing

data was pre-processed as described previously [9, 23] and variance stabilizing transformation was performed to normalize. The two-sided paired sample t-test was used to calculate significant differences in gene expression levels, considering p-value < 0.05 significant. Complete statistical output can be found in **Supplementary Table 2**. IBM SPSS Statistics, version 25 was used to perform all statistical analysis presented.

Declarations

Disclosures

The authors have no relevant financial or non-financial interests to disclose.

References

1. Chen, D., et al., *Osteoarthritis: toward a comprehensive understanding of pathological mechanism.* Bone Res, 2017. **5**: p. 16044.
2. Krishnan, Y. and A.J. Grodzinsky, *Cartilage diseases.* Matrix Biol, 2018. **71-72**: p. 51-69.
3. Wu, Y., et al., *Novel treatments for osteoarthritis: an update.* Open Access Rheumatol, 2018. **10**: p. 135-140.
4. Litwic, A., et al., *Epidemiology and burden of osteoarthritis.* Br Med Bull, 2013. **105**: p. 185-99.
5. Pan, J., et al., *Elevated cross-talk between subchondral bone and cartilage in osteoarthritic joints.* Bone, 2012. **51**(2): p. 212-7.
6. Goldring, S.R. and M.B. Goldring, *Changes in the osteochondral unit during osteoarthritis: structure, function and cartilage-bone crosstalk.* Nat Rev Rheumatol, 2016. **12**(11): p. 632-644.
7. Fellows, C.R., C. Matta, and A. Mobasheri, *Applying Proteomics to Study Crosstalk at the Cartilage-Subchondral Bone Interface in Osteoarthritis: Current Status and Future Directions.* EBioMedicine, 2016. **11**: p. 2-4.
8. Lories, R.J. and F.P. Luyten, *The bone–cartilage unit in osteoarthritis.* Nature Reviews Rheumatology, 2011. **7**(1): p. 43-49.
9. Coutinho de Almeida, R., et al., *RNA sequencing data integration reveals an miRNA interactome of osteoarthritis cartilage.* Ann Rheum Dis, 2019. **78**(2): p. 270-277.
10. den Hollander, W., et al., *Transcriptional associations of osteoarthritis-mediated loss of epigenetic control in articular cartilage.* Arthritis Rheumatol, 2015. **67**(8): p. 2108-16.
11. Bomer, N., et al., *Underlying molecular mechanisms of DIO2 susceptibility in symptomatic osteoarthritis.* Ann Rheum Dis, 2015. **74**(8): p. 1571-9.
12. Goldring, M.B. and S.R. Goldring, *Articular cartilage and subchondral bone in the pathogenesis of osteoarthritis.* Ann N Y Acad Sci, 2010. **1192**: p. 230-7.
13. Houtman, E., et al., *Human Osteochondral Explants: Reliable Biomimetic Models to Investigate Disease Mechanisms and Develop Personalized Treatments for Osteoarthritis.* Rheumatology and Therapy, 2021. **8**(1): p. 499-515.
14. Dreier, R., *Hypertrophic differentiation of chondrocytes in osteoarthritis: the developmental aspect of degenerative joint disorders.* Arthritis Res Ther, 2010. **12**(5): p. 216.
15. Bos, S.D., P.E. Slagboom, and I. Meulenbelt, *New insights into osteoarthritis: early developmental features of an ageing-related disease.* Curr Opin Rheumatol, 2008. **20**(5): p. 553-9.
16. Primorac, D., et al., *Knee Osteoarthritis: A Review of Pathogenesis and State-Of-The-Art Non-Operative Therapeutic Considerations.* Genes (Basel), 2020. **11**(8).
17. Lin, H., et al., *Stem cell-based microphysiological osteochondral system to model tissue response to interleukin-1β.* Mol

Pharm, 2014. **11**(7): p. 2203-12.

18. Lin, Z., et al., *Osteochondral Tissue Chip Derived From iPSCs: Modeling OA Pathologies and Testing Drugs.* Front Bioeng Biotechnol, 2019. **7**: p. 411.

19. Goldman, S.M. and G.A. Barabino, *Spatial Engineering of Osteochondral Tissue Constructs Through Microfluidically Directed Differentiation of Mesenchymal Stem Cells.* Biores Open Access, 2016. **5**(1): p. 109-17.

20. Wang, C.C., et al., *A highly organized three-dimensional alginate scaffold for cartilage tissue engineering prepared by microfluidic technology.* Biomaterials, 2011. **32**(29): p. 7118-26.

21. Ramos, Y.F., et al., *Genes involved in the osteoarthritis process identified through genome wide expression analysis in articular cartilage; the RAAK study.* PLoS One, 2014. **9**(7): p. e103056.

22. Bomer, N., et al., *Neo-cartilage engineered from primary chondrocytes is epigenetically similar to autologous cartilage, in contrast to using mesenchymal stem cells.* Osteoarthritis Cartilage, 2016. **24**(8): p. 1423-30.

23. Tuerlings, M., et al., *RNA sequencing reveals interacting key determinants of osteoarthritis acting in subchondral bone and articular cartilage.* Arthritis Rheumatol, 2020.

24. Miosge, N., et al., *Expression of collagen type I and type II in consecutive stages of human osteoarthritis.* Histochem Cell Biol, 2004. **122**(3): p. 229-36.

25. Komori, T., *Regulation of bone development and extracellular matrix protein genes by RUNX2.* Cell Tissue Res, 2010. **339**(1): p. 189-95.

26. Lui, J.C., et al., *Persistent Sox9 expression in hypertrophic chondrocytes suppresses transdifferentiation into osteoblasts.* Bone, 2019. **125**: p. 169-177.

27. Mueller, M.B., et al., *Hypertrophy in mesenchymal stem cell chondrogenesis: effect of TGF-beta isoforms and chondrogenic conditioning.* Cells Tissues Organs, 2010. **192**(3): p. 158-66.

28. Liu, W., et al., *Alpl prevents bone ageing sensitivity by specifically regulating senescence and differentiation in mesenchymal stem cells.* Bone Research, 2018. **6**(1): p. 27.

29. Duan, J., et al., *Irreversible cellular senescence induced by prolonged exposure to H2O2 involves DNA-damage-and-repair genes and telomere shortening.* The International Journal of Biochemistry & Cell Biology, 2005. **37**(7): p. 1407-1420.

30. Lee, H.-p., et al., *Mechanical confinement regulates cartilage matrix formation by chondrocytes.* Nature Materials, 2017. **16**(12): p. 1243-1251.

31. Houtman, E., et al., *Elucidating mechano-pathology of osteoarthritis: transcriptome-wide differences in mechanically stressed aged human cartilage explants.* Arthritis Research & Therapy, 2021. **23**(1): p. 215.

32. Piluso, S., et al., *Mimicking the Articular Joint with In Vitro Models.* Trends Biotechnol, 2019. **37**(10): p. 1063-1077.

33. Eslami Amirabadi, H., et al., *A novel method to understand tumor cell invasion: integrating extracellular matrix mimicking layers in microfluidic chips by "selective curing".* Biomedical Microdevices, 2017. **19**(4): p. 92.

34. Stern, A.R., et al., *Isolation and culture of primary osteocytes from the long bones of skeletally mature and aged mice.* Biotechniques, 2012. **52**(6): p. 361-73.

Supplementary files

Supplementary figures
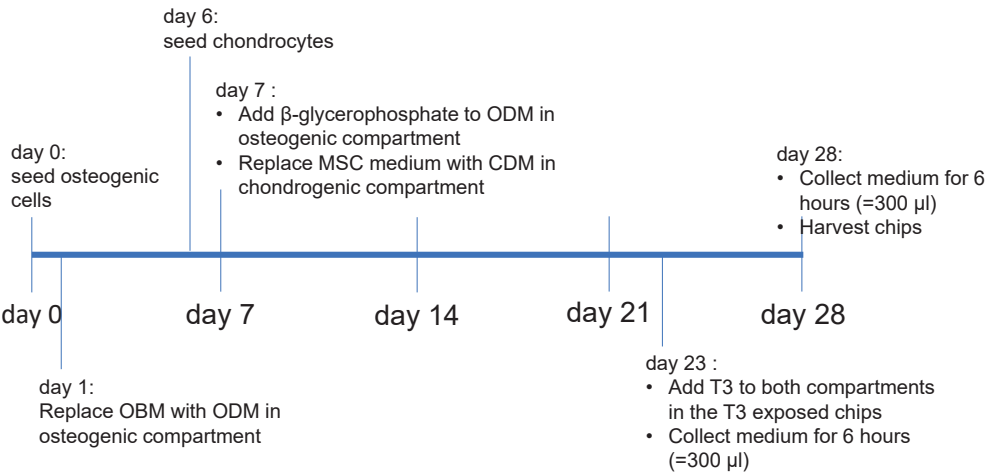
Supplementary Figure 1 – Timeline of cell culture in osteochondral unit-on-a-chip model system.
OBM: osteoblast medium/osteogenic expansion medium, ODM: osteogenic differentiation medium, and CDM: chondrogenic differentiation medium.
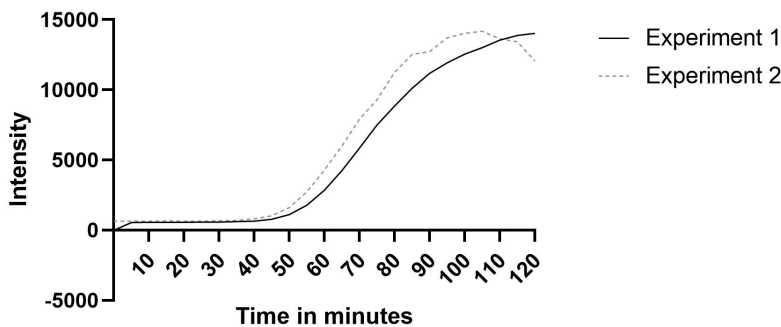

Supplementary Figure 2 – Diffusion of fluorescent Dextran over the PCL matrix.
Dextran was injected in the chondrogenic channel and average intensity was measured in the osteogenic channel, next to the matrix.
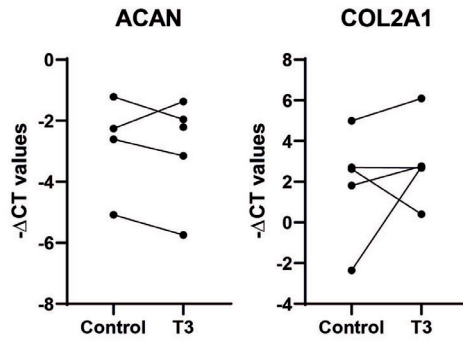
Supplementary Figure 3 – Gene expression levels of chondrogenic markers in the cartilage compartment of our model system upon exposure to T3 (n = 5 donors).
Two sided paired sample T-test was used for statistical assessment, with * $p < 0.05$, **$p < 0.005$, ***$p < 0.001$
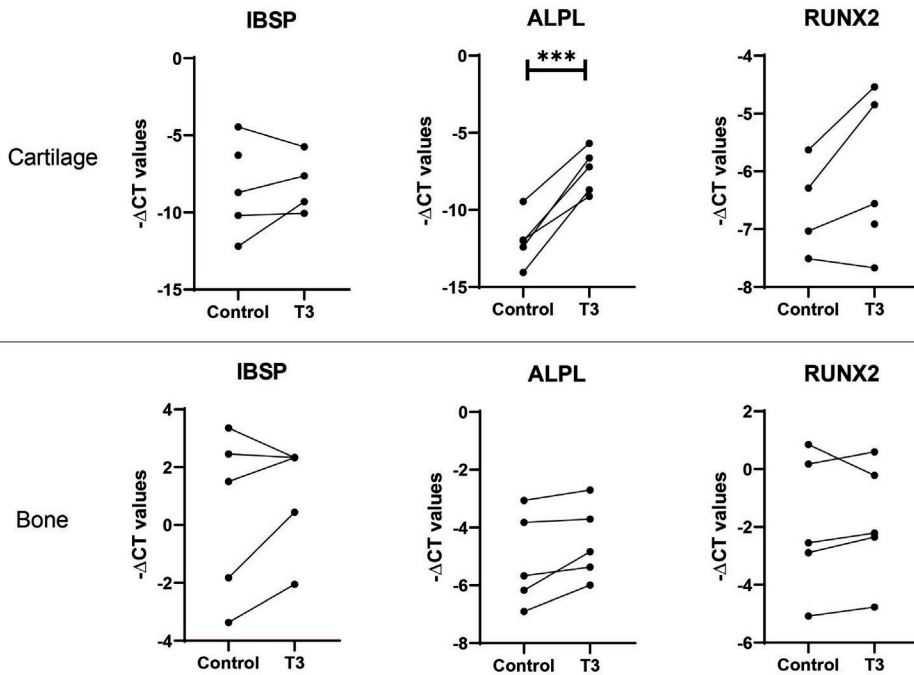
Supplementary Figure 4 – Gene expression levels of hypertrophy markers in the 3D chondrocyte cell pellet cultures (A) and in the 3D osteogenic cell pellet cultures (B) upon exposure to T3.
Two sided paired sample T-test was used for statistical assessment, with * $P < 0.05$, **$P < 0.005$, ***$P < 0.001$

8

Chapter 8

Supplementary tables

Supplementary Table 1 - Baseline characteristics
Supplementary Table 1A- Baseline characteristics of donors used in chip.

	Total (N=4)
Age	68.8 (8.0)
Females	2 out of 4

Supplementary Table 1B- Baseline characteristics of donors used in RNAseq.

	Total (N=15)
Age	67.5 (8.7)
Females	13 out of 15

Supplementary Table 1C- Baseline characteristics of donors used in implementation of an age-related disease model

	Total (N=5)
Age	67.0 (4.5)
Females	5 out of 5

Supplementary Table 2 – Statistical two-sided t-test output
Supplementary Table 2A – Gene expression analysis comparison of bone/cartilage

	Chip/ Pellet RNA-seq	Gene	Paired Differences							
			Mean	Std. Deviation	Std. Error Mean	95% Confidence Interval of the difference Lower	Upper	t	df	Sig. (2-tailed)
Pair 1	Chip	COL2A1	3.17216	1.9073	0.85297	0.80393	5.54038	3.719	4	0.02
Pair 2	Chip	ACAN	0.1257	1.24377	0.55623	-1.41865	1.67005	0.226	4	0.832
Pair 3	Chip	OPN	-3.06909	2.16151	0.96666	-5.75296	-0.38522	-3.175	4	0.034
Pair 4	Chip	RUNX2	-1.82933	1.22662	0.54856	-3.35239	-0.30628	-3.335	4	0.029
Pair 5	Chip	COL1A1	0.94232	1.45425	0.65036	-0.86336	2.74801	1.449	4	0.221
Pair 6	Pellet	COL2A1	10.21819	3.72916	2.15303	0.95445	19.48193	4.746	2	0.042
Pair 7	Pellet	ACAN	3.83059	2.13497	1.06749	0.43337	7.22781	3.588	3	0.037
Pair 8	Pellet	OPN	-7.34399	2.361	1.1805	-11.1009	-3.58712	-6.221	3	0.008

8

	Chip/ Pellet/ RNA-seq	Gene	Paired Differences							
			Mean	Std. Deviation	Std. Error Mean	95% Confidence Interval of the difference		t	df	Sig. (2-tailed)
						Lower	Upper			
Pair 9	Pellet	RUNX2	-3.21201	0.8514	0.4257	-4.56677	-1.85725	-7.545	3	0.005
Pair 10	Pellet	COL1A1	-0.35708	0.81123	0.40561	-1.64792	0.93376	-0.88	3	0.443
Pair11	RNA-seq	COL2A1	-5.73411	1.990794	0.514021	-6.83657	-4.63164	-11.1554	14	2.37E-08
Pair 12	RNA-seq	ACAN	-4.74167	2.118074	0.546884	-5.91462	-3.56872	-8.67033	14	5.3E-07
Pair 13	RNA-seq	OPN	3.026371	1.713188	0.442343	2.077639	3.975103	6.84168	14	8.04E-06
Pair 14	RNA-seq	RUNX2	3.30432	1.442733	0.372512	2.505361	4.103279	8.870373	14	4.04E-07
Pair 15	RNA-seq	COL1A1	1.085628	2.841655	0.733712	-0.48803	2.659284	1.479638	14	0.161

Supplementary Table 2B – Gene expression analysis comparison of an age-related disease model in the chip

| | Bone/ | Gene | Mean | Std. Deviation | Std. Error Mean | Paired Differences 95% Confidence Interval of the difference | | t | df | Sig. (2-tailed) |
						Lower	Upper			
	Cartilage									
Pair 1	Bone	*ISBP*	1.19103	1.53125	0.68480	-0.71027	3.09233	1.739	4	0.157
Pair 2	Bone	*ALPL*	1.36190	1.02431	0.45809	0.09005	2.63375	2.973	4	0.041
Pair 3	Bone	*RUNX2*	0.54400	0.95929	0.42901	-0.64711	1.73511	1.268	4	0.274
Pair 4	Cartilage	*ISBP*	2.33096	1.53169	0.68499	0.42912	4.23281	3.403	4	0.027
Pair 5	Cartilage	*ALPL*	1.49905	2.01954	0.90317	-1.00855	4.00664	1.660	4	0.172
Pair 6	Cartilage	*RUNX2*	0.94600	1.00925	0.45135	-0.30715	2.19915	2.096	4	0.104

8

CHAPTER 9

General Discussion and future perspectives

Summary

Osteoarthritis (OA) is a prevalent disabling age-related disease with multiple tissues involved. Due to a major backlog in development of disease modifying OA drugs (DMOADs), available treatment options are restricted to pain relief and costly total joint replacement (TJR) surgery at end-stage disease. Despite the societal burden of these large number of TJR surgeries, it provides the OA research society with an invaluable and continues supply of OA disease relevant tissues, such as articular cartilage, subchondral bone, synovium and synovial fluid. In the current thesis the joint tissues collected within the RAAK study were fully exploited to gain insight into the biological mechanisms and the diversity in pathophysiological processes in bone and cartilage [1-3]. Henceforth, three main intertwined strategies were applied 1) study of ongoing OA pathophysiology by molecular characterization of bone and cartilage in interaction, 2) identify non-invasive molecular biomarkers in the circulation that report on these pathophysiological processes, and 3) apply and advance functional genomic studies and *in vitro* disease modelling to study downstream actions of compelling OA risk variants and respective genes on joint tissue homeostasis and chondrocyte function.

Osteoarthritis molecular pathophysiology

The study of ongoing OA pathophysiological processes, thus far, focussed primarily on molecular analyses of articular cartilage, as exemplified by multiple differential -omic studies to date published on healthy, macroscopically preserved and lesioned articular cartilage of an OA joint (**Figure 1**). These studies provided valuable insight in the molecular OA landscapes e.g. mRNA, microRNAs (miRNAs), long non-coding RNAs (lncRNAs) of cartilage as well as the pathways in which these molecules act [3-6]. Nonetheless, insight in the molecular landscape of subchondral bone remained elusive. This despite the fact that multiple OA risk genes identified in genome wide association studies (GWAS) are involved in maintenance processes in both cartilage and bone, hence indicating that unfavorable processes in both tissues could drive OA onset and progression [7-10]. To fill this gap of knowledge, in **chapter 2** and **chapter 3** we applied RNA-sequencing (RNA-seq) of OA subchondral bone to identify mRNA and lncRNAs that mark OA pathophysiology herein. To study the interaction and overlap with OA pathophysiology in articular cartilage, previously assessed transcriptome wide data of matching cartilage [4] was introduced in these analyses. Moreover, the previously identified OA molecular endotypes in cartilage (**Figure 1**) [11-13] were further characterized in subchondral bone in **chapter 5**. Besides the heterogeneity between patients also heterogeneity between joint site is observed (**Figure 1**), which is also further discussed in this thesis (**chapter 2** and **chapter 3**).
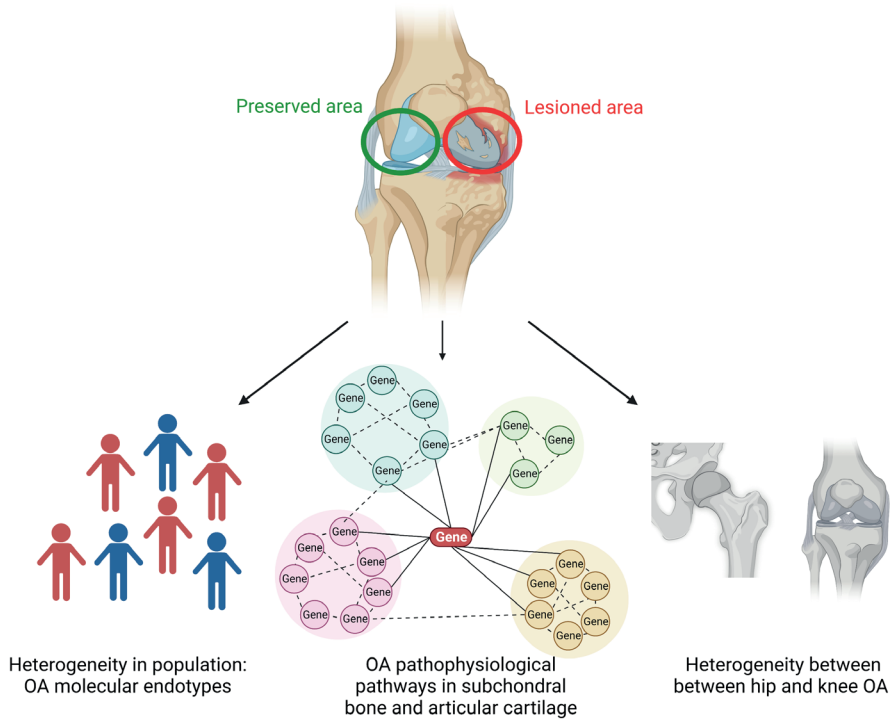
Figure 1 – Transcriptomic data analysis to characterize OA pathophysiology.
Transcriptomic data can be used to characterize pathophysiological pathways. In addition, transcriptomic data can be used to investigate OA heterogeneity either between patients or between joint site. (created with Biorender.com)

Non-invasive biomarkers for osteoarthritis

Thus far, classification and/or diagnosis of OA is solely based on radiography and clinical symptoms, such as pain and stiffness. This indicates that there is an unmet need for reliable biomarkers that reflect ongoing processes in joint tissues in general [14]. Most studied biomarkers for OA are biochemical markers in serum or urine, such as sCOMP and uCTX-II, which are often degradation products of joint tissues [15-17]. Nonetheless, only a few of these biochemical markers are tested for clinical use, as these markers often are a-specific with regard to OA pathophysiological tissue progression, they do not mark early OA, and they are not highly predictive [18-20]. For that matter, studies implicate circulating microRNAs as novel promising biomarkers, as they are stable in plasma and serum and could report on (patho-)physiological processes [21-23]. Recently, we showed for the first time that miRNAs in plasma were indeed able to reflect early OA related mRNA expression patterns in articular cartilage [24]. As proof-of-principle, in this thesis, we exploited plasma miRNA dataset for identification of miRNAs that could serve as biomarkers for classification of patients based on their

9
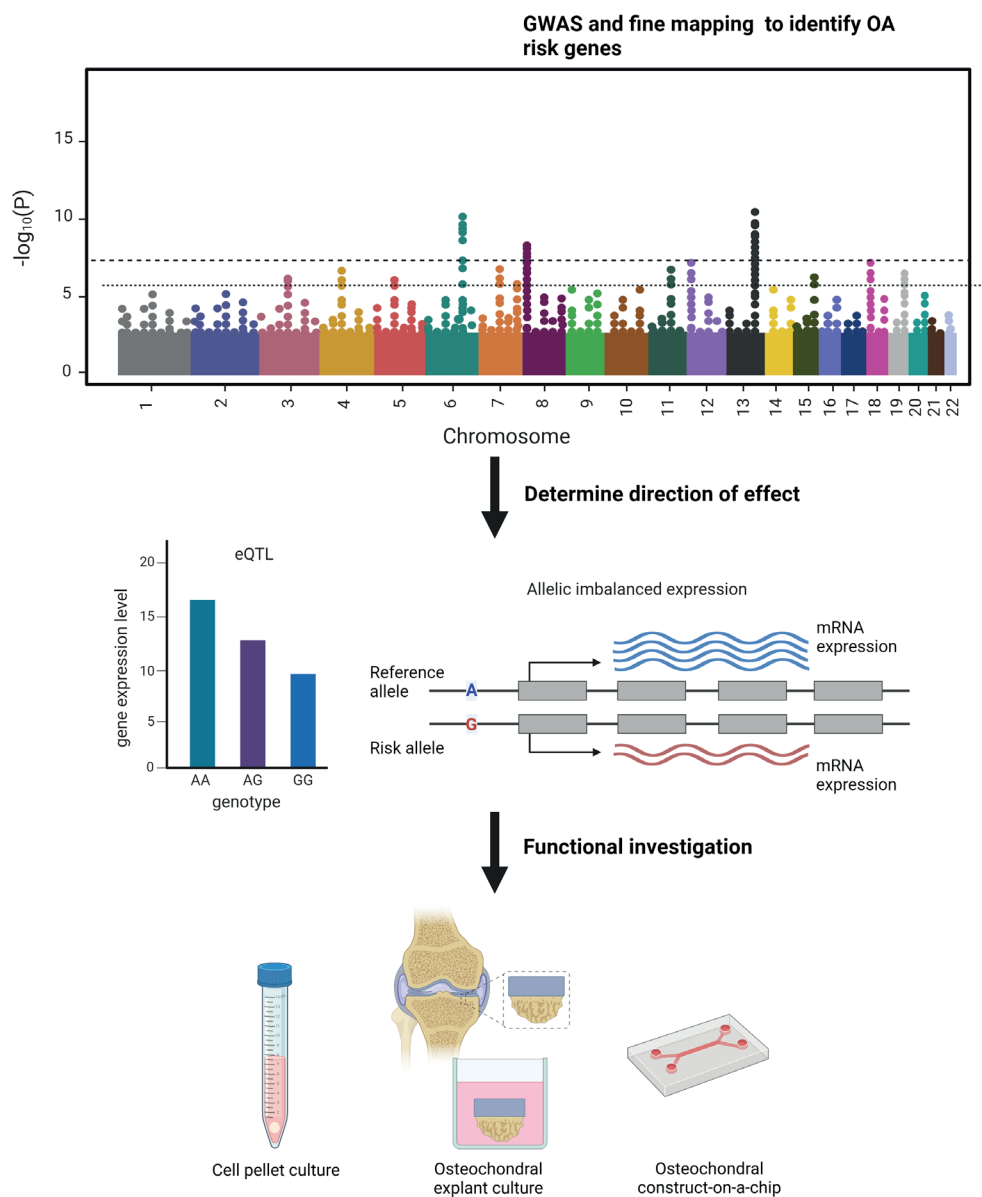
Figure 2 – Concept workflow for translation of OA risk genes towards development of DMOADs.
OA susceptibility genes are identified by performing genome-wide association studies and fine mapping. Subsequently, the direction of effect should be determined by either eQTL or allelic imbalanced expression analysis. Finally, the hypothesis on the direction of effect needs to be tested in an in vitro or ex vivo disease model system. (Created with Biorender.com)

previously identified OA molecular endotypes of preserved articular cartilage (**chapter 4**).

Genetic predisposition

Genetic predisposition is found to be a strong risk factor in many age-related chronic diseases [25], including OA [26]. The function of genes conferring this risk, that are identified by genome wide association studies (GWAs), provide valuable information on the biological pathways involved in disease aetiology [27]. For that matter, multiple comprehensive GWAS studies for OA have been performed with over 100 robust association signals [28-30]. The function of identified OA genes highlighted that OA aetiology is driven by dysfunctional maintenance processes in cartilage and bone. Nevertheless, strikingly little progress has been made in translating OA risk SNPs to underlying biological mechanisms, drug targets, and development of DMOADs [31]. In this thesis we, therefore, applied a functional genomic approach (**Figure 2**) to study two compelling OA risk alleles. Rs1052429-A, located in the 3'UTR of *WWP2* gene, was previously shown to be associated with increased expression of *WWP2* [32, 33] and rs4252548-T, located in *IL11* gene, that was shown to decrease stability of IL11. Hereto, we studied the downstream effects of *WWP2* upregulation in 3D chondrocyte pellet cultures in **chapter 6** and studied whether hrIL11 protein addition could rescue the OA state in osteochondral explant cultures in **chapter 7**. Finally, in **chapter 8** we developed a novel biomimetic *in vitro* model system representing functional articular cartilage and subchondral bone in interaction to study OA-related perturbations and/ or OA susceptibility genes.

Together in this thesis, we tried to make a step forward in transition from bench-to-bedside in OA by combining previously reported GWAS and allelic imbalance results, with molecular profiling of subchondral bone and articular cartilage and functional investigation of OA risk genes (**Figure 2**).

Molecular characterization of subchondral bone osteoarthritis pathophysiology in comparison to articular cartilage

To gain insight in OA pathophysiology of subchondral bone, in interaction with articular cartilage, in this thesis we have compared gene and lncRNA expression levels between macroscopically preserved and lesioned OA subchondral bone. Subsequently, we have compared these results with previously reported results on (differentially) expressed genes and lncRNAs in OA articular cartilage [4, 6]. Moreover, we have integrated these results with genetic findings [30] and allelic imbalanced expression [32, 33].

9
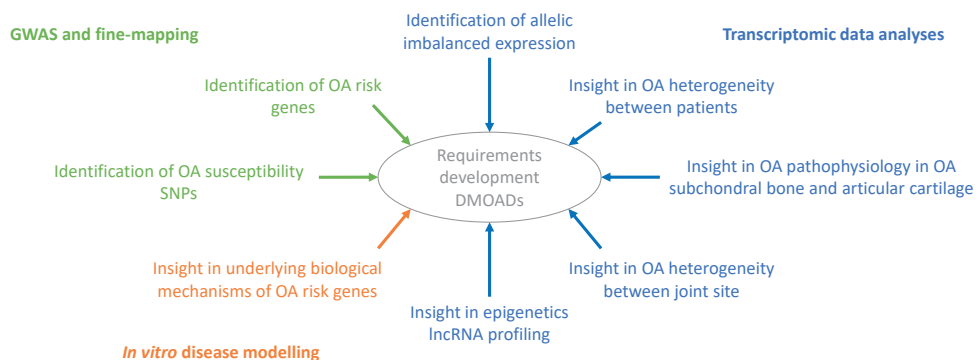
Figure 3 – overview of different requirements in the development of DMOADs.
Development of DMOADs requires combining GWAS, transcriptomic data analyses, and in vitro or ex vivo disease modeling.

In development of DMOADs (**Figure 3**) targeting genes or pathways that are active with OA pathophysiology in both articular cartilage and subchondral bone could be an attractive strategy, as targeting these genes or pathways would have therapeutic effects in these two most important joint tissues affected by OA. Since using transcriptomic data to identify genes and/or pathways based on differential expression analysis with ongoing OA per definition does not provide insight in cause or consequence, integration of these data with genetic studies is required to identify common genes in articular cartilage and subchondral bone that are most likely causal to OA. In this respect and given that drug targets founded by genetic evidence have at least two times higher success rates [34, 35], in **chapter 2** we have searched for genes that were responsive to OA pathophysiology in both articular cartilage and subchondral bone with similar directions of effects and filtered these genes for OA risk genes identified in previously reported comprehensive GWAS [30, 36]. In doing so, we have identified 305 genes marking the OA pathophysiological process in both articular cartilage and subchondral bone, of which *IL11* and *CHADL* were previously identified as OA risk gene. To make firm hypothesis on the direction of effect of *IL11* and *CHADL,* we have explored previous findings on these genes. Given that the *IL11* risk variant is a missense variant resulting in a thermally unstable protein [37], we and others hypothesized that decreased expression of IL11 confers risk to OA. As such, increasing IL11 protein levels was previously proposed as OA treatment strategy [36]. Remarkable is that *IL11* gene expression levels are highly upregulated in lesioned compared to preserved OA articular cartilage and subchondral bone, reflecting that there is not necessarily a lack of potency to produce IL11 or signal via IL11, unless translation of the protein or binding of IL11 to its receptors is hampered. Founded by expression quantitative trait loci (eQTL) in adipose and skeletal muscle tissue, the OA risk variant located in an intron of *CHADL* acts

via increased expression of *CHADL* [38]. It has previously been shown that recombinant CHADL binds to collagen and inhibits collage fibril formation *in vitro* [39]. Moreover, *CHADL* knockdown in a chondrogenic mice cell line was stated to increase chondrogenic differentiation as shown by increased deposition of *COL2* and *ACAN* [40]. Based on these findings, we hypothesize that increased levels of *CHADL* have negative effects in both articular cartilage and subchondral bone, by decreasing the extracellular matrix (ECM) stability in both tissues and thereby predisposing to OA. Hence, we propose inhibition of *CHADL* as a potential therapeutic strategy for OA. Thus far, no approved drugs are available to inhibit *CHADL* [41] and further functional investigation is required to better understand the mode-of-action of *CHADL* in predisposing to OA.

More recent, the largest GWAS meta-analysis so far was reported, identifying 100 independent SNPs being associated with OA [28]. Upon intersecting the nearest genes of these 100 SNPs with the 305 genes showing similar directions of effect in articular cartilage and subchondral bone, we additionally found *GLIS3, DGKI,* and *SLC44A2* as potential druggable targets (**Table 1**). The functions of *GLIS3, DGKI*, and *SLC44A2* in articular cartilage and/or subchondral bone are still unknown. Nonetheless, risk allele rs10405617-A, located in an intron of *SLC44A2,* marks higher expression of *SLC44A2* compared to rs10405617-G in skeletal muscle tissue according to GTEx project [38], suggesting that increased *SLC44A2* expression confers risk to OA. Functional *in vitro* or *ex vivo* studies on these potential therapeutic targets are still necessary to understand their mode-of-action and confirm their effects on articular cartilage and subchondral bone causing predisposal to OA.

LncRNAs are relatively new molecules being investigated in the OA field as they are poorly evolutionarily conserved and are generally less abundantly expressed, making them more difficult to study compared to for example mRNA or miRNAs [42]. Nonetheless, lncRNAs could serve as attractive potential druggable targets since they are known to be highly tissue specific and have regulatory roles in various transcriptional and (post-)translational processes [43, 44]. Given these unique features, targeting lncRNAs as therapeutic strategy for OA might be superior to targeting proteins in terms of potential unbeneficial side-effects associated with their targeting [45]. Henceforth, in **chapter 3** we have characterized lncRNAs that are (differentially) expressed in OA subchondral bone in comparison to OA articular cartilage to identify potential therapeutic targets. We found a relatively large number of lncRNAs (N=1090 lncRNAs) that were robustly expressed in both articular cartilage and subchondral bone. This large overlap in expressed lncRNAs might be due to the common mesodermal origin of these tissues. Among differentially expressed lncRNAs between preserved and lesioned OA tissue we have identified five lncRNAs overlapping between articular cartilage

9

and subchondral bone, including *AC005165.1* being downregulated in both lesioned tissues. In subchondral bone *AC005165.1* was even identified as the most significantly downregulated lncRNA. To explore which genes or pathways are targeted by *AC005165.1* in subchondral bone, we have performed spearman correlations between *AC005165.1* expression levels and all differentially expressed protein-coding genes in subchondral bone. The highest (positive) correlation was found between *AC005165.1* and *FRZB* and this potential interaction was confirmed by downregulation of *AC005165.1* in primary osteogenic cells using LNA GAPmeRs resulting in consistent downregulation of *FRZB*. Interestingly, *FRZB* is a well-known OA gene and it is known to inhibit canonical WNT-signaling [46]. Moreover, decreased expression of *FRZB* was previously shown to confer risk to OA [47-49]. These data, together with the fact that *AC005165.1* and *FRZB* are both significantly downregulated with OA in both articular cartilage and subchondral bone, suggest that dysregulated *AC005165.1* directly or indirectly causes dysregulation of *FRZB*. Therefore, upregulation of *AC005165.1* might be an attractive therapeutic strategy to maintain *FRZB* levels in both tissues. Nonetheless, the mode-of-action of how *AC005165.1* affects *FRZB* gene expression remains still unknown and additional functional investigation in both articular cartilage and subchondral bone is required. A first follow-up experiment could be generating a lentiviral mediated upregulation of *AC005165.1* in an advanced *in vitro* OA model representing cartilage and bone and perform RNA-seq to identify all direct and indirect targets of *AC005165.1* in both tissues. Compared to 2387 differentially expressed genes previously identified between preserved and lesioned articular cartilage [4], we have identified only 1569 genes differentially expressed in subchondral bone (**chapter 2**). Similar results were seen for differentially expressed lncRNAs, as we previously have identified 191 differentially expressed lncRNAs between preserved and lesioned articular cartilage [6] while only 21 lncRNAs have been identified in subchondral bone (**chapter 3**). These differences in number of differentially expressed genes and lncRNAs might reflect the fact that bone as multicellular tissue is more heterogeneous in terms of expression levels, while articular cartilage only resides one cell-type. The advantage of using bulk RNA-seq data of subchondral bone was that we were able to almost directly compare our findings with previous findings on articular cartilage. However, a disadvantage was that the identified genes and lncRNAs represent overall average expression changes, confounded by variation in cell type proportions and ignoring cell-specific changes present in subchondral bone. To overcome this issue of multicellular tissues, cellular deconvolution methods are computational methods that can be applied to correct for cell type proportions present in bulk data [50]. However, these methods require sensitive markers for each cell type expected to be present in the bulk data, which were not yet available for subchondral bone. Moreover, these cellular deconvolution methods are affected by normalization and transformation of the data. Alternative and more

Table 1 – OA risk genes identified in large GWAS that are differentially expressed between preserved and lesioned OA subchondral bone and articular cartilage, showing similar directions of effect.

SNP	Nearest gene	Suggested gene expression risk	Subchondral bone		Articular cartilage		GWAS reference
			FC gene	FDR gene	FC gene	FDR gene	
rs4252548	IL11	decreased expression	4,16	2,44E-03	22,80	1,53E-20	[28, 30, 36]
rs117018441	CHADL	increased expression	0,63	2,33E-02	0,63	1,29E-02	[30, 40]
rs10974438	GLIS3	Unknown	1,45	5,95E-03	1,88	1,02E-05	[28]
rs571734653	DGKI	Unknown	1,44	1,50E-02	2,07	5,49E-05	[28]
rs10405617	SLC44A2	increased expression	0,85	1,91E-02	0,80	2,85E-02	[28]

9

advanced methods to take into account multiple cell types present in bone are single-cell RNA-seq (scRNA-seq) or spatial transcriptomics [51, 52]. Next to providing valuable insight in cell types present subchondral bone or OA-disease state, scRNA-seq could also provide insight into cell-type specific alterations between preserved and lesioned tissue [53]. In spatial transcriptomics, this single-cell level expression pattern is linked to cellular location within the tissue [54]. Both methods could provide additional insight in OA pathogenesis and should be implemented in future studies.

Heterogeneity in osteoarthritis: molecular endotypes and non-invasive biomarkers

Failure of DMOADs development is partly caused by the fact that it has followed a "one-drug-fits-all-patients" approach, in which heterogeneity, such as OA molecular endotypes, is ignored [17, 55]. Previous studies have identified two consistent and robust OA endotypes based on unique molecular landscapes of OA preserved articular cartilage [12, 13]. Molecular endotype A and B described a hypertrophy-driven and inflammatory-driven OA pathophysiological process, respectively. Moreover, endotype B OA patients showed significantly more joint space narrowing compared to endotype A. Given this intrinsic difference in OA pathophysiology between endotype A and B patients, we evaluated whether the genes we put forward as potential druggable targets in this thesis are specific to one of the endotypes. As shown in **Table 2**, *CHADL, GLIS3, DGKI, SLC44A2, MAP2K6* and *WWP2* expression levels were only responsive to OA pathophysiology in endotype A patients, suggesting these targets may be particularly or only of interest for treatment of endotype A relative to endotype B patients. Vice versa, *HLA-DPA1* expression levels were only responsive to OA pathophysiology in endotype B patients, suggesting targeting *HLA-DPA1* may be particularly of interest for treatment of endotype B relative to A patients. These data indicate that different OA therapeutic strategies between these patients are necessary and endotype-based stratification of patients before starting clinical trials, for example, could potentially result in higher success rates [17, 55]. Nonetheless, since these potential druggable targets play a role in both articular cartilage and subchondral bone, knowledge on whether these OA molecular endotypes exist in subchondral bone is required to enable treatment of the osteochondral unit as a whole. Therefore, in this thesis we have identified blood-based biomarkers to enable OA endotype stratification before starting treatment and we have characterized these OA molecular endotypes in subchondral bone.

To enable molecular endotype-based stratification of patients before treatment starts, non-invasive biomarkers that reflect ongoing processes in articular cartilage are required. Based on our recent work showing that circulating miRNAs are able to reflect ongoing processes in articular cartilage of OA joints [24], in **chapter 4** we have

searched for circulating miRNAs that mark OA molecular endotypes. In doing so, we have identified four miRNAs that together with sex and age predicted OA molecular endotype with 86% accuracy in a dataset different from the training dataset. These miRNAs could potentially be used in the clinic to stratify patients on their OA molecular endotype before treatment starts. Of note is that the datasets used to identify and validate these circulating miRNAs were small and replication in a large dataset would be required to confirm these results. Nonetheless, circulating miRNAs as biomarker for OA molecular endotypes and OA pathophysiology in general could provide a new window of opportunities for effective personalized OA treatment strategies and might result in more successful clinical trials.

To gain knowledge on whether similar molecular differences are seen in subchondral bone between OA molecular endotypes identified in articular cartilage, in **chapter 5** we focused on characterization of these endotypes in subchondral bone of 14 patients. We have shown that endotype A and B patients indeed exhibit distinct transcriptomic profiles in preserved OA subchondral bone. This difference between endotypes was shown to be enriched for similar processes in articular cartilage, such as immune response and positive regulation of IL6 production, with higher expression of these markers in both tissues in endotype B relative to endotype A patients. Moreover, differential expression analysis between preserved and lesioned OA subchondral bone suggested that particularly endotype B patients showed excessive bone formation in response to OA pathophysiology, characterized by expression of *COL1A1, COL1A2, GDF6*, and *CXCL9,* which is in line with observed increased joint space narrowing. Altogether, these data indicate that endotype B patients exhibit an atypical OA disease process, with detrimental inflammation in both articular cartilage and subchondral bone, resulting in excessive cartilage degeneration and bone formation. Related to the potential druggable targets we put forward in this thesis (**Table 2**), we found *CHADL* and *FRZB* being responsive to OA pathophysiology in subchondral bone specifically in endotype A patients, while *GLIS3* was responsive specifically in endotype B patients. More extensive characterization of these OA molecular endotypes in subchondral bone in a larger dataset could provide additional information on the other potential druggable targets, as larger datasets are more sensitive to identify smaller gene expression differences.

Attractive druggable targets identified in this thesis: potential treatment strategies
Based on genetics, differential expression between macroscopically preserved and lesioned OA articular cartilage and subchondral bone, and/or molecular endotypes, in this thesis we have put forward nine genes (**Table 2**) as attractive potential targets for OA treatment strategies. Of these nine genes, *FRZB* and *IL11* gene expression levels were

Table 2 – Potential druggable targets put forward in this thesis and their expression differences stratified for molecular endotype in articular cartilage and subchondral bone

Gene	Articular cartilage			Subchondral bone		
	Fold change OA vs P endotype A	Fold change OA vs P endotype B	Fold difference B vs A	Fold change OA vs P endotype A	Fold change OA vs P endotype B	Fold difference B vs A
CHADL (chapter 2)	0.56	n.s.	n.s.	0.51	n.s.	n.s.
IL11 (chapter 2 and 7)	18.87	59.64	n.s.	n.s.	n.s.	n.s.
FRZB (chapter 3)	0.25	0.26	0.34	0.53	n.s.	n.s.
MAP2K6 (chapter 5)	0.70	n.s.	0.38	n.s.	n.s.	n.s.
HLA-DPA1 (chapter 5)	n.s.	0.33	5.89	n.s.	n.s.	n.s.
WWP2 (chapter 6)	0.74	n.s.	n.s.	n.s.	n.s.	n.s.
GLIS3 (chapter 9)	2.24	n.s.	n.s.	n.s.	2.46	n.s.
DGKI (chapter 9)	2.39	n.s.	2.39	n.s.	n.s.	n.s.
SLC44A2 (chapter 9)	0.71	n.s.	n.s.	n.s.	n.s.	n.s.

responsive to OA pathophysiology in both articular cartilage and subchondral bone and in both OA molecular endotypes, suggesting that targeting these genes could be a therapeutic strategy for all OA patients. The other genes were either more specific to OA molecular endotype A or molecular endotype B, stressing the importance of personalized medicine in OA treatment strategies. Because development of therapeutics is a time-consuming and expensive process with high failure rate, last decade drug repurposing strategies gained interest for various diseases [56, 57]. Drug repurposing is a strategy that involves application of approved drugs outside the scope of the original use [58]. Valuable tools in drug repurposing are publicly available online databases, such as drug-gene interaction database (DGIdb 4.0), in which drug-gene interactions are predicted [41]. For that matter, we have screened our genes of interest for interactions with FDA approved drugs (**Table 3**). We only have found drug-gene interactions for *IL11* and *MAP2K6.* Drug-gene interactions for *IL11* include bisphosphonates (alendronic acid and etidronic acid), usually prescribed for treatment of osteoporosis, anti-depressants (escitalopram and citalopram), and cancer therapeutics (azacytidine, fluorouracil, and doxorubicin). The directions of effect of these drugs on *IL11* remains unknown. Drug-gene interactions for *MAP2K6* were all three cancer therapeutics and are predicted to have inhibitory effects on *MAP2K6*, matching the direction of desired effect. Nevertheless, predicted drug-gene interactions does not necessarily reflect effectiveness of the drug with OA. Therefore, functional studies are required to first understand how these genes affect articular cartilage and subchondral bone homeostasis and second to understand what the effect of the drug is. Moreover, application of these drugs in the clinic require additional studies on administration methods, side-effects, and doses [59].

Proof-of-concept: in vitro investigation of OA risk genes *WWP2* and *IL11*
To enable translation from genetic and genomic studies towards the development of DMOADs, insight in underlying biological mechanisms of OA risk genes is essential. As proof-of-concept (**Figure 2**), the next step in this thesis was to functionally investigate OA risk genes *WWP2* and *IL11* using two models that we have set up previously: 3D primary chondrocyte pellet cultures [60, 61] and human osteochondral explant cultures [62-65].

One of the top findings in a previously performed screen for allelic imbalanced expression in articular cartilage was rs1052429, located in *WWP2* gene. This SNP showed highly significant allelic imbalanced expression and allele rs1051429-A was associated to minimal joint space width, a characteristic of OA, and marked increased expression of *WWP2*. Moreover, rs34195470, a proxy of rs1052429, was identified conferring genome-wide significant risk to OA in large comprehensive genome-wide meta-analyses [28, 30]. Comparison of macroscopically preserved and lesioned OA articular cartilage previously

9

revealed that *WWP2* gene expression was significantly downregulated in lesioned tissue [4]. Nevertheless, differential expression analysis reflects the tissue response to OA pathophysiological process and gene expression differences identified in such analysis are not necessarily causal to OA pathophysiology. Therefore, we advocate that is essential to formulate hypotheses on direction of effects of OA genes based on genetics, such as allelic imbalanced expression or eQTL (**Figure 2**). Based on allelic imbalanced expression [32], we made the firm hypothesis that rs1052429-A acts via increased expression levels of *WWP2* conferring risk to OA. Henceforth, to mimic this effect we have generated lentiviral particle-mediated upregulation of full length *WWP2* in 3D primary chondrocyte pellet cultures (**chapter 6**). After seven days of pellet culture, we have observed detrimental effects on cartilage matrix deposition in terms of gene expression levels upon *WWP2* upregulation. These detrimental effects were reflected by significant downregulation of *ACAN* and *COL2A1,* marking cartilage anabolism, and changed gene expression of *EPAS1, GJA1, GDF10,* and *STC2,* all four genes involved in chondrocyte dedifferentiation to bone [66-71]. Chondrocyte dedifferentiation results in a shift from collagen type 2 to collage type 1 production, resulting in more fibrotic cartilage [72]. Since *WWP2* is known to be involved in (post-)translational modifications [73], we have performed proteomics analysis on our 3D chondrocyte pellet cultures to gain insight in protein expression differences upon *WWP2* upregulation. As articular cartilage ECM consists of dense insoluble collagen networks, extracting proteins can be challenging [74]. Consequently, we have performed proteomics on day three (less ECM expected) and day seven (more ECM expected) of chondrocyte pellet cultures. Protein extraction of both days was successful and cartilage markers, such as COL2A1, ACAN, COMP, and FN1, were already abundantly expressed after three days of pellet culture. Based on these results we have pooled proteomic data of day three and seven (to increase power) to evaluate the effects of WWP2 upregulation. In total, 42 proteins were identified being differentially expressed, which were enriched for ubiquitin conjugating enzyme activity. Altogether, our hypothesis based on genetics was confirmed by functional investigation of *WWP2* in cartilage. Nonetheless, this study did not yet include cartilage in interaction with subchondral bone. Moreover, multiple differentially methylated CpGs located in *WWP2* are identified [75], of which the effects are not addressed in this thesis. Since WWP2 is a E3 ubiquitin ligase and differentially expressed proteins were enriched for ubiquitination-related processes, upregulation of WWP2 could also affect proteins cellular location, activity, and protein-protein interactions without changing expression levels itself [76, 77], which was not captured by our read-outs. Finally, in this thesis we suggested that miRNA-140 could potentially have a regulatory effect on *WWP2,* which should be further investigated. In conclusion, to get full understanding of the underlying mechanisms of how *WWP2* confers risk to OA, integration of multi-omics data and functional experiments, preferable in a model system representing functional

Table 3 – Predicted drug-gene interactions for genes of interest using DGIdb [41], showing interactions for IL11 and MAP2K6.

Gene	Gene expression risk	Reported drug-gene interactions (approved)[41]	Direction of drugs
CHADL (chapter 2)	Increased	none	-
IL11 (chapter 2 and 7)	*Decreased*	ALENDRONIC ACID, ETIDRONIC ACID, ESCITALOPRAM, CITALOPRAM, AZACITIDINE, FLUOROURACIL, DOXORUBICIN	unknown
FRZB (chapter 3)	*Decreased*	none	-
MAP2K6 (chapter 5)	*Increased*	COBIMETINIB, BINIMETINIB, TRAMETINIB	inhibitory
HLA-DPA1 (chapter 5)	*Increased*	none	-
WWP2 (chapter 6)	*Increased*	none	-
GLIS3 (chapter 9)	*Unkown*	none	-
DGKI (chapter 9)	*Unkown*	none	-
SLC44A2 (chapter 9)	*Increased*	none	-

cartilage and bone, should be performed in future studies.

Multiple GWAS meta-analysis have identified rs4252548, a missense mutation in *IL11*, conferring risk to OA [28, 30]. As the missense mutation results in a thermally unstable protein, it was hypothesized that this SNP confers risk to OA via reduced function of IL11 protein. Therefore, addition of hrIL11 protein was previously suggested as therapeutic strategy for OA [36]. Nonetheless, functional investigation is required to confirm these potential beneficial effects of hrIL11 on articular cartilage and subchondral bone. The importance of including subchondral bone in functional investigation of *IL11* is stressed by the fact that gene expression levels of *IL11* are among the top 25 genes being responsive to OA pathophysiology showing the highest foldchange in both articular cartilage and subchondral bone (**chapter 2**). Moreover, IL11 is known for its role in bone homeostasis and metabolism, as it regulates osteoclastogenesis via RANKL expression by osteoblasts [78-81]. To study the effects of hrIL11 on articular cartilage and subchondral bone with OA, we had available our human *ex vivo* osteochondral explant cultures (**chapter 7**) [62]. These osteochondral explants are isolated from preserved areas of a human OA joints and can be exposed to OA-related perturbations, such as mechanical loading, inflammation, and hypertrophy. Previously it was shown that excessive mechanical loading of 3D chondrocyte pellet cultures resulted in increased levels of *IL11*, comparable as seen between preserved and lesioned OA cartilage [61]. Based on these findings, we have applied mechanical loading on these osteochondral explant to model OA, with or without addition of hrIL11. Mechanical loading of explants

9

resulted in similar effects on articular cartilage as reported previously [64]. However, we did not observe any effects in articular cartilage and subchondral bone gene expression levels upon hrIL11 addition (data not shown). Since mechanical loading represents only a portion of OA pathophysiology, we decided to isolate osteochondral explants from the lesioned areas of the joint to fully recapitulate OA. Nonetheless, exposing lesioned osteochondral explants to hrIL11 had again minimal effects on both tissues. Based on the significant upregulation of *SPP1* and downregulation of *WNT16* upon hrIL11 exposure resulted in unbeneficial response of lesioned articular cartilage, while significant downregulation of *PTGES* in subchondral bone might potentially be beneficial. The latter might suggest rs4252548-T confers risk to OA via subchondral bone, however, more research is needed to confirm. Together, these results indicate the importance of functional investigation of OA risk genes in both articular cartilage and subchondral bone, as we showed that treating the whole joint with hrIL11 does not necessarily have beneficial outcomes. Additional studies including higher sample size are necessary to confirm our findings. Moreover, gene expression of IL11 receptor *IL11RA* was previously also shown to be dysregulated with OA in articular cartilage [4]. Hence, it might be valuable to include *IL11RA* in future functional investigations.

Novel biomimetic *in vitro* model system of osteochondral tissue: osteochondral-unit-on-a-chip

Since 3D chondrocyte pellet and osteochondral explant cultures both have their limitations (**Table 4**), development of a novel state-of-the-art model system based on microfluidic tissue-on-chip principles would be preferred. Therefore, in the last part of this thesis, we developed a novel dual-tissue microfluidic model system in which we cultured interacting neo-cartilage and neo-bone deposited by primary chondrocytes and osteogenic cells, respectively (**chapter 8**).

Table 4 – Advantages and limitations of 2D cell cultures, 3D chondrocyte or osteogenic cell pellet cultures, and ex vivo osteochondral explants.

Model	Advantages	Limitations
2D cell culture	• Easy to use • Easy to increase sample size	• Lack complexity • Lack interaction with ECM • Chondrocytes are prone to lose phenotype
3D chondrocyte/ osteogenic cell pellet culture	• Allow gene expression alterations by e.g. lentiviral transduction • Easy to increase sample size	• Neo- cartilage and bone are produced, being less prone to develop OA • Interaction between cartilage and bone is lacking
Ex vivo osteochondral explants	• Consist of aged ECM that is prone to OA onset • Represent interaction between cartilage and bone	• Sample size is dependent on joint replacement surgery and joint size/OA state

The main advantage of our developed osteochondral-unit-on-a-chip compared to available microfluidic systems is that cells deposit biological ECM instead of matrix island withing hydrogels [82, 83]. As proof-of-principle, we have implemented OA-related perturbation to our system to mimic a pathophysiological process. In our previous study on osteochondral explant cultures [62], we have showed that OA-related perturbations could be used to mimic inflammatory OA (IL1β), post-traumatic OA (mechanical loading), and age-related OA (hypertrophy-inducing thyroid hormone T3). Inducing inflammation using IL1β was shown to be very detrimental for cartilage tissue in osteochondral explants and application of mechanical loading in our microfluidic chip would require adaptations in chip design. Consequently, we choose to expose the system to hypertrophy-inducing thyroid hormone T3. Upon T3 exposure the chondrogenic compartment changed its gene expression pattern towards an osteogenic phenotype, similar to OA pathophysiology and to the effects observed in osteochondral explants. In the osteogenic compartment expression levels of hypertrophic markers were also increased. Together, this shows that our model system could serve as a platform to perform in depth investigations of underlying mechanisms of OA risk genes or OA-related stimuli in both cartilage and bone. Subsequently, our system could be used for the identification of druggable targets and eventually drug testing, which will contribute to cost-efficient preclinical research and reduce, refine, and replace animal experiments.

Enhancements to our developed osteo-chondral-unit-on-a-chip could still be accomplished. To completely overcome the dependency of patients that undergo total joint replacement surgery the use of a more stable cell line, such as induced pluripotent stem cells (iPSCs), could be an attractive alternative to produce neo-cartilage and neo-bone [84]. Another advantage of using iPSCs is that it allows genome editing techniques, such as CRISPR/Cas9, to knock-in or knock-out complete genes or to insert or repair specific mutations, after which these conditions can be compared to their isogenic control. Finally, CRISPR/Cas9 can also be used to create reporter iPSC lines that can provide real-time read-out upon perturbation and/or drug candidate testing [85-88]. Therefore, it would be of added value to optimize the iPSC culturing protocol in terms of differentiation towards chondrocytes and osteoblasts, seeding process and culturing time for the use in our microfluidic model system. This would allow in-depth investigation of specific mutations in interacting cartilage and bone tissue. Furthermore, implementation of other cell types, such as synoviocytes, adipocytes, osteoclasts, and immune cells would advance the system even further. The most simple way to add different cell types is by placing multiple microfluidic chips in parallel. Synoviocytes, for example, could be implemented to the system by placing a synoviocyte containing microfluidic chip in front of our osteochondral-unit-on-a-chip (**Figure 4**).

9

By doing so, chondrocytes will be exposed to synoviocyte-conditioned media. To allow complete remodeling of the ECM by cells present in the osteogenic compartment the polycaprolactone (PCL) matrix could be replaced by, for instance, a collagen type I or silk fibroin matrix [89]. Mechanical loading has been shown to be an important trigger in OA [64, 90-92]. To apply mechanical loading to neo-cartilage and neo-bone in our chip, we need to incorporate an actuation chamber or for example a controllable micro-piston to the design [93]. Finally, in order to use our system as part of pre-clinical studies screening for newly developed potential OA drugs, it would be necessary to further miniaturize our system and make it more compatible with high-throughput screens. In this respect, using iPSC reporter cell lines might provide faster and real-time read-out [85].
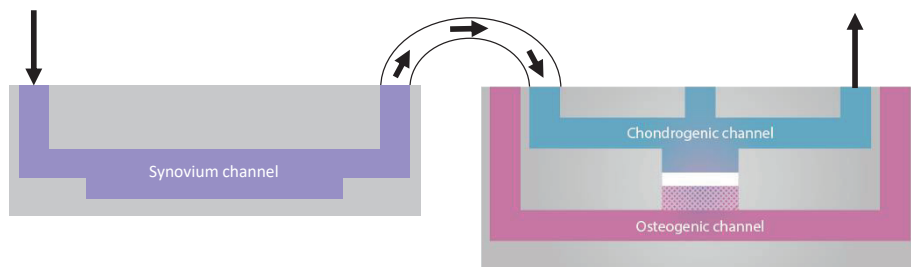
Figure 4 – Schematic overview of a relatively simple way to implement additional cell types, such as fibroblast to mimic the synovium, to our osteochondral-unit-on-a-chip system.

References

1. Knoop, J., et al., Identification of phenotypes with different clinical outcomes in knee osteoarthritis: Data from the osteoarthritis initiative. Arthritis Care & Research, 2011. 63(11): p. 1535-1542.
2. Waarsing, J.H., S.M. Bierma-Zeinstra, and H. Weinans, Distinct subtypes of knee osteoarthritis: data from the Osteoarthritis Initiative. Rheumatology (Oxford), 2015. 54(9): p. 1650-8.
3. Ramos, Y.F., et al., Genes involved in the osteoarthritis process identified through genome wide expression analysis in articular cartilage; the RAAK study. PLoS One, 2014. 9(7): p. e103056.
4. Coutinho de Almeida, R., et al., RNA sequencing data integration reveals an miRNA interactome of osteoarthritis cartilage. Ann Rheum Dis, 2019. 78(2): p. 270-277.
5. Katsoula, G., et al., A molecular map of long non-coding RNA expression, isoform switching and alternative splicing in osteoarthritis. Human Molecular Genetics, 2022: p. ddac017.
6. van Hoolwerff, M., et al., Elucidating Epigenetic Regulation by Identifying Functional cis-Acting Long Noncoding RNAs and Their Targets in Osteoarthritic Articular Cartilage. Arthritis Rheumatol, 2020. 72(11): p. 1845-1854.
7. Fellows, C.R., C. Matta, and A. Mobasheri, Applying Proteomics to Study Crosstalk at the Cartilage-Subchondral Bone Interface in Osteoarthritis: Current Status and Future Directions. EBioMedicine, 2016. 11: p. 2-4.
8. Goldring, S.R. and M.B. Goldring, Changes in the osteochondral unit during osteoarthritis: structure, function and cartilage-bone crosstalk. Nat Rev Rheumatol, 2016. 12(11): p. 632-644.
9. Funck-Brentano, T. and M. Cohen-Solal, Crosstalk between cartilage and bone: when bone cytokines matter. Cytokine Growth Factor Rev, 2011. 22(2): p. 91-7.
10. Pan, J., et al., Elevated cross-talk between subchondral bone and cartilage in osteoarthritic joints. Bone, 2012. 51(2): p. 212-7.
11. Yuan, C., et al., Classification of four distinct osteoarthritis subtypes with a knee joint tissue transcriptome atlas. Bone Research, 2020. 8(1): p. 38.
12. Soul, J., et al., Stratification of knee osteoarthritis: two major patient subgroups identified by genome-wide expression analysis of articular cartilage. Ann Rheum Dis, 2018. 77(3): p. 423.
13. Coutinho de Almeida, R., et al., Identification and characterization of two consistent osteoarthritis subtypes by transcriptome and clinical data integration. Rheumatology (Oxford), 2020.
14. Bernotiene, E., et al., Emerging Technologies and Platforms for the Immunodetection of Multiple Biochemical Markers in Osteoarthritis Research and Therapy. Frontiers in Medicine, 2020. 7.
15. Ramos, Y.F.M., et al., Meta-analysis identifies loci affecting levels of the potential osteoarthritis biomarkers sCOMP and

uCTX-II with genome wide significance. Journal of Medical Genetics, 2014. 51(9): p. 596-604.
16. Meulenbelt, I., et al., Urinary CTX-II levels are associated with radiographic subtypes of osteoarthritis in hip, knee, hand, and facet joints in subject with familial osteoarthritis at multiple sites: the GARP study. Annals of the rheumatic diseases, 2006. 65(3): p. 360-365.
17. Angelini, F., et al., Osteoarthritis endotype discovery via clustering of biochemical marker data. Annals of the Rheumatic Diseases, 2022. 81(5): p. 666-675.
18. Bay-Jensen, A.C., et al., Blood and urine biomarkers in osteoarthritis – an update on cartilage associated type II collagen and aggrecan markers. Current Opinion in Rheumatology, 2022. 34(1).
19. Lotz, M., et al., Value of biomarkers in osteoarthritis: current status and perspectives. Ann Rheum Dis, 2013. 72(11): p. 1756-63.
20. Valdes, A.M., et al., Large scale meta-analysis of urinary C-terminal telopeptide, serum cartilage oligomeric protein and matrix metalloprotease degraded type II collagen and their role in prevalence, incidence and progression of osteoarthritis. Osteoarthritis and Cartilage, 2014. 22(5): p. 683-689.
21. Cruz, M.S., et al., miRNAs emerge as circulating biomarkers of post-myocardial infarction heart failure. Heart Failure Reviews, 2020. 25(2): p. 321-329.
22. Vanhie, A., et al., Plasma miRNAs as biomarkers for endometriosis. Hum Reprod, 2019. 34(9): p. 1650-1660.
23. Bouvy, C., et al., Circulating MicroRNAs as Biomarkers in Diffuse Large B-cell Lymphoma: A Pilot Prospective Longitudinal Clinical Study. Biomark Cancer, 2018. 10: p. 1179299x18781095.
24. Ramos, Y.F.M., et al., Circulating MicroRNAs Highly Correlate to Expression of Cartilage Genes Potentially Reflecting OA Susceptibility-Towards Identification of Applicable Early OA Biomarkers. Biomolecules, 2021. 11(9): p. 1356.
25. Wehby, G.L., B.W. Domingue, and F.D. Wolinsky, Genetic Risks for Chronic Conditions: Implications for Long-term Wellbeing. J Gerontol A Biol Sci Med Sci, 2018. 73(4): p. 477-483.
26. Spector, T.D. and A.J. MacGregor, Risk factors for osteoarthritis: genetics11Supported by Procter & Gamble Pharmaceuticals, Mason, OH. Osteoarthritis and Cartilage, 2004. 12: p. 39-44.
27. Aubourg, G., et al., Genetics of osteoarthritis. Osteoarthritis and Cartilage, 2021.
28. Boer, C.G., et al., Deciphering osteoarthritis genetics across 826,690 individuals from 9 populations. Cell, 2021.
29. Zengini, E., et al., Genome-wide analyses using UK Biobank data provide insights into the genetic architecture of osteoarthritis. Nat Genet, 2018. 50(4): p. 549-558.
30. Styrkarsdottir, U., et al., Meta-analysis of Icelandic and UK data sets identifies missense variants in SMO, IL11, COL11A1 and 13 more new loci associated with osteoarthritis. Nat Genet, 2018. 50(12): p. 1681-1687.
31. Ramos, Y.F. and I. Meulenbelt, Implementation of Functional Genomics for Bench-to-Bedside Transition in Osteoarthritis. Curr Rheumatol Rep, 2015. 17(8): p. 53.
32. den Hollander, W., et al., Annotating Transcriptional Effects of Genetic Variants in Disease-Relevant Tissue: Transcriptome-Wide Allelic Imbalance in Osteoarthritic Cartilage. Arthritis Rheumatol, 2019. 71(4): p. 561-570.
33. Coutinho de Almeida, R., et al., Allelic expression imbalance in articular cartilage and subchondral bone refined genome-wide association signals in osteoarthritis. medRxiv, 2022: p. 2022.04.07.22273552.
34. Nelson, M.R., et al., The support of human genetic evidence for approved drug indications. Nat Genet, 2015. 47(8): p. 856-60.
35. King, E.A., J.W. Davis, and J.F. Degner, Are drug targets with genetic support twice as likely to be approved? Revised estimates of the impact of genetic support for drug mechanisms on the probability of drug approval. PLOS Genetics, 2019. 15(12): p. e1008489.
36. Tachmazidou, I., et al., Identification of new therapeutic targets for osteoarthritis through genome-wide analyses of UK Biobank data. Nat Genet, 2019. 51(2): p. 230-236.
37. Lokau, J., et al., The SNP rs4252548 (R112H) which is associated with reduced human height compromises the stability of IL-11. Biochim Biophys Acta Mol Cell Res, 2018. 1865(3): p. 496-506.
38. The Genotype-Tissue Expression (GTEx) project. Nat Genet, 2013. 45(6): p. 580-5.
39. Tillgren, V., et al., The Novel Small Leucine-rich Protein Chondroadherin-like (CHADL) Is Expressed in Cartilage and Modulates Chondrocyte Differentiation*. Journal of Biological Chemistry, 2015. 290(2): p. 918-925.
40. Styrkarsdottir, U., et al., Whole-genome sequencing identifies rare genotypes in COMP and CHADL associated with high risk of hip osteoarthritis. Nat Genet, 2017. 49(5): p. 801-805.
41. Freshour, S.L., et al., Integration of the Drug–Gene Interaction Database (DGIdb 4.0) with open crowdsource efforts. Nucleic Acids Research, 2020. 49(D1): p. D1144-D1151.
42. Quinn, J.J. and H.Y. Chang, Unique features of long non-coding RNA biogenesis and function. Nature Reviews Genetics, 2016. 17(1): p. 47-62.
43. Marchese, F.P., I. Raimondi, and M. Huarte, The multidimensional mechanisms of long noncoding RNA function. Genome Biology, 2017. 18(1): p. 206.
44. Morlando, M., M. Ballarino, and A. Fatica, Long Non-Coding RNAs: New Players in Hematopoiesis and Leukemia. Frontiers in medicine, 2015. 2: p. 23-23.
45. Wang, J., et al., Roles of long non-coding RNA in osteoarthritis (Review). Int J Mol Med, 2021. 48(1).
46. Lories, R.J., et al., Articular cartilage and biomechanical properties of the long bones in Frzb-knockout mice. Arthritis Rheum, 2007. 56(12): p. 4095-103.
47. Loughlin, J., et al., Functional variants within the secreted frizzled-related protein 3 gene are associated with hip osteoarthritis in females. Proc Natl Acad Sci U S A, 2004. 101(26): p. 9757-62.
48. Leijten, J.C., et al., GREM1, FRZB and DKK1 mRNA levels correlate with osteoarthritis and are regulated by osteoarthritis-associated factors. Arthritis Res Ther, 2013. 15(5): p. R126.
49. Enomoto-Iwamoto, M., et al., The Wnt antagonist Frzb-1 regulates chondrocyte maturation and long bone development during limb skeletogenesis. Dev Biol, 2002. 251(1): p. 142-56.
50. Avila Cobos, F., et al., Benchmarking of cell type deconvolution pipelines for transcriptomics data. Nature Communications, 2020. 11(1): p. 5650.
51. Longo, S.K., et al., Integrating single-cell and spatial transcriptomics to elucidate intercellular tissue dynamics. Nature Reviews Genetics, 2021. 22(10): p. 627-644.
52. Greenblatt, M.B., et al., The Unmixing Problem: A Guide to Applying Single-Cell RNA Sequencing to Bone. Journal of Bone and Mineral Research, 2019. 34(7): p. 1207-1219.
53. Ji, Q., et al., Single-cell RNA-seq analysis reveals the progression of human osteoarthritis. 2019. 78(1): p. 100-110.
54. Ståhl, P.L., et al., Visualization and analysis of gene expression in tissue sections by spatial transcriptomics. Science, 2016. 353(6294): p. 78-82.
55. Grässel, S. and D. Muschter, Recent advances in the treatment of osteoarthritis. F1000Research, 2020. 9: p. F1000 Faculty Rev-325.
56. Oprea, T.I. and J. Mestres, Drug Repurposing: Far Beyond New Targets for Old Drugs. The AAPS Journal, 2012. 14(4): p.

9

759-763.

57. Repositioning Bevacizumab: A Promising Therapeutic Strategy for Cartilage Regeneration. Tissue Engineering Part B: Reviews, 2016. 22(5): p. 341-357.
58. Pushpakom, S., et al., Drug repurposing: progress, challenges and recommendations. Nature Reviews Drug Discovery, 2019. 18(1): p. 41-58.
59. Ashburn, T.T. and K.B. Thor, Drug repositioning: identifying and developing new uses for existing drugs. Nature Reviews Drug Discovery, 2004. 3(8): p. 673-683.
60. Bomer, N., et al., Underlying molecular mechanisms of DIO2 susceptibility in symptomatic osteoarthritis. Ann Rheum Dis, 2015. 74(8): p. 1571-9.
61. Timmermans, R.G.M., et al., A human in vitro 3D neo-cartilage model to explore the response of OA risk genes to hyper-physiological mechanical stress. Osteoarthritis and Cartilage Open, 2022. 4(1): p. 100231.
62. Houtman, E., et al., Human Osteochondral Explants: Reliable Biomimetic Models to Investigate Disease Mechanisms and Develop Personalized Treatments for Osteoarthritis. Rheumatology and Therapy, 2021. 8(1): p. 499-515.
63. Houtman, E., et al., Inhibiting thyroid activation in aged human explants prevents mechanical induced detrimental signalling by mitigating metabolic processes. Rheumatology, 2022.
64. Houtman, E., et al., Elucidating mechano-pathology of osteoarthritis: transcriptome-wide differences in mechanically stressed aged human cartilage explants. Arthritis Research & Therapy, 2021. 23(1): p. 215.
65. Geurts, J., et al., Novel Ex Vivo Human Osteochondral Explant Model of Knee and Spine Osteoarthritis Enables Assessment of Inflammatory and Drug Treatment Responses. Int J Mol Sci, 2018. 19(5).
66. Gagliardi, A.D., et al., Human stanniocalcin-2 exhibits potent growth-suppressive properties in transgenic mice independently of growth hormone and IGFs. Am J Physiol Endocrinol Metab, 2005. 288(1): p. E92-105.
67. Chang, A.C., et al., The murine stanniocalcin 2 gene is a negative regulator of postnatal growth. Endocrinology, 2008. 149(5): p. 2403-10.
68. Gago-Fuentes, R., et al., The C-terminal domain of connexin43 modulates cartilage structure via chondrocyte phenotypic changes. Oncotarget, 2016. 7(45): p. 73055-73067.
69. Gelse, K., et al., Molecular differentiation between osteophytic and articular cartilage--clues for a transient and permanent chondrocyte phenotype. Osteoarthritis Cartilage, 2012. 20(2): p. 162-71.
70. Mayan, M.D., et al., Articular chondrocyte network mediated by gap junctions: role in metabolic cartilage homeostasis. Ann Rheum Dis, 2015. 74(1): p. 275-84.
71. Knight, M.M., et al., Articular chondrocytes express connexin 43 hemichannels and P2 receptors - a putative mechanoreceptor complex involving the primary cilium? J Anat, 2009. 214(2): p. 275-83.
72. Charlier, E., et al., Chondrocyte dedifferentiation and osteoarthritis (OA). Biochemical Pharmacology, 2019. 165: p. 49-65.
73. Chantry, A., WWP2 ubiquitin ligase and its isoforms: new biological insight and promising disease targets. Cell Cycle, 2011. 10(15): p. 2437-9.
74. Wilson, R., D. Belluoccio, and J.F. Bateman, Proteomic analysis of cartilage proteins. Methods, 2008. 45(1): p. 22-31.
75. Rice, S.J., et al., Discovery and analysis of methylation quantitative trait loci (mQTLs) mapping to novel osteoarthritis genetic risk signals. Osteoarthritis Cartilage, 2019. 27(10): p. 1545-1556.
76. Schnell, J.D. and L. Hicke, Non-traditional Functions of Ubiquitin and Ubiquitin-binding Proteins*. Journal of Biological Chemistry, 2003. 278(38): p. 35857-35860.
77. Miranda, M. and A. Sorkin, Regulation of receptors and transporters by ubiquitination: new insights into surprisingly similar mechanisms. Mol Interv, 2007. 7(3): p. 157-67.
78. Fung, K.Y., et al., Emerging roles for IL-11 in inflammatory diseases. Cytokine, 2022. 149: p. 155750.
79. Kespohl, B., et al., The cytokine interleukin-11 crucially links bone formation, remodeling and resorption. Cytokine & Growth Factor Reviews, 2021. 60: p. 18-27.
80. Sims, N.A., Cell-specific paracrine actions of IL-6 family cytokines from bone, marrow and muscle that control bone formation and resorption. Int J Biochem Cell Biol, 2016. 79: p. 14-23.
81. Sims, N.A., et al., Interleukin-11 Receptor Signaling Is Required for Normal Bone Remodeling. Journal of Bone and Mineral Research, 2005. 20(7): p. 1093-1102.
82. Lin, Z., et al., Osteochondral Tissue Chip Derived From iPSCs: Modeling OA Pathologies and Testing Drugs. Front Bioeng Biotechnol, 2019. 7: p. 411.
83. Lin, H., et al., Stem cell-based microphysiological osteochondral system to model tissue response to interleukin-1β. Mol Pharm, 2014. 11(7): p. 2203-12.
84. Rodríguez Ruiz, A., et al., Cartilage from human-induced pluripotent stem cells: comparison with neo-cartilage from chondrocytes and bone marrow mesenchymal stromal cells. Cell and Tissue Research, 2021. 386(2): p. 309-320.
85. Dicks, A., et al., Prospective isolation of chondroprogenitors from human iPSCs based on cell surface markers identified using a CRISPR-Cas9-generated reporter. Stem Cell Research & Therapy, 2020. 11(1): p. 66.
86. Rodríguez Ruiz, A., et al., Mutation in the CCAL1 locus accounts for bidirectional process of human subchondral bone turnover and cartilage mineralization. Rheumatology (Oxford), 2022.
87. van Hoolwerff, M., et al., High-impact FN1 mutation decreases chondrogenic potential and affects cartilage deposition via decreased binding to collagen type II. Sci Adv, 2021. 7(45): p. eabg8583.
88. Choi, Y.R., et al., Genome Engineering for Osteoarthritis: From Designer Cells to Disease-Modifying Drugs. Tissue Eng Regen Med, 2019. 16(4): p. 335-343.
89. Hofmann, S., et al., Remodeling of tissue-engineered bone structures in vivo. Eur J Pharm Biopharm, 2013. 85(1): p. 119-29.
90. van Haaften, E.E., K. Ito, and C.C. van Donkelaar, The initial repair response of articular cartilage after mechanically induced damage. J Orthop Res, 2017. 35(6): p. 1265-1273.
91. Chang, S.H., et al., Excessive mechanical loading promotes osteoarthritis through the gremlin-1-NF-κB pathway. Nat Commun, 2019. 10(1): p. 1442.
92. Zhu, J., et al., Instability and excessive mechanical loading mediate subchondral bone changes to induce osteoarthritis. Ann Transl Med, 2020. 8(6): p. 350.
93. Onal, S., M.M. Alkaisi, and V. Nock, A flexible micro-piston device for mechanical cell stimulation and compression in microfluidic settings. bioRxiv, 2021: p. 2021.01.11.426203.

9

Appendix

Nederlandse samenvatting
Lisf of publications
Curriculum vitae
Dankwoord

Appendix

Nederlandse samenvatting

Inleiding

Artrose is een complexe en leeftijd gerelateerde gewrichtsaandoening die wordt gekenmerkt door kraakbeen degeneratie, veranderingen in het onderliggende subchondrale bot en ontsteking. Er zijn verschillende risicofactoren die de kans op artrose vergroten, zoals overgewicht, overbelasting, een hoge leeftijd en een genetische aanleg. Wereldwijd is 7% van de bevolking gediagnostiseerd met artrose en naar verwachting zal dit nog flink oplopen door vergrijzing en het toenemend aantal mensen met overgewicht. De symptomen van artrose zijn pijn en stijfheid van het gewricht, wat leidt tot immobiliteit. Op dit moment zijn er geen medicijnen beschikbaar die het ziekteproces kunnen stoppen of omkeren. De behandeling bestaat daarom alleen uit het toedienen van pijnstilling en/of het uitvoeren van een kostbare gewrichtsvervangende operatie in het eindstadium van het ziekteproces. Dit zorgt voor een grote ziektelast, voor zowel de patiënt als de maatschappij.

Uitgangspunten van dit proefschrift

Om medicijnen te kunnen ontwikkelen hebben we meer inzicht nodig in het onderliggend pathofysiologisch proces van artrose. In kraakbeen is dit ziekteproces al vrij intensief onderzocht, maar het onderliggende subchondrale bot is tot nu toe onderbelicht gebleven. Genetische predispositie is een sterke risicofactor voor artrose. Genetische varianten die het risico op het krijgen van artrose verhogen worden geïdentificeerd in zogenoemde genome-wide association (GWA) studies. Het beter begrijpen van de onderliggende biologische oorzaken waarop deze genetische varianten verhoogd risico geven op artrose is noodzakelijk om effectieve translatie naar medicijnen of therapieën te kunnen maken, die het artroseproces kunnen stoppen of zelfs genezen. Om deze mechanismen te onderzoeken is er een grote behoefte aan laboratorium modellen van gewrichtsweefsel waarin we artrose nabootsen. Tenslotte zijn er signaalmoleculen, ofwel biomarkers, nodig die bijvoorbeeld in bloed gemeten kunnen worden en waarmee we verschillende ziektebeelden van artrose van elkaar kunnen onderscheiden. Dit laatste kan helpen om uiteindelijk een therapie op maat te ontwikkelen, waardoor de patiënt met het juiste medicijn behandeld kan worden.
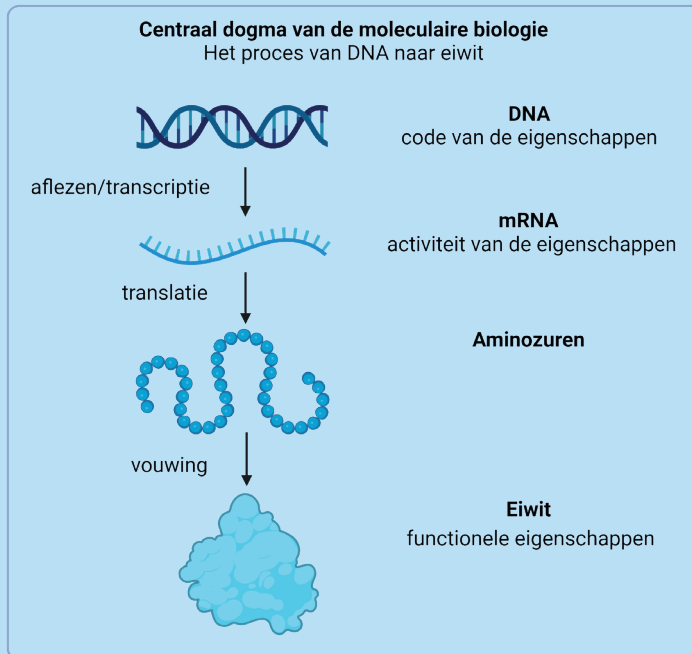
Doel van dit proefschrift

In dit proefschrift hebben we drie strategieën toegepast om aspecten van het ziekteproces in het gewrichtsweefsel te kunnen herkennen en om onderliggende mechanismen van artrose risico genen beter te begrijpen. Dit hebben we gedaan door:
1. De moleculaire pathofysiologie van het bot in interactie met kraakbeen te karakteriseren
2. Moleculen, zogenoemde microRNA (miRNA), aanwezig in bloed te identificeren

A

zodat we deze kunnen gebruiken om het type artrose te herkennen op een niet-invasieve manier

3. Verschillende *in vitro* of *ex vivo* modellen van gewrichtsweefsels toe te passen of te ontwikkelen om de onderliggende mechanismen van specifieke risico genen of factoren te kunnen onderzoeken in bot en kraakbeen.

Tekst box 1 – DNA, mRNA en eiwit

Centraal dogma van de moleculaire biologie
Het proces van DNA naar eiwit

DNA
code van de eigenschappen

aflezen/transcriptie

mRNA
activiteit van de eigenschappen

translatie

Aminozuren

vouwing

Eiwit
functionele eigenschappen

Ons DNA bestaat uit twee ketens van nucleotiden die samen een dubbele helix vormen. Het DNA bevat de genetische informatie (de code van de eigenschappen). De nucleotiden waar het DNA uit bestaat vormen samen een code die het lichaam informatie geeft over hoe eiwitten moeten worden aangemaakt. Deze eiwitten bepalen op hun beurt weer welke processen er plaats vinden in het lichaam. Voor het maken van een eiwit wordt een stuk DNA, ook wel gen genoemd, eerst afgelezen en gekopieerd. Dit proces noemen we transcriptie en het kopie wat hierbij ontstaat noemen we mRNA (de hoeveelheid mRNA bepaald de activiteit van de eigenschappen). Dit proces vindt plaats in de celkern. Vervolgens gaat het mRNA de celkern uit, naar een zogenoemde ribosoom. Hier wordt de code van het mRNA vertaald naar een volgorde van aminozuren. Dit proces noemen we translatie. Tenslotte vouwt de keten van aminozuren zichzelf op en ontstaat er een driedimensionale eiwit structuur (met functionele eigenschappen).

Tekst box 2 – Epigenetica
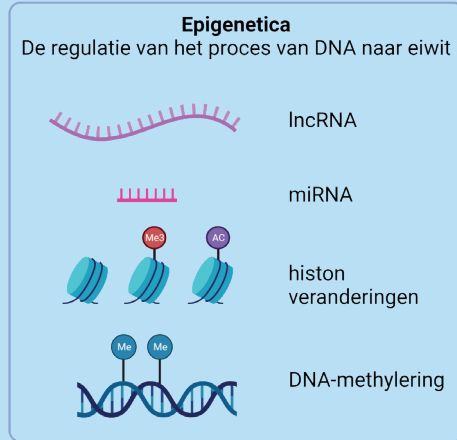
Epigenetica refereert naar een verandering in gen activiteit (Tekst box 1) die plaats vindt zonder dat de code van het DNA veranderd. Veranderingen van gen activiteit zijn vaak nodig om (tijdelijke) aanpassing aan de omgeving te kunnen bewerkstelligen. Er zijn meerdere manieren waarop de regulatie van een gen kan plaats vinden. Er bestaan bijvoorbeeld moleculen die erg veel lijken op mRNA (Tekst box 1), maar die er uiteindelijk niet voor zorgen dat er een eiwit gemaakt wordt. Deze moleculen noemen we niet-coderende RNA's (ncRNA's). Deze ncRNA's bestaan in een lange vorm, ook wel lange ncRNA's (lncRNA's) genoemd, en in een korte vorm, ook wel micro RNA's (miRNA's) genoemd. LncRNA's kunnen worden ingezet om transcriptie of translatie (Tekst box 1) te beïnvloeden. Zo kunnen sommige lncRNA's er voor zorgen dat het transcriptie proces niet plaats kan vinden, terwijl andere lncRNA's er juist voor kunnen zorgen dat mRNA of eiwitten worden afgebroken. MiRNA's kunnen de activiteit van een gen beïnvloeden door bijvoorbeeld aan het mRNA te binden waardoor het wordt afgebroken nog voor dat het eiwit gemaakt wordt. Een andere vorm van epigenetica is histon veranderingen. Histonen zijn eiwitten waar het DNA om zit opgerold. Door bepaalde moleculen, een methylgroep of een acetylgroep, te binden aan een histon wordt het aflezen van het DNA en daarmee de aanmaak van mRNA gereguleerd. Tenslotte kunnen er ook methylgroepen worden toegevoegd aan het DNA zelf. Het toevoegen of weghalen van een methylgroep zorgt er voor dat het DNA wel of niet toegankelijk is voor het aflezen en dus het maken van mRNA.

Moleculaire pathofysiologie van artrose; interactie tussen kraakbeen en subchondraal bot
Zoals eerder genoemd heeft het in kaart brengen van het artrose ziekteproces zich tot nu toe voornamelijk gericht op het kraakbeen. In zulke studies wordt vaak de moleculaire vergelijking gemaakt tussen macroscopisch aangedaan en niet-aangedaan weefsel

A

afkomstig van hetzelfde gewricht of tussen aangedaan en gezond weefsel afkomstig van verschillende personen. Deze studies hebben al veel waardevolle inzichten gegeven in de expressieprofielen van bijvoorbeeld messenger RNA (mRNA, **Tekst box 1**), miRNA (**Tekst box 2**) en lang niet-coderend RNA (lncRNA, **Tekst box 2**) in kraakbeen. Daarnaast hebben deze studies inzichten gegeven in de processen waar deze moleculen een rol in spelen. In tegenstelling tot de vele studies naar artrose in kraakbeen, is het onderliggende subchondrale bot onderbelicht gebleven. Dit ondanks het feit dat er wel degelijk structurele veranderingen plaats vinden in het subchondrale bot met artrose. Daarnaast zijn er ook meerdere genetische factoren gevonden die verhoogd risico geven op artrose en deze factoren spelen een belangrijke rol in zowel kraakbeen als bot. Dit wijst er op dat naast het kraakbeen ook het onderliggende bot van belang is in de oorzaak en progressie van artrose. Om deze leemte in kennis op te vullen hebben we in RNA-sequencing toegepast op het subchondrale bot en hebben we expressieprofielen vergeleken tussen macroscopisch aangedaan en niet-aangedaan weefsel van hetzelfde gewricht.

In **hoofdstuk 2** hebben we ons gericht op het identificeren van mRNA dat het artroseproces in bot markeert. Door een cluster analyse uit te voeren vonden we verschillen in het artroseproces in subchondraal bot tussen heupen en knieën. Dit verschil is belangrijk om in acht te nemen wanneer men op zoek gaat naar mogelijke aangrijpingspunten voor medicijnen tegen artrose. Idealiter hebben potentiële medicijnen een effect in zowel kraakbeen als bot, zodat het gehele gewricht behandeld kan worden. Daarom hebben we gezocht naar genen die het artroseproces markeren in zowel kraakbeen als bot, met eenzelfde richting van het effect. Om vervolgens hieruit die genen te selecteren die het meest waarschijnlijk artrose veroorzaken, hebben we deze overlappende genen tussen kraakbeen en bot gefilterd op artrose risicogenen. Dit resulteerde in de identificatie van twee genen, *IL11* en *CHADL*. Deze genen markeren in zowel bot als kraakbeen het artrose proces en zijn eerder ook zijn geïdentificeerd als artrose risicogenen, waardoor ze dus aantrekkelijke potentiële aangrijpingspunten zijn voor medicijnen.

Epigenetica refereert naar veranderingen in het fenotype zonder dat er veranderingen in de genetische code plaats vinden. Door expressielevels van genen tijdelijk aan te passen kunnen cellen reageren op omgevingsfactoren zoals mechanische belasting en trauma's. Een van deze epigenetische mechanismen is de expressie van lncRNA (**Tekst box 1**). LncRNA's zijn over het algemeen langer dan 200 nucleotiden en lijken op mRNA moleculen, maar waar mRNA transleert naar eiwit, is lncRNA niet eiwit coderend. LncRNA's kunnen op verschillende niveaus de activiteit van mRNA en eiwitten beïnvloeden en zo processen in het weefsel reguleren. Het gegeven

dat lncRNA's erg weefsel- en ziekte-specifiek kunnen zijn, maakt dat lncRNA een aantrekkelijk aangrijpingspunt is voor medicijnen. Daarom hebben wij in **hoofdstuk 3** lncRNA's geïdentificeerd die het artroseproces markeren in subchondraal bot in interactie met kraakbeen. Door de lncRNA's die tot expressie komen in macroscopisch aangedaan en niet-aangedaan weefsel met elkaar te vergelijken, hebben we vijf lncRNA's geïdentificeerd die zowel in subchondraal bot als in kraakbeen het artroseproces markeren. LncRNA *AC005165.1* kwam in zowel bot als kraakbeen significant lager tot expressie in het aangedane weefsel. Door correlaties te berekenen tussen de expressie levels van *AC005165.1* en mRNA vonden we *FRZB,* een welbekend artrose gen, als mogelijk doelwit van *AC005165.1*. Vervolgens hebben we experimenteel bevestigd dat een lagere expressie van *AC005165.1* in bot cellen direct of indirect leidt tot een lagere expressie van *FRZB.* Dit zien we ook terug in het artrose proces. Verhoging van *AC005165.1* zou daarom een mogelijke therapeutische strategie kunnen zijn om de expressie levels van *FRZB* stabiel te houden in zowel kraakbeen als bot.

Diversiteit van het pathofysiologisch proces in artrose; subtype A en B artrose
Naast de moleculaire verschillen tussen aangedaan en niet-aangedaan weefsel, kan moleculaire data van kraakbeen en subchondraal bot ook gebruikt worden voor het identificeren van subtypes van artrose. Eerdere studies hebben laten zien dat er consistente verschillen zijn in het artrose ziekteproces tussen patiënten. Er zijn twee subtypes van artrose geïdentificeerd op basis van moleculaire data van kraakbeen. In het kraakbeen van patiënten met subtype A artrose wordt voornamelijk een transitie van kraakbeen naar botachtig weefsel gezien, terwijl het kraakbeen van patiënten met subtype B artrose vooral inflammatie laat zien. Om te kijken of het artroseproces ook verschillend is in het onderliggende bot, hebben we ons in **hoofdstuk 5** gericht op het karakteriseren van deze artrose subtypes in het subchondrale bot. Als grootste verschil tussen het bot van de twee subtype artrose patiënten vonden we de mate waarin genen die het inflammatieproces markeren tot expressie kwamen. Vergelijkbaar met kraakbeen kwamen deze inflammatiemarkers, waaronder *IL1β*, *OSM* en *AIF1,* hoger tot expressie in het bot van subtype B patiënten. Daarnaast zagen we ook een hogere expressie van genen die duiden op de formatie van (nieuw) bot in subtype B patiënten. Deze verschillen tussen patiënten moet in acht worden genomen wanneer men medicijnen gaat ontwikkelen, zodat de patiënt met het juiste medicijn behandeld kan worden.

Classificatie van artrose subtypen; circulerende miRNA's
Tot nu toe is de diagnose en/of classificatie van artrose alleen gebaseerd op röntgenfoto's en klinische symptomen zoals pijn en stijfheid van het gewricht. Er is dus een onvervulde behoefte aan betrouwbare biomarkers die processen in gewrichtsweefsels, waaronder

A

kraakbeen en subchondraal bot, weerspiegelen. Tot dusver zijn afbraakproducten van gewrichtsweefsels aanwezig in serum of urine, zoals sCOMP en uCTX-II, bestudeerd als mogelijke biomarkers. Deze afbraakproducten zijn meestal niet specifiek voor het artrose ziekteproces dat plaats vindt in de gewrichtsweefsels. Biomarkers die wel specifieke ziekteprocessen in de gewrichtsweefsels markeren bieden de mogelijkheid om subtype A en B artrose te herkennen, wat vervolgens de ontwikkeling van een therapie op maat faciliteert. Een nieuwe richting in het identificeren van biomarkers voor artrose is het bestuderen van miRNA's die aanwezig zijn in bloed. MiRNA's zijn stabiel in plasma en uit recent onderzoek blijkt dat deze miRNA's inderdaad in staat zijn artrose-gerelateerde mRNA-expressiepatronen in kraakbeen te weerspiegelen. Op basis van deze gegevens hebben wij in **hoofdstuk 4** gezocht naar miRNA's in plasma die het verschil markeren tussen subtype A en subtype B artrose patiënten. In dit hoofdstuk hebben wij vier miRNA's in het plasma geïdentificeerd die samen kunnen voorspellen of een patiënt subtype A of subtype B artrose heeft. Dit kan worden ingezet om, voor een behandeling start, te bepalen welk subtype artrose een patiënt heeft en vervolgens de behandeling hierop af te stemmen.

Genetische predispositie en translationeel onderzoek; onderliggende mechanisme van risicogenen *WWP2* en *IL11*.
Tot op heden zijn er meer dan 100 associaties gevonden tussen variaties in het DNA, zogenoemde single nucleotide polymorphism (SNP), en het krijgen van artrose. Het is van belang dat deze risico SNPs voor artrose worden getransleerd naar onderliggende biologische mechanismen en uiteindelijk aangrijpingspunten voor medicijnen. Daarom hebben wij in **hoofdstuk 6** en **hoofdstuk 7** twee verschillende modellen van kraakbeen en/of bot gebruikt om de onderliggende biologische mechanismen van twee van deze risico SNPs te onderzoeken.

In **hoofdstuk 6** hebben we gekeken naar risico SNP rs1052429, die zich in de genetische code van het *WWP2* gen bevindt. Eerder is al laten zien dat het risico allel rs1052429-A geassocieerd is met hogere expressielevels van *WWP2*. Op basis hiervan was onze hypothese dat verhoogde expressielevels van *WWP2* een verhoogd risico geeft op artrose. Daarom hebben we met behulp van een lentivirus verhoogde expressielevels van *WWP2* in kraakbeencellen, zogenoemde chondrocyten, gegenereerd. Vervolgens hebben we 3D kraakbeen organoïden, of ook wel miniatuurorgaantjes, gemaakt van chondrocyten met en zonder verhoogde expressielevels van *WWP2*. Deze kraakbeen pellets hebben we met elkaar vergeleken om inzicht te krijgen in het mechanisme waarop *WWP2* verhoogd risico geeft op artrose. Verhoogde *WWP2* expressielevels resulteerde in verlaagde expressielevels van kraakbeenmarkers *COL2A1* en *ACAN.* Daarnaast zagen we ook verlaagde expressielevels van *GDF10, STC2* en *GJA1* en

verhoogde expressielevels van *EPAS1*, allemaal hypoxie-gerelateerde genen. Deze bevindingen suggereren dat verhoogd expressielevel van *WWP2* resulteert in een nadelig effect op kraakbeenmatrix. De genexpressie levels van *EPAS1, GDF10,* en *GJA1* zijn allemaal gevoelig voor zuurstoflevels, wat kan betekenen dat verhoogde levels van *WWP2* resulteert in hypoxie-gerelateerde chondrocyt dedifferentiatie. Naast het effect van verhoogde *WWP2* expressie levels, hebben we in **hoofdstuk 6** ook gekeken naar de eiwit expressie in 3D kraakbeen organoïden na drie en na zeven dagen kweken. Op zowel dag drie als dag zeven kwamen kraakbeen eiwitten zoals collageen type 2, aggrecan en fibronectine hoog tot expressie. Dit wijst er op dat chondrocyten in deze 3D kraakbeen organoïden al in drie dagen tijd kraakbeen matrix produceren.

In **hoofdstuk 7** hebben we gefocust op risico SNP rs4252548, die zich in het coderende deel van *IL11* bevindt. Risico allel rs4252548-T is een zogenoemde missense mutatie en resulteert in verminderde stabiliteit van het IL11 eiwit. De hypothese is daarom dat risico allel rs4252548-T verhoogd risico geeft op artrose door minder beschikbaarheid van het IL11 eiwit. Op basis hiervan werd humaan recombinant IL11 (hrIL11) eiwit als mogelijk medicijn voor artrose gesuggereerd. Het voordeel van hrIL11 is dat het gebruik van hrIL11 al is goedgekeurd door de FDA als medicijn tegen trombocytopenie. Een goedgekeurd medicijn is al getest op veiligheid en daarom is het risico op falen van het medicijn lager. Daarnaast kan de ontwikkeling van een al goedgekeurd medicijn veel sneller gaan, omdat er al verschillende testen zijn uitgevoerd. In tegenstelling tot bovengenoemde hypothese, zien we in zowel bot als kraakbeen een hoger level van *IL11* mRNA in aangedaan artrose weefsel in vergelijking tot niet-aangedaan weefsel uit hetzelfde gewricht. Dit zou er op kunnen wijzen dat het IL11 eiwit niet goed wordt aangemaakt of niet goed functioneert in aangedaan weefsel. Om te bestuderen of hrIL11 inderdaad gebruikt kan worden als medicijn tegen artrose, hebben we gebruik gemaakt van een *ex vivo* model van kraakbeen en bot, de zogenoemde osteochondrale biopten. Deze osteochondrale biopten zijn genomen van het aangedane gedeelte van het gewricht, waardoor deze biopten het artrose ziektebeeld in zowel kraakbeen als bot weerspiegelen. Vervolgens hebben we deze biopten behandeld met hrIL11 om te kijken wat het effect is van hrIL11 op het kraakbeen en bot. De effecten van hrIL11 bleken minimaal te zijn. In kraakbeen zorgde hrIL11 behandeling voor een verhoogde expressie van botmarker *SPP1* en voor een verlaagde expressie van *WNT16.* Dit wijst er op dat het kraakbeen meer hypertroof wordt door behandeling met hrIL11, wat een ongunstig effect is. In bot zagen we een verlaagde expressie van *PTGES* en *IL11RA*, wat mogelijk wijst op een verminderde osteoclast activiteit en daarom een voordelig effect zou kunnen zijn. Opvallend was dat de intrinsieke expressielevels van *IL11* niet significant veranderd waren na behandeling met het hrIL11 eiwit. Met name in het kraakbeen was er een grote variatie in intrinsieke *IL11* expressie te zien in reactie op behandeling

A

met het hrIL11 eiwit. Vooral patiënten die uit zichzelf een hoog expressielevel van *IL11* hadden reageerde wel op de hrIL11 eiwit behandeling. Dit zou er op kunnen wijzen dat het eigen IL11 eiwit mogelijk niet efficiënt bind aan zijn receptor. Meer onderzoek is nodig om te bekijken of dit daadwerkelijk zo is en wat dit precies betekent voor een mogelijke behandeling met hrIL11.

Nieuw model voor het bestuderen van kraakbeen en bot; osteochondrale unit-op-een-chip
De twee modellen die we in dit proefschrift gebruikt hebben zijn de 3D *in vitro* kraakbeen pellets en de *ex vivo* osteochondrale biopten. De kraakbeen pellets hebben als voordeel dat genexpressie kan worden aangepast, bijvoorbeeld door gebruik te maken van een lentivirus, om zo de effecten van een specifiek gen te kunnen onderzoeken (**hoofdstuk 6**). Het nadeel van 3D kraakbeen pellets is dat het model alleen maar uit kraakbeen bestaat, terwijl ook bot een belangrijke rol speelt in artrose. De interactie tussen kraakbeen en bot wordt wel gevangen door het gebruik van osteochondrale biopten (**hoofdstuk 7**). Echter, het nadeel van osteochondrale biopten is dat hier genexpressie niet kan worden aangepast. Om deze limitaties te voorkomen hebben we in **hoofdstuk 8** een nieuw model ontwikkeld waarbij we, gebruikmakende van chondrocyten en botcellen, kraakbeen en bot genereren in een microfluïdisch systeem, een zogenoemd gewricht-op-een-chip model. Naast het genereren van kraakbeen en bot in dit systeem hebben we ook laten zien dat we dit weefsel kunnen blootstellen aan artrose-gerelateerde verstoringen zoals hypertrofie-inducerend thyroïd hormoon T3. Dit model kan in de toekomst gebruikt worden voor het functioneel bestuderen van genen en factoren die verhoogd risico geven op artrose.

Conclusie en toekomstperspectieven
In dit proefschrift hebben we verschillende strategieën toegepast om meer inzicht te krijgen in het artrose ziekteproces. Op deze manier hebben we laten zien dat er een aantal belangrijke zaken zijn waar men rekening mee dient te houden bij de ontwikkeling van medicijnen tegen artrose. Ondanks dat genetica een goed startpunt is voor het vinden van aangrijpingspunten voor medicijnen, is het van essentieel belang dat het onderliggende mechanisme van deze risicogenen wordt onderzocht. Dit om te begrijpen hoe en via welk weefsel het gen verhoogd risico op artrose veroorzaakt. Daarnaast pleiten wij voor een medicijn wat aangrijpt op zowel kraakbeen als bot, om op deze manier zo effectief mogelijk te kunnen behandelen. Ook dient men rekening te houden met de heterogeniteit die artrose kent en niet uit te gaan van het one-drug-fits-all-patients principe. Zowel in dit proefschrift als in voorgaande studies is aangetoond dat het artrose ziekteproces verschillend is tussen zowel het type gewricht (heup en knie) als tussen patiënten (subtype A en subtype B artrose). Tenslotte hebben we in dit proefschrift de potentie van miRNA's in bloed als biomarker voor artrose subtypes

weergeven. Al met al hebben we in dit proefschrift geprobeerd een stap voorwaarts te maken in de transitie van bench-to-bed-side.

A

Appendix

Publication list

Characterizing the invasion of different breast cancer cell lines with distinct E-cadherin status in 3D using a microfluidic system
H. Eslami Amirabadi*, **M. Tuerlings***, A. Hollestelle, S. SahebAli, R. Luttge, C.C. van Donkelaar, J.W.M. Martens, J.M.J. den Toonder
Biomedical Microdevices (2019)

Elucidating Epigenetic Regulation by Identifying Functional cis-Acting Long Noncoding RNAs and Their Targets in Osteoarthritic Articular Cartilage
M. van Hoolwerff, P.I. Metselaar, **M. Tuerlings**, H.E.D. Suchiman, N. Lakenberg, Y.F.M. Ramos, D. Cats, R.G.H.H. Nelissen, D. Broekhuis, H. Mei, R. Coutinho de Almeida, I. Meulenbelt
Arthritis and Rheumatology (2020)

RNA Sequencing Reveals Interacting Key Determinants of Osteoarthritis Acting in Subchondral Bone and Articular Cartilage: Identification of IL11 and CHADL as Attractive Treatment Targets
M. Tuerlings, M. van Hoolwerff, E. Houtman, H.E.D. Suchiman, N. Lakenberg, H. Mei, H.M.J. van der Linden, R.R.G.H.H. Nelissen, Y.F.M. Ramos, R. Coutinho de Almeida, I. Meulenbelt
Arthritis and Rheumatology (2021)

Long non-coding RNA expression profiling of subchondral bone reveals AC005165.1 modifying FRZB expression during osteoarthritis
M. Tuerlings, M. van Hoolwerff, J.M. van Bokkum, H.E.D. Suchiman, N. Lakenberg, D. Broekhuis, R.G.H.H. Nelissen, Y.F.M. Ramos, H. Mei, D. Cats, R. Coutinho de Almeida, I. Meulenbelt
Rheumatology (2021)

Characterization of dynamic changes in Matrix Gla Protein (MGP) gene expression as function of genetic risk alleles, osteoarthritis relevant stimuli, and the vitamin K inhibitor warfarin
E. Houtman, R. Coutinho de Almeida, **M. Tuerlings**, H.E.D. Suchiman, D. Broekhuis, R.G.H.H. Nelissen, Y.F.M. Ramos, J.B.J. van Meurs, I. Meulenbelt
Osteoarthritis and Cartilage (2021)

Cartilage from human-induced pluripotent stem cells: comparison with neo-cartilage from chondrocytes and bone marrow mesenchymal stromal cells
A. Rodríguez Ruiz, A. Dicks, **M. Tuerlings**, K. Schepers, M. van Pel, R.G.H.H. Nelissen, C. Freund, C.L. Mummery, V. Orlova, F. Guilak, I. Meulenbelt, Y.F.M. Ramos
Cell and tissue research (2021)

A

Elucidating mechano-pathology of osteoarthritis: transcriptome-wide differences in mechanically stressed aged human cartilage explants
E. Houtman, **M. Tuerlings**, J. Riechelman, H.E.D. Suchiman, R.J.P. van der Wal, R.G.H.H. Nelissen, H. Mei, Y.F.M. Ramos, R. Coutinho de Almeida, I. Meulenbelt
Arthritis Research & Therapy (2021)

Deciphering osteoarthritis genetics across 826,690 individuals from 9 populations
C.G. Boer, K. Hatzikotoulas, L. Southam, L. Stefánsdóttir, Y. Zhang, R. Coutinho de Almeida, T.T. Wu, J. Zheng, A. Hartley, M. Teder-Laving, A.H. Skogholt, C. Terao, E. Zengini, G. Alexiadis, A. Barysenka, G. Bjornsdottir, M.E. Gabrielsen, A. Gilly, T. Ingvarsson, M.B. Johnsen, H. Jonsson, M. Kloppenburg, A.Luetge, S.H. Lund, R. Mägi, M. Mangino, R.R.G.H.H. Nelissen, M. Shivakumar, J. Steinberg, H. Takuwa, L.F. Thomas, **M. Tuerlings**, arcOGEN Consortium; HUNT All-In Pain; ARGO Consortium; Regeneron Genetics Center; G.C. Babis, J. Pui Yin Cheung, J. Hee Kang, P. Kraft, S.A. Lietman, D. Samartzis, P.E. Slagboom, K. Stefansson, U. Thorsteinsdottir, J.H. Tobias, A.G. Uitterlinden, B. Winsvold, J.A. Zwart, G.D. Smith, P.C. Sham, G. Thorleifsson, T.R. Gaunt, A.P. Morris, A.M. Valdes, A. Tsezou, K.S.E. Cheah, S. Ikegawa, K. Hveem, T. Esko, J.M. Wilkinson, I. Meulenbelt, M. Ta Michael Lee, J.B.J. van Meurs, U. Styrkársdóttir, E. Zeggini
Cell (2021)

Capturing Essential Physiological Aspects of Interacting Cartilage and Bone Tissue with Osteoarthritis Pathophysiology: A Human Osteochondral Unit-on-a-Chip Model
M. Tuerlings*, I. Boone*, H. Eslami Amirabadi, M.A.M. Vis, H.E.D. Suchiman, H.M.J. van der Linden, S. Hofmann, R.G.H.H. Nelissen, J.M.J. den Toonder, Y.F.M. Ramos, I. Meulenbelt
Advanced Materials Technologies (2022)

Inhibiting thyroid activation in aged human explants prevents mechanical induced detrimental signalling by mitigating metabolic processes
E. Houtman, **M. Tuerlings**, H.E.D. Suchiman, N. Lakenberg, F.M.F. Cornelis, H. Mei, D. Broekhuis, R.G.H.H. Nelissen, R. Coutinho de Almeida, Y.F.M. Ramos, R.J. Lories, L.J. Cruz, I. Meulenbelt
Rheumatology (2022)

A molecular map of long non-coding RNA expression, isoform switching and alternative splicing in osteoarthritis
G. Katsoula, J. Steinberg, **M. Tuerlings**, R. Coutinho de Almeida, L. Southam, D. Swift, I. Meulenbelt, J.M. Wilkinson, E. Zeggini
Human Molecular Genetics (2022)

A human in vitro 3D neo-cartilage model to explore the response of OA risk genes to hyper-physiological mechanical stress
R.G.M. Timmermans, N.G.C. Bloks, **M. Tuerlings**, M. van Hoolwerff, R.G.H.H. Nelissen, R.J.P. van der Wal, P.M. van der Kraan, A.B. Blom, M.H.J. van den Bosch, Y.F.M. Ramos, I. Meulenbelt
Osteoarthritis and Cartilage Open (2022)

The role of TNFRSF11B in development of osteoarthritic cartilage
A. Rodríguez Ruiz, **M. Tuerlings**, A. Das, R. Coutinho de Almeida, H.E.D. Suchiman, R.G.H.H. Nelissen, Y.F.M. Ramos, I. Meulenbelt
Rheumatology (2022)

Allelic expression imbalance in articular cartilage and subchondral bone refined genome-wide association signals in osteoarthritis.
R. Coutinho de Almeida, **M. Tuerlings**, Y.F.M. Ramos, W. Den Hollander, H.E.D. Suchiman, N. Lakenberg, R.G.H.H. Nelissen, H. Mei, I. Meulenbelt
Rheumatology (2022)

Identification and functional characterization of imbalanced osteoarthritis-associated fibronectin splice variants
M. van Hoolwerff, **M. Tuerlings**, I.J.L. Wijnen, H.E.D. Suchiman, D. Cats, H. Mei, R.G.H.H. Nelissen, H.M.J. van der Linden, Y.F.M. Ramos, R. Coutinho de Almeida, I. Meulenbelt
Rheumatology (2023)

WWP2 confers risk to osteoarthritis by affecting cartilage matrix deposition via hypoxia associated genes
M. Tuerlings, G.M.C. Janssen, I. Boone, M. van Hoolwerff, A. Rodriguez Ruiz, E. Houtman, H.E.D. Suchiman, R.J.P. van der Wal, R.G.H.H. Nelissen, R. Coutinho de Almeida, P.A. van Veelen, Y.F.M. Ramos, I. Meulenbelt
Osteoarthritis and cartilage (2023)

*Shared first author

A

Appendix

Curriculum Vitae

Margo Tuerlings was born in 1992 on December 3 in Eindhoven, the Netherlands. She graduated from secondary school in 2011 at Beatrix College in Tilburg.

In 2011 she started a surgical assistant training at Fontys University of Applied Sciences in Eindhoven and St. Elizabeth hospital in Tilburg. After six months she decided to challenge herself a bit more, she quit the surgical assistant training and she enrolled in the study Medical Sciences and Technology at Eindhoven University of Technology (TU/e) in 2012. Margo obtained her bachelor's degree in 2016 and she continued her academic career by enrolling in the Biomedical Engineering master's program at the TU/e. During this master's program she followed the track Regenerative Medicine and Technology, which was a collaboration between the department of Biomedical Engineering of the TU/e and the department of Medicine of Utrecht University (UU). Moreover, she chose to specialize in orthopedic biomechanics. Her first internship was at the department of Mechanical Engineering of the TU/e in the microsystems research group of Prof. Jaap den Toonder. Within this internship, Margo focused on the characterization of breast cancer cell lines with distinct E-cadherin status using a microfluidic system. For her master-thesis she wanted to combine her specialization on orthopedic biomechanics with the experience of her first master internship, by working on the development of a microfluidic model system of an osteochondral construct to eventually study underlying biological mechanisms of osteoarthritis (OA) risk genes. The research in this master-thesis was performed in a collaboration between the Microsystems research group of Prof. Jaap den Toonder within the department of Mechanical Engineering at the TU/e and the Osteoarthritis research group of Prof. Ingrid Meulenbelt within the department of Biomedical Data Sciences, section Molecular Epidemiology at Leiden University Medical Center (LUMC). Margo presented this work at the Human Organ and Disease Model Technologies (HDMT) annual meeting 2018 and she won the "Best Show Case Idea" award.

After Margo obtained her master's degree in 2018, she started as PhD student in the Osteoarthritis research group of Prof. Ingrid Meulenbelt. During her PhD, she focused on the characterization of OA pathophysiology in subchondral bone in interaction with articular cartilage, by analyzing large RNA-sequencing datasets of these tissues. Moreover, she used miRNA-sequencing data of plasma, together with RNA-sequencing data of articular cartilage and subchondral bone, to identify potential non-invasive biomarkers in plasma that mark OA-related processes within the joint. To investigate underlying mechanisms of previously identified OA risk genes, she exploited two model systems of OA: *in vitro* 3D primary chondrocyte pellet cultures and *ex vivo* human osteochondral explant cultures. Finally, she further optimized the osteochondral

A

unit-on-a-chip as a model system for OA. Margo presented her work (oral and poster presentations) on national and international conferences, including the Dutch Society for Matrix Biology (NVMB) annual meeting, the HDMT annual meeting, the Orthopaedic Research Society annual meeting (ORS), and the joint meeting of the Hellenic Society for the Study of Bone Metabolism and the Dutch Society for Calcium and Bone Metabolism.

In 2022, Margo continued her academic career within the Osteoarthritis research group of Prof. Ingrid Meulenbelt as post-doctoral researcher. She will optimize the osteochondral unit-on-a-chip for the use of human induced pluripotent stem cell derived mesenchymal stem cells (hiMSCs) to eventual study high impact mutation OPG-XL.

A

Appendix

Dankwoord

Na iets meer dan vier jaar komt er een einde aan mijn promotietraject. Een tijd die voorbij is gevlogen en een tijd waarin ik enorm veel heb geleerd. Natuurlijk heb ik dit niet alleen gedaan en wil ik graag alle mensen bedanken die aan het tot stand komen van dit proefschrift hebben bijgedragen.

Professor Meulenbelt, beste Ingrid, allereerst wil ik je bedanken voor de mogelijkheid om mijn promotietraject binnen jouw groep te kunnen doen. Daarnaast wil ik je bedanken voor alles wat je mij hebt geleerd, voor je vertrouwen, voor alle feedback en voor de sparsessies tijdens de maandelijkse f2f meetings die meestal langer duurde dan het daarvoor geschreven uur. Ik vind het erg fijn dat ik ook de komende jaren bij jou in de groep mag blijven werken.

Doctor Coutinho de Almeida, dear Rodrigo, thank you for your patience, for learning me how to work with R and for all the help with making scripts. I could not have done it without your help and I really learned a lot from you.

Doctor Ramos, beste Yolande, dankjewel voor alles wat ik van jou geleerd heb op het lab en daarbuiten, ook wil ik je bedanken voor alle feedback op mijn manuscripten. Ik waardeer het enorm dat ik met vragen en/of twijfels over experimenten altijd bij jou kan binnenlopen.

Graag wil ik mijn collega's van de OA groep bedanken voor de bijdrage aan dit proefschrift. Allereerst Ilja, bedankt voor alle uren die we samen in het lab, in de trein, op kantoor en op borrels hebben doorgebracht, zonder jou was mijn promotietijd niet hetzelfde geweest. Daarnaast wil ik je ook bedanken dat je mijn paranimf wilt zijn. Eka, dankjewel voor je ondersteuning op het lab en voor je luisterend oor. Marcella, Alejandro en Evelyn, bedankt voor al jullie hulp en voor alles wat jullie mij geleerd hebben. Verder wil ik ook alle (ex-)collega's van de OA groep bedanken: Ritchie, Niek, Nicoline, Ghazaleh, Mathew, Rick en Nico. Bedankt allemaal voor de hulp in en rondom het lab, de feedback tijdens besprekingen, maar ook voor de gezelligheid en goede gesprekken. Natuurlijk wil ik ook de collega's van MolEpi bedanken, in het bijzonder Eline en Inge. Mijn dank gaat ook uit naar de studenten die ik tijdens mijn promotietraject heb mogen begeleiden: Jessica, Janneke, Maurice en Elisa. Dankjewel voor jullie hulp.

Verder wil ik graag iedereen bedanken die betrokken is bij de RAAK-studie, zowel binnen het LUMC als in Alrijne ziekenhuis Leiderdorp. Zonder al het waardevolle materiaal wat jullie voor ons hebben verzameld was dit proefschrift niet tot stand kunnen komen. Ook de patiënten die hebben meegewerkt aan de RAAK-studie wil ik graag bedanken.

A

A